

**AN UNSUPERVISED CLASSIFICATION-BASED TIME SERIES CHANGE
DETECTION APPROACH FOR MAPPING FOREST DISTURBANCE**

ILIA PARSHAKOV
Master of Science, University of Lethbridge, 2012

A thesis submitted
in partial fulfilment of the requirements for the degree of

DOCTOR OF PHILOSOPHY

in

EARTH, SPACE, AND PHYSICAL SCIENCE

Department of Geography and Environment
University of Lethbridge
LETHBRIDGE, ALBERTA, CANADA

© Ilia Parshakov, 2021

AN UNSUPERVISED CLASSIFICATION-BASED TIME SERIES CHANGE DETECTION
APPROACH FOR MAPPING FOREST DISTURBANCE

ILIA PARSHAKOV

Date of Defence: December 22, 2020

Dr. Derek R. Peddle Supervisor	Professor	Ph.D.
Dr. Karl Staenz Thesis Examination Committee Member	Professor Emeritus	Ph.D.
Dr. Howard Cheng Thesis Examination Committee Member	Associate Professor	Ph.D.
Dr. Craig Coburn Internal External Examiner Department of Geography and Environment Faculty of Arts and Science	Professor	Ph.D.
Dr. H. Peter White External Examiner Canada Centre for Remote Sensing Division Natural Resources Canada Ottawa, Ontario	Research Scientist	Ph.D.
Dr. René Barendregt Chair	Professor	Ph.D.

ABSTRACT

Unsupervised Classification to Change (UC-Change) is a new remote sensing approach for mapping areas affected by logging and wildfires. It addresses the main limitations of existing image time-series change detection techniques, such as limited multi-sensor capabilities, use of purely spectral-based forest recovery metrics, and poor detection of salvage harvesting. UC-Change detects disturbances and tracks forest recovery by analyzing changes in the spatial distribution of spectral classes over time. The algorithm detected approximately 85% and 70% of reference cutblock and fire scar pixels at a ± 2 -year temporal agreement, respectively, consistently outperforming existing algorithms across different biogeoclimatic zones of British Columbia, Canada. The results indicate an upper estimate of 7.5 million ha of forest cleared between 1984 and 2014, which is above estimates based on existing maps and databases (6.3 – 6.7 million ha). Also presented is a new framework for using open-access data for validation of change detection results.

ACKNOWLEDGEMENTS

This research was conducted within the Alberta Terrestrial Imaging Centre (ATIC) and the Department of Geography and Environment of the University of Lethbridge and supported primarily by a Natural Sciences and Engineering Research Council of Canada (NSERC) Collaborative Research and Training Experience (CREATE) grant entitled Advanced Methods, Education and Training in Hyperspectral Science and Technology (AMETHYST – P.I.'s D. Peddle, K. Staenz, P. Teillet), and by the University of Lethbridge.

I would like to thank my Supervisor Dr. Derek Peddle, Committee Members Dr. Karl Staenz and Dr. Howard Cheng, Internal-External Examiner Dr. Craig Coburn, External Examiner Dr. H. Peter White (Canada Centre for Remote Sensing), as well as Dr. Jinkai Zhang (Alberta Agriculture and Forestry), Subir Chowdhury (Alberta Geological Survey), Trevor Armstrong (AMETHYST Program Coordinator), and graduate student Peter Kennedy, for all the help, expertise, advice and comments they provided. I am also very grateful to my friends and family for their moral support and encouragement.

TABLE OF CONTENTS

ABSTRACT	iii
ACKNOWLEDGEMENTS	iv
LIST OF TABLES	ix
LIST OF FIGURES	x
LIST OF ABBREVIATIONS	xiii
CHAPTER 1 INTRODUCTION	1
1.1. Ecological Consequences of Forest Harvesting	1
1.2. Transition to Sustainable Silviculture	4
1.3. Role of Remote Sensing in Forestry	5
1.4. Research Goal and Objectives	7
1.5. Thesis Overview	9
1.6. References	9
CHAPTER 2 BACKGROUND	15
2.1. Factors Affecting Forest Change Detection	15
2.1.1. Data type	16
2.1.2. Spatial resolution.....	22
2.1.3. Image quality.....	25
2.1.4. Sun-target-sensor geometry.....	28
2.2. Types of Change Detection Techniques	29
2.2.1. Bi-temporal change detection techniques	29

2.2.2.	Time-series change detection techniques	32
2.3.	Change Attribution	44
2.4.	Forest Recovery Monitoring.....	45
2.5.	Accuracy Assessment of Forest Change Maps	47
2.6.	References	50
CHAPTER 3	A CLASSIFICATION-BASED TIME SERIES CHANGE DETECTION	
	TECHNIQUE FOR MAPPING STAND-REPLACING FOREST DISTURBANCES	
	USING MULTI-SENSOR REMOTE SENSING DATA	63
	Abstract.....	63
3.1.	Introduction	64
3.2.	Study Area and Data	71
3.3.	UC-Change Algorithm	79
3.3.1.	Unsupervised classification.....	80
3.3.2.	Stable pixel detection	82
3.3.3.	Primary change pixel detection.....	87
3.3.4.	Secondary change pixel detection.....	88
3.3.5.	Removal of false positives and analysis of post-disturbance recovery	90
3.3.6.	Accuracy assessment and comparison with LandTrendr, C2C, and GFC	94
3.4.	Results.....	98
3.5.	Discussion	106
3.5.1.	Performance of the UC-Change technique.....	106

3.5.2.	Comparison with existing change detection techniques and maps	107
3.5.3.	Forest recovery monitoring	110
3.6.	Conclusions	112
3.7.	References	116
CHAPTER 4	A COMPARISON OF THE UC-CHANGE AND C2C CHANGE	
	DETECTION ALGORITHMS FOR MAPPING CUTBLOCKS AND ESTIMATING THE	
	RATE OF FOREST HARVESTING IN BRITISH COLUMBIA, CANADA	123
	Abstract.....	123
4.1.	Introduction	124
4.2.	Study Area and Data	126
4.2.1.	Forest disturbance maps	129
4.2.2.	Forest inventory map and protected areas as validation data.....	132
4.2.3.	Other datasets	133
4.3.	Experimental Design	134
4.4.	Results.....	140
4.4.1.	Evaluation of the VRI forest inventory map	140
4.4.2.	Evaluation of the UC-Change and C2C forest change maps	140
4.4.3.	Harvest rate estimation.....	146
4.5.	Discussion	149
4.5.1.	VRI as validation data	149
4.5.2.	False detection of cutblock pixels in the UC-Change and C2C maps	150

4.5.3.	Effect of terrain slope and aspect on cutblock detection.....	152
4.5.4.	Effect of forest type and harvest practices on cutblock detection.....	154
4.5.5.	Accuracy of harvest rate estimation	158
4.6.	Conclusions	159
4.6.1.	Future work	163
4.7.	References	164
CHAPTER 5	CONCLUSIONS AND FUTURE WORK.....	171
5.1.	Conclusions	171
5.2.	Future work	177
5.3.	References	179
APPENDIX 1	Pseudocode.....	182
1.	Parameters	182
2.	Global Variables	183
3.	Local Variables	184
4.	Functions	185
5.	Processing.....	187

LIST OF TABLES

Table 3-1. The characteristics of maps and algorithms used in the study.	77
Table 3-2. Default LandTrendr parameters (Kennedy et al., 2018).....	78
Table 3-3. Percent reference clearcut pixels detected at a temporal agreement of ± 1 and ± 3 years. The available C2C and GFC maps covered limited time periods.	98
Table 3-4. Total area of the reference forest fire polygons per year and percent of the area detected by the four change detection techniques. The table only shows the years for which the total size of reference polygons was greater than 1 km ²	100
Table 3-5. False detection of cutblocks (commission errors) in the UC-Change and C2C maps for the period 2001 – 2015. The LandTrendr and GFC maps may contain disturbances other than logging and forest fires and were added for comparison only.	101
Table 4-1. The characteristics of forested BGC zones spanning the study area and information relevant to forest disturbance mapping.	128
Table 4-2. Percent 1988–2012 iVRI pixels visually confirmed as cutblock pixels using the LandTrendr Pixel Time Series Plotter.....	140
Table 4-3. Percent 1988 – 2012 iVRI clearcut pixels present in the UC-Change and C2C maps.	141
Table 4-4. Total area (km ²) and percent of BC forest (~55 million ha) harvested between 1985 and 2014 (inclusive). UCC = UC-Change.	149
Table A1-1. The values of some of the variables for the nineteenth image (1990-06-23_L5.dat) in a hypothetical dataset.	185

LIST OF FIGURES

Figure 2-1. Left: a subset of a 30-m Landsat 7 ETM+ false-color (green-red-NIR) image showing a 13.5 km x 13.5 km area near Prince George, British Columbia. Right: the same subset resampled to a 250-m resolution to match the spatial resolution of the red and NIR bands of the MODIS sensor. The white and pink patches are clearcuts. 23

Figure 2-2. Temporal segmentation process as proposed by Kennedy et al. (2010). Grey lines represent yearly NBR values for a single pixel. Potential vertices are identified by fitting regression lines to the temporal trajectory of a pixel (a) and then removed one by one to produce a simple model with the best fit (b). Image modified from: Kennedy et al. (2010), some steps removed. 36

Figure 2-3. Disturbance detection using the BFAST Monitor (Source: Verbesselt et al., 2012). The black line represents NDVI fluctuations before disturbance (“history period”). The blue dashed line is the model based on those normal fluctuations. The red line within the grey background (“monitoring period”) shows where data persistently deviates from the model, resulting in disturbance detection (vertical green line)..... 39

Figure 3-1. Number of Google Scholar returns for "change detection", "Landsat", and "time series". 66

Figure 3-2. Original NBR values (blue) and LandTrendr segmentation results (orange) for a pixel in a 1993 clearcut in Oregon, USA. Parameters best suited for the area were used to produce this segmentation (Kennedy et al., 2018). 69

Figure 3-3. Biogeoclimatic zones and subzones (in brackets) in the study area (based on BEC, 2020). 72

Figure 3-4. Number of images per year per sensor used in the study. The light grey bars in the background represent study area coverage (percent area covered per year) provided by the data. 73

Figure 3-5. The spectral response functions of the ten sensors used in this study. The bands that were not used are grayed out. The thermal and panchromatic bands of the Landsat sensors were not used and are not shown here. Data obtained from the USGS and ESA websites. 75

Figure 3-6. Flowchart of the UC-Change algorithm..... 80

Figure 3-7. Main steps of the UC-Change change detection: a) original multispectral images in false color (green-red-NIR; $t_1 - t_7$ are the acquisition dates of the images; bright areas are fresh clearcuts); b) K-means classification output (10 classes); c) stable pixels derived from the K-means maps; d) primary change pixels derived from stable pixels; and e) multitemporal classification using the stable and change pixels as training samples and a stack of the four corresponding original images together with the final output product..... 83

Figure 3-8. Top: Changes in the distribution of SWIR-ranked spectral classes in a 1987-07-01 clearcut over time. Bottom: forest recovery in the same clearcut measured by the cumulative percentage of dominant (containing 90% or more pixels) pre-disturbance and post-disturbance spectral classes, as well as average NBR and NDVI values. The spectral indices (NDVI and NBR) reached pre-disturbance values within 13 years after disturbance. The percentage of pre-disturbance classes reached 90% only after 28 years..... 93

Figure 3-9. VRI (blue), NBAC (white), and Kluskoil Lake Provincial Park (green) polygons overlaid on a Landsat 8 image (RGB: red, NIR, SWIR-2) acquired on 2014-09-13 (top) and the UC-Change map (bottom). Colors in the UC-Change map represent the year of disturbance. A large number of false positives (highlighted with red circles) can be seen inside the park, mainly due to changing wetland conditions.	97
Figure 3-10. Percent reference clearcut pixels detected at a temporal agreement of ± 1 year (solid lines) and ± 3 years (dashed lines). The grey line represents the total area of VRI clearcut polygons per year.	99
Figure 3-11. UC-Change and C2C forest change maps of the entire study area (100 km \times 100 km; north is up) for the period 1985 – 2015. Brighter shades of grey indicate more recent changes. Note the differences in the south-west corner.	102
Figure 3-12. 2001 – 2015 clearcuts and clearcuts with reserves (patches of undisturbed forest) as they appear in the reference data (VRI) and the four change detection maps compared in the Chapter. The UC-Change map was the most similar to the reference map. It accurately represented clearcuts with reserves and had a cleaner look overall, whereas other maps had a strong “salt-and-pepper” effect with many missing or only partially represented cutblocks.	103
Figure 3-13. Forest recovery in 1986 and 1987 clearcuts per biogeoclimatic zone and subzone (in brackets; followed by the total area of 1986 and 1987 clearcuts in km ²) as estimated using UC-Change forest recovery metrics (top) and average NBR values (bottom). Low 2017 and 2018 values are due to forest fires that affected recovering areas. .	105
Figure 4-1. The extent of the study area (dashed line) and biogeoclimatic zones (based on BEC, 2020) in British Columbia. See also Table 4.1.	127
Figure 4-2. LandTrendr-generated NBR trajectory for a pixel in a clearcut dated 1993 in both the UC-Change and C2C maps and 1996 in the VRI. Based on the dramatic fall in NBR values, the forest was harvested some time between summer 1992 and summer 1993 (only July and August Landsat data were used to produce this plot). Therefore, the VRI timestamp was deemed incorrect.	135
Figure 4-3. Positive and negative 30-m buffers were applied to each VRI clearcut polygon. The positive buffer allowed assessment of clearcut edge detections, which are subject to various geometric errors and the mixed-pixel problem. Inner VRI polygons (iVRI) were used to evaluate the ability of change detection techniques to detect pure clearcut pixels.	136
Figure 4-4. Percent reference clearcut pixels detected inside iVRI (e.g., UC-Change inner), VRI (UC-Change), and bVRI (UC-Change ± 1 pixel) polygons with a temporal agreement of ± 2 years, represented by solid, dashed, and dotted lines, respectively. If there were no geometric errors and mixed pixels were labelled accurately, the three lines per change detection technique would coincide. Using original VRI polygons for the assessment of clearcut detection produced the lowest numbers due to a misalignment between the map and reference dataset (VRI).	142
Figure 4-5. UC-Change map (translucent) and a VRI polygon (red) overlaid on top of a high-resolution Google Earth image (© Maxar Technologies). The size of the clearcut in the change map is clearly too large and the change pixels are shifted eastward relative to the actual location of the clearcut. This example illustrates false detection resulting from the mixed-pixel problem and image misregistration.	143

Figure 4-6. Percent iVRI clearcut pixels detected depending on the slope and aspect for the years 1987 - 2013.....	145
Figure 4-7. Percent iVRI clearcut pixels detected per BGC zone for the years 1987 - 2013.	146
Figure 4-8. Forest harvest rates in British Columbia, estimated using five different sources....	147
Figure 4-9. Forest harvest rate estimates with UC-Change and C2C results adjusted for commission and omission errors. The “VRI U CC adjusted” numbers were produced by merging VRI and CC maps and dividing the results by 0.95 to produced estimates for the entire province (the original VRI and C2C maps contain information about logging occurring on public lands only, which accounts for approximately 95% of all logging in the province).	148
Figure 4-10. 1998 (bottom) and 1989 (middle) partial cuts (examples of selection management) next to a 2002 clearcut with reserves (top-left) as seen in a 2004 high-resolution Google Earth image. Location: 51°40'55"N, 121°51'12"W; Biogeoclimatic zone: IDF. Imagery © Maxar Technologies.....	155
Figure 4-11. NBR trajectories (blue lines) of Landsat pixels (red squares in high-resolution Google Earth images; 30 m × 30 m) in cutblocks representative of various BGC zones. Y-axis = NBR; X-axis = year. Red lines are LandTrendr-fitted segments. Imagery © CNES / Airbus, Province of British Columbia, and Maxar Technologies.	157

LIST OF ABBREVIATIONS

AAFC	Agriculture and Agri-Food Canada
ALOS	Advanced Land Observing Satellite
AVHRR	Advanced Very High Resolution Radiometer
BAP	Best Available Pixel
BC	British Columbia
BEC	Biogeoclimatic Ecosystem Classification
BFAST	Breaks For Additive Season and Trend
BGC	Biogeoclimatic. BGC zone abbreviations:
BWBS	Boreal White and Black Spruce
CWH	Coastal Western Hemlock
ESSF	Englemann Spruce – Subalpine Fir
ICH	Interior Cedar – Hemlock
IDF	Interior Douglas-fir
MS	Montane Spruce
SBPS	Sub-Boreal Pine – Spruce
SBS	Sub-Boreal Spruce
BRDF	Bidirectional Reflectance Distribution Function
C2C	Composite2Change
CC	Consolidated Cutblocks
CCDC	Continuous Change Detection and Classification
CPCAD	Canadian Protected and Conserved Areas Database
DBEST	Detecting Breakpoints and Estimating Segments in Trend
DEM	Digital Elevation Model
ECCC	Environment and Climate Change Canada
ERTS	Earth Resources Technology Satellite (Landsat 1)
ESA	European Space Agency
ETM+	Enhanced Thematic Mapper Plus
FGC	Forest Genetics Council of British Columbia
FOV	Field Of View
GCP	Ground Control Point
GFC	Global Forest Change
ISODATA	Iterative Self-Organizing DATA analysis technique
LiDAR	Light Detection and Ranging
MMU	Minimum Mapping Unit
MODIS	MODerate-Resolution Imaging Spectroradiometer
MPB	Mountain Pine Beetle
MSS	Multispectral Scanner System
NBAC	National Burned Area Composite
NBR	Normalized Burn Ratio
NDVI	Normalized Difference Vegetation Index
NDWI	Normalized Difference Water Index
NFD	National Forestry Database
NIR	Near-InfraRed
NRCan	Natural Resources Canada

OLI	Operational Land Imager
PALSAR	Phased Array type L-band Synthetic Aperture Radar
PCA	Principal Component Analysis
RESULTS	Reporting Silviculture Updates and Land status Tracking System
RMSE	Root-Mean-Square Error
SAR	Synthetic Aperture Radar
SMA	Spectral Mixture Analysis
SPOT	Satellite Pour l'Observation de la Terre (French; English translation: satellite for observation of Earth)
SWIR	Short-Wave InfraRed
TCW	Tasseled Cap Wetness
TM	Thematic Mapper
TMA	Temporal Mixture Analysis
UC-Change	Unsupervised Classification to Change
USGS	United States Geological Survey
UTM	Universal Transverse Mercator
VNIR	Visible and Near-InfraRed
VRI	Vegetation Resources Inventory
	bVRI buffered VRI
	iVRI inner VRI

CHAPTER 1

INTRODUCTION

1.1. Ecological Consequences of Forest Harvesting

Global forest cover has undergone tremendous changes due to human activities (Kaplan *et al.*, 2016). Remote sensing plays a crucial role in documenting, monitoring, and mitigating these changes. It has been estimated that there are from 35% to 46% fewer trees on the planet today than there were at the start of human civilization (Crowther *et al.*, 2015; Mackey *et al.*, 2015) and that intact forests account for only 18% of the remaining forest cover (Venter *et al.*, 2016; Potapov *et al.*, 2017; Watson *et al.*, 2018). Deforestation (i.e., removal of forest not followed by reforestation), caused by the clearing of forested land for agricultural and other land uses, has resulted in the extinction or habitat loss of many species of plants, animals, and other organisms (Gibson *et al.*, 2011, Betts *et al.*, 2017). In many areas, deforestation has caused soil degradation and desertification (Glantz and Orlovsky, 1983; Oldeman, 1992; De la Paix *et al.*, 2013), changed hydrology (De la Paix *et al.*, 2013; Bagley *et al.*, 2014) and altered microclimate (Betts, 2001; Bounoua *et al.*, 2002; Li *et al.*, 2016), and had various negative socio-economic effects. For example, deforestation affects the livelihoods of people who depend on forest products and services (Sunderlin *et al.*, 2005; Mamo *et al.*, 2007). A significant portion of the carbon stored in felled trees ends up in the atmosphere, contributing to the rising concentration of atmospheric greenhouse gases (Bala *et al.*, 2007) and this contributes to anthropogenic climate change.

Deforestation is less common in developed countries (Leckie *et al.*, 2002; Clement *et al.*, 2015), where forests are usually allowed to partially regrow with or without human assistance (e.g., planting and/or seeding) before being harvested again. However, conversion of natural

forests into managed, repeatedly harvested forests can have similar consequences to deforestation mentioned in the previous paragraph, although to a lesser extent. For example, clearcutting (i.e., cutting of all trees in an area of at least a few hectares at one time), which is the most common harvesting method in Canada (Bergeron and Fenton, 2012) and many other countries (Brassard and Chen, 2006; Lundmark *et al.*, 2013), results in even-aged stands after regeneration and can have a less diverse understory compared with old-growth forests and forests recovering from natural disturbances, such as fire and insect infestations (Burton *et al.*, 2003; Bergeron and Fenton, 2012). Animal biodiversity is also much lower due to the lack of coarse woody debris, which is a critical habitat component for small mammals (Carey and Johnson, 1995), birds (Carey *et al.*, 1991), and amphibians (Bury *et al.*, 1991; Corn and Bury, 1991).

Whereas natural disturbances, including wildfires (Kutiel and Shaviv, 1992; Yildiz *et al.*, 2010), return nutrients like phosphorus, potassium, calcium, and magnesium from the trees back into the soil, logging removes nutrients directly and through post-harvest leaching (McRae *et al.*, 2001; Palviainen *et al.*, 2014; Swinfield *et al.*, 2019), depleting the soil after every harvest. Soils also suffer from erosion caused by heavy equipment involved with logging (Startsev *et al.*, 1998), including the need for access roads. Finally, unlike natural forests, which can continue to accumulate carbon for many centuries (Pregitzer and Euskirchen, 2004; Luysaert *et al.*, 2008), managed forests are harvested about every 100 years or even more frequently, typically well before they reach their maximum carbon capacity. To maximize financial return, managed forests are cut before reaching peak biomass (Hyde, 1981) and contain as little as 20% of the carbon on average over the rotation period compared to surrounding intact old-growth forests, depending on the type of forest and climate (less in tropics and more in boreal forests; Cooper, 1983). For example, in British Columbia, considering that only half of the harvested wood is turned into long-lived

products (e.g., lumber and panels; BC Ministry of Forests, 2010), those products would need to last for at least two harvest rotations (~ 200 years) to make logging in the province carbon neutral, which is not realistic (Pingoud, 2010).

Intensive silviculture often replaces native tree species with monocultural plantations. For example, the Province of British Columbia, by far the largest timber producer in Canada (NRCan, 2020), replants 80% of harvested areas (BC Ministry of Forests, 2017), of which 55% are replanted as lodgepole pine plantations instead of a mixture of native tree species (BC Ministry of Forests, 2009; Mather *et al.*, 2010; FGC, 2018). This practice is common even in areas with very high pre-harvest tree species diversity (Roach *et al.*, 2015). Lodgepole pine has been deemed as a highly attractive species by the timber industry due to its commercial suitability and also rapid growth rate under various conditions (Burns and Honkala 1990, Klinka *et al.* 2000) and has been planted in many countries outside its native range (e.g., Sweden and New Zealand; Gundale *et al.*, 2014), where it and its pests threaten to become invasive species (Engelmark *et al.*, 2001; Ledgard *et al.*, 2001). While lodgepole pine is native to North America and a common, dominant, or seral species in parts of British Columbia, it is now being recognized that monospecific plantations of this species suffer high mortality rates compared to the natural forest they replace for several reasons. Due to low species diversity, they are less resilient to diseases (e.g., western gall rust and dohistroma needle blight) and insect infestations (e.g., mountain pine beetle and lodgepole pine terminal weevil) and are prone to damage by wildlife (e.g., bears), ice, and snow press (Mather *et al.*, 2010; Roach *et al.*, 2015). In addition, the health of lodgepole pine plantations may become compromised in the future as the climate gets warmer. According to Coops and Waring (2010), lodgepole pine prefers relatively cold climates, with harsh spring frosts and average summer

temperatures below 15°C, and as a result, they predicted that this species will disappear in many parts of its current range by 2070 due to global warming.

1.2. Transition to Sustainable Silviculture

To protect biodiversity and maintain ecosystem integrity, forestry must transition from an agricultural model to one that mimics natural disturbance processes. One such alternative to clearcutting and monocultural plantations is variable retention harvesting, which leaves behind coarse woody debris, shrubs, single trees, and patches of intact forest that have high biodiversity and/or are important for forest recovery (Franklin *et al.*, 1997). Many researchers, such as Curtis (1997), Burton *et al.* (1999), and Harvey *et al.* (2003), also argue that an extended rotation period of up to 200 years is necessary to ensure that older cutblocks provide at least some of the habitat value and other ecological functions of the old-growth forest they replace. While the use of these sustainable practices (variable retention harvesting and extended rotation) is still very limited (Beese *et al.*, 2019), somewhat less ecologically-oriented partial-harvest, clearcutting-with-reserves, and small-area-clearcutting methods have become common in some places, such as British Columbia and Ontario (Thorpe and Thomas, 2007; BC Ministry of Forests, 2018).

There are often competing objectives between what will generate the most profit, particularly in the short term, and what is best ecologically. Sustainable methods, especially those using extended rotation periods, may require larger areas and higher expenses to maintain the same rate of timber extraction as clearcutting. In addition, there is no systematic approach to determining what kind of forest management methods are best suited for each particular area. For example, lone trees left behind by variable retention harvest may suffer high mortality in areas where strong winds are frequent (Beese *et al.*, 2019). In drier areas, moisture competition from residual trees

can also slow down forest regeneration (Beese *et al.*, 2019). Thus, there is a distinct need for information to help properly drive these forest harvest and management decisions, both for short term harvesting decisions and longer-term forest integrity (which has both ecological and economic benefits).

1.3. Role of Remote Sensing in Forestry

While field visits are crucial for studying forest recovery in individual cutblocks, it is impractical to monitor hundreds of thousands of them without using remote sensing tools. Therefore, remote sensing plays an important role in helping to find a compromise between ecological and economic objectives. Using satellite data, it is possible not only to map the extent and date of harvest, but also to monitor forest recovery. A combination of satellite, airborne, and near-surface remote sensing data can be used to determine if the composition and structure of recovering forest stands meet the goals of sustainable forestry. This information makes it possible to evaluate the success of different forest management practices. Likewise, biomass can be estimated regularly, and this can also help monitor greenhouse gas emissions and carbon sequestration (De Sy *et al.*, 2012).

Aerial photography has been used for high-definition forest mapping for approximately a century (e.g., Robbins, 1929; Parsons, 1930; Husch *et al.*, 2002). British Columbia's Forest Inventory is still primarily based on human interpretation of aerial photographs (Bourgeois *et al.*, 2018). However, while this method makes it possible to map forest disturbance and analyze post-disturbance forest recovery at a high level of spatial accuracy and detail, it is labour intensive and time consuming, expensive, subjective based on individual interpreter

variations, limited to a few regions where sufficient spatial and temporal coverage of the area is available, and rarely provides up-to-date information.

Satellite sensors can acquire data for any forested area on the planet at regular and relatively short (compared to aerial photography) time intervals. Most cutblocks can be easily identified on images acquired by the multispectral scanner (MSS) that was on board the Landsat 1 satellite launched in 1972 (originally called ERTS/1). Landsat data have been continuously recorded for nearly half a century and, therefore, can be used to determine the baseline for monitoring both recent and older forest disturbances. Such a long record of satellite data can provide essential information on how forest disturbances of the past affect forest communities, flora, and fauna today. For example, Landsat sensors captured the rapid growth in commercial harvesting of northern forests which was facilitated by the mechanization and automation of the timber industry in the 1970s and 1980s (Burton *et al.*, 2003).

Despite the long and continuous record of satellite observations, there are few detailed large-area maps of anthropogenic forest disturbances that are openly available today. Prior to the opening of the Landsat archive in 2008, satellite-based forest disturbance mapping was mostly limited to small-area medium-resolution (10m – 100m) or large-area but coarse resolution (>100m) studies (Banskota *et al.*, 2014; Zhu, 2017). Even today, the use of medium-resolution 1972 – 1983 Landsat data is hindered by the quality of data preprocessing (Wulder *et al.*, 2019). In contrast, the preprocessing of data acquired by Landsat 5 TM (launched in 1984) and newer sensors has been continuously improving (Zhu *et al.*, 2015; Qiu *et al.*, 2019; Wulder *et al.*, 2019), resulting in analysis-ready imagery that can be used in multi-temporal studies without any additional preparation on the user side. This presents an important opportunity. However, a key

challenge is the much larger size and temporal extent of these datasets, and the need for a better approach and new processing methods. This forms the focus of this thesis.

The goal of forest disturbance mapping is to determine how (e.g., fire, logging, and insect infestation), where (location and boundary of disturbed forest), and when changes in forest cover occur, as well as to provide information on the temporal dynamics of such changes. Only time-series change detection techniques, which use large, temporally dense sets of satellite data, can be used to address these questions. Many researchers (e.g., Hansen and Loveland, 2012; Banskota *et al.*, 2014) predicted that automated time-series algorithms would largely replace traditional techniques that compare a small number (as few as two) of images as they provide a deeper understanding of forest changes and trends and can be used to map large areas.

1.4. Research Goal and Objectives

The goal of this research was to develop a new technique for mapping stand-replacing forest disturbances (i.e., disturbances resulting in a complete or near complete removal of forest cover) that would address some of the limitations of existing methods, such as limited multi-sensor capabilities, use of purely spectral-based forest recovery metrics, and poor detection of salvage harvesting. The technique, named Unsupervised Classification to Change (UC-Change), represents a completely new approach to time-series change detection. It can utilize both spectral and spatial information contained in data of variable spatial, spectral, and radiometric resolutions from multiple sensors to map forest disturbances. It offers new, object-based metrics for monitoring forest recovery that can provide unique ecological information. It may also have utility for other time-series applications. The objectives of the thesis were as follows:

- 1) Develop a technique that detects forest disturbances using unsupervised classification maps derived from time-series Landsat and Sentinel-2 data. Compared to existing methods, it was expected that such a technique would require fewer data preprocessing steps and be able to more fully utilize the spectral and spatial information offered by different sensors in multi-sensor datasets.
- 2) The second objective with this new UC-Change approach was focused on the analysis of post-disturbance dynamics. Its basis is tracking changes in the distribution of spectral classes inside a disturbed area over time to better monitor forest recovery than by using pixel-based metrics only. To test this, the saturation rate for the two types of metrics (existing pixel-based metrics and the new object-based metrics) was compared. Pixel-based methods use spectral indices that, in Canada, reach pre-disturbance values within 20 years after a disturbance event (White *et al.*, 2017), well before the forest reaches maturity (80 – 120 years, depending on the species), not to mention the old-growth status (>200 years) (Cooper, 1983; Burton *et al.*, 1999). It was expected that the proposed object-based metrics would take longer to saturate than pixel-based metrics. In addition, they were expected to be able to provide basic information about changes in stand composition (e.g., whether regenerating stands are deciduous, coniferous, or mixed).
- 3) Develop a framework for the assessment of forest disturbance maps using high-quality open-access data, such as the forest inventory data of British Columbia.
- 4) The final objective was to evaluate the ability of the UC-Change technique to accurately estimate the rate of forest harvesting in different biogeoclimatic zones and over large areas. To do so, a map produced for the province of British Columbia was validated against forest inventory data and compared with existing forest disturbance maps and databases.

1.5. Thesis Overview

This thesis follows a journal paper format. In Chapter 2, the literature is reviewed to identify issues associated with existing approaches to forest disturbance mapping. Chapter 3 (draft of Paper 1) presents the new UC-Change method created with the purpose of addressing those issues. Chapter 4 (draft of Paper 2) analyzes the utility of the UC-Change approach for estimating the scale and rate of forest harvesting at a regional scale. Chapters 3 and 4 are intended as self-contained, stand-alone manuscripts in draft form to be updated and submitted for peer-review and publication at a later date. Chapter 5, the Conclusion, summarizes the thesis findings, highlights the significance of the research, provides major conclusions, and suggests areas for future research.

1.6. References

- Bagley, J. E., Desai, A. R., Harding, K. J., Snyder, P. K., & Foley, J. A. (2014). Drought and deforestation: Has land cover change influenced recent precipitation extremes in the Amazon? *Journal of Climate*, 27(1), 345-361.
- Bala, G., Caldeira, K., Wickett, M., Phillips, T. J., Lobell, D. B., Delire, C., & Mirin, A. (2007). Combined climate and carbon-cycle effects of large-scale deforestation. *Proceedings of the National Academy of Sciences*, 104(16), 6550-6555.
- Banskota, A., Kayastha, N., Falkowski, M. J., Wulder, M. A., Froese, R. E., & White, J. C. (2014). Forest monitoring using Landsat time series data: a review. *Canadian Journal of Remote Sensing*, 40(5), 362-384.
- BC Ministry of Forests (2009). Annual Service Plan Report: 2002–2009 annual reports. The Ministry of Forests, Lands, Natural Resource Operations and Rural Development of British Columbia, Canada. <http://www.for.gov.bc.ca/mof/annualreports.htm> [Accessed on 2020-10-30]
- BC Ministry of Forests (2010). The State of British Columbia's Forests, third Edition. The Ministry of Forests, Lands, Natural Resource Operations and Rural Development of British Columbia, Canada. https://www2.gov.bc.ca/assets/gov/environment/research-monitoring-and-reporting/reporting/envreportbc/archived-reports/sof_2010.pdf [Accessed on 2020-10-30].
- BC Ministry of Forests (2017). Factsheet: reforestation in B.C. The Ministry of Forests, Lands, Natural Resource Operations and Rural Development of British Columbia, Canada. <https://news.gov.bc.ca/factsheets/factsheet-reforestation-in-bc> [Accessed on 2020-10-30].

- BC Ministry of Forests (2018). Area harvested in 2017/18 by silvicultural systems on crown land by area. The Ministry of Forests, Lands, Natural Resource Operations and Rural Development of British Columbia, Canada. https://www2.gov.bc.ca/assets/gov/farming-natural-resources-and-industry/forestry/silviculture/silviculture-statistics/annual-reports/2017-18-annual-reports/area_harvested_in_2017-2018_by_silv_system_on_cl_by_fr.xlsx [Accessed on 2020-10-30]
- BC Ministry of Forests (2020). Managing vegetation in provincial forests. The Ministry of Forests, Lands, Natural Resource Operations and Rural Development of British Columbia, Canada. <https://www.for.gov.bc.ca/hfp/publications/00183/> [Accessed on 2020-10-30].
- Beese, W. J., Deal, J., Dunsworth, B. G., Mitchell, S. J., & Philpott, T. J. (2019). Two decades of variable retention in British Columbia: a review of its implementation and effectiveness for biodiversity conservation. *Ecological Processes*, 8(1), 33.
- Bergeron, Y., & Fenton, N. J. (2012). Boreal forests of eastern Canada revisited: old growth, nonfire disturbances, forest succession, and biodiversity. *Botany*, 90(6), 509-523.
- Betts, M.G., Wolf, C., Ripple, W.J., Phalan, B., Millers, K.A., Duarte, A., Butchart, S.H. and Levi, T. (2017). Global forest loss disproportionately erodes biodiversity in intact landscapes. *Nature*, 547(7664), 441.
- Betts, R. A. (2001). Biogeophysical impacts of land use on present-day climate: Near-surface temperature change and radiative forcing. *Atmospheric Science Letters*, 2(1-4), 39-51.
- Bounoua, L., DeFries, R., Collatz, G. J., Sellers, P., & Khan, H. (2002). Effects of land cover conversion on surface climate. *Climatic Change*, 52(1-2), 29-64.
- Brassard, B. W., & Chen, H. Y. (2006). Stand structural dynamics of North American boreal forests. *Critical Reviews in Plant Sciences*, 25(2), 115-137.
- Brumelis, G., & Carleton, T. J. (1988). The vegetation of postlogged black spruce lowlands in central Canada. I. Trees and tall shrubs. *Canadian Journal of Forest Research*, 18(11), 1470-1478.
- Burns, R. M., & Honkala, B. H. (1990). Silvics of North America. Volume 1. Conifers. *Agriculture Handbook* (Washington), (654).
- Burton, P. J., Kneeshaw, D. D., & Coates, K. D. (1999). Managing forest harvesting to maintain old growth in boreal and sub-boreal forests. *The Forestry Chronicle*, 75(4), 623-631.
- Burton, P. J., Messier, C., Weetman, G. F., Prepas, E. E., Adamowicz, W. L., & Tittler, R. (2003). The current state of boreal forestry and the drive for change. *Towards Sustainable Management of the Boreal Forest*, 1-40.
- Bury, R. B., Corn, P. S., & Aubry, K. B. (1991). Regional patterns of terrestrial amphibian communities in Oregon and Washington. Pages 341-352 in L. E Ruggiero, K. B. Aubry, A. B. Carey, and M. H. Huff, technical coordinators. Wildlife and vegetation of unmanaged Douglas-fir forests. *United States Forest Service General Technical Report*, PNW-285.

- Carey, A. B., & Johnson, M. L. (1995). Small mammals in managed, naturally young, and old-growth forests. *Ecological Applications*, 5(2), 336-352.
- Carey, A. B., Hardt, M. M., Horton, S. P., & Biswell, B. L. (1991). Spring bird communities in the Oregon Coast Range. Pages 123-144 in L. F Ruggiero, K. B. Aubry, A. B. Carey, and M. H. Huff, technical coordinators. Wildlife and vegetation of unmanaged Douglas-fir forests. *United States Forest Service General Technical Report*, PNW-285.
- Carleton, T. J., & MacLellan, P. (1994). Woody vegetation responses to fire versus clear-cutting logging: a comparative survey in the central Canadian boreal forest. *Ecoscience*, 1(2), 141-152.
- Clement, M. T., Chi, G., & Ho, H. C. (2015). Urbanization and land-use change: A human ecology of deforestation across the United States, 2001–2006. *Sociological Inquiry*, 85(4), 628-653.
- Cooper, C. F. (1983). Carbon storage in managed forests. *Canadian journal of forest research*, 13(1), 155-166.
- Coops, N. C., & Waring, R. H. (2010). A process-based approach to estimate lodgepole pine (*Pinus contorta Dougl.*) distribution in the Pacific Northwest under climate change. *Climatic Change*, 105(1-2), 313-328.
- Corn, P. S., & Bury, R. B. (1991). Terrestrial amphibian communities in the Oregon Coast Range. Pages 305-318 in L. F Ruggiero, K. B. Aubry, A. B. Carey, and M. H. Huff, technical coordinators. Wildlife and vegetation of unmanaged Douglas-fir forests. *United States Forest Service General Technical Report*, PNW-285.
- Cremer, M., & Prietzel, J. (2017). Soil acidity and exchangeable base cation stocks under pure and mixed stands of European beech, Douglas fir and Norway spruce. *Plant and Soil*, 415(1-2), 393-405.
- Crowther, T.W., Glick, H.B., Covey, K.R., Bettigole, C., Maynard, D.S., Thomas, S.M., Smith, J.R., Hintler, G., Duguid, M.C., Amatulli, G. and Tuanmu, M.N. (2015). Mapping tree density at a global scale. *Nature*, 525(7568), 201.
- Curtis, R.O. (1997). The role of extended rotations. pp. 165-170 in K.A. Kohm and J.F. Franklin (eds.), *Creating a Forestry for the 21st Century: The Science of Ecosystem Management*. Island Press, Washington, DC.
- De la Paix, M. J., Lanhai, L., Xi, C., Ahmed, S., & Varennyam, A. (2013). Soil degradation and altered flood risk as a consequence of deforestation. *Land Degradation & Development*, 24(5), 478-485.
- De Sy, V., Herold, M., Achard, F., Asner, G. P., Held, A., Kellndorfer, J., & Verbesselt, J. (2012). Synergies of multiple remote sensing data sources for REDD+ monitoring. *Current Opinion in Environmental Sustainability*, 4(6), 696-706.
- Engelmark, O., Sjöberg, K., Andersson, B., Rosvall, O., Ågren, G.I., Baker, W.L., Barklund, P., Björkman, C., Despain, D.G., Elfving, B. and Ennos, R.A. (2001). Ecological effects and

- management aspects of an exotic tree species: the case of lodgepole pine in Sweden. *Forest Ecology and Management*, 141(1-2), 3-13.
- FGC, 2018. Annual Report 2017/2018. Forest Genetics Council of British Columbia. <http://www.fgcouncil.bc.ca/FGC-Annual-Report-2017-18-Web.pdf> [Accessed on 2020-10-30].
- Franklin, J. F., Berg, D. F., Thornburg, D., & Tappeiner, J. C. (1997). Alternative silvicultural approaches to timber harvesting: variable retention harvest systems. In *Creating a Forestry for the 21st Century: The Science of Ecosystem Management*. K.A. Kohn and J. F. Franklin (eds.), Island Press, Washington, D.C. pp. 111–139.
- Gibson, L., Lee, T.M., Koh, L.P., Brook, B.W., Gardner, T.A., Barlow, J., Peres, C.A., Bradshaw, C.J., Laurance, W.F., Lovejoy, T.E., & Sodhi, N. S. (2011). Primary forests are irreplaceable for sustaining tropical biodiversity. *Nature*, 478(7369), 378.
- Glantz, M. H., & Orlovsky, N. S. (1983). Desertification: A review of the concept. *Desertification Control Bulletin*, 9, 15-22.
- Gundale, M. J., Kardol, P., Nilsson, M. C., Nilsson, U., Lucas, R. W., & Wardle, D. A. (2014). Interactions with soil biota shift from negative to positive when a tree species is moved outside its native range. *New Phytologist*, 202(2), 415-421.
- Hansen, M. C., & Loveland, T. R. (2012). A review of large area monitoring of land cover change using Landsat data. *Remote Sensing of Environment*, 122, 66-74.
- Harvey, B. D., T. Nguyen-Xuan, Y. Bergeron, S. Gauthier & A. Leduc (2003). Forest management planning based on natural disturbance and forest dynamics. Pages 395–432 in P. J. Burton, C. Messier, D. W. Smith & W. L. Adamowicz (eds.). *Towards Sustainable Management of the Boreal Forest*. NRC Research Press, Ottawa, Ontario.
- Hyde, W. F. (1981). Volume or value maximization in forestry: An historical rationale and a glance at emerging technologies. *The Annals of Regional Science*, 15(2), 55-71.
- Kaplan, J. O., Pfeiffer, M., Kolen, J. C., & Davis, B. A. (2016). Large scale anthropogenic reduction of forest cover in Last Glacial Maximum Europe. *PLoS One*, 11(11), e0166726.
- Klinka, K., Worrall, J., Skoda, L., Varga, P., & Krajina, V. J. (2000). The distribution and synopsis of ecological and silvical characteristics of tree species of British Columbia's forests. *Canadian Cartographics Ltd., Coquitlam, BC*.
- Kutiel, P., & Shaviv, A. (1992). Effects of soil type, plant composition and leaching on soil nutrients following a simulated forest fire. *Forest Ecology and Management*, 53(1-4), 329-343.
- Leckie, D. G., Gillis, M. D., & Wulder, M. A. (2002). Deforestation estimation for Canada under the Kyoto Protocol: a design study. *Canadian Journal of Remote Sensing*, 28(5), 672-678.
- Ledgard, N. (2001). The spread of lodgepole pine (*Pinus contorta*, Dougl.) in New Zealand. *Forest Ecology and Management*, 141(1-2), 43-57.

- Li, Y., Zhao, M., Mildrexler, D.J., Motesharrei, S., Mu, Q., Kalnay, E., Zhao, F., Li, S. & Wang, K. (2016). Potential and actual impacts of deforestation and afforestation on land surface temperature. *Journal of Geophysical Research: Atmospheres*, 121(24), 14-372.
- Lundmark, H., Josefsson, T., & Östlund, L. (2013). The history of clear-cutting in northern Sweden—driving forces and myths in boreal silviculture. *Forest Ecology and Management*, 307, 112-122.
- Luyssaert, S., Schulze, E.D., Börner, A., Knohl, A., Hessenmöller, D., Law, B.E., Ciais, P., & Grace, J. (2008). Old-growth forests as global carbon sinks. *Nature*, 455(7210), 213.
- Mackey, B., DellaSala, D.A., Kormos, C., Lindenmayer, D., Kumpel, N., Zimmerman, B., Hugh, S., Young, V., Foley, S., Arsenis, K. and Watson, J.E. (2015). Policy options for the world's primary forests in multilateral environmental agreements. *Conservation Letters*, 8(2), 139-147.
- Mamo, G., Sjaastad, E., & Vedeld, P. (2007). Economic dependence on forest resources: A case from Dendi District, Ethiopia. *Forest Policy and Economics*, 9(8), 916-927.
- Mather, W. J., Simard, S. W., Heineman, J. L., & Sachs, D. L. (2010). Decline of planted lodgepole pine in the southern interior of British Columbia. *The Forestry Chronicle*, 86(4), 484-497.
- McRae, D. J., Duchesne, L. C., Freedman, B., Lynham, T. J., & Woodley, S. (2001). Comparisons between wildfire and forest harvesting and their implications in forest management. *Environmental Reviews*, 9(4), 223-260.
- NRCan (2020). National Forestry Database: forest area harvested on private and Crown lands in Canada. Canadian Forest Service, Natural Resources Canada. <http://nfdp.ccfm.org/en/data/harvest.php> [Accessed on 2020-10-31].
- Oldeman, L. R. (1992). Global extent of soil degradation. In *Bi-Annual Report 1991-1992/ISRIC* (pp. 19-36). ISRIC.
- Palviainen, M., Finér, L., Laurén, A., Launiainen, S., Piirainen, S., Mattsson, T., & Starr, M. (2014). Nitrogen, phosphorus, carbon, and suspended solids loads from forest clear-cutting and site preparation: long-term paired catchment studies from eastern Finland. *Ambio*, 43(2), 218-233.
- Pingoud, K., Pohjola, J., & Valsta, L. (2010). Assessing the integrated climatic impacts of forestry and wood products. *Silva Fennica*, 44(1), 155-175.
- Pregitzer, K. S., & Euskirchen, E. S. (2004). Carbon cycling and storage in world forests: biome patterns related to forest age. *Global Change Biology*, 10(12), 2052-2077.
- Qiu, S., Lin, Y., Shang, R., Zhang, J., Ma, L., & Zhu, Z. (2019a). Making Landsat Time Series Consistent: Evaluating and Improving Landsat Analysis Ready Data. *Remote Sensing*, 11(1), 51.
- Qiu, S., Zhu, Z., & He, B. (2019b). Fmask 4.0: Improved cloud and cloud shadow detection in Landsats 4–8 and Sentinel-2 imagery. *Remote Sensing of Environment*, 231, 111205.

- Roach, W. J., Simard, S. W., & Sachs, D. L. (2015). Evidence against planting lodgepole pine monocultures in the cedar–hemlock forests of southeastern British Columbia. *Forestry: An International Journal of Forest Research*, 88(3), 345-358.
- Startsev, N. A., McNabb, D. H., & Startsev, A. D. (1998). Soil biological activity in recent clearcuts in west-central Alberta. *Canadian Journal of Soil Science*, 78(1), 69-76.
- Sunderlin, W. D., Angelsen, A., Belcher, B., Burgers, P., Nasi, R., Santoso, L., & Wunder, S. (2005). Livelihoods, forests, and conservation in developing countries: an overview. *World Development*, 33(9), 1383-1402.
- Swinfield, T., Both, S., Riutta, T., Bongalov, B., Elias, D., Majalap-Lee, N., Ostle, N., Svátek, M., Kvasnica, J., Milodowski, D., & Jucker, T. (2019). Imaging spectroscopy reveals the effects of topography and logging on the leaf chemistry of tropical forest canopy trees. *Global Change Biology*, 26(2), 989-1002.
- Thorpe, H. C., & Thomas, S. C. (2007). Partial harvesting in the Canadian boreal: success will depend on stand dynamic responses. *The Forestry Chronicle*, 83(3), 319-325.
- Venter, O., Sanderson, E.W., Magrath, A., Allan, J.R., Beher, J., Jones, K.R., Possingham, H.P., Laurance, W.F., Wood, P., Fekete, B.M. and Levy, M.A. (2016). Sixteen years of change in the global terrestrial human footprint and implications for biodiversity conservation. *Nature Communications*, 7, 12558.
- Watson, J.E., Evans, T., Venter, O., Williams, B., Tulloch, A., Stewart, C., Thompson, I., Ray, J.C., Murray, K., Salazar, A. and McAlpine, C. (2018). The exceptional value of intact forest ecosystems. *Nature Ecology & Evolution*, 2(4), 599.
- White, J. C., Wulder, M. A., Hermosilla, T., Coops, N. C., & Hobart, G. W. (2017). A nationwide annual characterization of 25 years of forest disturbance and recovery for Canada using Landsat time series. *Remote Sensing of Environment*, 194, 303-321.
- Wulder, M.A., Loveland, T.R., Roy, D.P., Crawford, C.J., Masek, J.G., Woodcock, C.E., Allen, R.G., Anderson, M.C., Belward, A.S., Cohen, W.B. & Dwyer, J. (2019). Current status of Landsat program, science, and applications. *Remote Sensing of Environment*, 225, 127-147.
- Yildiz, O., Esen, D., Sarginci, M., & Toprak, B. (2010). Effects of forest fire on soil nutrients in Turkish pine (*Pinus brutia*, Ten) Ecosystems. *Journal of Environmental Biology*, 31(1-2), 11-13.
- Zhu, Z. (2017). Change detection using Landsat time series: A review of frequencies, preprocessing, algorithms, and applications. *ISPRS Journal of Photogrammetry and Remote Sensing*, 130, 370-384.
- Zhu, Z., Wang, S., & Woodcock, C. E. (2015). Improvement and expansion of the Fmask algorithm: Cloud, cloud shadow, and snow detection for Landsats 4–7, 8, and Sentinel 2 images. *Remote Sensing of Environment*, 159, 269-277.

CHAPTER 2

BACKGROUND

In the context of remote sensing, change detection can be defined as the process of detecting changes in land cover by comparing multitemporal observations. For example, two Landsat images of the same area can be compared to identify areas of forest loss and forest gain that occurred between the acquisition dates of the two images. Usually the term is applied to semi-automated and automated procedures (Lu *et al.*, 2004; Hansen and Loveland, 2012; Banskota *et al.*, 2014).

This chapter starts with a summary of main factors affecting forest change detection, which is followed by a review of current methods, including their strengths and weaknesses. Separate sections will analyze the ability of existing algorithms to characterize change and monitor post-disturbance forest recovery. Finally, the chapter will discuss the unique aspects of the accuracy assessment of change detection products.

2.1. Factors Affecting Forest Change Detection

There are numerous factors that can affect the performance of any change detection technique. Understanding these factors and knowing which of them a particular technique is most sensitive to may help select and pre-process imagery to maximize the accuracy of resulting maps. Using suitable data allows the algorithm of choice to separate the disturbances of interest from other changes and from noise, and to improve the mapping of individual disturbance events.

2.1.1. Data type

2.1.1.1. Optical remote sensing

Most forest change detection techniques use primarily or exclusively optical remote sensing data, which covers the visible (0.4 μm – 0.7 μm), near-infrared (NIR; 0.7 μm – 1.4 μm) and short-wave infrared (SWIR; 1.4 μm – 2.4 μm) parts of the electromagnetic spectrum (Lu *et al.*, 2004; Hussain *et al.*, 2013). All three regions (visible, NIR, and SWIR) can be used to identify and separate forested areas from other land-cover types and particularly bare ground (e.g., fresh clearcuts). What sets forest cover apart are the strong canopy shadowing effects and absorption of light in the SWIR region by canopy moisture (Steiner and Gutermann, 1966; Colwell, 1974; Horler and Ahern, 1986; Gemmell, 1995). Strong absorption of light in the visible spectrum by chlorophyll and other pigments (carotenoids and xanthophylls) can also be used to distinguish forest pixels from areas lacking vegetation (e.g., fresh clearcuts and fire scars) (Huete, 2012).

Trees can be distinguished from non-vegetated surfaces by using the visible and NIR bands. For this reason, many studies used the Normalized Difference Vegetation Index (NDVI) to map forest disturbances (e.g., Lunetta *et al.*, 2006; Verbesselt *et al.*, 2010; Reiche *et al.*, 2015):

$$\text{NDVI} = \frac{\text{NIR} - \text{red}}{\text{NIR} + \text{red}}, \quad (2-1)$$

where NIR and red are spectral reflectance values from the corresponding spectral bands. NDVI is sensitive to the health and density of green vegetation (Tucker, 1979; Sellers *et al.*, 1992); therefore, fresh cutblock and fire scars have low NDVI values compared to pre-disturbance values.

There are two main challenges associated with using NDVI for mapping forest disturbances. Compared to longer wavelengths, the NIR and especially red (due to strong chlorophyll absorption) bands can only sense the very top layer of tree canopies (Gao, 1996). As a

result, NDVI is known to saturate (plateau) at leaf area index¹ values far below those of mature forest stands (Gao, 1996). Consequently, NDVI has a limited application when it comes to monitoring forest recovery, as it can only be used to detect the initial emergence of any leafy vegetation, not just trees (Pickell *et al.*, 2016). In addition, it is not always easy to separate forest from non-woody vegetation using NDVI alone, for the same reason.

While other VNIR spectral indices exist, they perform similarly to NDVI when used for forest disturbance mapping (Xue and Su, 2017; Huo *et al.*, 2019; Cohen *et al.*, 2018). It is noteworthy that many sensors either do not have bands other than in the visible and NIR wavelength regions (e.g., Landsat MSS, SPOT 1 – 7, and most sensors with sub-10-m spatial resolution), or the spatial resolution of other bands is too low to accurately map the spatial extent of most cutblocks and small fire scars. For example, only two bands, red and NIR, of the MOderate-Resolution Imaging Spectroradiometer (MODIS) sensors have a spatial resolution of 250 m (other bands are 500 m or 1000 m). Therefore, using other indices is not always an option.

Landsat 5 TM (launched in 1984) and newer Landsat and some other sensors (e.g., Sentinel-2) have two spectral bands measuring radiance in two short-wave infrared (SWIR) atmospheric windows: 1500 nm – 1750 nm and 2000 nm – 2400 nm; these bands are commonly referred to as SWIR-1 and SWIR-2. It has been known that SWIR bands are extremely important for forest mapping (Horler and Ahern, 1986). Gemmell (1995) found strong inverse correlation between the SWIR bands of Landsat 5 TM data and timber volume. Hermosilla *et al.* (2015a) found the SWIR-1 bands of Landsat 5 TM and Landsat 7 ETM+ to be more important for the classification of forest disturbances than any other band, vegetation index, or other characteristic

¹ Leaf area index (LAI) is the ratio of one-sided leaf area per unit of ground area (Jordan, 1969).

that they tested. Cohen *et al.* (2018) had similar findings, in which the Normalized Burn Ratio (NBR) and Tasseled Cap Wetness (TCW) performed slightly better at detecting forest disturbances in Landsat data than just SWIR-1 or SWIR-2 bands alone. These indices are defined as follows:

$$\text{NBR} = \frac{\text{NIR} - \text{SWIR2}}{\text{NIR} + \text{SWIR2}} \text{ and} \quad (2-2)$$

$$\text{TCW} = 0.0315 \times \text{Blue} + 0.2021 \times \text{Green} + 0.3102 \times \text{Red} + 0.1594 \times \text{NIR} - 0.6806 \times \text{SWIR1} - 0.6109 \times \text{SWIR2}, \quad (2-3)$$

where Blue, Green, Red, NIR, SWIR1 and SWIR2 are spectral reflectance values for the corresponding Landsat spectral bands; coefficients used for TCW may differ depending on the sensor. Both NBR and TCW contrast SWIR bands with other spectral bands and have been found very useful for forest change detection because these regions (visible, NIR, and SWIR) react to forest disturbances differently (Huang *et al.*, 2010; Kennedy *et al.*, 2010; Hermosilla *et al.*, 2015a; Hughes *et al.*, 2017).

There are several reasons why SWIR bands are particularly useful for mapping forest disturbances and monitoring regrowth. First of all, the SWIR reflectance is inversely related to water content, which is typically higher in tree canopies than in other vegetation and bare soil (Horler and Ahern, 1986; Fiorella and Ripple, 1995; Schultz *et al.*, 2016). Secondly, the SWIR reflectance of a forest stand is even more affected by canopy shadowing than visible and NIR bands due to lower diffusive radiation in the shadows at longer wavelengths (Horler and Ahern, 1986; Zhu and Woodcock, 2012), which makes the difference between trees and non-woody vegetation or bare ground even greater. Thirdly, because SWIR wavelengths can penetrate multiple layers of leaves, SWIR-based vegetation indices do not saturate as quickly and are more sensitive to LAI than VNIR indices; therefore, they can provide more information about forest recovery than indices that use shorter wavelengths, such as NDVI (Hardisky *et al.*, 1983; Buma, 2012; Bartels *et al.*, 2016). Finally, SWIR bands are less sensitive to atmospheric conditions like

haze and thin clouds than visible and NIR bands because they are less affected by atmospheric scattering (USGS, 2020a). All these factors make cutblocks and fire scars easier to spot in SWIR bands than in VNIR bands.

While it is not surprising that most Landsat time-series forest change detection methods rely solely on SWIR bands (Kennedy *et al.*, 2007) or indices that contrast SWIR against other spectral bands (Huang *et al.*, 2010; Kennedy *et al.*, 2010; Hermosilla *et al.*, 2015a; Hughes *et al.*, 2017), the fact that SWIR bands are sensitive not only to canopy moisture, but also soil moisture, may present a challenge. In fact, the TCW transformation (Equation 2-3) was initially developed for mapping soil moisture (Crist, 1985). For this reason, precipitation events may affect the detection of some forest disturbances when using only TCW, SWIR bands, or SWIR-based vegetation indices because wet cutblocks and fire scars may have forest-like values in these spectral bands and indices.

It is now being recognized that using more than one band or vegetation index can significantly improve forest change detection. Cohen *et al.* (2018) compared the performance of their change detection algorithm (LandTrendr) using different combinations of 13 optical bands and indices, from singular bands/indices to a combination of all thirteen, and found that the combined use of all 13 bands and indices produced the lowest commission and omission errors when mapping forest disturbances using Landsat data. Healey *et al.* (2018) achieved similar results when they combined the outputs from multiple change detection algorithms that used different combinations of spectral bands. These studies indicate that every spectral band contains unique information that can be related to forest disturbance. Several methods have adopted a multispectral approach in the last decade (Jin *et al.*, 2013; Zhu and Woodcock, 2014; Cohen *et al.*, 2018), and among them, the one presented in this thesis.

2.1.1.2. Synthetic Aperture Radar

Multispectral satellite instruments do not always provide enough cloud-free data to accurately map disturbances, especially in areas with frequent cloud cover. To address this issue, some studies used Synthetic Aperture Radar (SAR) data (Almeida-Filho *et al.*, 2007; Lehmann *et al.*, 2013, Reiche *et al.*, 2015), which are largely unaffected by clouds. SARs are active sensors that transmit long-wavelength microwaves and then record the amount of backscattered radiation. The proportion of energy backscattered towards the receiver depends of the geometry of the target, its surface roughness and moisture content, as well as various sensor parameters (Leberl, 1990). These characteristics are different for various vegetation types and non-vegetated areas, which makes it possible to map changes in forest cover using SAR data. It has been found that low frequency radar bands, such as the L-band (1 – 2 GHz; 15 – 30 cm) and P-band (0.23 – 1 GHz; 30 – 130 cm), are more useful for detecting forest disturbances than the C-band (4 – 8 GHz; 3.75 – 7.5 cm) and other high-frequency radar bands as they can penetrate tree canopies deeper, and therefore, provide information about canopy structure (Luckman *et al.*, 1997; Ribbes *et al.*, 1997; van der Sanden and Hoekmen, 1999). In these two bands, forested pixels appear brighter than other types of vegetation and bare ground, because the signal can penetrate foliage but bounces off trunks and branches.

Optical and L-band radar time-series data can be combined to improve the detection of forest disturbances. For example, Reiche *et al.* (2015) used a regression model based on optimized weighted correlation of Landsat NDVI and ALOS PALSAR L-band backscatter time series in order to create a fused times series. In case of PALSAR data, they used the ratio of horizontally polarized and vertically polarized backscatter of horizontally transmitted waves (HVHH). High HVHH ratios indicate high volume scattering, where emitted waves become

polarized as they bounce off branches and trunks (Rignot *et al.*, 1997). By using the fused NDVI and SAR data, the authors achieved an overall accuracy of 95.5% with a 1.59-month mean time lag when mapping deforestation in the tropical forests of Fiji.

The C-band is another SAR band that is worth mentioning in this brief summary as its availability has increased dramatically in recent years. Many radar satellites (e.g., Sentinel-1 and the RADARSAT constellations) now provide C-band data at a high temporal resolution. In the C-band, woody and some non-woody vegetation appear similar because the pulses reflect from not only trunks and branches, but also leaves and, therefore, cannot penetrate deep into the canopy, resulting in a low sensitivity to aboveground biomass (Wang *et al.*, 1994). In addition, the C-band is also more sensitive to soil moisture than longer wavelengths (Wang *et al.*, 1994). Despite these limitations, Reiche *et al.* (2018) used Sentinel-1 data in combination with Landsat and ALOS-2 PALSAR-2 L-band imagery to increase the temporal resolution of their time series dataset, which resulted in a reduced detection lag (31 days).

SAR is generally less preferred to optical data for several reasons. One of them is the difficulty related to data interpretation. The side-looking viewing geometry causes SAR layover and shadow in hilly and mountainous areas and makes the spatial resolution and backscatter dependent on the distance from the sensor (slant range) and topography. The SAR speckle has also been cited as a deterring factor (Quegan and Yu, 2001; Reiche *et al.*, 2015), although methods exist to reduce speckle (Quegan and Yu, 2001; Trouvé *et al.*, 2003). Finally, SAR data acquired when soil moisture is high may present a problem because backscatter depends on canopy and soil water content, making it harder to separate disturbed areas from undisturbed (Lucas *et al.*, 2010; Mitchell *et al.*, 2017).

2.1.1.3. LiDAR

Light Detection and Ranging (LiDAR) is a very useful technology for forest mapping as it provides highly detailed three-dimensional information (Wulder *et al.*, 2013; White *et al.*, 2016). However, its spatial and temporal coverage are very limited compared to radar and optical satellite platforms due to the fact that currently only airborne LiDAR sensors can provide sufficient detail to map forest disturbances (Wulder *et al.*, 2013; White *et al.*, 2016). One notable exception is the Global Ecosystem Dynamics Investigation (GEDI) that was launched to the International Space Station in December 2018. This instrument was designed specifically for studying Earth's forests. However, it is expected to sample only 4% of the Earth's land surface during its two-year mission (Dubayah *et al.*, 2020). Similarly, regional airborne LiDAR data acquisition programs are generally too expensive to be carried out frequently (Hansen *et al.*, 2014; Guo *et al.*, 2017). Therefore, LiDAR is outside the scope of this thesis, because the focus is on time-series forest change detection of large areas for which LiDAR data sets do not exist.

2.1.2. Spatial resolution

While coarse-resolution data can be used to map large-area disturbances, satellite imagery with sufficiently high spatial (< 100 m) and temporal resolution is required to accurately map individual forest clearings and fire scars (Mantovani and Setzer, 1996; Pape and Franklin, 2008; Potapov *et al.*, 2011; De Sy *et al.*, 2012; Banskota *et al.*, 2014). Landsat satellites have been continuously collecting such data since 1972. Landsat pixels are small enough to discern the shape of small clearcuts (Figure 2-1) and have a temporal resolution that is high enough to provide cloud-free observations for most years. However, before the opening of the Landsat archive in 2008, data costs were high, the processing power of computers was more limited, and data storage was challenging. As a result of all these factors, higher spatial resolution (< 100 m) time-series change

detection was rarely used for mapping forest disturbances (Lu *et al.*, 2004; Kennedy *et al.*, 2007; Banskota *et al.*, 2014; Zhu, 2017). Landsat data becoming available for free resulted in a dramatic increase in the number of studies and publications using time-series change detection in the 2010s (Banskota *et al.*, 2014; Zhu, 2017). Nonetheless, it is worth mentioning that many routines used in time-series forest disturbance mapping today, such as curve-fitting change detection and image compositing, were first developed to process coarse resolution MODIS data (250 m – 1000 m; Luo *et al.*, 2008; Verbesselt *et al.*, 2010) and AVHRR data (1100 m; Holben, 1986; Roerink *et al.*, 2000; Bradley *et al.*, 2007).

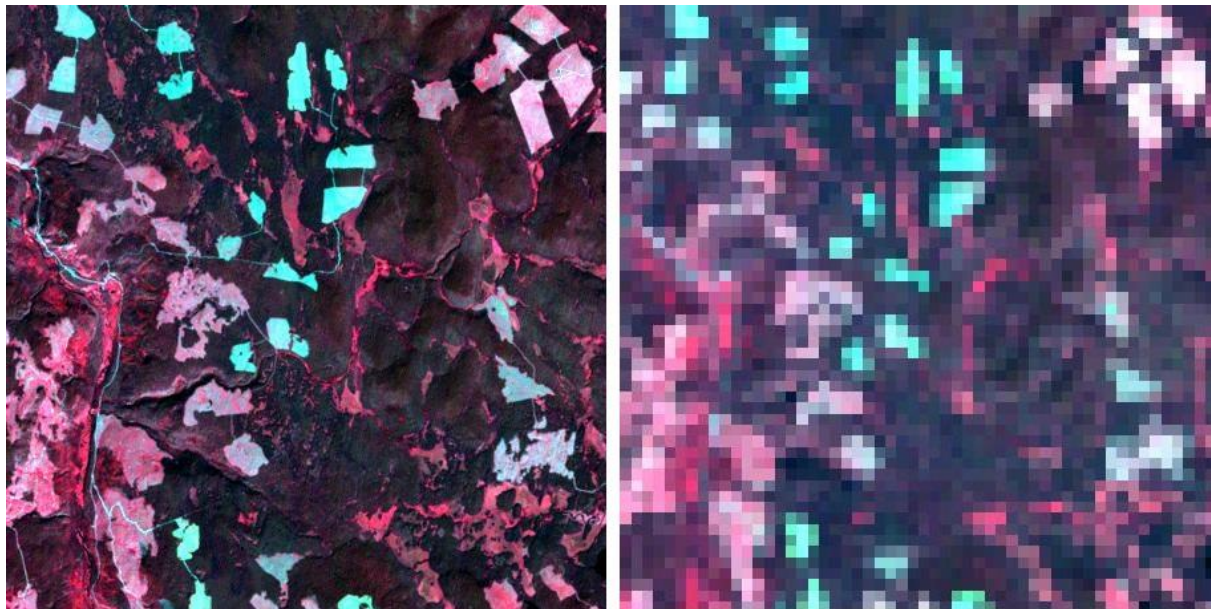


Figure 2-1. Left: a subset of a 30-m Landsat 7 ETM+ false-color (green-red-NIR) image showing a 13.5 km x 13.5 km area near Prince George, British Columbia. Right: the same subset resampled to a 250-m resolution to match the spatial resolution of the red and NIR bands of the MODIS sensor. The white and pink patches are clearcuts.

Sustainable forest harvest practices leave behind small patches of trees that require a spatial resolution that exceed what Landsat provides (i.e., smaller than 30 m) to be mapped accurately. Recently launched (2015 and 2017) Sentinel-2 sensors provide free high-quality and

high-temporal-resolution (5 days) data at spatial resolutions of 10 m and 20 m that can make this possible. One can predict that future forest disturbance studies will primarily use Sentinel-2 or even higher resolution data. High-spatial-resolution (< 10 m) satellite data typically lack SWIR bands and are still prohibitively expensive for most users when it comes to large-area time-series analysis over multiple years ($\geq \$1.2/\text{km}^2/\text{image}$; Sozzi et al., 2018). In addition, currently only large constellations of small satellites can provide such data for large areas at high temporal frequencies (Planet, 2020). Small satellites are relatively inexpensive, but they have small imaging sensors, which cannot provide the same image quality as larger sensors (Planet, 2020). Finally, forest change mapping techniques designed for medium-resolution data (from 10 m to 100 m) may not work for high-spatial-resolution (< 10 m and especially < 1 m) data. There are two main reasons: 1) such techniques require sub-pixel geometric accuracy and 2) forest stands and disturbed areas should appear relatively homogenous in the imagery for these techniques to work. Neither is typically true for very-high-resolution data. For example, 3-m PlanetScope images have a positional accuracy of 5-8 m (<https://spacedata.copernicus.eu/planetscope>). This makes it difficult to analyze a time series of pixel values, because a pixel can fall on a treetop in one image and in the shadow between trees in the next image. Therefore, change detection using very-high-resolution data requires object-based approaches to information extraction to achieve accurate results (Ferreira *et al.*, 2019).

Aerial photography has been used for high-definition forest mapping for approximately a century (e.g., Robbins, 1929; Parsons, 1930; Husch *et al.*, 2002). British Columbia's Forest Inventory is still primarily based on human interpretation of aerial photographs (color-infrared stereo-pairs) collected at a scale ranging between 1:10,000 and 1:15,000 (Bourgeois *et al.*, 2018). Approximately \$15 million (Canadian) is required to map one tenth of

the province per year using this method (Bourgeois *et al.*, 2018). However, the budget has decreased substantially since the 1990s and is now well below this number. Due to the 10-year gap between subsequent photo acquisitions, the temporal information for disturbances is collected using a reporting system. This indicates that using aerial photos for highly detailed forest mapping at a regional scale is possible, but requires additional sources of information and is very expensive.

2.1.3. Image quality

The detection of changes can be affected by numerous data quality factors, such as image noise, pixel or line/column drop-outs, geometric correction, and cloud and cloud shadow masking. Changes in pixel values caused by any of these factors can be mistakenly identified as forest change. Techniques that directly compare pixel values also require accurate atmospheric correction or data normalization to reduce the effect of atmospheric conditions on pixel values (Banskota *et al.*, 2014; Zhu, 2017).

The quality of data is limited by sensor technology. Increased sensitivity and quantization level (radiometric resolution) allow newer sensors to convert smaller number of photons to pixel values more accurately and precisely. For example, Landsat 8 OLI has 6 – 12 times higher signal-to-noise ratios, depending on the spectral band, compared to Landsat 7 ETM+ at a radiance level typical of land observations, as specified in Morfitt *et al.* (2015). Despite having narrower bands, Landsat 8 data are not only more accurate, but also more precise due to the increased radiometric resolution: Landsat 7 records 8-bit data (256 different values), while Landsat 8 pixels are 12-bit data (4096 values); Landsat MSS images are only 6 bit (64 different values). Sensors that have more spectral bands, lower signal-to-noise ratios, and higher radiometric resolutions provide more useful information that can be used to separate similar forest types and detect subtle forest disturbances.

The quality of cloud-masking and atmospheric correction has also been improving based on new algorithms (Zhu *et al.*, 2015; Qiu *et al.*, 2019a; Wulder *et al.*, 2019). These procedures are especially accurate when coupled with the additional spectral bands of newer multispectral instruments, such as the Coastal Aerosol (442.7 nm), Cirrus (945.1 nm), and Water Vapor (1373.5 nm) bands of the Sentinel-2 sensors (Qiu *et al.*, 2019b). While the quality of Landsat MSS preprocessing still leaves much to be desired at the time of writing, efforts are being made to bring it closer to the level achieved for newer Landsat sensors (Braaten *et al.*, 2015; Wulder *et al.*, 2019). This is a primary reason why relatively few studies have used Landsat MSS data in time-series forest disturbance mapping (Pflugmacher *et al.*, 2014; Vogeler *et al.*, 2018).

Snow cover can be a problem when mapping disturbances. For example, in mountainous areas, warmer years expose bare ground that is normally covered by snow in high alpine areas during the summer. Variable snow cover can also be more prevalent in the “shoulder” seasons of the spring and fall, depending on latitude and also extent of seasonal time series in a given year. Areas with variable snow cover can be misidentified as forest disturbance due to large temporal variation in the SWIR spectral reflectance (as seen in the Composite2Change map; C2C, 2019). Although most techniques reviewed in this chapter use only mid-summer data, some use all available data throughout the year (including winter). For these techniques, winter snow cover can also be a challenge, as discussed separately in Section 2.2.2.2.

Many change detection algorithms also require that agricultural areas are masked out in input data. Due to crop rotation, pixel values can change dramatically from year to year, which may result in crop fields being incorrectly identified as a forest change class (Huang *et al.*, 2010). For this reason, croplands are masked before change detection (Stueve *et al.*, 2011; Hermosilla *et*

al., 2015a), removed after change detection (Zhao *et al.*, 2018), or omitted from accuracy assessment (Hughes *et al.*, 2017).

Finally, accurate geometric correction and image-to-image co-registration are crucial for any time-series analysis. The goal of these procedures is to project multitemporal images onto the same grid so that change detection algorithms can compare the values of pixels that are most similar in their ground coverage (Fisher, 1997; Banskota *et al.*, 2014). Nowadays, orthorectification is performed by data providers using sophisticated routines, digital elevation models (DEMs), and ground control points (GCPs) (ESA, 2020; USGS, 2020b). Landsat 5 – 8 geometrically corrected products typically have a cartographic accuracy of 12 m or better (Wulder *et al.*, 2019). For Sentinel-2, the number is 12.5 m with GCPs and 20 m without (ESA, 2020), which means the geometric error can be equal or greater than the size of a pixel. The terrain correction of imagery acquired over mountainous areas is particularly difficult due to relief displacement (Itten and Meyer, 1993; Stumpf *et al.*, 2018).

Image noise and co-registration errors contribute to the “salt-and-pepper” effect (speckle) seen in many forest disturbance maps, where there are many pixels inside clearcuts and other homogeneous disturbed areas that are mislabelled as undisturbed (Hughes *et al.*, 2017). Due to variations in the spatial coverage of pixels, pixel values can change slightly from image to image. Combined with image noise and other factors (e.g., spatial resampling of data of various spatial resolution), these changes can result in algorithms producing errors (pixels labeled incorrectly as disturbed). To combat this effect, the user can set stricter thresholds, but this in turn can result in false negatives (pixels labeled incorrectly as undisturbed) in disturbed areas, especially in highly heterogeneous forest stands (e.g., old-growth and mixed stands).

2.1.4. Sun-target-sensor geometry

The spectral reflectance of an object varies depending on the illumination and viewing angles, and this variation is characterized using the Bidirectional Reflectance Distribution Function (BRDF; Nicodemus, 1965). The illumination component of the function changes in a predictable way depending on the time of year and, therefore, does not present a problem for pixel-based change detection techniques as it is either avoided by using only mid-summer data or incorporated in phenological reflectance models (Zhu and Woodcock, 2014). Scene-level techniques² that use multi-season data are more sensitive. For example, in mountainous areas, shadows cast in areas of high relief have different positions at different times of year and can be mistakenly identified as forest change (Hansen and Loveland, 2012; Banskota *et al.*, 2014). Therefore, imagery acquired over such areas may require some form of terrain illumination correction (Tan *et al.*, 2013).

The view-angle component of BRDF affects both pixel-based and scene-level techniques. Pixel-based techniques that use satellite imagery acquired from neighbouring orbital paths require BRDF correction to remove variation caused by large differences in viewing angles for pixels located within the overlap of two paths (Hansen and Loveland, 2012). Scene-level classification-based techniques may suffer from inconsistent across-track classification of pixels. One way to avoid this problem for this type of technique without BRDF correction is to use subsets

² Hereinafter, the term *scene-based* or *scene-level* refers to routines that process data in such a way that the output (e.g., class assignment) for one pixel depends on the values of other pixels in the image (e.g., the K-means classifier). Similarly, *object-based* routines are routines where the output for a pixel depends on the values of other pixels in the same object. *Object* is a spatially contiguous cluster of pixels (e.g., a group of detected change pixels representing a clearcut). Finally, *pixel-based* routines process each pixel independently (e.g., the Maximum Likelihood classifier or the LandTrendr change detection algorithm).

of images (e.g., 100 km × 100 km). However, this may not work for mountainous areas and/or off-nadir imagery, which may still require some form of correction.

BRDF effects also present an opportunity. Using BRDF information has been shown to improve forest type and species classification (Deering, 1999; Kayitakire and Defourny, 2004; Fassnachta and Koch, 2012). Consequently, such information can potentially improve the detection of subtle changes and provide useful information about forest recovery.

2.2. Types of Change Detection Techniques

There are two main types of change detection techniques. Bi-temporal techniques use image pairs: one image acquired before the disturbance event (or events) that the user wishes to map, and one after. Alternatively, time-series techniques use a large number (or “stack”) of multitemporal images (usually one or more image per year, over a series of years) to determine not only the spatial extent, but also the date of change. Because the focus of the thesis is on time-series change detection, these are considered in more detail than bi-temporal techniques in the following review.

2.2.1. Bi-temporal change detection techniques

Bi-temporal change detection techniques detect changes by comparing two images. The goal is to detect changes that occurred between the acquisition dates of the two images. Most commonly used methods are image differencing, change vector analysis, principal component analysis (PCA), and post-classification comparison.

Image differencing techniques simply subtract one image from another on a pixel by pixel basis (Hayes and Sader, 2001). In the resulting image, a pixel value close to zero indicates no change, while any significant (i.e., exceeding predefined thresholds) deviations from zero

indicate a change. For this to work, the two original images must be atmospherically corrected or normalized to each other prior to subtraction. Because one cannot subtract more than one band at a time, the most important band or spectral index (e.g., NDVI) must be selected depending on what type of change is being detected, or if multiple bands are differenced, a way to reconcile different outcomes from different bands is also needed. One advantage of this approach is that it provides some information about the direction of change (e.g., whether NDVI increased or decreased).

Change vector analysis is a similar approach that works with multiple bands by calculating the Euclidean distance between the spectrum of a pixel at time T_1 and the spectrum of the same pixel at time T_2 (Cohen and Fiorella, 1998). Both image differencing and change vector analysis are sensitive to image noise and use thresholds that are often arbitrary or based on trial and error.

In PCA-based change detection, a transform is performed on a stack of all spectral bands of the two images (Fung and LeDrew, 1987; Collins and Woodcock, 1996; Macleod and Congalton; 1998; Hayes and Sader, 2001). In PCA, the original image is transformed into principal components, where the first principal component accounts for most variance in the data, the second shows most variance unaccounted for in the first principal component, and so on. Pixels values (eigenvalues) in individual components are calculated in a similar way to tasseled cap transformation (Equation 2-3), but coefficients (eigenvectors) are calculated automatically for each image or stack of images. Major components typically account for variation in pixel values that can be explained by spectral differences among land-cover types. Because changed areas have low inter-image correlation but represent only a small portion of the study area, most of the change information is contained in the second or, sometimes, lower components (Collins and Woodcock, 1996). PCA-based change detection is far less sensitive to noise, can use all spectral bands,

typically does not require image normalization, and can even be used with multisource data (Deng *et al.*, 2008). However, the user must find the principal components that represent change and select thresholds to extract change pixels. In addition, this approach provides no information about the type or direction of change, so labeling detected changes can be difficult.

Post-classification methods compare class labels in a pair of classified images, providing a clearer understanding of the type of change (e.g., forest to clearcut or forest to agriculture) (Gregory *et al.*, 1981; El-Hattab, 2016). This includes comparing results from several images, one pair at a time. It is important to note, however, that the resulting change map typically combines the classification errors of the two images. This can often be a problem, considering that a common accuracy expectation for land cover and ecological classifications is 85% (Anderson, 1971; Foody, 2008; Congalton and Green, 2009). Accordingly, comparing two maps with an 85% accuracy may yield a change map of even lower accuracy. In addition, knowledge of the study area is required to select training data (in case of supervised classification) or label spectral classes (in case of unsupervised classification).

Bi-temporal change detection techniques are still commonly used in small local studies (e.g., Deng *et al.*, 2008; El-Hattab, 2016). These techniques are simple and easy to understand, but rely heavily on human input, as the user has to select images, training areas, and/or thresholds. Each pair of images must be cloud-free and acquired in the same season and growing stage because bi-temporal methods cannot distinguish between phenological changes and land-cover changes (DeVries *et al.*, 2015b; Zhu *et al.*, 2012). In addition, bi-temporal techniques miss many disturbances when the difference in the acquisition date between the two images they compare is larger than a few years, because disturbed areas become harder to separate spectrally from the surrounding intact forest as they regenerate (Masek *et al.* 2008; Schroeder *et al.*, 2011). For

example, Masek *et al.* (2008) found that they missed between 30% to 60% of stand-replacing disturbances (i.e., disturbances resulting in the removal of forest cover) when comparing 1990 and 2000 imagery. Schroeder *et al.* (2011) reported a similar finding, where change detection accuracies gradually decreased as the temporal gap between images increased. When the gap was 10 years, the results were not different from random.

Regional and global studies require a completely different approach. In the last decade, increased computer processing power and availability of remote sensing data have allowed the development of highly automated and flexible time-series techniques that extract information by looking through hundreds of multitemporal images. These are reviewed in the next section.

2.2.2. Time-series change detection techniques

Many time-series change detection techniques have been developed, especially in the last decade. They typically use one or more images per year, where a series of images covers a long period of time (usually a decade or longer). Most such techniques that are used in forest disturbance mapping can be grouped into three types: classification-based, trajectory-based, and hybrid.

2.2.2.1. Classification-based time-series change detection techniques

Classification-based routines either compare a series of classification maps (Knudby *et al.*, 2010) or classify entire stacks of multitemporal images at once (Schroeder *et al.*, 2011). Often, classification-based time-series change detection techniques use the same routines as bi-temporal methods. For example, Knudby *et al.* (2010) used a supervised classifier to classify every scene in a 1984 – 2009 time series (one Landsat 5 TM or Landsat 7 ETM+ image per year). A total

of 728 field observations were used to delineate training areas. The authors concluded that this approach was more time consuming and less reliable than using direct visual interpretation.

Other studies produced more encouraging results. Schroeder *et al.* (2011) used 16 growing-season Landsat 5 TM and Landsat 7 ETM+ images spanning the years from 1987 to 2008. They manually delineated training areas representing clearcuts and fire scars for every image in the time series. Training areas were also produced for persistent forest, persistent non-forest, and water classes. This was interesting as it introduced a multi-temporal component to the definition of a given class (i.e., a training pixel referred to properties spanning several image dates). Instead of classifying images separately, the authors used the training areas to classify a stack of the SWIR-1 bands from all the images in the time series with the minimum-distance-to-means classifier. The resulting forest disturbance map had an overall spatio-temporal accuracy of 93%. The main source of error was the misclassification of wetland pixels as forest disturbances and some fire scar pixels as forest harvest. Wetlands spectral characteristics may vary from year to year depending on the weather, water level, and time of vegetation flushing, which confused the algorithm.

Subpixel classification techniques like Spectral Mixture Analysis (SMA; Horwitz *et al.*, 1971) have been adapted to process time series datasets, where instead of spectral bands there are layers representing individual dates in the time series. SMA classification produces fractional images for each endmember (i.e., a pure spectrum of a thematic class), where pixel values in each image represent the fraction of the corresponding endmember. Piwowar *et al.* (1998) introduced a new approach called “Temporal Mixture Analysis” (TMA) and applied it to a stack of 12 images derived from passive microwave imagery acquired by the Nimbus-7 Scanning Multichannel Microwave Radiometer (SMMR), where each “time slice” represented monthly Arctic sea ice

concentrations averaged over a 9-year period spanning the years 1978 – 1987. They found that one non-seasonal sea ice and three seasonal sea ice endmembers could accurately characterize intra-annual changes in sea ice in most pixels. Resulting fraction images represented long-term normals. The same endmembers could then be used to produce fraction maps for individual years and find years that deviated from the normals. The work was later repeated for a longer time series (20 years) using more endmembers (nine) (Piwowar, 2008). A similar approach was also used to analyze changes in plant vigor interpreted from NDVI values in Central North America (Piwowar *et al.*, 1999). The authors concluded this method showed promise, however, to date it has received only limited attention by others.

2.2.2.2. Change detection based on temporal trajectory analysis

There are two main types of techniques that use the temporal trajectories of individual pixels to detect change: trajectory-segmentation and curve-fitting. Both approaches analyze how pixel values change over time. They extract information about forest disturbances by fitting simple models in the form of straight lines or polynomial curves to segments of the temporal profiles of individual pixels representing pre-disturbance, disturbance, and post-disturbance states. Each approach has a number of advantages and disadvantages.

Segmentation-based time series change detection techniques

Trajectory-segmentation techniques typically use yearly mid-summer imagery (Kennedy *et al.*, 2010; Hermosilla *et al.*, 2015a). Because such data are largely unaffected by seasonal reflectance fluctuations, segments in the temporal trajectories of individual pixels representing pre-disturbance, disturbance, and post-disturbance states appear as nearly straight lines. Segmentation algorithms fit straight lines to these segments, making it possible to extract information about forest change in an automated fashion. Such information as the date of change,

its magnitude, and the rate of forest recovery can be determined based on the location of vertices and the slope of regression lines.

LandTrendr (Kennedy *et al.*, 2010) is perhaps the most established segmentation-based algorithm (cited 914 times as of 2020-09-27, according to Google Scholar), and it is also available to the public through the Google Earth Engine platform. For every year between 1985 and 2007, the authors created a single mosaic from images acquired between mid-July and late August using only clear-sky pixels. Such mosaics are sometimes referred to as Best-Available-Pixel (BAP) composites (White *et al.*, 2014; Hermosilla *et al.*, 2015a). After creating BAP composites, LandTrendr identifies straight-line segments in a time series of NBR values (Figure 2-2a). The algorithm then removes vertices that are deemed to be unimportant or caused by noise (Figure 2-2b). Based on the slope of individual segments, the algorithm identifies not only abrupt events (i.e., forest disturbances), but also long-term trends (e.g., forest regrowth).

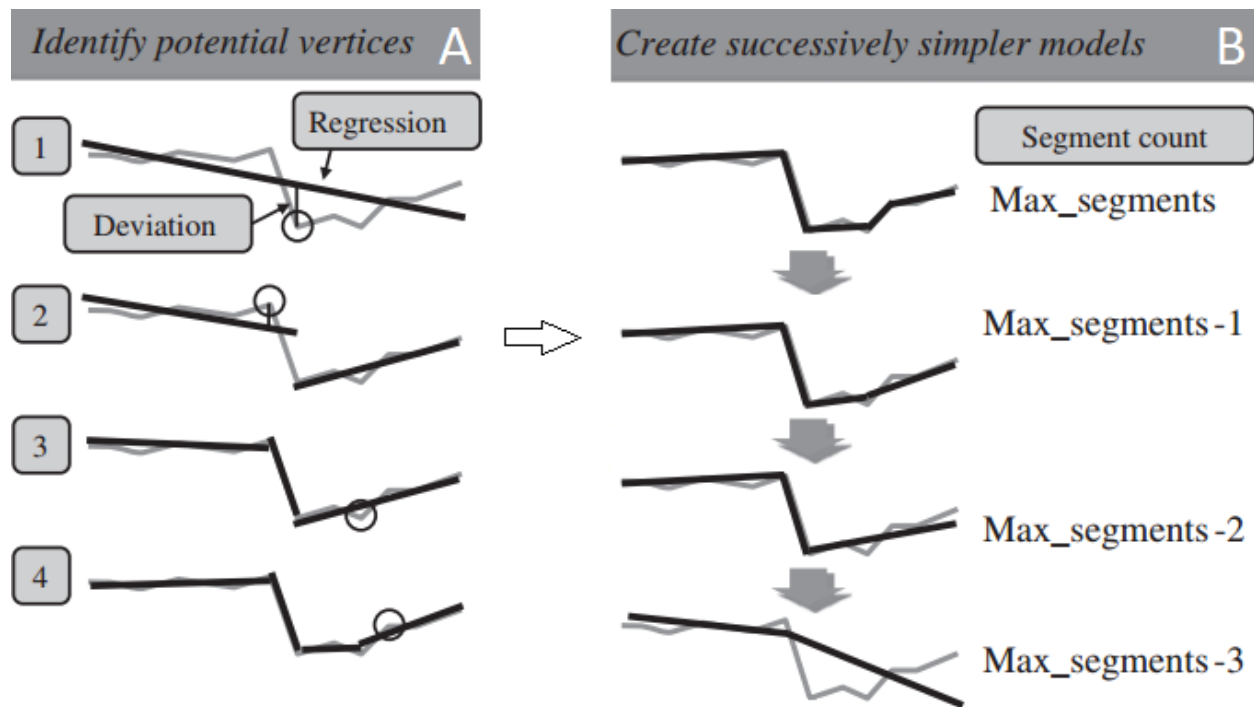


Figure 2-2. Temporal segmentation process as proposed by Kennedy *et al.* (2010). Grey lines represent yearly NBR values for a single pixel. Potential vertices are identified by fitting regression lines to the temporal trajectory of a pixel (a) and then removed one by one to produce a simple model with the best fit (b). Image modified from: Kennedy *et al.* (2010), some steps removed.

The Composite2Change (C2C; Hermosilla *et al.*, 2015a) technique also uses mid-summer image composites to avoid vertices that do not represent disturbance events (e.g., seasonal variation caused by normal phenological changes in reflectance). However, other approaches can use a wider range of dates. For example, the Detecting Breakpoints and Estimating Segments in Trend (DBEST) technique can use images acquired during any part of the year (Jamali *et al.*, 2015). It uses a procedure called Seasonal-Trend decomposition based on Loess (STL; Cleveland *et al.*, 1990; LOESS stands for LOcally Estimated Scatterplot Smoothing) to decompose temporal trajectories of pixels into “trend (low frequency variation), seasonal (variation at or near the seasonal frequency), and remainder (remaining variation) components”. Temporal segmentation is then applied only to the trend component.

LandTrendr, C2C, and DBEST all use different approaches to perform the same tasks. For example, LandTrendr and DBEST start with a single segment and gradually increase the number until the maximum number of segments, defined by the user, is reached or a good enough fit between the segments and data values is achieved (the threshold for which is also user-defined). In contrast, C2C starts with the maximum number of segments and iteratively reduces their number. All three techniques utilize different goodness-of-fit measures: C2C uses the Root-Mean-Square Error (RMSE), LandTrendr uses the F statistic, and DBEST uses the Bayesian information criterion (Schwarz, 1978).

The performance of a segmentation-based technique is highly dependent on what parameters and thresholds it employs and what values the user assigns to them. For example, the threshold that defines the maximum number of segments determines the ability to detect whether an area was affected by more than one disturbance during the study period (Hermosilla *et al.*, 2017). The ability to detect more subtle changes and the edges of disturbed areas depends on the magnitude-of-change threshold, which must be selected carefully to minimize commission and omission errors. For example, Kennedy *et al.* (2010) used aerial photos to determine what threshold values result in the best detection of forest disturbances of interest. Finally, one goodness-of-fit measure can work better than another depending on circumstances (e.g., amount of noise and temporal autocorrelation; Banskota *et al.*, 2014).

Like other pixel-based techniques, segmentation-based change detection algorithms produce maps with a noticeable “salt-and-pepper” or speckle effect (see Section 2.1.3 Image Quality). To reduce map speckle, Hughes *et al.* (2017) performed spatial segmentation on yearly mid-summer image composites of vegetation index values to identify patches of forest and other land-cover types with similar spectral characteristics. The spatial segmentation algorithm removed

local variation while preserving object edges, resulting in same-valued objects. The value assigned to all pixels inside an object was calculated using a spatial de-noising algorithm. This was followed by a pixel-based temporal segmentation. While both steps (spatial segmentation and temporal segmentation) are still univariate, the technique utilizes at least some spatial information for change detection, unlike other purely pixel-based trajectory-based techniques. The authors found that the addition of spatial segmentation resulted in a slightly more accurate detection of forest change. However, this approach has its own weaknesses. Firstly, the user must specify the parameter which controls the intensity of spatial “de-noising” and, consequently, the size of patches, which can be both difficult to determine and site-specific. Secondly, pixels on the edges of patches may produce errors as they can become associated with a different patch from one image to the next in a time series of images.

Curve-fitting time series change detection methods

One inherent weakness of segmentation-based techniques is that they completely ignore phenological information. In contrast, curve-fitting techniques use every single clear-sky observation to construct models (polynomial curves representing phenological change in spectral reflectance) that allow precise (both spatially and temporally) detection of changes with a minimal detection lag (i.e., the length of time between the actual date of occurrence and the date of acquisition for the image in which the change was detected). They have much more information available to them to distinguish different vegetation types and disturbances compared to techniques like LandTrendr and C2C, which use only mid-summer data. Seasonal data contain such information as the amplitude (difference between the summer and winter spectral reflectance), timing (e.g., of the beginning and end of the growing season), and shape (e.g., rate of green-up and

senescence) of phenology-driven changes in reflectance, which can potentially allow a more accurate detection and classification of changes (Zhu and Woodcock, 2014).

Breaks For Additive Season and Trend (BFAST) was among the first curve-fitting time-series change detection methods (Verbesselt *et al.*, 2010). It was initially used to detect forest disturbances in MODIS data. The high temporal resolution of MODIS data allowed it to automatically generate a model for each pixel that predicted normal seasonal variations in pixel values. Any lasting deviations from the modelled trends were labeled as disturbances (Figure 2-3). This approach allowed them to detect changes soon after they occurred. In comparison, segmentation-based techniques, which typically use only one image composite per year, cannot reliably detect changes for the last year in the time series (Kennedy *et al.*, 2010).

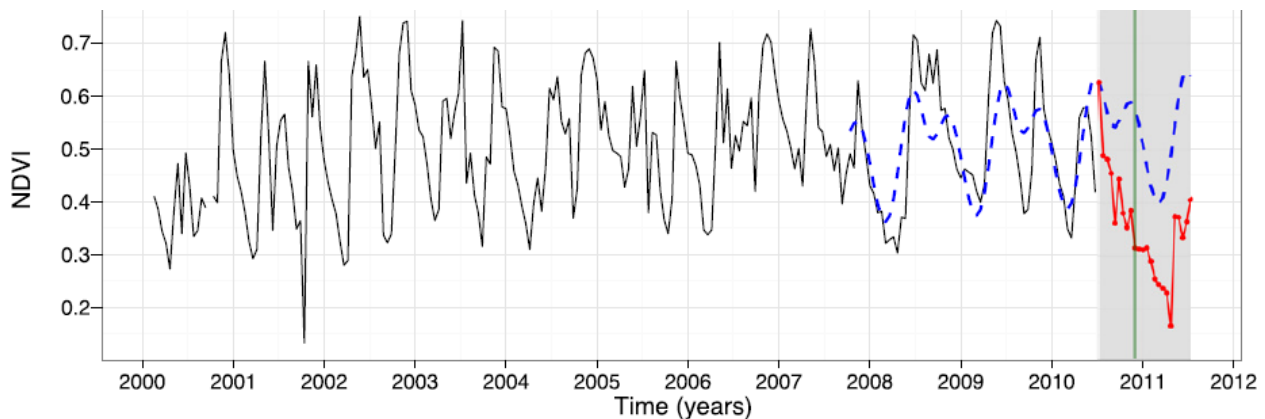


Figure 2-3. Disturbance detection using the BFAST Monitor (Source: Verbesselt *et al.*, 2012). The black line represents NDVI fluctuations before disturbance (“history period”). The blue dashed line is the model based on those normal fluctuations. The red line within the grey background (“monitoring period”) shows where data persistently deviates from the model, resulting in disturbance detection (vertical green line).

While the 250-m resolution of MODIS data is sufficient to locate most clearcuts or fire scars, it is insufficient to accurately map the spatial extent of individual disturbance events (see Section 2.1.2; Figure 2-1). Up until recently, the temporal resolution of coarse-resolution remote sensing data (e.g., AVHRR and MODIS) was superior to that of freely available moderate-

resolution Landsat data, and it was not possible to derive complex time-series models for the latter. Nonetheless, multiple studies, such as by Zhu *et al.* (2012), Zhu and Woodcock (2014), DeVries *et al.* (2015a,b), and Schultz *et al.* (2016), have shown that simple first-order harmonic models can be used to accurately detect small-area forest disturbances using Landsat data.

Newer BFAST-based techniques have evolved to provide more detailed outcomes, not just initial disturbances. DeVries *et al.* (2015b; 2016) used all available Landsat 5 TM, Landsat 7 ETM+, and Landsat 8 OLI data not only to detect initial forest disturbances, but also to monitor regrowth and repeat disturbances that followed. Another modification of the BFAST algorithm can detect permanent shifts in vegetation activity trends (de Jong *et al.*, 2013).

Continuous Change Detection and Classification (CCDC) is another notable example of a curve-fitting technique (Zhu and Woodcock, 2014). Unlike other existing BFAST-like methods that rely on a single vegetation index based on two bands, the authors used all seven Landsat spectral bands. This allowed them to detect not only forest change, but also other types of land-cover change. In addition, the technique also classified pre- and post-disturbance time-series models into land-cover types. Using all available phenological and spectral information allowed them to produce a hypertemporal map for 16 land-cover types, such as bare soil, grassland, mixed forest, deciduous forest, coniferous forest, and pasture/crops, at an overall accuracy of 90%. Reference data produced from airphoto interpretation and field visits were used for training the Random Forest classifier. However, no attempts were made to classify changes by disturbance agent (e.g., fire and harvest).

The combined temporal resolution of Landsat and Sentinel-2 sensors (less than 3 days; Gómez *et al.*, 2016; Li and Roy, 2017) is now close to that of MODIS (daily coverage). Using both Landsat and Sentinel-2 data can potentially allow curve-fitting methods to use more complex

models to achieve better results. However, the issue of spectral band dissimilarities among sensors must be addressed to make this possible. For example, Sentinel-2 and the various Landsat sensors have similar (but in some cases not corresponding) spectral band ranges, and of the bands that do correspond, their spectral response functions differ, which further affects pixel values and derived vegetation indices (Teillet and Ren, 2008; Roy *et al.*, 2016; Sulla-Menashe *et al.*, 2016). In addition, the Sentinel-2 sensors have more optical bands than Landsat sensors. Existing algorithms, for example, use either one band, or a vegetation index, sometimes within the context of index-based monitoring protocols (e.g., BFAST), or, they can use the same set of bands (e.g., CCDC) across the entire time series, however, in these and other cases, they still cannot fully utilize datasets with variable number of spectral bands across multiple sensors.

There is another limitation that can potentially affect curve-fitting change detection algorithms when mapping forest disturbances in northern countries, such as Canada. While this type of algorithms produced good results when tested on several areas in the USA (Zhu and Woodcock, 2014), large-area tests are required to determine how well they can map disturbances in northern forests. Winter snow cover can make it difficult to generate accurate models of seasonal reflectance fluctuations, which is necessary for good change detection results (Zhu and Woodcock, 2014).

Common limitations of trajectory-based techniques

Trajectory-based techniques assume that pixel values for undisturbed land cover stay the same or change in a predictable manner from year to year. However, there is always variation due to such factors as incomplete cloud and snow masking, image noise, the quality of atmospheric correction, differences in the relative spectral response functions of sensors, BRDF effects, and interannual variation in plant vigor and phenology (e.g., length of the growing season). The user

must carefully tune the parameters and thresholds of an algorithm to minimize the effects of these factors, mainly to reduce false detection. However, a threshold that is too strict can also make the algorithm less sensitive to some forest changes. Cohen *et al.* (2017) compared maps produced with seven different time-series change detection algorithms using the same Landsat dataset and found that the maps that had low commission errors had high omission errors, and vice versa.

Availability of clear-sky data can be an issue for both segmentation-based and curve-fitting time-series change detection techniques, although to a much lesser extent compared to bi-temporal techniques owing to data redundancy. These techniques use tens or hundreds of images, and if a disturbance event is not visible in one of the images due to cloud cover, it can potentially be detected in another. Segmentation-based techniques typically use only mid-summer data (Kennedy *et al.*, 2010, Hermosilla *et al.*, 2015a), which rarely provide a complete spatial coverage for each year in the time series even for areas with abundant sunshine (Hermosilla *et al.*, 2015b). The larger the temporal gap between observations, the more difficult it is for such techniques to detect change. This is due to the fact that the difference between pre- and post-disturbance pixel values quickly diminishes with time (Schroeder *et al.*, 2011). Although curve-fitting algorithms can use much more data than segmentation-based algorithms because they are not limited to the peak of the growing season, they also *need* more data to generate accurate time-series models. Therefore, clouds can present a problem for this type of techniques too, for example from 1984 – 1998, when data were available primarily from Landsat-5 only (Landsat-4 provided sporadic data during parts of this period).

Trajectory-based methods are inherently univariate. In other words, they process individual bands/indices and pixels independently. The only way for trajectory-based techniques to utilize multiple bands/indices is to combine the outputs derived from the temporal trajectories

of individual bands/indices (Zhu and Woodcock, 2014; Schultz *et al.*, 2016; Cohen *et al.*, 2018). The disadvantage of this approach is the assumption that disturbances are easily detectable in at least some of the spectral bands; i.e., the difference between the actual pixel values and predicted values exceeds the thresholds set for one or more bands. As this thesis will demonstrate, a truly multispectral technique can detect changes that have a very mild effect on individual bands but are more easily discernable when multiple bands are considered simultaneously.

2.2.2.3. Hybrid approaches

The Global Forest Change (GFC) map shows forest gain and loss for every year between 2000 and present (Hansen *et al.*, 2013). It is the first such map that has a 30-m spatial resolution and is updated yearly for all forested area on the planet and is readily available for viewing, analysis, and downloading via the Google Earth Engine platform (GFC, 2020). The map was produced using a change detection algorithm that blurs the line between classification-based and temporal trajectory analysis approaches. Various modifications of the algorithm have been developed by the authors (Hansen *et al.*, 2008; Potapov *et al.*, 2011, 2012, and 2015). The following paragraph is a brief summary of Potapov *et al.* (2015).

The core part of the GFC technique is classification-based change detection, where instead of classifying a stack of images the authors classified multitemporal metrics derived from a Landsat time series. The metrics were computed for Landsat bands 3, 4, 5, and 7, as well as for the vegetation indices NDVI and Normalized Difference Water Index (NDWI; what formulation the authors used is unclear), and include “*the first and last cloud-free observation, slope of linear regression between reflectance value and observation date, largest reflectance drop or gain between consecutive observations*”, among many others. To compute some of these metrics, as

well as to determine the date of disturbance, the technique analyzed the temporal trajectories of individual pixels. Therefore, the technique is characterized as hybrid.

To classify the metrics, the authors used a bagged decision-tree algorithm (Breiman, 1996). This is a supervised classifier that requires training data, which was manually produced using visual interpretation with a particular emphasis on edge pixels to ensure that the maps comply with the definition of forest that was used by the authors: 25% or greater canopy closure of trees taller than 5 m (Hansen *et al.*, 2013). Thus, unlike most developers of change detection techniques, the authors provided a clear definition of forest and emphasized the importance of accurate detection of boundary pixels.

2.3. Change Attribution

To better understand the impact of human activities and natural phenomena on forested ecosystems, it is important not only to detect a change, but also to determine the disturbance agent. Disturbances can be distinguished based on a number of spectral, spatial, and temporal characteristics derived from remote sensing data. For example, clearcuts cause a more dramatic change in the SWIR spectral reflectance (Schroeder *et al.*, 2011) and are more homogeneous compared to fire scars (Chu and Guo, 2014). Cutblocks are usually also much smaller than fire scars (Hermosilla *et al.*, 2015a). Low-magnitude spatially discontinuous changes can typically be characterized as due to wind or insect damage. Long-term changes with linear shapes can be considered as paved or unpaved roads.

Most classification-based techniques detect and classify changes simultaneously, as a single process. Their ability to classify changes depends on the training data or endmembers selected by the user, among other factors. In contrast, trajectory-based techniques require separate

routines to perform change attribution (Hermosilla *et al.*, 2015a; Kennedy *et al.*, 2015; DeVries *et al.*, 2016). For example, the C2C technique has an algorithm that attributes detected changes to the following four classes: fire, harvesting, road, and non-stand-replacing changes (Hermosilla *et al.*, 2015a). In the first step, the algorithm performs spatial aggregation of change pixels with the same date of occurrence and duration of event, creating “change objects”. These change objects are then classified using a Random Forest classifier based on 17 different spectral, spatial, and temporal characteristics. The spectral characteristics are based on average and standard deviation values before and after disturbance for various spectral bands and indices, the spatial characteristics are based on properties such as object area and compactness, and the temporal characteristics are based on the duration of the disturbance event. To produce training samples for the supervised classification, the authors labeled some of the detected change objects using photointerpretation. The resulting change attribution was 91.6% accurate at the object level. Kennedy *et al.* (2015) used a nearly identical approach to reach an overall accuracy of 84%, although for a different study area and set of change classes.

2.4. Forest Recovery Monitoring

The goal of forest recovery monitoring is to determine if, how fast, and in what form tree cover returns to disturbed areas. Time-series remote sensing data are well suited for this purpose as they provide a continuous, nearly half century record of satellite observations. Trajectory-based change detection techniques can be used not only to detect changes, but also to monitor the initial stages of regrowth. However, the ability to monitor forest regeneration depends on what information is available to a particular technique.

Segmentation-based techniques either use mid-summer spectral reflectance data (Kennedy *et al.*, 2010; Hermosilla *et al.*, 2015a) or generalize winter and summer data into straight-line segments devoid of seasonal information (Jamali *et al.*, 2015) to track forest recovery in individual pixels. Therefore, their ability to monitor forest recovery is limited. Pickell *et al.* (2016) compared several indices (NDVI, NBR, and tasseled cap greenness) and the SWIR-1 band of Landsat sensors and concluded that the SWIR band and NBR were more useful for monitoring forest regrowth using only mid-summer data, because indices based on shorter wavelengths saturated too quickly, before forest cover could even establish. However, even the NBR reached pre-disturbance values in disturbed boreal and sub-boreal forest stands within 20 years (White *et al.*, 2017). This occurs well before a forest reaches maturity (80 – 120 years, depending on species), and old-growth status (>140 years) (Cooper, 1983; Burton *et al.*, 1999).

Curve-fitting techniques like BFAST and CCDC, which utilize all available summer and winter data, can potentially provide much more information. Depending on the temporal density of cloud-free and snow-free observations, these procedures are able to derive such information as the amplitude and shape of seasonal changes in reflectance, the length of the growing season, and the timing of leaf emergence, peak greenness, and defoliation. This information has been used to distinguish between evergreen and deciduous stands (Huete, 2012; Zhu and Woodcock, 2014). For example, the CCDC technique can simultaneously detect changes and classifies images in the time series into land-cover types such as bare soil, mixed forest, deciduous forest, and coniferous forest (Zhu and Woodcock, 2014). First, the CCDC algorithm produces a time series model for each pixel; the coefficients of these models are then used to classify forest types.

Most existing approaches are pixel-based and, therefore, cannot measure spatial characteristics like stand composition and structure, which are critical for monitoring forest recovery from an ecological perspective (Foster *et al.*, 1998; Reyes and Kneeshaw, 2008; Chen *et al.*, 2009; Ilisson and Chen, 2009; Bartels *et al.*, 2016). A successful recovery of the ecological properties of a forest stand does not necessarily mean that every pixel inside the stand has reached its pre-disturbance reflectance value (and vice versa), because the spatial distribution of tree species in a recovered forest stand can be different from the pre-disturbance distribution. What matters is the overall stand composition, which can only be determined using an object-based method. While trajectory-based change detection techniques can use objects instead of pixels, they must average pixel values inside objects due to the univariate nature of such techniques (Hughes *et al.*, 2017), resulting in loss of crucial information.

Finally, using LiDAR technology and/or photogrammetry is the only reliable way to derive detailed information about the composition and structure of forest stands over larger areas (Goodbody *et al.*, 2017). Existing trajectory-based methods cannot use mixed data type datasets and, therefore, cannot incorporate data produced with LiDAR and photogrammetry into their processing chains. In contrast, some classification-based approaches can potentially utilize multisource data, but due to the very limited spatial and temporal coverage, the use of various data types is rarely considered except for smaller, local studies (Falkowski *et al.*, 2009; Chu and Guo, 2014).

2.5. Accuracy Assessment of Forest Change Maps

Many studies presenting new time-series forest change detection techniques report near or higher than 90% accuracies. However, these accuracies may represent best-case scenarios,

because many authors used parameters fine-tuned for a particular study area or training data available for that study area. Using the same parameters or training data outside the initial study areas may yield substantially lower accuracies. For example, Cohen *et al.* (2017) assessed forest disturbance maps produced using seven different change detection algorithms for five different areas across the United States and found that the omission errors for cutblocks and fire scars ranged between 54% and 82%.

Prior to mapping a new area, the user of a change detection algorithm must re-calibrate the algorithm's thresholds using a process called sensitivity analysis, where different threshold values are tested on one or few small areas within the study area (Kennedy *et al.*, 2010; Hermosilla *et al.*, 2015b). Because sensitivity analysis requires reference data, it can rarely be performed at a regional or national scale. Therefore, selected thresholds are not guaranteed to produce good change detection outside the test areas. Sensitivity analysis is also very time consuming as it implies numerous re-runs. The more thresholds and parameters an algorithm has, the more difficult it is to fine tune it for a particular geographical area, as every combination must be tested separately. Similarly, supervised methods may require additional or new training data when used to map a new area to properly capture its land cover type and variability.

Accuracy estimates can vary greatly depending on the reference data used. Unlike traditional land-cover maps, forest disturbance maps have a temporal component that must be examined as carefully as the spatial component. For this reason, reference data must contain temporal information (e.g., the date of disturbance). Field observations rarely provide such information because it is difficult to determine the date or at least the year of disturbance if it occurred decades ago. Therefore, to produce reference data, especially the temporal component, authors often resort to human interpretation of images from the same dataset that is fed to the

change detection algorithm (Kennedy *et al.*, 2010; Hermosilla *et al.*, 2015a, Kennedy *et al.*, 2015; Potapov *et al.*, 2015). This approach produces biased results as it simply compares the ability of an algorithm to detect change to that of a human interpreter, which itself is not error-free (e.g., visual interpretation of Landsat data to produce validation data for maps produced using the same Landsat data). Validation data produced using an independent, high-quality set of data (e.g., aerial photos, high-resolution satellite imagery, LiDAR, and field reports) can provide a more accurate estimation of the actual accuracy (Olofsson *et al.*, 2014; Zhu and Woodcock, 2014). Where available, forest inventory can be used for this purpose. For example, the Vegetation Resources Inventory (VRI) of British Columbia is produced by human analysts using high-resolution aerial photos and, more recently, LiDAR data (BC Ministry of Forests, 2019), resulting in accurate polygons representing most clearcuts that occurred in the province in the 20th and 21st century.

Because the “no change” class is disproportionately large in forest disturbance maps, commission errors can easily be overlooked. To avoid underestimation of false positives, it is important to know the weaknesses of a change detection technique when designing a validation dataset. For example, areas that are subject to high interannual variation in spectral reflectance, such as wetlands (due to variations in hydrology) and agricultural land (due to crop rotation), must be examined carefully as they can be misidentified as forest change (Huang *et al.*, 2010; Stueve *et al.*, 2011; Zhao *et al.*, 2018). In addition, particular attention must be given to boundary pixels between disturbed areas and surrounding forest, because the detection of mixed pixels is highly sensitive to the algorithm’s thresholds. A change threshold that is too high or too low can make disturbed areas appear smaller or larger in the resulting map than their actual size, which in turn leads to omission or commission errors, respectively.

Chapters 3 and 4 will discuss additional aspects related to the evaluation of forest change maps. For example, they will discuss how protected areas (e.g., provincial parks) can be used to assess false detection of forest harvest. Another example is an accuracy assessment approach focused on the temporal accuracy of forest disturbance maps. Good practices developed for the accuracy assessment of traditional bi-temporal forest change maps overlook this important aspect of time-series change detection (Olofsson *et al.*, 2014).

2.6. References

- Almeida-Filho, R., Rosenqvist, A., Shimabukuro, Y. E., & Silva-Gomez, R. (2007). Detecting deforestation with multitemporal L-band SAR imagery: A case study in western Brazilian Amazonia. *International Journal of Remote Sensing*, 28(6), 1383-1390.
- Anderson, J. R. (1971). Land-use classification schemes. *Photogrammetric Engineering*, 37: 379-387.
- Banskota, A., Kayastha, N., Falkowski, M. J., Wulder, M. A., Froese, R. E., & White, J. C. (2014). Forest monitoring using Landsat time series data: a review. *Canadian Journal of Remote Sensing*, 40(5), 362-384.
- Bartels, S. F., Chen, H. Y., Wulder, M. A., & White, J. C. (2016). Trends in post-disturbance recovery rates of Canada's forests following wildfire and harvest. *Forest Ecology and Management*, 361, 194-207.
- BC Ministry of Forests (2019). Forest Inventory Section Highlights: December 2019. The Ministry of Forests, Lands, Natural Resource Operations and Rural Development of British Columbia, Canada. https://www2.gov.bc.ca/assets/gov/farming-natural-resources-and-industry/forestry/stewardship/forest-analysis-inventory/newsletter/forest_inventory_newsletter_december_2019.pdf [Accessed on 2020-10-31].
- Bourgeois, W., Binkley, C., LeMay, V., Moss, I., & Reynolds, N. (2018). British Columbia forest inventory review panel technical background report. Prepared for the Office of the Chief Forester Division, British Columbia Ministry of Forests, Lands, Natural Resource Operations and Rural Development. https://www2.gov.bc.ca/assets/gov/farming-natural-resources-and-industry/forestry/stewardship/forest-analysis-inventory/brp_technical_document_final.pdf [Accessed 2020-10-31].
- Braaten, J. D., Cohen, W. B., & Yang, Z. (2015). Automated cloud and cloud shadow identification in Landsat MSS imagery for temperate ecosystems. *Remote Sensing of Environment*, 169, 128-138.

- Bradley, B. A., Jacob, R. W., Hermance, J. F., & Mustard, J. F. (2007). A curve fitting procedure to derive inter-annual phenologies from time series of noisy satellite NDVI data. *Remote Sensing of Environment*, 106(2), 137-145.
- Breiman, L. (1996). Bagging predictors. *Machine Learning*, 24(2), 123-140.
- Buma, B. (2012). Evaluating the utility and seasonality of NDVI values for assessing post-disturbance recovery in a subalpine forest. *Environmental Monitoring and Assessment*, 184(6), 3849-3860.
- Burton, P. J., Kneeshaw, D. D., & Coates, K. D. (1999). Managing forest harvesting to maintain old growth in boreal and sub-boreal forests. *The Forestry Chronicle*, 75(4), 623-631.
- C2C (2019). Satellite forest information for Canada: C2C map. Canadian Council of Forest Ministers. https://opendata.nfis.org/mapserver/nfis-change_eng.html [Maps downloaded on 2019-02-10].
- Chen, H. Y., Vasilias, S., Kayahara, G. J., & Ilisson, T. (2009). Wildfire promotes broadleaves and species mixture in boreal forest. *Forest Ecology and Management*, 257(1), 343-350.
- Chu, T., & Guo, X. (2014). Remote sensing techniques in monitoring post-fire effects and patterns of forest recovery in boreal forest regions: A review. *Remote Sensing*, 6(1), 470-520.
- Cleveland, R.B., Cleveland, W.S., McRae, J.E., & Terpenning, I. (1990). STL: A seasonal-trend decomposition procedure based on loess. *Journal of official statistics*, 6, 3-73.
- Cohen, W. B., & Fiorella, M. (1998). Comparison of methods for detecting conifer forest change with Thematic Mapper imagery. *Remote sensing change detection: Environmental monitoring methods and applications*, 89-102.
- Cohen, W. B., Yang, Z., Healey, S. P., Kennedy, R. E., & Gorelick, N. (2018). A LandTrendr multispectral ensemble for forest disturbance detection. *Remote Sensing of Environment*, 205, 131-140.
- Cohen, W.B., Healey, S.P., Yang, Z., Stehman, S.V., Brewer, C.K., Brooks, E.B., Gorelick, N., Huang, C., Hughes, M.J., Kennedy, R.E., & Loveland, T. R. (2017). How similar are forest disturbance maps derived from different Landsat time series algorithms? *Forests*, 8(4), 98.
- Collins, J. B., & Woodcock, C. E. (1996). An assessment of several linear change detection techniques for mapping forest mortality using multitemporal Landsat TM data. *Remote sensing of Environment*, 56(1), 66-77.
- Colwell, J. E. (1974). Vegetation canopy reflectance. *Remote sensing of environment*, 3(3), 175-183.
- Congalton, R. G., & Green, K. (2008). *Assessing the accuracy of remotely sensed data: principles and practices*. CRC press.
- Cooper, C. F. (1983). Carbon storage in managed forests. *Canadian journal of forest research*, 13(1), 155-166.

- Crist, E. P. (1985). A TM tasseled cap equivalent transformation for reflectance factor data. *Remote Sensing of Environment*, 17(3), 301-306.
- Deering, D. W. (1999). Structure analysis and classification of boreal forests using airborne hyperspectral BRDF data from ASAS. *Remote Sensing of Environment*, 69(3), 281-295.
- de Jong, R., Verbesselt, J., Zeileis, A., & Schaepman, M. E. (2013). Shifts in global vegetation activity trends. *Remote Sensing*, 5(3), 1117-1133.
- De Sy, V., Herold, M., Achard, F., Asner, G. P., Held, A., Kellndorfer, J., & Verbesselt, J. (2012). Synergies of multiple remote sensing data sources for REDD+ monitoring. *Current Opinion in Environmental Sustainability*, 4(6), 696-706.
- Deng, J. S., Wang, K., Deng, Y. H., & Qi, G. J. (2008). PCA-based land-use change detection and analysis using multitemporal and multisensor satellite data. *International Journal of Remote Sensing*, 29(16), 4823-4838.
- DeVries, B., Decuyper, M., Verbesselt, J., Zeileis, A., Herold, M., & Joseph, S. (2015a). Tracking disturbance-regrowth dynamics in tropical forests using structural change detection and Landsat time series. *Remote Sensing of Environment*, 169, 320-334.
- DeVries, B., Pratihast, A. K., Verbesselt, J., Kooistra, L., & Herold, M. (2016). Characterizing Forest change using community-based monitoring data and Landsat time series. *PloS one*, 11(3), e0147121.
- DeVries, B., Verbesselt, J., Kooistra, L., & Herold, M. (2015b). Robust monitoring of small-scale forest disturbances in a tropical montane forest using Landsat time series. *Remote Sensing of Environment*, 161, 107-121.
- Dubayah, R., Blair, J. B., Goetz, S., Fatoyinbo, L., Hansen, M., Healey, S., Hofton, M., Hurtt, G., Kellner, J., Luthcke, S., & Armston, J. (2020). The Global Ecosystem Dynamics Investigation: High-resolution laser ranging of the Earth's forests and topography. *Science of Remote Sensing*, 1, 100002.
- El-Hattab, M. M. (2016). Applying post classification change detection technique to monitor an Egyptian coastal zone (Abu Qir Bay). *The Egyptian Journal of Remote Sensing and Space Science*, 19(1), 23-36.
- ESA (2020). Sentinel-2 MSI calibration and validation: performance. European Space Agency <https://earth.esa.int/web/sentinel/technical-guides/sentinel-2-msi/performance> [Accessed on 2020-10-31].
- Falkowski, M. J., Evans, J. S., Martinuzzi, S., Gessler, P. E., & Hudak, A. T. (2009). Characterizing forest succession with lidar data: An evaluation for the Inland Northwest, USA. *Remote Sensing of Environment*, 113(5), 946-956.
- Fassnachta, F., & Koch, B. (2012). Review of forestry oriented multi-angular remote sensing techniques. *International Forestry Review*, 14(3), 285-298.

- Ferreira, M. P., Wagner, F. H., Aragão, L. E., Shimabukuro, Y. E., & de Souza Filho, C. R. (2019). Tree species classification in tropical forests using visible to shortwave infrared WorldView-3 images and texture analysis. *ISPRS journal of photogrammetry and remote sensing*, 149, 119-131.
- Fisher, P. (1997). The pixel: a snare and a delusion. *International Journal of Remote Sensing*, 18(3), 679-685.
- Foody, G. M. (2008). Harshness in image classification accuracy assessment. *International Journal of Remote Sensing*, 29(11), 3137-3158.
- Foster, D. R., Knight, D. H., & Franklin, J. F. (1998). Landscape patterns and legacies resulting from large, infrequent forest disturbances. *Ecosystems*, 1(6), 497-510.
- Fiorella, M., & Ripple, W. J. (1995). Analysis of conifer forest regeneration using Landsat Thematic Mapper data. *Photogrammetric Engineering and Remote Sensing*, 59, 1383–1388.
- Fung, T., & LeDrew, E. (1987). Application of principal components analysis to change detection. *Photogrammetric engineering and remote sensing*, 53(12), 1649-1658.
- Gao, B. C. (1996). NDWI—A normalized difference water index for remote sensing of vegetation liquid water from space. *Remote sensing of environment*, 58(3), 257-266.
- Gemmell, F. M. (1995). Effects of forest cover, terrain, and scale on timber volume estimation with Thematic Mapper data in a Rocky Mountain site. *Remote Sensing of Environment*, 51(2), 291-305.
- GFC (2020). Hansen Global Forest Change v1.7 (2000-2019). Google Earth Engine. https://developers.google.com/earth-engine/datasets/catalog/UMD_hansen_global_forest_change_2019_v1_7 [Accessed on 2020-10-31].
- Gómez, C., White, J. C., & Wulder, M. A. (2016). Optical remotely sensed time series data for land cover classification: A review. *ISPRS Journal of Photogrammetry and Remote Sensing*, 116, 55-72.
- Goodbody, T. R., Coops, N. C., Marshall, P. L., Tompalski, P., & Crawford, P. (2017). Unmanned aerial systems for precision forest inventory purposes: A review and case study. *The Forestry Chronicle*, 93(1), 71-81.
- Gregory, M. S., Walsh, S. J., & Vitek, J. (1981). Mechanics of monitoring forest clearcuts and their regeneration. *LARS Symposia*, Paper 461.
- Guo, X., Coops, N. C., Tompalski, P., Nielsen, S. E., Bater, C. W., & Stadt, J. J. (2017). Regional mapping of vegetation structure for biodiversity monitoring using airborne lidar data. *Ecological informatics*, 38, 50-61.

- Hansen, A. J., Phillips, L. B., Dubayah, R., Goetz, S., & Hofton, M. (2014). Regional-scale application of lidar: Variation in forest canopy structure across the southeastern US. *Forest Ecology and Management*, 329, 214-226.
- Hansen, M. C., & Loveland, T. R. (2012). A review of large area monitoring of land cover change using Landsat data. *Remote sensing of Environment*, 122, 66-74.
- Hansen, M. C., Potapov, P. V., Moore, R., Hancher, M., Turubanova, S., Tyukavina, A., Thau, D., Stehman, S. V., Goetz, S. K., Loveland, T. R., Kommareddy, A., Egorov, A., Chini, L., Justice, C. O., Townshend, J. R. G. (2013). High-resolution global maps of 21st-century forest cover change. *Science*, 342(6160), 850-853.
- Hansen, M.C., Egorov, A., Potapov, P.V., Stehman, S.V., Tyukavina, A., Turubanova, S.A., Roy, D.P., Goetz, S.J., Loveland, T.R., Ju, J. and Kommareddy, A. (2014). Monitoring conterminous United States (CONUS) land cover change with web-enabled Landsat data (WELD). *Remote sensing of Environment*, 140, 466-484.
- Hansen, M.C., Roy, D.P., Lindquist, E., Adusei, B., Justice, C.O., & Altstatt, A. (2008). A method for integrating MODIS and Landsat data for systematic monitoring of forest cover and change and preliminary results for Central Africa. *Remote Sensing of Environment*, 112, 2495–2513.
- Hardisky, M. A., Klemas, V., & Smart, M. (1983). The influence of soil salinity, growth form, and leaf moisture on the spectral radiance of *Spartina alterniflora* canopies. *Photogrammetric engineering and remote sensing*, 49(1), 77-83.
- Harvey, B. D., Nguyen-Xuan, T., Bergeron, Y., Gauthier, S., & Leduc, A. (2003). Forest management planning based on natural disturbance and forest dynamics. *Towards Sustainable Management of the Boreal Forest*. NRC Research Press, Ottawa, Ontario, 395-432.
- Hayes, D. J., & Sader, S. A. (2001). Comparison of change-detection techniques for monitoring tropical forest clearing and vegetation regrowth in a time series. *Photogrammetric engineering and remote sensing*, 67(9), 1067-1075.
- Healey, S. P., Cohen, W. B., Yang, Z., Brewer, C. K., Brooks, E. B., Gorelick, N., Hernandez, A. J., Huang, C., Hughes, M. J., Kennedy, R. E., and Loveland, T. R. (2018). Mapping forest change using stacked generalization: An ensemble approach. *Remote Sensing of Environment*, 204, 717-728.
- Hermosilla, T., Wulder, M. A., White, J. C., Coops, N. C., & Hobart, G. W. (2015a). Regional detection, characterization, and attribution of annual forest change from 1984 to 2012 using Landsat-derived time-series metrics. *Remote Sensing of Environment*, 170, 121-132.
- Hermosilla, T., Wulder, M. A., White, J. C., Coops, N. C., & Hobart, G. W. (2015b). An integrated Landsat time series protocol for change detection and generation of annual gap-free surface reflectance composites. *Remote Sensing of Environment*, 158, 220-234.

- Hermosilla, T., Wulder, M. A., White, J. C., Coops, N. C., & Hobart, G. W. (2017). Updating Landsat time series of surface-reflectance composites and forest change products with new observations. *International Journal of Applied Earth Observation and Geoinformation*, 63, 104-111.
- Holben, B. N. (1986). Characteristics of maximum-value composite images from temporal AVHRR data. *International Journal of Remote Sensing*, 7(11), 1417-1434.
- Horler, D. N. H., & Ahern, F. J. (1986). Forestry information content of Thematic Mapper data. *International Journal of Remote Sensing*, 7(3), 405-428.
- Horwitz, H.M., Nalepka, R.F., Hyde, P.D. and Morgenstern, J.P (1971), Estimating the proportions of objects within a single resolution element of a multispectral scanner, *Proceedings, 7th International Symposium on Remote Sensing of Environment*, ERIM, Ann Arbor MI, 2:1307- 1320.
- Huang, C., Goward, S. N., Masek, J. G., Thomas, N., Zhu, Z., & Vogelmann, J. E. (2010). An automated approach for reconstructing recent forest disturbance history using dense Landsat time series stacks. *Remote Sensing of Environment*, 114(1), 183-198.
- Huete, A. R. (2012). Vegetation indices, remote sensing and forest monitoring. *Geography Compass*, 6(9), 513-532.
- Hughes, M. J., Kaylor, S. D., & Hayes, D. J. (2017). Patch-based forest change detection from Landsat time series. *Forests*, 8(5), 166.
- Huo, L. Z., Boschetti, L., & Sparks, A. M. (2019). Object-based classification of Forest disturbance types in the conterminous United States. *Remote Sensing*, 11(5), 477.
- Husch, B., Beers, T. W., & Kershaw Jr, J. A. (2002). *Forest mensuration*. John Wiley & Sons. Chapter 13, page 431
- Hussain, M., Chen, D., Cheng, A., Wei, H., & Stanley, D. (2013). Change detection from remotely sensed images: From pixel-based to object-based approaches. *ISPRS Journal of photogrammetry and remote sensing*, 80, 91-106.
- Ilisson, T., & Chen, H. Y. (2009). Response of six boreal tree species to stand replacing fire and clearcutting. *Ecosystems*, 12(5), 820-829.
- Itten, K. I., & Meyer, P. (1993). Geometric and radiometric correction of TM data of mountainous forested areas. *IEEE Transactions on geoscience and remote sensing*, 31(4), 764-770.
- Jamali, S., Jönsson, P., Eklundh, L., Ardö, J., & Seaquist, J. (2015). Detecting changes in vegetation trends using time series segmentation. *Remote Sensing of Environment*, 156, 182-195.
- Jin, S., Yang, L., Danielson, P., Homer, C., Fry, J., & Xian, G. (2013). A comprehensive change detection method for updating the National Land Cover Database to circa 2011. *Remote Sensing of Environment*, 132, 159-175.

- Jordan, C. F. (1969). Derivation of leaf area index from quality of light on the forest floor. *Ecology*, 50(4), 663-666.
- Kayitakire, F., & Defourny, P. (2004). Forest type discrimination using multi-angle hyperspectral data. In *Proc. 2nd CHRIS/PROBA Workshop, ESA SP* (pp. 72-84).
- Kennedy, R. E., Cohen, W. B., & Schroeder, T. A. (2007). Trajectory-based change detection for automated characterization of forest disturbance dynamics. *Remote Sensing of Environment*, 110, 370 – 386.
- Kennedy, R. E., Yang, Z., & Cohen, W. B. (2010). Detecting trends in forest disturbance and recovery using yearly Landsat time series: 1. LandTrendr—Temporal segmentation algorithms. *Remote Sensing of Environment*, 114(12), 2897-2910.
- Kennedy, R. E., Yang, Z., Braaten, J., Copass, C., Antonova, N., Jordan, C., & Nelson, P. (2015). Attribution of disturbance change agent from Landsat time-series in support of habitat monitoring in the Puget Sound region, USA. *Remote Sensing of Environment*, 166, 271-285.
- Key, C. H., & Benson, N. C. (1999). Measuring and remote sensing of burn severity. In L. F. Neuenschwander, & K. C. Ryan (Eds.), *Proceedings Joint Fire Science Conference and Workshop*, vol. II (p. 284). Moscow, ID: University of Idaho and International Association of Wildland Fire.
- Knudby, A., Newman, C., Shaghude, Y., & Muhando, C. (2010). Simple and effective monitoring of historic changes in nearshore environments using the free archive of Landsat imagery. *International Journal of Applied Earth Observation and Geoinformation*, 12, S116-S122.
- Leberl, F. W. (1990). *Radargrammetric Image Processing*. Norwood: Artech House, 595 p.
- Lehmann, E. A., Wallace, J. F., Caccetta, P. A., Furby, S. L., & Zdunic, K. (2013). Forest cover trends from time series Landsat data for the Australian continent. *International Journal of Applied Earth Observation and Geoinformation*, 21, 453-462.
- Li, J., & Roy, D. P. (2017). A global analysis of Sentinel-2A, Sentinel-2B and Landsat-8 data revisit intervals and implications for terrestrial monitoring. *Remote Sensing*, 9(9), 902.
- Lu, D., Mausel, P., Brondizio, E., & Moran, E. (2004). Change detection techniques. *International journal of remote sensing*, 25(12), 2365-2401.
- Lucas, R., Armston, J., Fairfax, R., Fensham, R., Accad, A., Carreiras, J., ... & Metcalfe, D. (2010). An evaluation of the ALOS PALSAR L-band backscatter—Above ground biomass relationship Queensland, Australia: Impacts of surface moisture condition and vegetation structure. *IEEE Journal of Selected Topics in Applied Earth Observations and Remote Sensing*, 3(4), 576-593.
- Luckman, A., Baker, J., Kuplich, T. M., Yanasse, C. D. C. F., & Frery, A. C. (1997). A study of the relationship between radar backscatter and regenerating tropical forest biomass for spaceborne SAR instruments. *Remote Sensing of Environment*, 60(1), 1-13.

- Lunetta, R. S., Knight, J. F., Ediriwickrema, J., Lyon, J. G., & Worthy, L. D. (2006). Land-cover change detection using multi-temporal MODIS NDVI data. *Remote Sensing of Environment*, 105(2), 142-154.
- Luo, Y., Trishchenko, A. P., & Khlopenkov, K. V. (2008). Developing clear-sky, cloud and cloud shadow mask for producing clear-sky composites at 250-meter spatial resolution for the seven MODIS land bands over Canada and North America. *Remote Sensing of Environment*, 112(12), 4167-4185.
- Macleod, R. D., & Congalton, R. G. (1998). A quantitative comparison of change-detection algorithms for monitoring eelgrass from remotely sensed data. *Photogrammetric Engineering and Remote Sensing*, 64(3), 207-216.
- Mantovani, A. D. M., & Setzer, A. W. (1996). A Change Detection Methodology for the Amazon Forest Using Multitemporal NOAA/AVHRR Data and GIS—Preliminary Results. In *Remote Sensing and GIS for Site Characterization: Applications and Standards*. ASTM International.
- Masek, J. G., Huang, C., Wolfe, R., Cohen, W., Hall, F., Kutler, J., & Nelson, P. (2008). North American forest disturbance mapped from a decadal Landsat record. *Remote Sensing of Environment*, 112(6), 2914-2926.
- Mitchell, A. L., Rosenqvist, A., & Mora, B. (2017). Current remote sensing approaches to monitoring forest degradation in support of countries measurement, reporting and verification (MRV) systems for REDD+. *Carbon Balance and Management*, 12(1), 9.
- Nicodemus, F. E. (1965). Directional reflectance and emissivity of an opaque surface. *Applied Optics*, 4(7), 767-775.
- Olofsson, P., Foody, G. M., Herold, M., Stehman, S. V., Woodcock, C. E., & Wulder, M. A. (2014). Good practices for estimating area and assessing accuracy of land change. *Remote Sensing of Environment*, 148, 42–57.
- Pape, A. D., & Franklin, S. E. (2008). MODIS-based change detection for Grizzly Bear habitat mapping in Alberta. *Photogrammetric Engineering and Remote Sensing*, 74(8), 973-985.
- Parsons, H. H. (1930). Aerial forest surveying. *The Forestry Chronicle*, 6(1), 56-60.
- Peddle, D.R., 2011. Partial-blind model inversion of mountain forest structure from MODIS imagery. *International Journal of Remote Sensing*. 32(22):7087-7096. doi:10.1080/01431161.2011.620033
- Peddle, D. R., Huemmrich, K. F., Hall, F. G., Masek, J. G., Soenen, S. A., & Jackson, C. D. (2011). Applications of the BIOPHYS algorithm for physically-based retrieval of biophysical, structural and forest disturbance information. *IEEE Journal of Selected Topics in Applied Earth Observations and Remote Sensing (IEEE J-STARS)*. 4(4):971-982. DOI: 10.1109/JSTARS.2011.2164899

- Pflugmacher, D., Cohen, W. B., Kennedy, R. E., & Yang, Z. (2014). Using Landsat-derived disturbance and recovery history and lidar to map forest biomass dynamics. *Remote Sensing of Environment*, 151, 124-137.
- Pickell, P. D., Hermosilla, T., Frazier, R. J., Coops, N. C., & Wulder, M. A. (2016). Forest recovery trends derived from Landsat time series for North American boreal forests. *International Journal of Remote Sensing*, 37(1), 138-149.
- Piowar, J. M. (2008). The derivation of an Arctic sea ice normal through temporal mixture analysis of satellite imagery. *International Journal of Applied Earth Observation and Geoinformation*, 10(1), 92-108.
- Piowar, J. M., Peddle, D. R., & Davidson, D. P. (1999). Assessing annual forest ecological change in western Canada using temporal mixture analysis of regional scale AVHRR imagery over a 14 year period. In, *Proceedings of the 4th International Airborne Remote Sensing Conference and Exhibition, /21st Canadian Symposium on Remote Sensing, Ottawa, Canada.*
- Piowar, J. M., Peddle, D. R., & LeDrew, E. F. (1998). Temporal mixture analysis of Arctic sea ice imagery: a new approach for monitoring environmental change. *Remote Sensing of Environment*, 63(3), 195-207.
- Planet (2020). Planet imagery product specification: Planetscope & RapidEye. Planet Labs, Inc. https://www.planet.com/products/satellite-imagery/files/1610.06_Spec%20Sheet_Combined_Imagery_Product_Letter_ENGv1.pdf [Accessed on 2020-10-31].
- Potapov, P. V., Turubanova, S. A., Tyukavina, A., Krylov, A. M., McCarty, J. L., Radeloff, V. C., & Hansen, M. C. (2015). Eastern Europe's forest cover dynamics from 1985 to 2012 quantified from the full Landsat archive. *Remote Sensing of Environment*, 159, 28-43.
- Potapov, P., Turubanova, S., & Hansen, M. C. (2011). Regional-scale boreal forest cover and change mapping using Landsat data composites for European Russia. *Remote Sensing of Environment*, 115(2), 548-561.
- Potapov, P., Turubanova, S., & Hansen, M. C. (2011). Regional-scale boreal forest cover and change mapping using Landsat data composites for European Russia. *Remote Sensing of Environment*, 115(2), 548-561.
- Potapov, P.V., Turubanova, S.A., Hansen, M.C., Adusei, B., Broich, M., Altstatt, A., Mane, L., & Justice, C.O. (2012). Quantifying forest cover loss in Democratic Republic of the Congo, 2000–2010, with Landsat ETM+ data. *Remote Sensing of Environment*, 122, 106–116.
- Stueve, K. M., Housman, I. W., Zimmerman, P. L., Nelson, M. D., Webb, J. B., Perry, C. H., Chastain, R. A., Gormanson, D. D., Huang, C., Healey, S. P. & Cohen, W. B. (2011). Snow-covered Landsat time series stacks improve automated disturbance mapping accuracy in forested landscapes. *Remote Sensing of Environment*, 115(12), 3203-3219.

- Qiu, S., Lin, Y., Shang, R., Zhang, J., Ma, L., & Zhu, Z. (2019a). Making Landsat Time Series Consistent: Evaluating and Improving Landsat Analysis Ready Data. *Remote Sensing*, 11(1), 51.
- Qiu, S., Zhu, Z., & He, B. (2019b). Fmask 4.0: Improved cloud and cloud shadow detection in Landsats 4–8 and Sentinel-2 imagery. *Remote Sensing of Environment*, 231, 111205.
- Quegan, S., & Yu, J. J. (2001). Filtering of multichannel SAR images. *IEEE Transactions on Geoscience and Remote Sensing*, 39(11), 2373-2379.
- Reiche, J., Hamunyela, E., Verbesselt, J., Hoekman, D., & Herold, M. (2018). Improving near-real time deforestation monitoring in tropical dry forests by combining dense Sentinel-1 time series with Landsat and ALOS-2 PALSAR-2. *Remote Sensing of Environment*, 204, 147-161.
- Reiche, J., Verbesselt, J., Hoekman, D., & Herold, M. (2015). Fusing Landsat and SAR time series to detect deforestation in the tropics. *Remote Sensing of Environment*, 156, 276-293.
- Reyes, G. P., & Kneeshaw, D. (2008). Moderate-severity disturbance dynamics in *Abies balsamea*–*Betula* spp. forests: the relative importance of disturbance type and local stand and site characteristics on woody vegetation response. *Ecoscience*, 15(2), 241-249.
- Ribbes, F., Le Toan, T. L., Bruniquel, J., Floury, N., Stussi, N., Liew, S. C., & Wasrin, U. R. (1997, August). Deforestation monitoring in tropical regions using multitemporal ERS/JERS SAR and INSAR data. In *IGARSS'97. 1997 IEEE International Geoscience and Remote Sensing Symposium Proceedings. Remote Sensing-A Scientific Vision for Sustainable Development* (Vol. 4, pp. 1560-1562). IEEE.
- Rignot, E., Salas, W. A., & Skole, D. L. (1997). Mapping deforestation and secondary growth in Rondonia, Brazil, using imaging radar and thematic mapper data. *Remote Sensing of Environment*, 59(2), 167-179.
- Robbins, C. R. (1929). Air survey and forestry. *Empire Forestry Journal*, 8(2), 205-228.
- Roerink, G. J., Menenti, M., & Verhoef, W. (2000). Reconstructing cloudfree NDVI composites using Fourier analysis of time series. *International Journal of Remote Sensing*, 21(9), 1911-1917.
- Roy, D. P., Kovalskyy, V., Zhang, H. K., Vermote, E. F., Yan, L., Kumar, S. S., & Egorov, A. (2016). Characterization of Landsat-7 to Landsat-8 reflective wavelength and normalized difference vegetation index continuity. *Remote Sensing of Environment*, 185, 57–70.
- Schroeder, T. A., Wulder, M. A., Healey, S. P., & Moisen, G. G. (2011). Mapping wildfire and clearcut harvest disturbances in boreal forests with Landsat time series data. *Remote Sensing of Environment*, 115(6), 1421-1433.
- Schultz, M., Clevers, J. G., Carter, S., Verbesselt, J., Avitabile, V., Quang, H. V., & Herold, M. (2016). Performance of vegetation indices from Landsat time series in deforestation monitoring. *International Journal of Applied Earth Observation and Geoinformation*, 52, 318-327.

- Schwarz, Gideon E. (1978). Estimating the dimension of a model. *Annals of Statistics* 6 (2): 981-461-464.
- Sellers, P. J., Berry, J. A., Collatz, G. J., Field, C. B., & Hall, F. G. (1992). Canopy reflectance, photosynthesis, and transpiration. III. A reanalysis using improved leaf models and a new canopy integration scheme. *Remote sensing of environment*, 42(3), 187-216.
- Sozzi, M., Marinello, F., Pezzuolo, A., & Sartori, L. (2018, July). Benchmark of satellites image services for precision agricultural use. In Proceedings of the AgEng Conference, Wageningen, The Netherlands (pp. 8-11).
- Steiner, D., & Gutermann, T. (1966), Russian data on spectral reflectance of vegetation, soil and rock types. *Technical Report AD815418*, University of Zurich, Department of Geography, Switzerland.
- Stueve, K.M., Housman, I.W., Zimmerman, P.L., Nelson, M.D., Webb, J.B., Perry, C.H., Chastain, R.A., Gormanson, D.D., Huang, C., Healey, S.P. and Cohen, W.B. (2011). Snow-covered Landsat time series stacks improve automated disturbance mapping accuracy in forested landscapes. *Remote Sensing of Environment*, 115(12), 3203-3219.
- Stumpf, A., Michéa, D., & Malet, J. P. (2018). Improved co-registration of Sentinel-2 and Landsat-8 imagery for earth surface motion measurements. *Remote Sensing*, 10(2), 160.
- Sulla-Menashe, D., Friedl, M. A., & Woodcock, C. E. (2016). Sources of bias and variability in long-term Landsat time series over Canadian boreal forests. *Remote Sensing of Environment*, 177, 206-219.
- Tan, B., Masek, J. G., Wolfe, R., Gao, F., Huang, C., Vermote, E. F., Sexton, J. O., & Ederer, G. (2013). Improved forest change detection with terrain illumination corrected Landsat images. *Remote Sensing of Environment*, 136, pp.469-483.
- Teillet, P. M., & Ren, X. (2008). Spectral band difference effects on vegetation indices derived from multiple satellite sensor data. *Canadian Journal of Remote Sensing*, 34(3), 159-173.
- Trouvé, E., Chambenoit, Y., Classeau, N., & Bolon, P. (2003). Statistical and operational performance assessment of multitemporal SAR image filtering. *IEEE Transactions on Geoscience and Remote Sensing*, 41(11), 2519-2530.
- Tucker, C. J. (1979). Red and photographic infrared linear combinations for monitoring vegetation. *Remote Sensing of Environment*, 8(2), 127-150.
- USGS (2020a). What are the best Landsat spectral bands for use in my research? United States Geological Survey. https://www.usgs.gov/faqs/what-are-best-landsat-spectral-bands-use-my-research?qt-news_science_products=0#qt-news_science_products [Accessed on 2020-10-31].
- USGS (2020b). Landsat levels of processing. United States Geological Survey. <https://www.usgs.gov/land-resources/nli/landsat/landsat-levels-processing> [Accessed on 2020-10-31].

- van der Sanden, J. J., & Hoekmen, D. H. (1999). Potential of Airborne Radar to Support the Assessment of Land Cover in a Tropical Rain Forest Environment. *Remote Sensing of Environment*, 68: 26-40.
- Verbesselt, J., Hyndman, R., Newnham, G., & Culvenor, D. (2010). Detecting trend and seasonal changes in satellite image time series. *Remote Sensing of Environment*, 114(1), 106-115.
- Verbesselt, J., Zeileis, A., & Herold, M. (2012). Near real-time disturbance detection using satellite image time series. *Remote Sensing of Environment*, 123, 98-108.
- Vogeler, J. C., Braaten, J. D., Slesak, R. A., & Falkowski, M. J. (2018). Extracting the full value of the Landsat archive: Inter-sensor harmonization for the mapping of Minnesota forest canopy cover (1973–2015). *Remote Sensing of Environment*, 209, 363-374.
- Wang, Y., Kasischke, E. S., Melack, J. M., Davis, F. W., & Christensen Jr, N. L. (1994). The effects of changes in loblolly pine biomass and soil moisture on ERS-1 SAR backscatter. *Remote Sensing of Environment*, 49(1), 25-31.
- White, J. C., Coops, N. C., Wulder, M. A., Vastaranta, M., Hilker, T., & Tompalski, P. (2016). Remote sensing technologies for enhancing forest inventories: A review. *Canadian Journal of Remote Sensing*, 42(5), 619-641.
- White, J. C., Wulder, M. A., Hobart, G. W., Luther, J. E., Hermosilla, T., Griffiths, P., Coops, N. C., Hall, R. J., Hostert, P., Dyk, A., & Guindon, L. (2014). Pixel-based image compositing for large-area dense time series applications and science. *Canadian Journal of Remote Sensing*, 40(3), 192-212.
- White, J. C., Wulder, M. A., Hermosilla, T., Coops, N. C., & Hobart, G. W. (2017). A nationwide annual characterization of 25 years of forest disturbance and recovery for Canada using Landsat time series. *Remote Sensing of Environment*, 194, 303-321.
- Wulder, M. A., Coops, N. C., Hudak, A. T., Morsdorf, F., Nelson, R., Newnham, G., & Vastaranta, M. (2013). Status and prospects for LiDAR remote sensing of forested ecosystems. *Canadian Journal of Remote Sensing*, 39(sup1), S1-S5.
- Wulder, M.A., Loveland, T.R., Roy, D.P., Crawford, C.J., Masek, J.G., Woodcock, C.E., Allen, R.G., Anderson, M.C., Belward, A.S., Cohen, W.B. & Dwyer, J. (2019). Current status of Landsat program, science, and applications. *Remote Sensing of Environment*, 225, 127-147.
- Xue, J., & Su, B. (2017). Significant remote sensing vegetation indices: A review of developments and applications. *Journal of Sensors*, 2017.
- Zhao, F., Huang, C., Goward, S.N., Schleeweis, K., Rishmawi, K., Lindsey, M.A., Denning, E., Keddell, L., Cohen, W.B., Yang, Z. & Dungan, J.L. (2018). Development of Landsat-based annual US forest disturbance history maps (1986–2010) in support of the North American Carbon Program (NACP). *Remote Sensing of Environment*, 209, 312-326.

- Zhu, Z. (2017). Change detection using landsat time series: A review of frequencies, preprocessing, algorithms, and applications. *ISPRS Journal of Photogrammetry and Remote Sensing*, 130, 370-384.
- Zhu, Z., & C. E. Woodcock (2014). Continuous Change Detection and Classification of Land Cover Using All Available Landsat Data, *Remote Sensing of Environment*, (144):152-171.
- Zhu, Z., Wang, S., & Woodcock, C. E. (2015). Improvement and expansion of the Fmask algorithm: Cloud, cloud shadow, and snow detection for Landsats 4–7, 8, and Sentinel 2 images. *Remote Sensing of Environment*, 159, 269-277.
- Zhu, Z., Woodcock, C. E., & Olofsson, P. (2012). Continuous monitoring of forest disturbance using all available Landsat imagery. *Remote Sensing of Environment*, 122, 75-91.

CHAPTER 3

**A CLASSIFICATION-BASED TIME SERIES CHANGE DETECTION TECHNIQUE
FOR MAPPING STAND-REPLACING FOREST DISTURBANCES USING MULTI-
SENSOR REMOTE SENSING DATA**

Abstract

Unsupervised Classification to Change (UC-Change) is a new approach developed to address key limitations of existing time-series change detection techniques. Instead of using temporal trajectories of individual pixels (reflectance or spectral index values), UC-Change analyzes changes in the spatial distribution of spectral classes over time. Unlike existing classification-based methods, the new technique does not require training data and can process dense and lengthy time-series and multi-sensor data with minimal user input.

The algorithm is described in full, and tested using a dataset containing 268 Landsat and Sentinel-2 images acquired over a forested area south of Prince George, British Columbia, Canada throughout a 47-year period (1972 to 2019). The 100 km × 100 km study site has been actively harvested in recent decades and experienced many wildfires and a mountain pine beetle (MPB) outbreak. The spatio-temporal accuracy of clearcut and fire scar detection was assessed using the Vegetation Resources Inventory (VRI) and National Burned Area Composite (NBAC) products, respectively, and compared against the Canadian Forest Service's Composite2Change 1984 – 2015 (C2C) and Hansen's Global Forest Change 2000 – 2019 (GFC) maps, as well as a map produced using an open-source version of the LandTrendr algorithm (1984 – 2019). The UC-Change algorithm detected 85.4% of the reference VRI 1974-2017 cutblock pixels at a temporal resolution of ±1 year (90.4% at ±3 years). It detected 86.6% of 1985 – 2015 VRI pixels,

compared to 46.1% and 46.8% in case of C2C and LandTrendr, respectively. For the period 2000 – 2019, UC-Change mapped 87.6% of the reference cutblock pixels, much more than LandTrendr (34.1%) and GFC (70.7). It also detected 23.6%, 19.2%, and 19.9% more reference forest fire pixels than the LandTrendr, C2C, and GFC approaches, respectively.

The UC-Change algorithm does not require atmospheric correction or any other preprocessing, except for image-to-image spatial co-registration and topographic correction in mountainous areas. It also performed much better than the other methods at detecting forest harvest and fire scars in areas heavily affected by the MPB outbreak. The potential of using the technique to measure forest recovery was tested and compared with a commonly used pixel-based method that uses temporal trajectories of spectral-index values in individual pixels. The new object-based metrics from UC-Change showed various rates of recovery depending on forest type (e.g. pine stands recovered faster than spruce stands), which was not the case for the pixel-based method using the Normalized Burn Ratio (NBR), and took longer to saturate.

3.1. Introduction

The goal of forest disturbance mapping is to determine how (e.g., fire, logging, and insect infestation), where (location and boundary of disturbed forest), and when changes in forest cover occurred, as well as to provide information on the temporal dynamics of such changes. Only time-series change detection techniques, which use large (tens or hundreds of images), temporally continuous (typically one or more images per year) sets of satellite data, can answer all of these questions in a timely fashion and over large areas. Many researchers, such as Hansen and Loveland (2012) and Banskota *et al.* (2014), predicted that automated time-series algorithms would largely replace traditional bi-temporal (i.e., comparing image pairs) and multitemporal (i.e., comparing

several images) techniques as they provide a deeper understanding of forest changes and trends and can be used to map large areas.

While coarser spatial resolution (>100 m) data can be used to map large-area disturbances, satellite imagery with sufficiently high spatial (<100 m) and temporal resolution is required to accurately map individual cutblocks and fire scars (Mantovani and Setzer, 1996; Pape and Franklin, 2008; Potapov *et al.*, 2011; De Sy *et al.*, 2012; Banskota *et al.*, 2014). Landsat satellites have been continuously collecting such data since 1972. Landsat pixels are small enough to discern the shape of small clearcuts (10 – 20 ha) and have a temporal resolution that is high enough to provide cloud-free observations for most years. However, due to the high cost of data and limited processing power of computers, high-resolution (<100 m) time-series change detection had rarely been used for mapping forest disturbances before the opening of the Landsat archive in 2008 (Lu *et al.*, 2004; Kennedy *et al.*, 2007; Banskota *et al.*, 2014; Zhu, 2017). Free Landsat data resulted in a dramatic increase in the number of publications on time-series change detection in the 2010s (Figure 3-1). This period also corresponded with considerable improvements in computing power and storage capacity options that further contributed to processing these larger datasets.

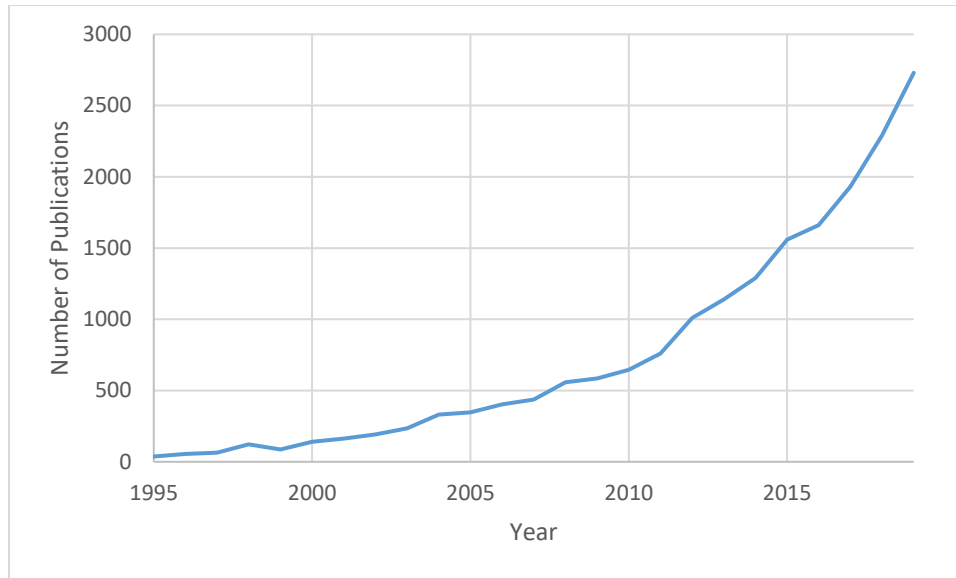


Figure 3-1. Number of Google Scholar returns for "change detection", "Landsat", and "time series".

Time-series change detection techniques can be classified based on the types of disturbances they detect and how they detect them. There are three types of forest disturbances: stand-replacing, partial, and gradual. The first causes a complete removal or mortality of trees in the area, whereas the latter two cause either the death of only some trees or slow degradation of a forested area. Few techniques detect all three types, although most can detect stand-replacing disturbances. When using a change detection map, one must understand what types of changes it shows and what definition of forest it follows. Different countries and disturbance mapping techniques use different definitions of forest, ranging in canopy cover and height and, sometimes, stand area. For example, the Global Forest Change (GFC) map follows two criteria: 25% or greater canopy closure, for trees taller than 5 m (Hansen *et al.*, 2013). Canada, on the other hand, uses the forest definition from the Food and Agriculture Organization of the United Nations: >0.5 ha area, >10% canopy cover, and >5 m height (NRCan, 2020a). The definition of forest used in this study

includes any area where timber can or could be (if the area was not protected) harvested commercially (i.e., any area where cutblocks can occur).

There are three main approaches to time-series change detection: classification-based, trajectory-based, and hybrid. Classification-based routines either compare a series of classification maps (Knudby *et al.*, 2010) or classify entire stacks of multitemporal images together (Schroeder *et al.*, 2011). For example, Schroeder *et al.* (2011) used 16 growing-season Landsat 5 TM and Landsat 7 ETM+ images from 1987 to 2008. They manually delineated training areas representing clearcuts and fire scars for every image in the time series. Training areas were also produced for persistent forest, persistent non-forest, and water classes. The resulting forest disturbance map had an overall spatio-temporal accuracy of 93%. Techniques like this can be very flexible as they can potentially use auxiliary information and data acquired during any part of the growing season, any number of spectral bands, sensors, and data types without atmospheric correction or data normalization. However, they typically require a considerable amount of user input and are not practical for larger time series or areas.

Trajectory-based change detection is a more popular approach because it is more automated and can be used to not only detect forest disturbances, but also monitor post-disturbance recovery (Kennedy *et al.*, 2010; Zhu and Woodcock, 2014; Hermosilla *et al.*, 2015a). This approach analyzes how pixel values change over time. Trajectory-based techniques extract information about forest disturbances by fitting simple models in the form of straight lines or polynomial curves to segments of the temporal profiles of individual pixels representing pre-disturbance, disturbance, and post-disturbance states.

LandTrendr (Kennedy *et al.*, 2010) is one of the most established trajectory-based algorithms (cited 914 times as of 2020-09-27, according to Google Scholar), and it is also available

to the public through the Google Earth Engine platform (Kennedy *et al.*, 2018). For every year in the time series, the algorithm creates a single mosaic from a number of midsummer images using only clear-sky pixels. Such mosaics are sometimes referred to as Best-Available-Pixel (BAP) composites (White *et al.*, 2014; Hermosilla *et al.*, 2015a; Chowdhury *et al.*, 2021). After creating BAP composites, LandTrendr identifies straight-line segments in a time series of normalized pixel values. The algorithm then removes vertices that are deemed to be unimportant or caused by noise. Based on the slope of individual segments, the algorithm identifies not only abrupt events (i.e., forest disturbances), but also long-term trends (e.g., forest regrowth). An example of such segmentation is presented in Figure 3-2, where LandTrendr identified four segments in a time series of Normalized Burned Ratio (NBR) values. NBR is a spectral index calculated using the following equation (Key and Benson, 2006):

$$\text{NBR} = \frac{\text{NIR} - \text{SWIR2}}{\text{NIR} + \text{SWIR2}}, \quad (3-1)$$

where NIR and SWIR2 are spectral reflectance values for the corresponding near-infrared and shortwave infrared Landsat spectral bands. This index was initially found to be sensitive to burn severity (Key and Benson, 1999) but has since been widely adopted for mapping other forest disturbances (Huang *et al.*, 2010; Hermosilla *et al.*, 2015b; Hughes *et al.*, 2017).

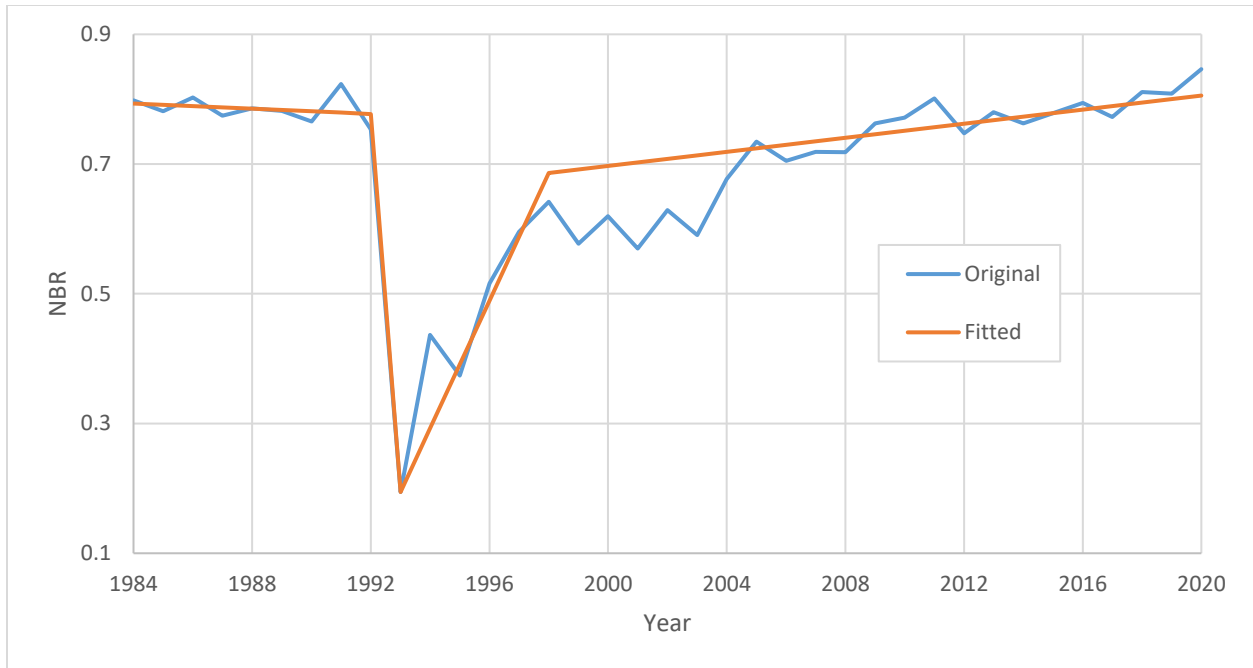


Figure 3-2. Original NBR values (blue) and LandTrendr segmentation results (orange) for a pixel in a 1993 clearcut in Oregon, USA. Parameters best suited for the area were used to produce this segmentation (Kennedy *et al.*, 2018).

Composite2Change (C2C) is another technique based on temporal trajectory analysis (Hermosilla *et al.*, 2015b; White *et al.*, 2017) that will also be used for comparison in this study. It follows the same approach as LandTrendr with a few minor differences. For example, LandTrendr starts with a single segment and gradually increases the number until a maximum number of segments, defined by the user, is reached or a good enough fit between the segments and data values is achieved (the threshold for which is also user-defined). In contrast, C2C starts with the maximum number of segments and iteratively reduces their number. Both algorithms have change-attribution extensions that classify detected disturbances into harvest, fire, and other classes (Hermosilla *et al.*, 2015a; Kennedy *et al.*, 2015).

The GFC map, produced using a hybrid approach, shows forest gain and loss for every year between 2000 and present (Hansen *et al.*, 2013). It is the only forest change map that has a

30 m spatial resolution and is updated yearly for the entire planet (GFC, 2020). The GFC change detection algorithm blurs the line between classification-based and temporal trajectory analysis approaches. Various modifications of the algorithm have been developed by the researchers (Hansen *et al.*, 2008; Potapov *et al.*, 2011, 2012, and 2015). The following paragraph is a brief summary of the publication by Potapov *et al* (2015).

The core part of the GFC technique is classification-based change detection, but instead of classifying a stack of images, the authors classified a diverse set of multitemporal metrics derived from a Landsat time series (e.g., the slope of linear regression between reflectance value and observation date). To compute some of these metrics, as well as to determine the date of disturbance, the technique analyzed the temporal trajectories of individual pixels. Therefore, the technique can be characterized as hybrid. This approach has the advantages of post-classification and pixel-based methods; however, it also has disadvantages such as requiring training data, atmospheric correction and/or normalization of data.

This Chapter presents a new classification-based technique named Unsupervised Classification to Change (UC-Change) and compares generated forest change maps against LandTrendr, C2C, and GFC maps for a complex mosaic of forest disturbance in western Canada. UC-Change combines the flexibility of classification-based routines with the high automation and ability to track forest recovery usually attributed to trajectory-based techniques. This approach can use multi-sensor data without losing the unique spectral and spatial information provided by each individual sensor. Unlike trajectory-based methods, it does not require atmospheric correction or any other preprocessing except for image-to-image spatial co-registration. Finally, it offers new, object-based metrics for measuring forest recovery.

3.2. Study Area and Data

To demonstrate various aspects of the new technique, a forested area was selected based on several criteria, such as the availability of reference data for the entire 1972 – 2019 period, sufficient amount of forest disturbances to test the temporal and spatial accuracy of the produced maps for every year in the time series, and a variety of forest types in terms of species composition and stand density. The study area in British Columbia (BC), Canada, corresponds to grid square T10UDD in the Universal Transverse Mercator (UTM) coordinate system (Sentinel-2 data are tiled based on this system) and is 100 km by 100 km in size (center coordinate: 52° 45' N; 123° 40' W; Figure 3-3). It is located south of Prince George, BC, and lies within the Montane Cordillera ecozone (Wiken 1986; Leckie *et al.*, 2016). The dominant tree species is lodgepole pine (*Pinus contorta* var. *latifolia*), followed by white spruce (*Picea glauca*) and subalpine fir (*Abies lasiocarpa*). The south part (coloured amber in Figure 3-3) of the study area has a low canopy cover of approximately 30% (VRI, 2020), which is still sufficient for land to be classified as forest based on the definition of forest adopted by Natural Resources Canada (NRCan, 2020a). The terrain is characterized as gently rolling (Leckie *et al.*, 2016). A mountain pine beetle (MPB) outbreak in the 2000s killed most lodge-pole pines in the area (BC Gov, 2020). Major forest fires occurred in 2006, 2010, 2014, 2016, and especially 2017 with many smaller fires over the years.

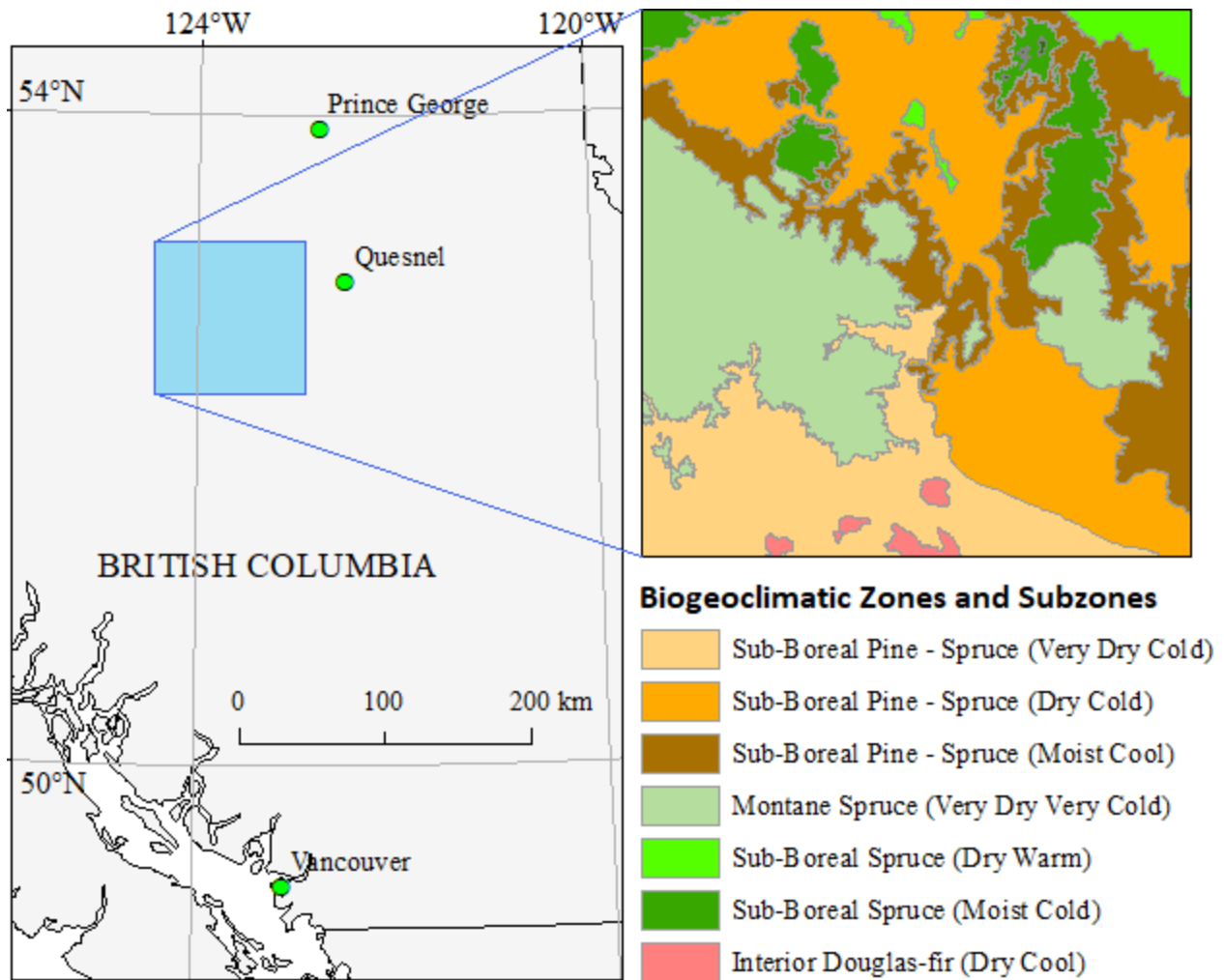


Figure 3-3. Biogeoclimatic zones and subzones (in brackets) in the study area (based on BEC, 2020).

The main dataset comprised 193 Landsat 5 TM, Landsat 7 ETM+, Landsat 8 OLI, and Sentinel-2 images acquired between 1984-06-22 and 2019-09-06 (Figure 3-4). Landsat Collection 1 Level-1 (terrain corrected but not atmospherically corrected) and Sentinel-2 Level-1C (ortho-rectified, top-of-atmosphere reflectance) data were selected and cropped automatically based on cloud cover. To reduce the processing time, only images with $\leq 50\%$ cloud cover were selected, except for particularly cloudy years. For those years, identified as when the 50% threshold resulted in $< 90\%$ yearly coverage of the study area, the threshold was reduced to 25% cloud cover.

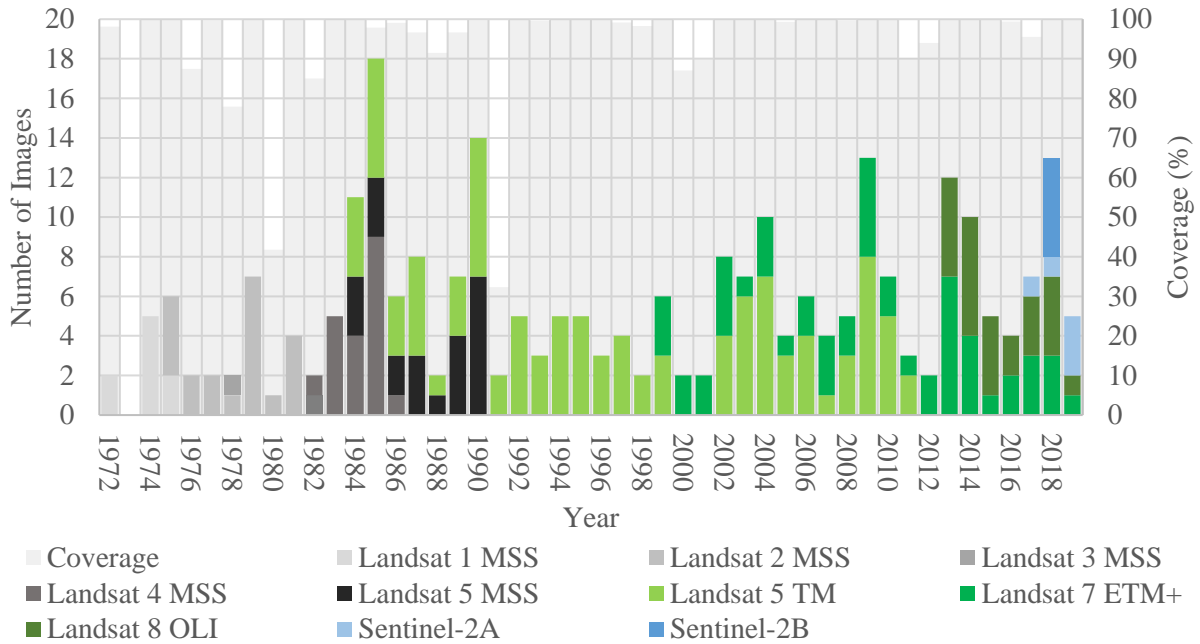


Figure 3-4. Number of images per year per sensor used in the study. The light grey bars in the background represent study area coverage (percent area covered per year) provided by the data.

The “Quality” band included with Landsat and Sentinel-2 images was used to mask clouds. Two additional steps were required for the Sentinel-2 data due to the low quality of the provided cloud masks. Firstly, a blue-band threshold (top-of-atmosphere reflectance > 16.5%) was used to mask most remaining clouds. The threshold was determined empirically to ensure that no clearcuts, which also have a high blue reflectance, are masked together with clouds. Secondly, a mask for cloud shadows was produced by shifting the cloud mask according to the mean solar azimuth angle at the time of image acquisition and an offset of 1,800 meters. The value (1,800 m = distance of 60 Landsat pixels) accounts for low-level clouds (<2000 m above ground) and most sun elevation angles (from 38° in September to 59° in June) possible at the acquisition time of Sentinel-2 data (~11:30 am) in the study area. While this value is not sufficient for mid- and high-level clouds (>2000 m), a higher value would result in the removal of a large number of useful pixels. A buffer of 300 meters was applied to both Landsat and Sentinel-2 cloud and cloud shadow

masks to remove most residual cloudy pixels. Despite such an excessive cloud masking, it was still possible to achieve a nearly 100% coverage of the study areas for most years.

Like many other change detection algorithms, UC-Change requires that agricultural areas be masked in input data. Preliminary tests showed that unmasked crop fields resulted in many false detections. Due to crop rotation, pixel values can change dramatically from year to year, which may result in crop fields being incorrectly identified as a forest change class by change detection algorithms (Huang *et al.*, 2010). For this reason, croplands were either masked in input data (Stueve *et al.*, 2011; Hermosilla *et al.*, 2015a), removed after change detection (Zhao *et al.*, 2018), or omitted from accuracy assessment (Hughes *et al.*, 2017). In this study, agriculture and water bodies were masked using the Agriculture and Agri-Food Canada's 2017 crop inventory map (AAFC, 2020). Using only the 2017 map for all years (1972 – 2019) was deemed a valid approach because there was little change in the extent of agricultural areas in Canada (NRCan, 2020b) and because no crop maps older than 2009 were available.

Spectral bands most affected by atmospheric conditions (e.g., blue, and from Sentinel-2: coastal aerosol, and cirrus bands) and phenomena unrelated to forest change (e.g., Landsat thermal infrared band) were not used in this study, resulting in a total of five Landsat and nine Sentinel-2 bands (Figure 3-5). To match the resolution of Landsat data, the 10 m (visible and near-infrared) and 20 m (red edge and short-wave infrared) spectral bands of Sentinel-2 data were resampled to 30 m by averaging the values within the nearest neighbor 30 m × 30 m area. However, it is noteworthy that errors of co-registration of Landsat 8 OLI and Sentinel-2 data can exceed 16 m (Stumpf *et al.*, 2018) and, therefore, introduce new issues, such as incorrect mapping of boundaries between patches of disturbed and undisturbed forest (this is expected to improve with future sensors and satellite imaging programs, as in the past).

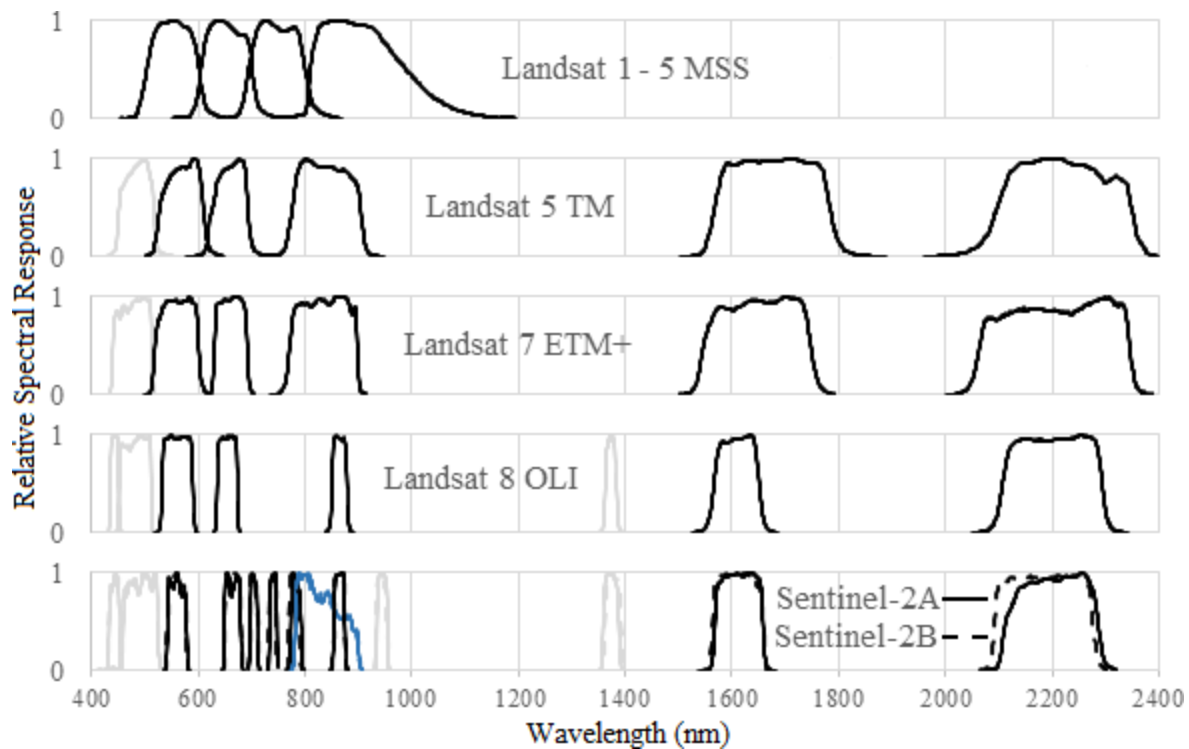


Figure 3-5. The spectral response functions of the ten sensors used in this study. The bands that were not used are grayed out. The thermal and panchromatic bands of the Landsat sensors were not used and are not shown here. Data obtained from the USGS and ESA websites.

In addition to the main dataset, a separate one containing 75 Landsat 1 – 5 MSS images was used to expand the time series to 1972. Only Tier 2 data were available for the study area. Tier 2 data are geometrically and radiometrically corrected but do not meet the Tier 1 quality criterion that requires a Root-Mean-Square Error (RMSE) of less than 12 m geometric correction error. The spatial resolution of Tier 2 data is 60 m, resampled from the original MSS resolution of 57 m × 79 m. Data values represent scaled top-of-atmosphere radiance and reflectance (scaling factors are provided in the metadata). The initial set of 92 images was selected automatically using the same approach that was used for the other sensors; however, based on visual examination, 17 images had to be discarded due to poor cloud masks or large geometric errors. The images were cloud masked the same way as Sentinel-2 images, but using a different threshold for clouds (the lowest wavelength available was used, which was the green band, with a top-of-atmosphere

reflectance threshold of $> 13\%$). Produced masks were of lower quality than those generated for the Sentinel-2 data because the green band does not allow a clear separation of clouds and fresh clearcuts. All four MSS spectral bands (green, red, NIR-1, and NIR-2) were used for change detection.

Clearcut detection was evaluated using Vegetation Resources Inventory (VRI, 2020) forest harvest polygons. The National Burned Area Composite (NBAC, 2020) database was used to assess the detection of wildfire burn scars. A set of polygons representing provincial parks and other protected areas were used to estimate false detections in the UC-Change and C2C maps (ECCC, 2020). It was assumed that only wildfires and biotic factors, but not harvesting, could cause disturbances in protected areas after they were established.

UC-Change maps were compared with maps produced by three methods already described in the Introduction section: LandTrendr, C2C, and GFC v1.7. Table 3-1 compares some aspects of these maps that are relevant to this study. For example, the LandTrendr and GFC maps used in this study show disturbances other than fire and harvest but lack change type information; therefore, it was not possible to evaluate false detection in these maps using the method described in the previous paragraph. While the C2C algorithm can also detect non-target disturbances, the available map contains only disturbances caused by wildfire and harvest (Hermosilla *et al.*, 2016; C2C, 2019).

Table 3-1. The characteristics of maps and algorithms used in the study.

Characteristic	UC-Change	LandTrendr	C2C	GFC
Approach to time-series change detection	Classification-Based	Temporal Trajectory Analysis	Temporal Trajectory Analysis	Hybrid
Are forest change maps available for the study area?	Yes ³	No	Yes	Yes
Is the algorithm open source?	Yes ⁴	Yes	No	No
Does the open-access map or algorithm show only stand-replacing disturbances?	Yes ⁵	No	Yes	No
Does the open-access map or algorithm classify changes?	No	No	Yes	No
Forest recovery monitoring capabilities	Object-based	Pixel-based	Pixel-based	N/A
Minimum mapping unit (in Landsat pixels and ha) for the study area	40 pixels (3.6 ha)	11 pixels (1.0 ha)	6 pixels (0.5 ha)	1 pixel (0.1 ha)
Temporal coverage	1984 – 2019	1984 – 2019	1984 – 2015	2000 – 2019
Input data date range	June 1 – Sep 20	June 20 – Sep 10	Aug 1 ± 30 days	Jan 1 – Dec 31
Were agricultural lands masked out?	Before processing	After processing	Before processing	No

There were no LandTrendr maps available online for the study area at the time of writing, but the algorithm itself is open-source (Kennedy *et al.*, 2018). The map used in this study was therefore generated, and using the default parameters (Table 3-2). These parameters were found optimal for multiple locations across the United States (Kennedy *et al.*, 2018) and were deemed appropriate for this study area as it is similar to forests in the Pacific northwest and interior forests south of BC. Sensitivity analysis confirmed this assumption. While increasing the size of

³ The UC-Change map for British Columbia can be made available by contacting the author.

⁴ See Appendix 1 for pseudocode.

⁵ UC-Change can potentially detect non-stand-replacing disturbances using a different set of parameters and/or classification routines.

the LandTrendr minimum mapping unit (MMU⁶) from the default 11 Landsat pixels to 40 pixels and the change magnitude threshold from 0.2 to 0.3 drastically reduced false detection and/or detection of non-stand-replacing disturbances, such as MPB damage, it also negatively affected the detection of disturbances of interest (cutblocks and fire scars). A change-attribution algorithm, such as the one used by Hermosilla *et al.* (2016), could potentially solve this problem without parameter adjustment by separating cutblocks and burned areas from other disturbances. Therefore, using the default parameters allowed a fairer comparison with other maps.

Table 3-2. Default LandTrendr parameters (Kennedy et al., 2018).

Parameter	Value
Magnitude of change ($\Delta\text{NBR} = \text{NBR}_{\text{post-disturbance}} - \text{NBR}_{\text{pre-disturbance}}$)	< -0.2
Pre-disturbance NBR	> 0.3
Duration of disturbance event	< 4 years
Number of segments	≤ 6
MMU	11 pixels

The available C2C and GFC maps are two-dimensional, showing all changes in a single layer instead of multiple layers (i.e., one per year). This means that they do not show repeat disturbances. The C2C map shows only disturbances with the greatest magnitude of change (C2C, 2019). Based on the analysis of areas affected by multiple disturbances, the GFC map shows the disturbances that occurred first. To account for these limitations and to make the comparison of the maps fair, all repeat disturbances were removed from the 1985 – 2015 reference VRI and NBAC data and only secondary disturbances were removed from the 2016 – 2018 reference data.

⁶ In the thesis, MMU refers to the minimum size of spatial clusters of change pixels that are allowed in change detection output. For example, an MMU of 11 pixels means that all clusters of change pixels smaller than 11 pixels are removed in the final change detection map. The main goal of this threshold is to reduce false detections. It is based on the assumption that disturbances of interest typically affect areas larger than the MMU (e.g., clearcuts are typically larger than 11 Landsat pixels, or 1 ha).

3.3. UC-Change Algorithm

The UC-Change algorithm detects groups of pixels (e.g., patches of disturbed forest) that break away from other groups of pixels (undisturbed forest of various types). A key concept in the algorithm is identification and use of *stable* and *change* pixels. Each image in a time series has its own set of **stable pixels**. This is where ground cover either does not change (e.g., undisturbed old-growth forest) or changes in the same way (e.g., regenerating clearcuts) for some duration of time from the date of image acquisition. To detect stable pixels, the algorithm processes small sets of images in a sliding time window fashion, starting from the first image in the dataset: $[t_1, t_2, t_3, t_4]$, then $[t_2, t_3, t_4, t_5]$, then $[t_3, t_4, t_5, t_6]$, etc.⁷ Each temporal subset contains a primary image, which is the first image in the subset, and all the others are secondary images. Only those pixels where no disturbances occurred in any of the secondary images are considered to be stable for the particular primary image.

Change pixels are defined as stable pixels that were not stable in temporally overlapping previous sets of images. For example, if the acquisition date of the image that is currently being processed is t_x , the overlapping sets are those where the primary image was acquired before the current image and at least one of the secondary images was acquired on or after t_x . For example, clearcuts that first appeared in t_x are stable in the corresponding subset of images $[t_x, t_{x+1}, t_{x+2}, t_{x+3}]$ but not in the preceding subsets $[t_{x-3}, t_{x-2}, t_{x-1}, t_x]$, $[t_{x-2}, t_{x-1}, t_x, t_{x+1}]$, and $[t_{x-1}, t_x, t_{x+1}, t_{x+2}]$. The subtraction of the t_{x-3} , t_{x-2} , and t_{x-1} stable pixels from the t_x stable pixels

⁷ Note: examples provided in this section refer to a hypothetical dataset where there are no clouds in any of the images. In real scenarios, when selecting secondary images, the algorithm skips images where cloud-free areas do not overlap with cloud-free areas in the primary image. For example, the second image (t_2) in a time series may not necessarily be a secondary of the first image (t_1), depending on the cloud cover in the two images.

removes all undisturbed forest and disturbances that occurred before t_x , leaving only disturbances that first appeared in the t_x image.

UC-Change detects stable and change pixels through a number of steps involving image classification and re-classification (Figure 3-6). Although the algorithm utilizes traditional unsupervised and supervised classification routines, it does not require any user input once the parameters are selected. The following paragraphs describe each processing step in detail.

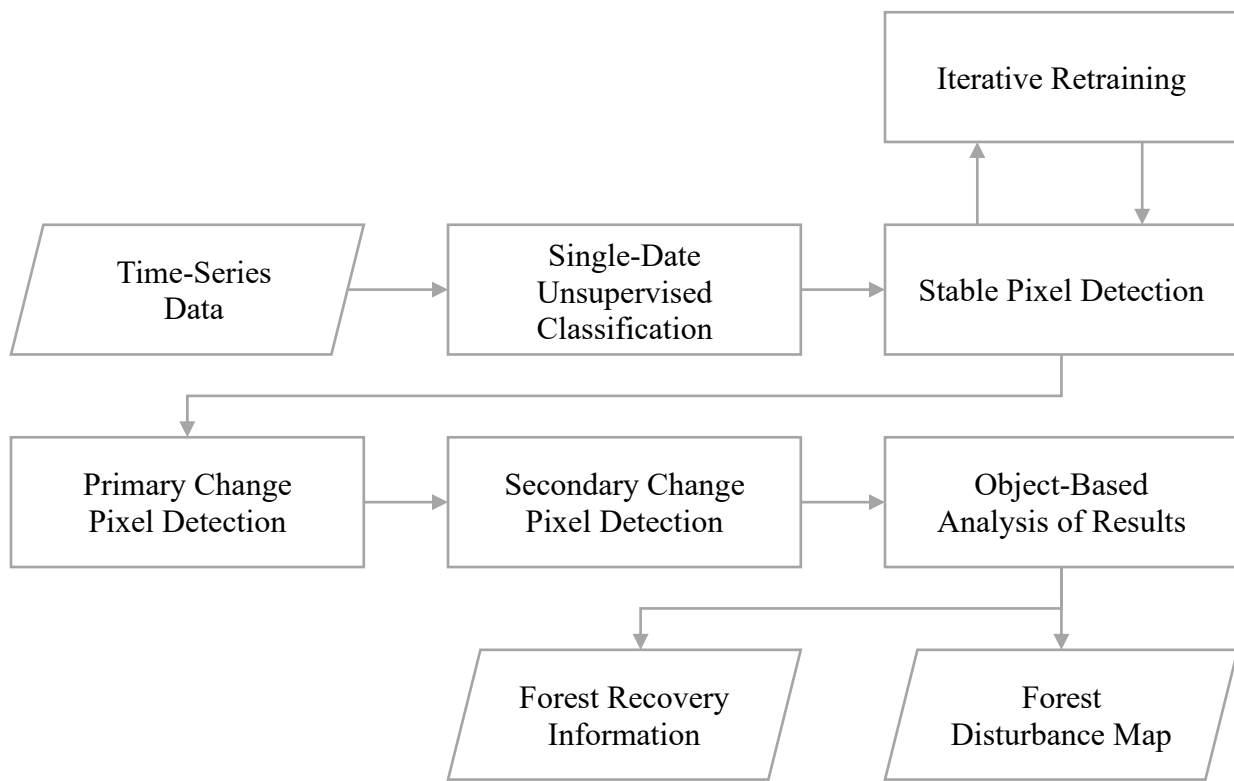


Figure 3-6. Flowchart of the UC-Change algorithm.

3.3.1. Unsupervised classification

To detect stable and change pixels, original numerical data must be converted into categorical data (i.e., classification maps). The UC-Change algorithm uses maps derived by unsupervised image classification, or clustering. The choice of classifier was based on several

criteria: 1) disturbed areas and pre-disturbance forest must be classified into different spectral classes; 2) the spatial distribution of spectral classes must remain similar in a sequence of images except for newly disturbed areas; 3) different stages of forest regrowth should be represented by different spectral classes to allow forest recovery information extraction; and 4) the classifier should be able to process hundreds of images in an automated and timely fashion. Based on these criteria, the K-means classifier (Steinhaus, 1956) was found well suited for this study. K-means reclusters pixels through an iterative process until it finds groups that are most separable from one another in the spectral domain. In the first iteration, pixels are classified based on the minimum Euclidean distance to evenly-distributed arbitrary class means. During each following iteration, class means are recalculated and pixels are reclassified based on the same minimum-distance-to-mean rule.

It is noteworthy that K-means is highly sensitive to canopy shadowing and topographic effects because these factors strongly affect all optical spectral bands. On the one hand, high sensitivity to canopy shadowing is beneficial to change detection and forest recovery monitoring, as older stands have stronger canopy shadowing (Gemmell, 1995). On the other hand, topographic effects (e.g., lower illumination and stronger canopy shadowing on north-facing slopes) may result in spatial inconsistencies in K-means classification maps. In the study area, some pixels containing one forest type were in fact classified into two separate spectral classes depending on whether they were located on north- or south-facing slopes. Nonetheless, based on visual analysis, the effect of terrain slope and aspect on change detection was minimal in the study area because the 10-class K-means maps still satisfied the four criteria in the previous paragraph. If this became a concern in a different study area, the fact that north and south facing aspects were separated into two spectral classes yet still associated with a given forest type could permit those spectral classes to

be combined in an automated environment to provide an integrated class for that forest type. The choice of 10 spectral classes is explained in the next section (Section 3.3.2).

3.3.2. Stable pixel detection

Although the spectral characteristics of land-cover types change through seasons and years, the spatial distribution of classes stays mostly unchanged through time for any particular land-cover type, at least when the number of classes is small. This is also the case for clearcuts and fire scars. For example, when images were classified into 10 classes, nearly all clearcut pixels remained in one class for at least four years. Therefore, to extract stable pixels from 10-class classification maps, the algorithm locates pixels that continue sharing one class for up to four years (Figure 3-7a-c).

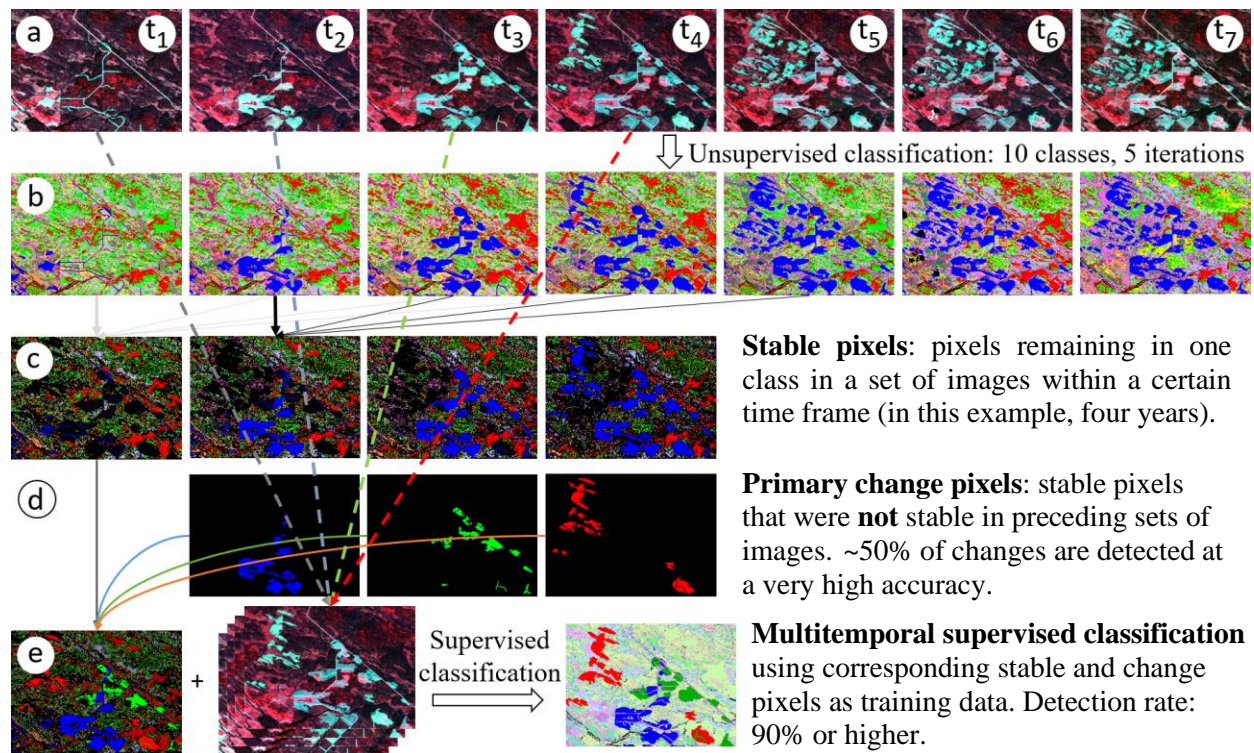


Figure 3-7. Main steps of the UC-Change change detection: a) original multispectral images in false color (green-red-NIR; $t_1 - t_7$ are the acquisition dates of the images; bright areas are fresh clearcuts); b) K-means classification output (10 classes); c) stable pixels derived from the K-means maps; d) primary change pixels derived from stable pixels; and e) multitemporal classification using the stable and change pixels as training samples and a stack of the four corresponding original images together with the final output product.

It is important to note that in order to detect stable pixels, the UC-Change algorithm matches only the spatial distribution of spectral classes and completely ignores whichever arbitrary class numbers are assigned to them. For example, K-means can assign different numbers (e.g., “Class 4” and “Class 5”) to a spectral class that contains a particular type of deciduous forest depending on the time of the year, because the spectral characteristics of the trees change with seasons. However, the spatial extent of the spectral class stays mostly unchanged because trees of the same species usually change their spectral characteristics in unison through seasons and years based on the leaf phenological cycle (Lechowicz, 1984; Hill *et al.*, 2010). The same is true for cutblocks and fire scars, and this is how UC-Change can detect stable pixels. This is a very

important point regarding the use of an unsupervised classification approach within the UC-Change algorithm. Some of the main challenges (and indeed, disadvantages) of unsupervised classification include the general need for cluster integration and class labeling, and associated with that, the rather arbitrary numbering of classes in intermediate steps. The UC-Change approach instead essentially bypasses those concerns by integrating a spatial-structural approach to unsupervised output management.

It should also be noted that a separate set of stable pixels is detected for each set of primary and secondary images. In other words, stable pixels are only detected for periods of time that do not exceed the length of time of the processing window. Therefore, from the algorithm's perspective, stable pixels are areas that do not experience abrupt changes between the acquisition dates of the first and last images in the time processing window. Examples of stable areas include undisturbed forest stands and areas disturbed before or after the stable period (four years in this study).

Stable pixel detection depends on three inter-dependent parameters: the number of spectral classes, the length of time with the processing window, and the number of secondary images. The K-means classifier set to produce *10 classes* was used in this study. The choice of 10 classes was found optimal after a series of tests on several datasets representing various forest types across Canada, including mixed and deciduous forests in the Province of New Brunswick. The algorithm could not find enough stable pixels when using 15-class K-means images, because the distribution of spectral classes varied too much from image to image. In contrast, the K-means classifier could not separate clearcuts and fire scars from some types of undisturbed forest when it was set to produce five or fewer classes. Based on additional testing using reference data produced by visual interpretation of Landsat data, excellent (>90% of reference cutblock pixels detected in

all test sites) and very similar (less than $\pm 1\%$ deviation in producer accuracies) results were produced when using images classified into 6 to 14 classes, because in those cases disturbances of interest (clearcuts and fire scars) were classified into a class of their own and remained so for the duration of the time processing window, which is the main requirement for the algorithm to work. Consequently, the middle value (10 classes) was used as reasonable value to work best for a wide variety of forest environments.

The maximum length of time of the processing window was set to *four years* based on two factors: the length of time patches of disturbed forest remain homogeneous in K-means classification maps (i.e., contain only one spectral class) and the availability of spatially overlapping images. The former determines the maximum value for this parameter, while the latter determines the minimum value. In 10-class K-means maps, cutblocks and fire scars contain only one spectral class for at least four years. Therefore, in order for the UC-Change algorithm to detect as many stable pixels as possible for disturbed areas, the length of the processing period should not exceed four years.

UC-Change is a scene-based technique and, therefore, when processing a subset of images, it can only utilize the parts of images that overlap. Instead of using all four years of data within the time window, which can contain as many as 40 images, the algorithm selects the *three images* where cloud-free areas have the largest spatial overlap with the cloud-free portion the primary image that is currently being processed. Using fewer than four images (i.e., primary plus three secondary) per set increased the probability of detecting unmasked cloud pixels as stable pixels, while using a larger number of images resulted in an insufficient number of stable pixels. A time window size of less than four years made it difficult for the algorithm to find overlapping images in the 1984 – 1998 data, where only Landsat 5 data were available. Note that all secondary

images can be from the same year as the primary one, as long as they have the largest overlap among all combinations of images acquired within the time window (i.e., within four years after the primary image).

3.3.2.1. Iterative retraining option

To detect changes accurately, the algorithm must locate as many stable pixels as possible. While it is not possible to detect all of them due to image noise, unmasked clouds and cloud shadows, and other factors, the number of detected stable pixels can be increased through a process called iterative retraining, whereby stable pixels derived from K-means classification output for a subset of images are used as training data in single-date Maximum Likelihood classifications of the images in the subset. For example, stable pixels detected for each K-means cluster in image X are used as training samples for the Maximum Likelihood classification of the same image, producing a new 10-class map that replaces the original K-means map. The resulting classified images can then be used again to locate stable pixels, this time in much larger quantities. This process can be repeated multiple times. The goal is to minimize multitemporal differences in the distribution of spectral classes caused by atmospheric conditions, phenology, and differences in sensor characteristics, and to maximize those caused by forest disturbances.

Iterative retraining can be viewed as a continuation of the single-date K-means classification with the addition of temporal and spatial (i.e., based on the spatial extent of spectral classes) information. Similar to when using the K-means classifier, the user can either set a fixed number of iterations or use a stopping criterion. In the latter case, the algorithm can be set to stop the retraining process if it no longer increases the number of stable pixels.

Although iterative retraining brings only minor improvements when the primary and secondary images are from the same type of sensor (e.g., Landsat 5 – 8), it proved highly beneficial in sets that contained a mixture of Sentinel-2 and Landsat images. K-means maps derived from Sentinel-2 images were noticeably different from those derived from Landsat 8 images acquired on the same day, because Sentinel-2 images contained more spectral bands, including three red-edge bands that have no analogues in Landsat data. Two iterations of retraining helped increase the number of detected stable pixels for such mixed sets of images by up to 70%. Considering that iterative retraining has the greatest impact on the processing time and that the third iteration improved the resulting change map only by a fraction of one percent, two iterations were found optimal for a number of test sites in Canada, and this fixed number of iterations was used in this study as well. The goal of iterative retraining is to make the spatial distribution of spectral classes more consistent among the primary image and the three secondary images, and this was achieved.

For the next step (primary change pixel detection) to work, no stable pixels should be detected in areas disturbed during the processing time window period. Such areas indeed remained free of stable pixels, even after multiple iterations of retraining.

3.3.3. Primary change pixel detection

After the first primary image is processed, the second image in the time series becomes a primary image and three images acquired after it become the secondary images for this next processing set. Once stable pixels are detected for the new set of images, disturbances that occurred before the new primary image but after the previous one are now detected and designated as stable. Primary change pixels are then extracted by subtracting old stable pixels from the new ones (Figure 3-7d).

The main purpose of primary change pixel detection is to automatically generate training sample for the next step (secondary change pixel detection). Therefore, it is important that they represent only forest disturbances of interest. However, in addition to true disturbances, some pixels representing undisturbed forested areas can also be mistakenly labeled “change” pixels if the algorithm failed to detect them as stable in previous sets of images due to image noise and other factors. These mislabeled “change” pixels are usually spread out and can be removed by deleting change pixels that are not spatially clustered or occur in groups smaller than *40 Landsat pixels* (3.6 ha). While smaller patches of disturbed forest (< 3.6 ha), which account for 0.9% (by area) of all clearcuts and 0% of fire scars in the study area (according to the VRI and NBAC data), are not represented by the resulting set of primary change pixels, the removal of non-clustered pixels is a sacrifice worth making as it removes the vast majority of false detections. The goal of this step is to produce training areas (e.g. even if cutblocks < 3.6 ha are removed, the training pixels still represent 99.1% of cutblocks). This approach also improves the training data for the following step of secondary change pixel detection.

3.3.4. Secondary change pixel detection

After stable and primary change pixels are detected for the entire time series, more changes can be detected by performing a series of multitemporal supervised classifications using the same subsets of images that were used in the previous steps (Figure 3-7e). Stable pixels detected for a primary image and primary change pixels detected for the secondary images are used as training data in a supervised classification of the corresponding four-image stack. This process is then repeated for all temporal subsets throughout the time series. The following is an example of one of such multitemporal classifications:

Input data:

- A stack of four images: 1990-06-23_L5, 1992-08-15_L5, 1993-09-03_L5, and 1994-07-20_L5, where 1990-06-23_L5 is the primary image and the rest are secondary images selected based on the maximum spatial overlap with the primary images (in this case, 97% overlap). The spectral bands of the four images are combined to produce a single image stack with 24 bands.

Training data:

- Stable pixels detected for all ten classes in the primary image:
1990-06-23_L5_c1_stable, 1990-06-23_L5_c2_stable, 1990-06-23_L5_c3_stable, ..., and 1990-06-23_L5_c10_stable.
- Primary change pixels detected for all images within entire processing window period:
1990-08-10_L5_primary_change, 1990-08-26_L5_primary_change,
1990-09-11_L5_primary_change, 1991-06-10_L5_primary_change,
1991-07-28_L5_primary_change, 1991-08-13_L5_primary_change,
1991-08-22_L5_primary_change, 1991-09-07_L5_primary_change,
1992-07-23_L5_primary_change, 1992-08-15_L5_primary_change,
1992-08-24_L5_primary_change, 1993-08-11_L5_primary_change,
1993-09-03_L5_primary_change, 1994-06-02_L5_primary_change, and
1994-07-20_L5_primary_change.

Output:

- 1990-06-23_L5-1994-07-20_L5_ML, a Maximum Likelihood classification map with 24 labelled classes

Combining same-date change classes from consecutive multitemporal classification maps produces secondary change pixels for each acquisition date. For example, change class ‘1994-07-20’ is contained in 15 different multitemporal classification maps: 1990-06-23_L5-1994-07-20_L5_ML, 1990-08-10_L5-1994-07-20_L5_ML, ..., 1997-06-10_L5-2001-08-16_L7_ML, and 1994-06-02_L5-1996-07-25_L5_ML.

The Maximum Likelihood classifier was found well suited for multitemporal classification, as it was much faster than the other two classifiers tested (Support Vector Machines and Neural Network) and was not prone to overfitting. Due to the very large number of training samples (>3,000,000 training pixels per image) and a large number of classifications to perform, the processing speed was an important consideration. In addition, it was important that the resulting spectral classes were normally distributed to prevent classes containing a mixture of disturbed and undisturbed forest. The Maximum Likelihood classifier aligned with this requirement due to its parametric statistical properties.

3.3.5. Removal of false positives and analysis of post-disturbance recovery

Although the multitemporal classification step described in Section 3.3.4 improves the detection rate, it can also introduce unwanted false detections of disturbance. Similar to the primary-change-pixel-detection step, clusters smaller than 40 Landsat pixels (3.6 hectares) were removed first. Doing so decreased the detection of clearcuts by 0.3% while reducing false positives and non-target disturbances by nearly 20% compared to results produced with the minimum cluster size set to 20 pixels.

Once non-clustered change pixels are removed, change maps are segmented into individual spatial clusters and the distribution of spectral classes before and after disturbance are

analyzed for every cluster. Spatial clusters that do not have substantially different pre- and post-disturbance distributions of spectral classes are rejected as described in the next paragraph. This filter requires ordinal categorical input with consistent class numbering. To meet this requirement, spectral classes in the K-means maps were ranked based on their average SWIR-2 pixel values. The SWIR-2 bands were chosen for three main reasons: 1) SWIR bands are the most important bands in forest disturbance mapping (Zhu and Woodcock, 2014; Hermosilla *et al.*, 2015a; Cohen *et al.*, 2018); 2) SWIR-2 is least affected by thin clouds and haze compared to other optical spectral bands; and 3) SWIR-2 bands of the Landsat and Sentinel-2 sensors have relatively similar spectral response curves (Figure 3-5). Such a ranking system assigns the highest rank to spectral classes representing disturbances and the lowest rank to classes representing dense forest. The ranking is relative and, therefore, does not require atmospheric correction and intra-sensor normalization to produce consistent results across the time series. The NIR band was used for Landsat MSS data due to the lack of SWIR bands.

The presented technique uses cumulative percentage of dominant pre- and post-disturbance spectral classes to remove clusters that do not represent clearcuts or fire scars. Dominant pre-disturbance classes are classes that, when combined, make up at least 90% of clustered pixels in images acquired up to four years before disturbance. In the study area, undisturbed coniferous stands were represented by Classes 1 to 5 in the 10-class SWIR-2-ranked K-means maps. Dominant post-disturbance classes are determined the same way, but using images acquired up to four years *after* disturbance. In the study area, most cutblocks and fire scars were represented by Classes 10 and Classes 7 – 10, respectively⁸. A filter threshold of 2 was used to

⁸ Spectral class 10 contained both clearcuts and severely burned areas due to similar spectral characteristics. Importantly, UC-Change uses classification maps from an unsupervised classifier (K-means in this study) that produces unlabelled spectral classes that do not necessarily match any specific thematic classes, and instead are handled in UC-Change using spatial-structural metrics.

produce the results presented in this Chapter. This means that the percentage of dominant pre-disturbance classes must drop twofold and the percentage of post-disturbance classes must increase twofold following a disturbance event in order for the cluster of pixels to be labelled “disturbed”. This threshold was determined to produce the lowest commission and omission errors. A stricter threshold would not affect the detection of clearcuts, because the distribution of spectral classes changes dramatically. This is true even for low-canopy-cover stands despite the small absolute difference between the pre- and post-disturbance SWIR-2 pixel values. This confirms that the SWIR-2 ranking does not discard the unique information contained in other spectral bands, as the results will demonstrate. However, unlike clearcuts, fire scars are more heterogeneous and sometimes contain a similar set of spectral classes to the forest they replace. Therefore, the user must adjust this threshold carefully to balance false detection and fire-scar detection.

The two metrics (percentage of dominant pre- and post-disturbance spectral classes) can also be used to analyze **forest recovery** (Figure 3-8). After disturbance, clearcuts and fire scars become increasingly heterogeneous. Consequently, the percentage of dominant post-disturbance classes starts to decrease, and reach 0% (absent) typically 15 to 20 years after disturbance. The percentage of dominant pre-disturbance classes starts to increase after that, plateauing between 90% and 100% from 25 to 30 years after disturbance, depending on forest type.

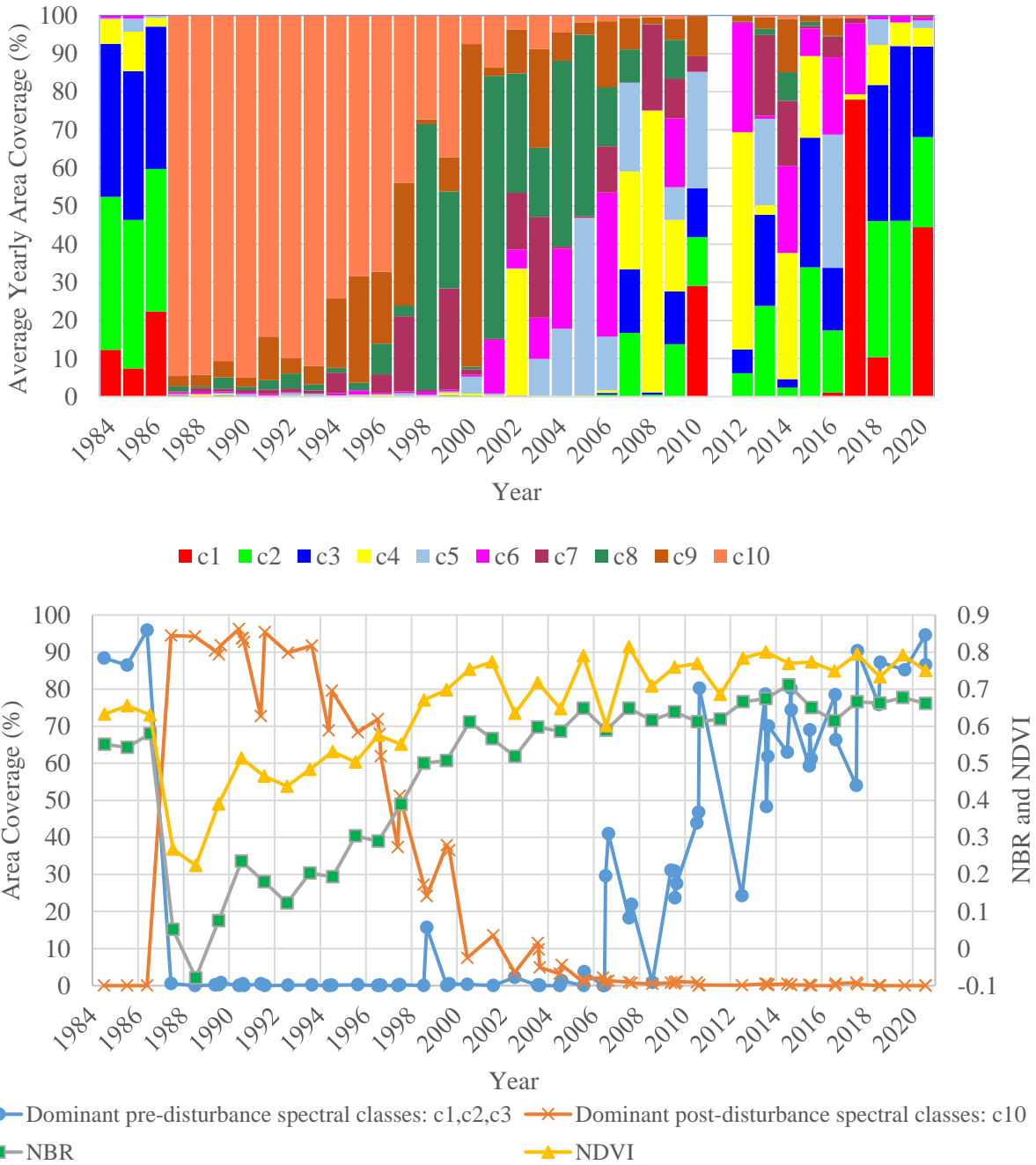


Figure 3-8. Top: Changes in the distribution of SWIR-ranked spectral classes in a 1987-07-01 clearcut over time. Bottom: forest recovery in the same clearcut measured by the cumulative percentage of dominant (containing 90% or more pixels) pre-disturbance and post-disturbance spectral classes, as well as average NBR and NDVI values. The spectral indices (NDVI and NBR) reached pre-disturbance values within 13 years after disturbance. The percentage of pre-disturbance classes reached 90% only after 28 years.

Finally, the proposed metrics can improve the classification of changes (i.e., change attribution). Clearcuts usually contain only one dominant post-disturbance class, whereas fire scars contain many. This is an area for future work.

It is important to note that while the algorithm that filters out false positives and tracks forest recovery is somewhat sensor-dependent, the technique itself is not. Only a few images in the time series are required to perform these routines. For example, in multi-source datasets, the user may choose to use only Landsat 5 - 8 for this step (filtering and forest recovery information extraction), as they showed consistent SWIR-2 ranking.

3.3.6. Accuracy assessment and comparison with LandTrendr, C2C, and GFC

VRI forest harvest polygons were used to assess the spatial and temporal accuracy of clearcut detection. At least some temporal discrepancy between the maps and VRI dataset was expected for two reasons. Firstly, VRI polygons are produced using aerial photographs and, therefore, are precise and accurate spatially. However, they are not always as accurate temporally, because the precise harvest date is often not reported for clearcuts (i.e., only the year but not the month and day of disturbance). Secondly, different change detection techniques time-stamp change pixels differently. For example, changes labelled “2010” in the C2C map could actually occur any time between July 1st 2009 and August 31st 2010, because the C2C technique used only July and August data.

Based on our own set of reference data, containing 3,545 manually delineated polygons produced through consecutive bi-temporal image interpretations of 1984-2016 Landsat data, the VRI polygons represented approximately 86.3% of all clearcuts in the study area. 93.7% of VRI polygons had a temporal accuracy of ± 1 year. There were two reasons why the VRI dataset

was chosen over our own set of polygons for the assessment of cutblock detection. First of all, VRI maps are produced by an independent group of analysts using an independent set of data (stereo aerial photos) and are freely available to the public, and thus allow an unbiased, reproduceable, and transparent evaluation of Landsat-based change detection products. Secondly, VRI polygons show the full spatial extent of individual cutblocks, making it possible to assess the detection of cutblock edges.

Cutblock detection was evaluated at a temporal agreement of ± 1 year and ± 3 years to exclude as many change pixels detected by chance as possible. The difference between ± 1 -year and ± 3 -year results was indicative of detection lag, which is defined as the offset between the acquisition date of the image in which a forest disturbance is first detected and the actual date of the disturbance. However, ± 1 -year and ± 3 -year results should only be interpreted in a relative sense due to temporal inaccuracies in the reference dataset itself (VRI).

NBAC polygons were used to assess the detection of forest fire scars. Only polygons produced using aerial photos and satellite data with a spatial resolution < 55 m were selected for this study. It is noteworthy that NBAC polygons do not indicate variation in burn severity. Many burned areas have surviving patches of trees that can be indistinguishable from undisturbed forest in Landsat images. Such unburned areas were removed from 90% of NBAC polygons by area (Hall et al., 2020). Using generalized vector data for the accuracy assessment of highly heterogeneous classes, such as fire scars, in classification maps is known to result in considerably underestimated accuracies (Wulder *et al.*, 2006). For this reason, a relatively low agreement between the NBAC map and change detection maps was expected. Nonetheless, the NBAC polygons can still be used as the basis for comparison to assess the relative performance of different

change detection techniques. Confidence intervals for this dataset were estimated at $\pm 4.3\%$ (Hall et al., 2020).

Polygons representing provincial parks and other protected areas were used to estimate false detection of forest harvest activities in the UC-Change and C2C maps (ECCC, 2020). The study area was heavily affected by a MPB outbreak, including the protected areas (NRCan, 2020c). However, MPB-affected areas were not detected by the UC-Change algorithm due to the lack of abrupt and localized changes in infested areas. Therefore, any change pixels detected within protected areas except those located inside NBAC forest fire polygons were considered false positives in the UC-Change map (Figure 3-9). The same rule was applied to the C2C map because it also shows only harvested and burned areas. However, this was not applied to the LandTrendr and GFC maps as they do show MPB-affected areas. False detection of cutblocks was evaluated only for the period mapped in all four maps (2001 – 2015). Lack of protected areas before 1995, and devastating forest fires after 2016 made it difficult to produce reliable estimates of commission errors outside this period.

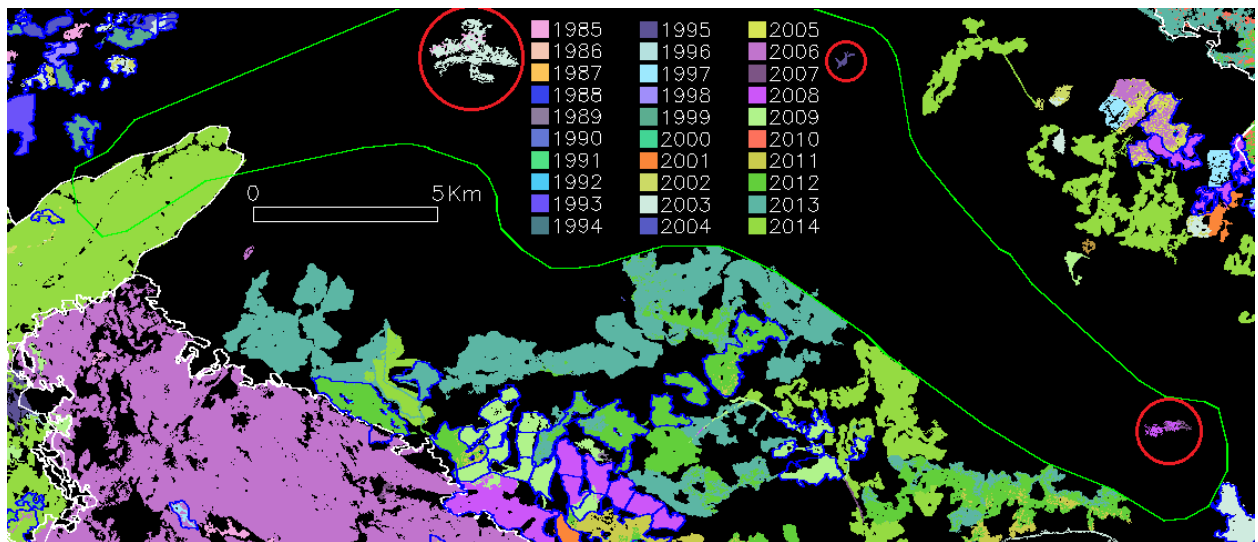


Figure 3-9. VRI (blue), NBAC (white), and Kluskoil Lake Provincial Park (green) polygons overlaid on a Landsat 8 image (RGB: red, NIR, SWIR-2) acquired on 2014-09-13 (top) and the UC-Change map (bottom). Colors in the UC-Change map represent the year of disturbance. A large number of false positives (highlighted with red circles) can be seen inside the park, mainly due to changing wetland conditions.

3.4. Results

Overall, UC-Change detected 85.4% of all 1974 – 2017 VRI cutblock pixels with a temporal agreement of ± 1 year; 89.0% were detected at ± 2 years and 90.4% at ± 3 years (Table 3-3). UC-Change outperformed all other techniques used for comparison across all years in the time series (Figure 3-10). C2C and LandTrendr both had much lower results than UC-Change, and they both performed very similarly to each other, detecting only 46.8% and 46.1% of 1985 – 2015 VRI cutblock pixels, respectively. For the same period, UC-Change mapped 86.6% of forest harvest pixels using June 1 – September 20 data and 79.0% using July 1 – August 31 data. In terms of cutblock detection, the GFC map was more similar to the UC-Change map, except for the period 2012 – 2015, where it contained 26.7% – 35.3% fewer VRI pixels. In addition, GFC detected 9.1% more cutblock pixels at ± 3 years than at ± 1 year (77.1% vs. 70.7%), indicating a relatively large detection lag in this map. In other maps, the difference for the same period was less than 5%.

Table 3-3. Percent reference clearcut pixels detected at a temporal agreement of ± 1 and ± 3 years. The available C2C and GFC maps covered limited time periods. UCC = UC-Change; LT = LandTrendr.

Years	Detection at ± 1 year (%)				Detection at ± 3 years (%)				Total area of VRI polygons (km ²)
	UCC	LT	C2C	GFC	UCC	LT	C2C	GFC	
1974-2017	85.4	-	-	-	90.4	-	-	-	2720.1
1974-1984	76.3	-	-	-	85.1	-	-	-	245.4
1985-2015	86.6	46.1	46.8	-	91.3	49.0	50.2	-	2414.9
2001-2017	87.6	34.1	-	70.7	91.9	35.7	-	77.1	1405.6

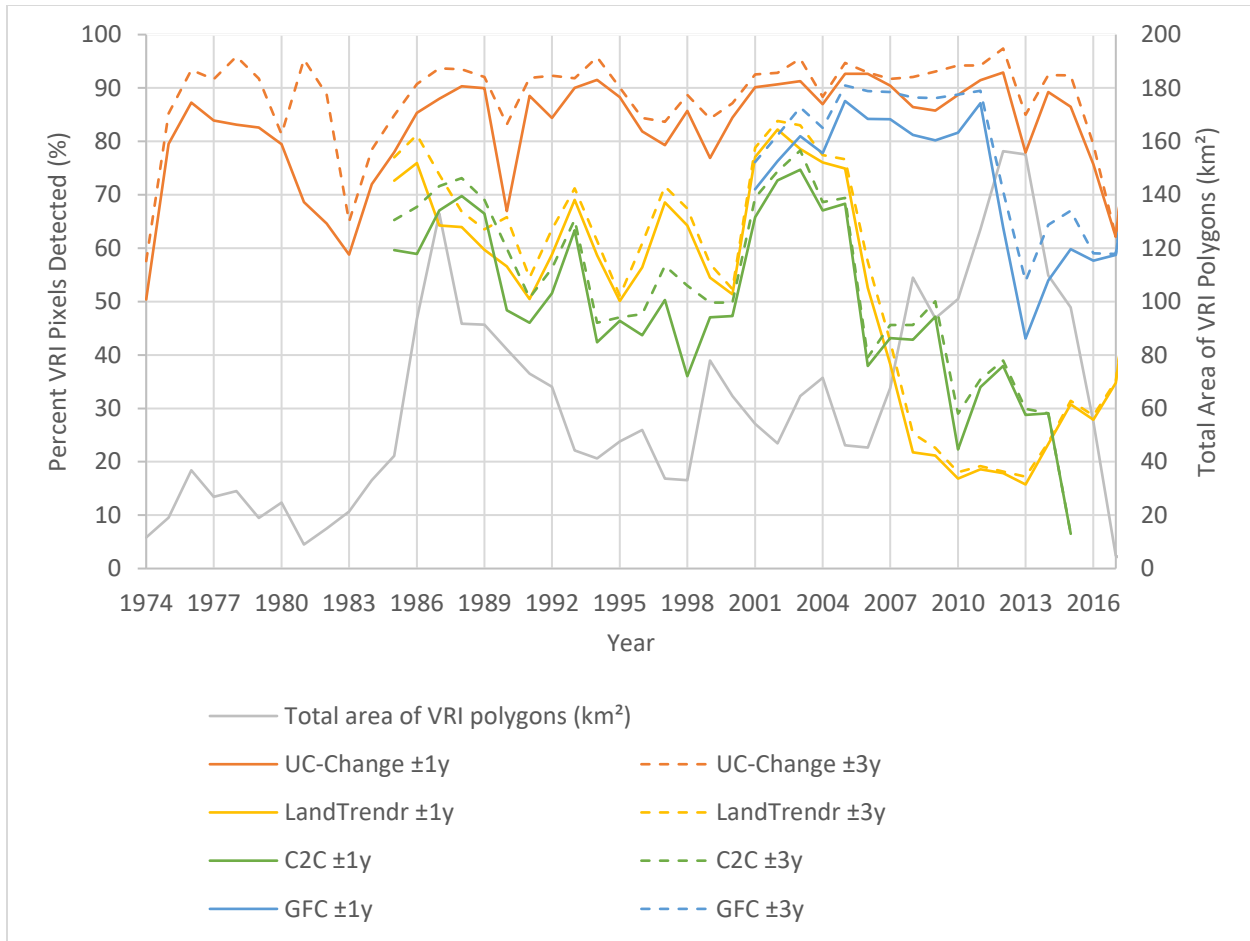


Figure 3-10. Percent reference clearcut pixels detected at a temporal agreement of ± 1 year (solid lines) and ± 3 years (dashed lines). The grey line represents the total area of VRI clearcut polygons per year.

UC-Change also outperformed other techniques in fire scar detection (Table 3-4). It detected 74.1% of reference 1987 – 2014 forest fire pixels at a ± 1 -year agreement (78.2% at ± 3 years), while LandTrendr detected 60.0% and C2C detected 62.2%. Similarly, UC-Change detected 72.1% of reference 2006 – 2017 forest fire polygons at a ± 1 -year agreement (73.3% at ± 3 years), while GFC mapped 60.1% (62.6% at ± 3 years). LandTrendr detected only 28.2% of the 2017 fire, which affected a seven times larger area than all 1987 – 2016 fires combined.

Table 3-4. Total area of the reference forest fire polygons per year and percent of the area detected by the four change detection techniques. The table only shows the years for which the total size of reference polygons was greater than 1 km². UCC = UC-Change; LT = LandTrendr.

Year	Detection at ±1 year (%)				Detection at ±3 years (%)				Total area of NBAC polygons (km ²)
	UCC	LT	C2C	GFC	UCC	LT	C2C	GFC	
1987	0.6	7.8	13.0	-	2.0	11.1	13.7	-	1.6
1988	92.7	79.9	84.2	-	94.9	79.9	85.1	-	1.4
1990	38.1	31.3	24.9	-	41.0	33.2	26.4	-	3.2
1995	56.3	47.4	53.5	-	56.4	47.4	53.5	-	19.2
2006	93.4	88.3	82.9	76.9	93.5	88.8	83.0	81.1	149.5
2009	68.2	35.0	56.4	54.1	69.4	35.8	58.2	57.3	53.9
2010	40.2	37.5	33.0	44.4	45.5	38.5	35.3	52.7	112.5
2014	87.5	60.2	68.3	50.6	87.6	60.2	68.4	57.3	134.3
2016	7.1	22.3	-	35.1	7.9	22.4	-	35.4	2.1
2017	71.7	28.2	-	60.4	72.2	28.8	-	62.4	3500.3

The C2C map had very few false cutblock pixels in protected areas (0.06% of the total protected area) (Table 3-5). In contrast, UC-Change mapped 2.6% of protected areas unaffected by forest fires as disturbed between 2001 and 2015 inclusive. Most false detections were along rivers and around lakes and ponds due to long-term fluctuations (4 – 5 years) in water level and wetland conditions. The LandTrendr map had somewhat fewer change pixels in unburned protected areas (1.8%) than the UC-Change map, but those pixels were more spread out and were mostly found in forested areas. Finally, 9.8% of protected areas were labelled disturbed in the GFC map.

Table 3-5. False detection of cutblocks (commission errors) in the UC-Change and C2C maps for the period 2001 – 2015. The LandTrendr and GFC maps may contain disturbances other than logging and forest fires and were added for comparison only.

Percent area, excluding agriculture and water bodies, mapped as disturbed...	UC-Change (%)	LandTrendr (%)	C2C (%)	GFC (%)
...in protected areas unaffected by forest fires (out of 226.4 km ²)	2.55	1.79	0.06	9.83
...outside protected areas (out of 10,418.4 km ²)	24.16	13.31	12.00	29.35

Outside protected areas, UC-Change, LandTrendr, C2C, and GFC found change in 24.2%, 13.3%, and 12.0%, and 29.3% of pixels in the 2001 – 2015 data, respectively. According to the VRI and NBAC data, 14.9% and 6.4% of the unprotected area was harvested and burned during that period, respectively, resulting in a total of 20.2% of the area affected by stand-replacing disturbances, including areas disturbed twice (fire and harvest). Considering that the VRI dataset contains approximately 90.6% of cutblocks that occurred in the study area during the period 2001 – 2015 (based on our own set of reference cutblock polygons), the actual percentage of disturbed forest is likely greater than 20.2%. Therefore, the UC-Change approach likely produced a better estimation of the total area affected by logging and forest fires compared to LandTrendr and C2C.

A visual comparison of the maps revealed that C2C and LandTrendr failed to detect most clearcuts in the Very Dry Cold subzone of the Sub-Boreal Pine - Spruce biogeoclimatic zone (south-west part of the map in Figure 3-11). In this subzone, C2C detected only 18.0% (LandTrendr: 21.9%) of 1985 – 2015 VRI clearcut pixels compared to 53.0% (LandTrendr: 50.0%) in the rest of the study area. GFC also struggled to detect cutblocks in this subzone (59.0% of 2001 – 2015 VRI pixels detected in the subzone and 72.8% outside). In contrast, UC-Change had nearly the same detection rate throughout the study area (84.7% and 87.0% at ± 1 year, respectively).

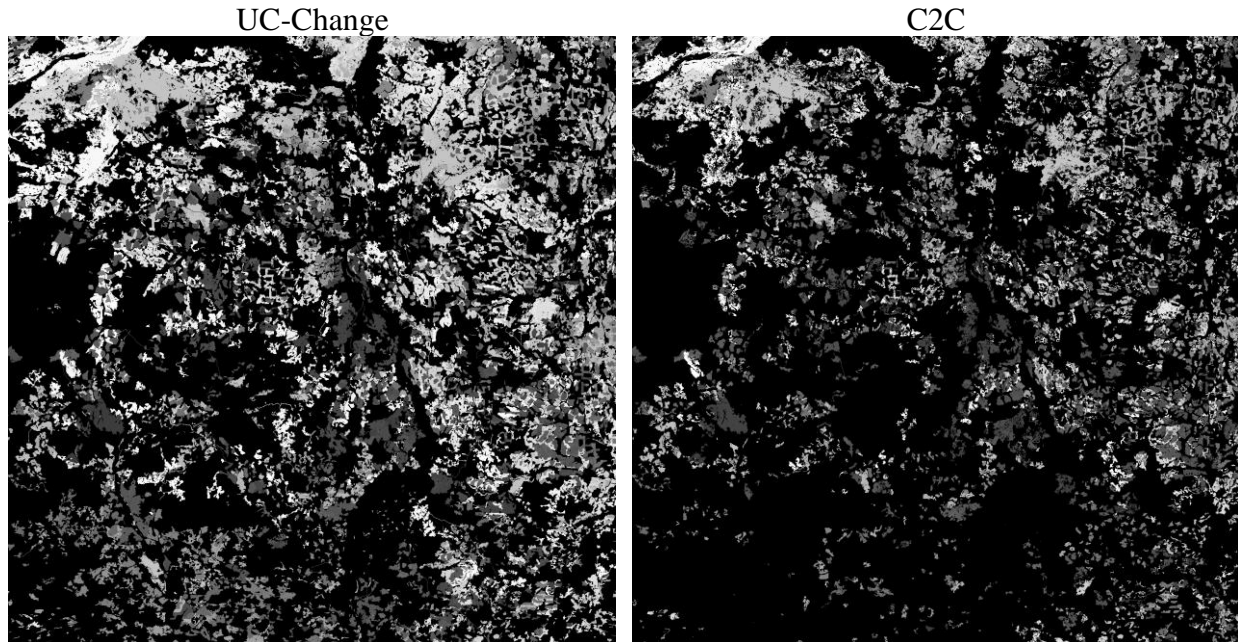


Figure 3-11. UC-Change and C2C forest change maps of the entire study area (100 km × 100 km; north is up) for the period 1985 – 2015. Brighter shades of grey indicate more recent changes. Note the differences in the south-west corner.

Clearcuts in the UC-Change map had a more homogenous, spatially contiguous appearance with almost no “salt-and-pepper” (speckle) effect compared to other maps (Figure 3-12). Unlike the GFC map, it accurately represented forest reserves inside clearcuts. In contrast, many cutblocks were absent or only partially present in the C2C and LandTrendr maps (e.g., Figure 3.12).

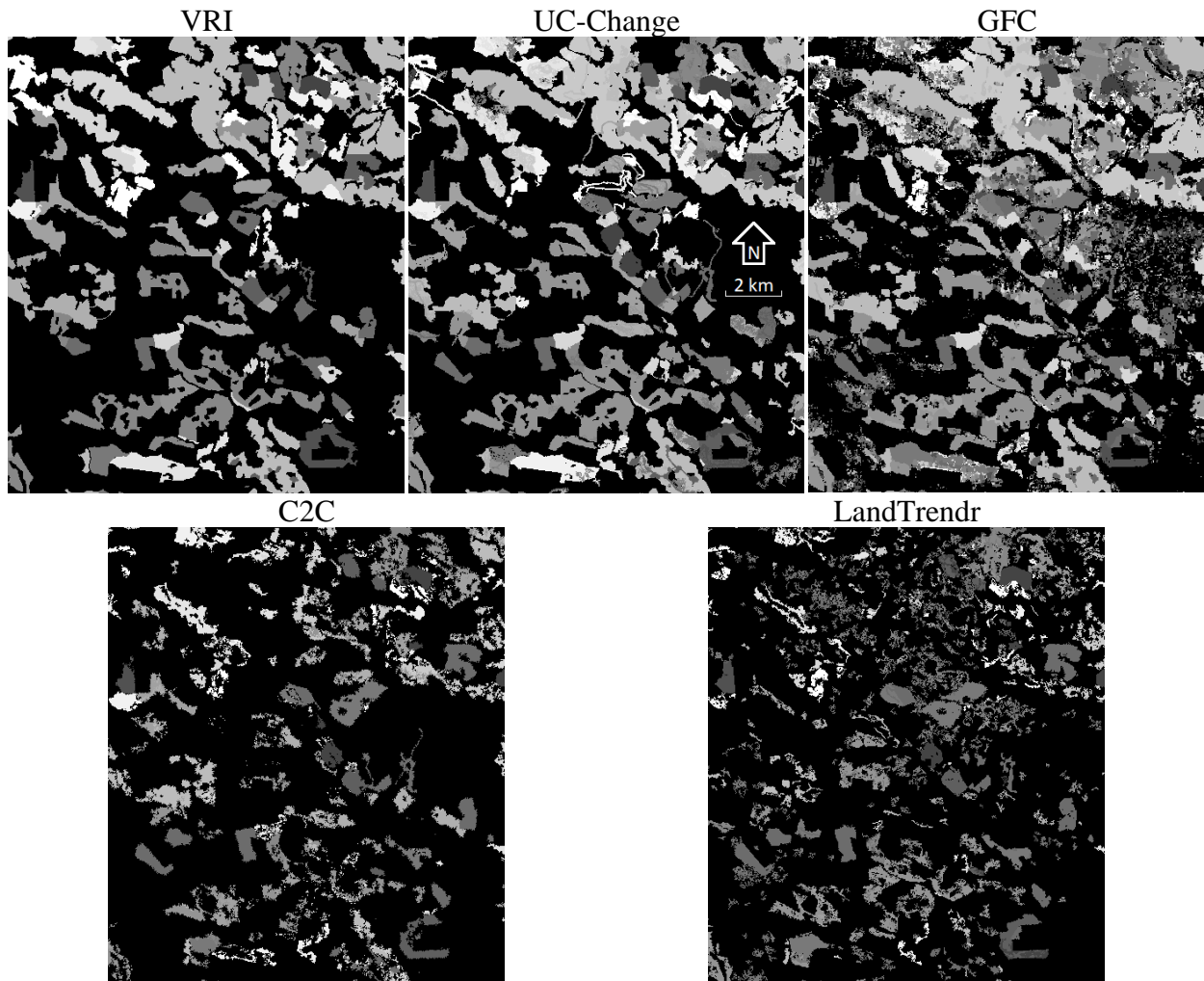


Figure 3-12. 2001 – 2015 clearcuts and clearcuts with reserves (patches of undisturbed forest) as they appear in the reference data (VRI) and the four change detection maps compared in the Chapter. The UC-Change map was the most similar to the reference map. It accurately represented clearcuts with reserves and had a cleaner look overall, whereas other maps had a strong “salt-and-pepper” effect with many missing or only partially represented cutblocks.

The UC-Change classification-based forest recovery metrics showed good potential. Unlike average NBR values, which followed the same recovery pattern in most clearcuts, the recovery of these areas in the UC-Change maps depended on forest type (Figure 3-13). Pine-dominated stands showed a faster recovery compared to spruce-dominated stands. For example, the UC-Change metrics reached their pre-disturbance values in 70.6% (by area) of 1986 and 1987 clearcuts in the Moist Cool subzone of the Sub-Boreal Pine – Spruce biogeoclimatic zone by 2016.

The number for the Very Dry Very Cold subzone of the Montane Spruce zone was only 54.8%. The VRI data shows that the lodgepole pine became the dominant tree species in many clearcuts in the subzone. The Very Dry Cold subzone of the Sub-Boreal Pine - Spruce zone was an exception: only 18.8% of 1986 and 1987 clearcuts fully recovered by 2016 in this part of the study area, according to the UC-Change metrics. According to the VRI dataset, trembling aspen became the dominant (14.3% of clearcuts) or common (accounting for 10% or more trees in 42.9% of clearcuts) species in most clearcuts in this subzone, and very few clearcuts reached a crown closure of 25% or higher 28 years after being harvested. Seral deciduous stands are common in naturally regenerating cutblocks due to serotinous cones (most cutblocks in the study area were replanted with lodgepole pine).

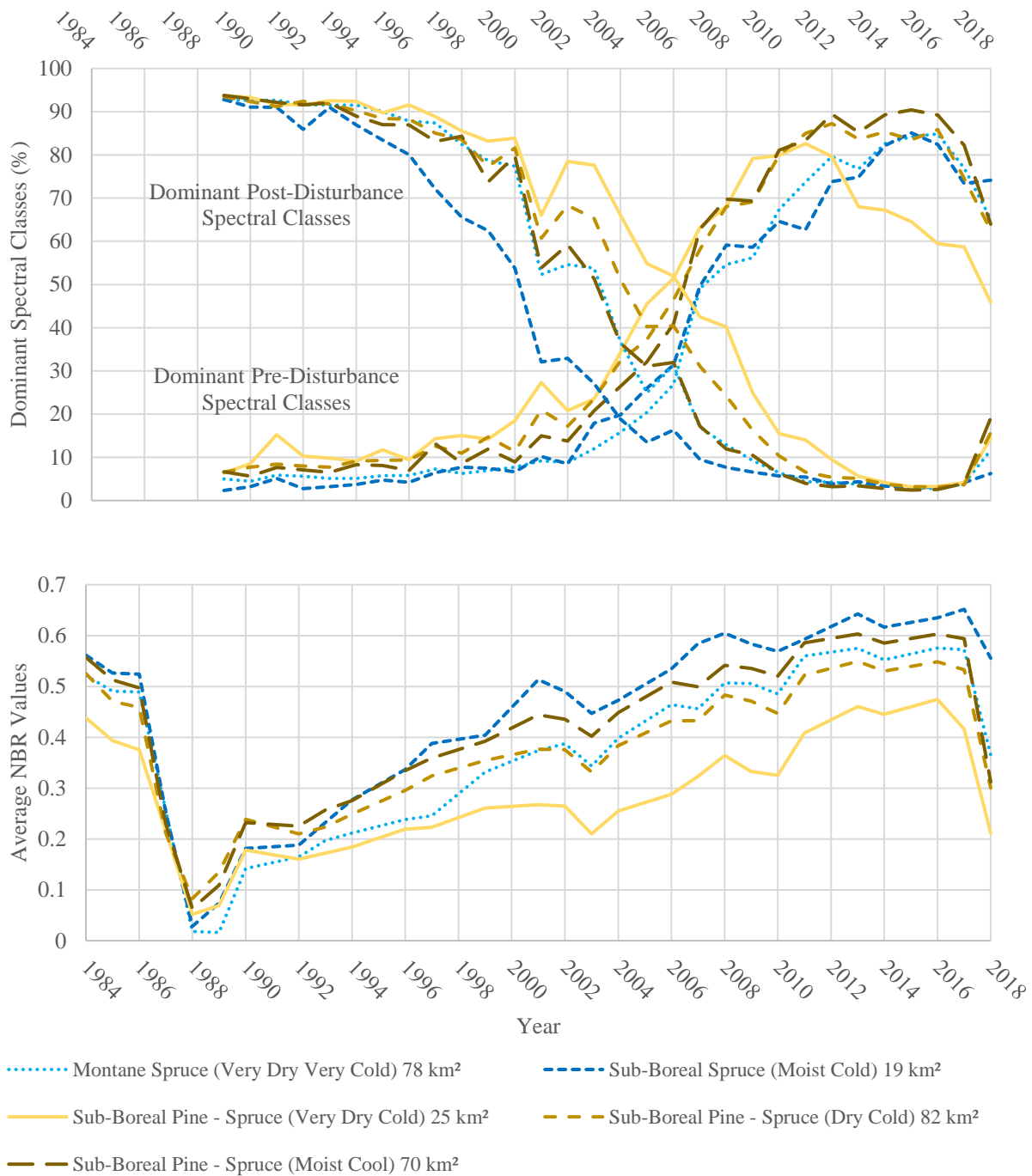


Figure 3-13. Forest recovery in 1986 and 1987 clearcuts per biogeoclimatic zone and subzone (in brackets; followed by the total area of 1986 and 1987 clearcuts in km²) as estimated using UC-Change forest recovery metrics (top) and average NBR values (bottom). Low 2017 and 2018 values are due to forest fires that affected recovering areas.

3.5. Discussion

3.5.1. Performance of the UC-Change technique

The UC-Change technique detected 85.4% of reference cutblock pixels at a temporal agreement of ± 1 year (90.4% at ± 3 years), outperforming all other techniques that were tested by a large margin. Somewhat lower detection of clearcuts in the 1974 – 1983 time period, for which only Landsat MSS data were available, can be attributed to several factors: lack of SWIR bands, image quality (e.g., low signal-to-noise ratio and large geometric errors), and low spatial resolution (57 m x 79 m resampled to 60 m). Only 76.3% of 1974 – 1984 cutblocks were detected and dated within ± 1 year from the corresponding VRI timestamps, while 85.1% were detected at a ± 3 -year accuracy, which indicates a delayed detection of affected clearcuts. These temporal inaccuracies in the UC-Change map were likely caused by the aggressive cloud masking that was applied to the input MSS data, which created large temporal data gaps between consequent observations.

The higher quality of Landsat 5 TM data and available cloud masks improved the temporal accuracy and overall detection of 1984 – 1998 disturbances. The addition of Landsat 7 ETM+ observations resulted in the highest agreement with the reference data, maintaining a detection rate close to 90% between the years 2000 and 2012.

The results after 2013 had lower accuracies, despite the availability of high-quality Landsat 8 OLI and Sentinel-2 data. This was likely due to the inability of the algorithm to detect multiple disturbances if they occur within the processing time window, which was four years in this study. In this case, a 2017 wildfire engulfed more than a third of the study area. Because of the 2017 fire, fewer stable pixels were detected in the 2013 – 2017 data, resulting in fewer primary change pixels and, consequently, secondary change pixels, because primary change pixels are

derived from stable pixels and secondary change pixels are derived using primary change pixels. Removal of post-2016 images from the dataset improved the detection of 2013 – 2015 clearcuts by 21.6%, confirming the hypothesis that the relatively low performance in this period was caused by the 2017 fire.

UC-Change detected relatively fewer reference forest fire pixels (72.0% at ± 1 year for the period 1987 – 2017) than reference cutblock pixels (86.5%), and this was expected. Compared to clearcuts, fire scars are heterogeneous and may contain unaffected trees, information that is not contained in the reference polygons. If the NBAC polygons represented only areas with fully burned canopies, the detection rate would likely be only slightly lower than that of cutblocks. The spatial distribution of spectral classes within fire scars continues to change months and even years following a fire, making it difficult to detect stable and, consequently, change pixels.

3.5.2. Comparison with existing change detection techniques and maps

The resulting UC-Change maps were considerably different from the maps produced with existing change detection methods. The most obvious difference was the total area mapped as disturbed. UC-Change, LandTrendr, C2C, and GFC mapped 2363 km², 1269 km², 1150 km², and 2865 km² as disturbed during the period of 2001 – 2015, respectively. Such a large difference can be partially explained by a MPB outbreak in the 2000s, which killed most lodgepole pine trees in the area (BC Ministry of Forests, 2020). The GFC map shows the MPB damage, whereas the UC-Change map and the available C2C map do not. Based on visual interpretation, LandTrendr also detected some MPB-affected areas, but for a more accurate detection the change-duration threshold would need to be set to a higher value than the one used in this study (3 years), because MPB-affected stands undergo a more gradual, longer-duration decline than cutblocks (Liang *et al.*, 2014). However, detection of MPB damage itself was outside the scope of this Chapter and thesis.

Instead, the focus of the study was on the detection of cutblocks and fire scars, including salvage harvesting of MPB-affected stands.

The MPB outbreak can explain why the LandTrendr and C2C technique detected so few 2006 – 2015 reference cutblocks pixels (32.8% and 38.8% at a temporal agreement of ± 1 year, respectively). Salvage logging accounted for a significant proportion of wood harvested in the area during this period (Kurz *et al.*, 2008). Because many trees were already dead, the difference between pre- and post-harvest NBR values in MPB-affected stands was too low for LandTrendr and C2C to detect cutblocks. However, it is noteworthy that compared to UC-Change these techniques also detected fewer reference cutblock pixels before the outbreak. LandTrendr and C2C mapped 73.3% and 67.8% of 1985 – 1999 VRI cutblock pixels at a ± 1 -year agreement, whereas UC-Change mapped 83.6%. This indicates that UC-Change was more capable at detecting cutblocks, at least partially due to its ability to use more spectral bands and approximately double as many images per year (June – September imagery vs July and August).

In comparison to other methods, UC-Change showed a much more consistent performance over both time and space. The performance of the technique was unaffected by the MPB outbreak. In many respects, this is especially interesting as it illustrates the robustness of the UC-Change approach in terms of the cutblock detection. Intuitively, it could easily be expected that not accounting for major disturbance such as MPB would impact other disturbance detection; however, that was not the case.

UC-Change also performed very well in the Very Dry Cold subzone of the Sub-Boreal Pine - Spruce biogeoclimatic zone, where the other three techniques (LandTrendr, C2C, and GFC) struggled the most. Due to the low soil moisture and stand density, undisturbed forest stands in

this part of the study area have relatively low NBR values, making clearcuts and forest fires harder to detect for techniques that rely exclusively on this spectral index, such as LandTrendr and C2C.

One of the main advantages of the UC-Change technique is its flexibility. It can use datasets containing any number of images per year and any number of bands per image. Because the technique can use data acquired during any part of the growing season, the availability of cloud-free data was much less of an issue. June to September data provided a full coverage of the study area for most years in the time series. In contrast, the C2C map was produced using only data acquired during the peak of the growing season (July and August). This limitation likely affected the performance of the C2C algorithm in a negative way. For example, Hermosilla *et al.* (2015b) found that cloud-free July and August Landsat data covered only 85% of the forested area of Saskatchewan on average per year during the period 2000 to 2010. Considering Saskatchewan is the sunniest province in Canada (Saskatchewan Research Council, 2014), July and August data coverage for interior British Columbia, where the study area is located, was likely lower, especially for the years 1984 to 1998, for which only Landsat 5 TM imagery was available. This may be the reason why LandTrendr, being a very similar technique to C2C, detected 10.7% more reference cutblock pixels during this period. LandTrendr used a slightly wider date range (June 20 – September 10) than C2C, and therefore, had more data to fill gaps in yearly image composites. However, UC-Change still detected 29.4% more cutblock pixels for the same period than LandTrendr when only July and August data were used (79.7% vs. 61.5%) instead of June 1st – September 20th data (84.5%), which indicates that the narrow date range used by LandTrendr and C2C was a significant but not the most important factor that affected their ability to detect forest harvesting.

Using protected areas, such as provincial parks, to quantify commission errors helped identify a problem in the current version of the UC-Change algorithm. Most false detections in the UC-Change map were found in wetlands, where spectral changes resulting from interannual variation in water levels and precipitation were often misidentified as forest disturbances. Coincidentally, most parks in the study area were established around large lakes and contain many wetlands. As a result, there were relatively more errors of commission in parks than in the rest of the study area. Based on a visual analysis, false detections in other maps (LandTrendr, C2C, and GFC) occurred mostly in forested areas and were more evenly spread out throughout the study area. Therefore, it was not surprising that the UC-Change map had more commission errors in parks (2.55% of the total park area) than C2C (0.06%) and LandTrendr (1.79%).

3.5.3. Forest recovery monitoring

Existing change detection techniques use spectral indices to track forest recovery. It took ~20 years for most clearcuts in the study area to fully recover their average NDVI and NBR values. These pixel-based metrics can be useful for monitoring disturbed areas from a purely economic standpoint. From this point of view, what matters the most is whether a disturbed area becomes a free-growing stand and, eventually, reaches a stocking target or, on the contrary, degrades to a not-satisfactorily-restocked (NSR) area (i.e., an area where there is not enough commercially valuable trees). For example, White et al. (2018) found that a metric named Years to Recovery (Y2R), defined as the number of years it takes for a pixel to reach 80% of its pre-disturbance NBR value, provided a realistic way to detect the re-establishment of forest cover, defined in the study as an area with canopy cover > 10% and tree height > 5 m. UC-Change has a completely different approach to monitoring forest recovery. It uses two metrics, the percentage of dominant pre- and post-disturbance spectral classes, to monitor recovery, and this is performed

at the object level. These object-based metrics make it possible to track changes in stand composition, which is a crucial determinant of forest recovery from an ecological perspective (Foster *et al.*, 1998; Reyes and Kneeshaw, 2008; Chen *et al.*, 2009; Ilisson and Chen, 2009; Bartels *et al.*, 2016). The rate at which clearcuts regain their pre-disturbance composition of spectral classes depends in part on the number of classes the classifier is set to generate; however, even at 10 classes, UC-Change offers more realistic measures of forest recovery compared to spectral indices as it uses all spectral bands that the user chooses to include in data processing (rather than only two). The new metrics in UC-Change take longer to saturate (up to 30 years) than NDVI and NBR (10 - 20 years). Most importantly, they capture differences in the recovery rate between different forest types. For example, stands dominated by the lodgepole pine showed a faster recovery in the UC-Change map than spruce stands, which was expected based on the literature (Armit, 1966; Burton *et al.*, 1999). This capability that UC-Change provides is very important to forest management, both for sustainability and for improved harvest planning.

Interestingly, the percentage of dominant pre-disturbance classes for many clearcuts plateaued or even declined before reaching 90%. There are several factors that could explain this. Clearcuts in northern forests often become populated with deciduous trees (Brumelis and Carleton, 1988; Carleton and MacLellan, 1994; Brassard and Chen, 2006). This makes clearcutting different from wildfires, which promote the regeneration of coniferous species (McRae *et al.*, 2001; Harvey *et al.*, 2014). Analysis of high-resolution Google Earth and Bing imagery produced by DigitalGlobe, as well as VRI data, revealed that some disturbed areas indeed became overgrown with deciduous species. However, most cutblocks in the study area met a completely different fate, becoming monocultural lodgepole pine plantations. Such plantations grow fast but do not have the stand composition and structure of the native forest they replace. In addition, lodgepole

pine plantations are often affected by various biotic agents, resulting in high mortality (Mather *et al.*, 2010). Both lodgepole pine plantations and seral deciduous stands often have a different composition of spectral classes in unsupervised classification maps compared to the original undisturbed forest, and this is the reason why UC-Change metrics did not reach their pre-disturbance values in these areas.

3.6. Conclusions

The UC-Change technique represents a new approach to forest disturbance mapping. As the name suggests, the technique uses classified images to detect and date stand-replacing disturbances, as well as monitor post-disturbance vegetation recovery, which makes it primarily independent of spectral resolution and data type, be it radiance or reflectance. For the same reason, the algorithm can use any number of spectral bands of any sensor to detect disturbances, unlike many existing change detection methods that use only one or two bands. The technique is also very flexible in terms of requirements to the temporal resolution of input data. While other methods either use only mid-summer data (e.g., LandTrendr and C2C use July and August data; Kennedy *et al.*, 2010; Hermosilla *et al.*, 2015a) or require all available data to achieve good results (i.e., every single available image between January 1st and December 31st; Verbesselt *et al.*, 2010; Zhu and Woodcock, 2014), the proposed method can use any number of non-winter images. Therefore, data availability is much less of an issue for UC-Change compared to these two approaches. Furthermore, unlike existing classification-based methods, UC-Change is an unsupervised algorithm that requires little user input⁹.

⁹ Parameter adjustment may be required when applying the algorithm to new geographical areas.

The new UC-Change approach is based on three steps. Images classified with an unsupervised classifier are used in the first step to detect a small number of highly accurate change pixels that are then used as training data in a series of multitemporal supervised classifications in the second step. The third step is object-based and filters clusters of change pixels based on their pre- and post-disturbance spectral class composition. This step not only removes false positives, but also provides information on forest recovery and can help classify changes by disturbance type (e.g., forest fire, clearcut, or road).

This Chapter has presented results produced using a very challenging study region and datasets. The dataset consisted of Landsat and Sentinel-2 data acquired over an area south of Prince George, British Columbia. The area contains diverse forests ranging in species composition and canopy cover, from sparse and dry pine-dominated forests in the south to dense spruce-dominated forests in the north. Overall, UC-Change detected 85.4% of the reference 1974 – 2017 clearcut pixels and 72.0% of the reference 1987 – 2017 fire scar pixels at a temporal agreement of ± 1 year (90.4% and 73.2% at ± 3 years, respectively). The resulting UC-Change maps were compared with a map generated using an open-source version of the LandTrendr algorithm, as well as with the C2C and GFC maps available online. Within the period of 1985 – 2015, the proposed technique detected 87.8% and 84.8% more reference clearcut pixels and 23.6% and 19.2% more reference forest fire pixels when compared to the C2C and LandTrendr maps, respectively. It also outperformed the GFC technique by 24.0% and 19.9% in clearcut and fire scar detection, respectively, in the period of 2001 – 2017.

The UC-Change technique detected the vast majority of 1972-1984 clearcuts using Landsat MSS data (85.1% at ± 3 years), showing that MSS data could be quite valuable for time series studies. However, the quality of MSS data is inconsistent, requiring manual image selection.

Therefore, it is recommended that data providers improve image quality (including reprocessing older archive data), as well as cloud and cloud shadow detection and geometric correction algorithms, particularly for Landsat 1 - 4.

The UC-Change algorithm uses two object-based metrics to derive information about forest recovery: percentage of dominant pre- and post-disturbance spectral classes inside spatial clusters of change pixels (see also Figure 3.8). While many factors affect the distribution of spectral classes (e.g., unmasked clouds and cloud shadows, seasonality, and spectral properties of data), the study showed that the two metrics can provide useful information about long-term changes in stand composition, which is a crucial determinant of forest recovery. Another strength of the UC-Change metrics is that they do not saturate as quickly as spectral indices used by other change detection methods. Unlike spectral indices, the UC-Change metrics also follow different recovery patterns depending on forest type and they better capture differences in the actual growth rate.

UC-Change was applied for the detection of clearcuts and fire scars. It was not used to detect any mountain pine beetle damage, even though the study area had a major outbreak. For the algorithm to be able to detect a disturbance, the distribution of spectral classes must change dramatically between consecutive images. No such drastic changes were observed in the K-means classification maps used in this study for this ongoing MPB disturbance. This was not a concern, as it was not part of this study's goal. In fact, it is noteworthy that, given this level of other disturbance, the new UC-Change method could capture the disturbances of interest (forest harvest and fire scars) even in the presence of these other disturbance agents. This suggests the robustness of the approach given the greater complexity and number of disturbances present. If other types of

disturbance were of interest, the unsupervised classifier and subsequent steps could be designed to separate those disturbances, including with respect to their unique temporal signatures.

The two main limitations of the UC-Change technique are related to its scene-based nature and the size of the processing time window. First of all, large-area disturbances (e.g., a major forest fire), unmasked clouds, and agricultural land may affect the detection of disturbances in the surrounding areas, because they affect the distribution of spectral classes in the rest of the image. However, the iterative retraining step largely negates this problem, as it makes classification consistent among images. Secondly, the technique cannot detect a disturbance event if another disturbance occurred in the same area within a time period equal to or smaller than the length of the time processing window. It is expected that using a smaller time window (e.g., 2 years instead of 4 years) would improve the detection of repeat disturbances, but would also require more images. Fortunately, with new sensors available (e.g. two Sentinel-2 sensors, and others planned from many other programs internationally), this is not viewed as a problem and in fact provides even further rationale for using algorithms such as UC-Change that can better take advantage of these data, while being designed to ingest data with different properties and attributes.

The next research steps with UC-Change include testing it over even larger areas (e.g., the entire province of British Columbia), with further algorithm refinements, such as change attribution, automatic parameter adjustment, and support for data of various spatial resolution without resampling (e.g., 10-m and 20-m Sentinel-2 data). False detection of change in wetlands is also an issue that needs to be addressed. In addition, it is worth investigating if a different, perhaps custom classifier could be used instead of K-means for the initial unsupervised classification to improve the separation of disturbed and undisturbed forest and reduce the processing time.

The flexibility and robustness of UC-Change may also create synergies with other powerful approaches, such as improved topographic correction (Soenen *et al.*, 2005, 2008, 2010), canopy reflectance modeling including work in mountainous terrain with various sensors (e.g. airborne, Landsat, MODIS, and others), applied to various types of forest disturbance (e.g. fire, MPB, partial harvesting), as improvements to classification (e.g. large area unsupervised cluster labeling) and involving considerable new algorithm development with a focus on automated methods (Peddle *et al.*, 2003, 2004, 2011), as well as possible linkages to other time series approaches, such as the development of temporal mixture analysis (TMA: Piwowar *et al.*, 1998) and applications involving other longer time series assessments of multiple disturbances (Chowdhury *et al.*, 2021).

3.7. References

- AAFC (2020). Annual crop inventory 2017. Agriculture and Agri-Food Canada. http://www.agr.gc.ca/atlas/data_donnees/agr/annualCropInventory/tif/2017/ [Accessed on 2020-10-30].
- Armit, D. (1966). Silvics and silviculture of lodgepole pine in the North Central Interior of British Columbia. *Research Notes (Forest Service, Department of Lands, Forests and Water Resources, British Columbia)*, 40.
- Axelson, J. N., Alfaro, R. I., & Hawkes, B. C. (2009). Influence of fire and mountain pine beetle on the dynamics of lodgepole pine stands in British Columbia, Canada. *Forest Ecology and Management*, 257(9), 1874-1882.
- Banskota, A., Kayastha, N., Falkowski, M. J., Wulder, M. A., Froese, R. E., & White, J. C. (2014). Forest monitoring using Landsat time series data: a review. *Canadian Journal of Remote Sensing*, 40(5), 362-384.
- Bartels, S. F., Chen, H. Y., Wulder, M. A., & White, J. C. (2016). Trends in post-disturbance recovery rates of Canada's forests following wildfire and harvest. *Forest Ecology and Management*, 361, 194-207.
- BC Ministry of Forests (2020). History of mountain pine beetle infestation in B.C. The Ministry of Forests, Lands, Natural Resource Operations and Rural Development of British Columbia <https://www2.gov.bc.ca/assets/gov/farming-natural-resources-and->

- [industry/forestry/forest-health/bark-beetles/history_of_the_mountain_pine_beetle_infestation.pdf](#) [Accessed on 2020-10-30]
- BEC (2020). Biogeoclimatic Ecosystem Classification program. The Ministry of Forests, Lands, Natural Resource Operations and Rural Development of British Columbia. <https://www.for.gov.bc.ca/hre/becweb/> [Accessed on 2020-10-30].
- Brassard, B. W., & Chen, H. Y. (2006). Stand structural dynamics of North American boreal forests. *Critical Reviews in Plant Sciences*, 25(2), 115-137.
- Brumelis, G., & Carleton, T. J. (1988). The vegetation of post-logged black spruce lowlands in central Canada. I. Trees and tall shrubs. *Canadian Journal of Forest Research*, 18(11), 1470-1478.
- Burton, P. J., Kneeshaw, D. D., & Coates, K. D. (1999). Managing forest harvesting to maintain old growth in boreal and sub-boreal forests. *The Forestry Chronicle*, 75(4), 623-631.
- C2C (2019). Satellite forest information for Canada. Canadian Council of Forest Ministers. https://opendata.nfis.org/mapserver/nfis-change_eng.html [Maps downloaded on 2019-02-10].
- Carleton, T. J., & MacLellan, P. (1994). Woody vegetation responses to fire versus clear-cutting logging: a comparative survey in the central Canadian boreal forest. *Ecoscience*, 1(2), 141-152.
- Chen, H. Y., Vasiliauskas, S., Kayahara, G. J., & Ilisson, T. (2009). Wildfire promotes broadleaves and species mixture in boreal forest. *Forest Ecology and Management*, 257(1), 343-350.
- Chowdhury, S., Peddle, D. R., Wulder, M. A., Heckbert, S., Shipman, T. C., & Chao, D. K. (2021). Estimation of land-use/land-cover changes associated with energy footprints and other disturbance agents in the Upper Peace Region of Alberta Canada from 1985 to 2015 using Landsat data. *International Journal of Applied Earth Observation and Geoinformation*, 94, 102224. DOI: <https://doi.org/10.1016/j.jag.2020.102224>
- Cohen, W. B., Yang, Z., Healey, S. P., Kennedy, R. E., & Gorelick, N. (2018). A LandTrendr multispectral ensemble for forest disturbance detection. *Remote Sensing of Environment*, 205, 131-140.
- De Sy, V., Herold, M., Achard, F., Asner, G. P., Held, A., Kellndorfer, J., & Verbesselt, J. (2012). Synergies of multiple remote sensing data sources for REDD+ monitoring. *Current Opinion in Environmental Sustainability*, 4(6), 696-706.
- ECCC (2020). Canadian Protected and Conserved Areas Database (CPCAD). Environment and Climate Change Canada (ECCC), Government of Canada. <https://www.canada.ca/en/environment-climate-change/services/national-wildlife-areas/protected-conserved-areas-database.html> [Accessed on 2020-10-30].
- Foster, D. R., Knight, D. H., & Franklin, J. F. (1998). Landscape patterns and legacies resulting from large, infrequent forest disturbances. *Ecosystems*, 1(6), 497-510.

- GFC, 2020. Hansen Global Forest Change v1.7 (2000-2019). Google Earth Engine. https://developers.google.com/earth-engine/datasets/catalog/UMD_hansen_global_forest_change_2019_v1_7 [Accessed on 2020-10-30].
- Hall, R. J., Skakun, R. S., Metsaranta, J. M., Landry, R., Fraser, R. H., Raymond, D., Gartrell, M., Decker, V., & Little, J. (2020). Generating annual estimates of forest fire disturbance in Canada: The National Burned Area Composite. *International journal of wildland fire*, 29(10), 878-891.
- Hansen, M. C., & Loveland, T. R. (2012). A review of large area monitoring of land cover change using Landsat data. *Remote Sensing of Environment*, 122, 66-74.
- Hansen, M. C., Potapov, P. V., Moore, R., Hancher, M., Turubanova, S., Tyukavina, A., Thau, D., Stehman, S. V., Goetz, S. K., Loveland, T. R., Kommareddy, A., Egorov, A., Chini, L., Justice, C. O., Townshend, J. R. G. (2013). High-resolution global maps of 21st-century forest cover change. *Science*, 342(6160), 850-853.
- Hansen, M. C., Roy, D. P., Lindquist, E., Adusei, B., Justice, C. O., & Altstatt, A. (2008). A method for integrating MODIS and Landsat data for systematic monitoring of forest cover and change in the Congo Basin. *Remote Sensing of Environment*, 112(5), 2495-2513.
- Harvey, B. J., Donato, D. C., & Turner, M. G. (2014). Recent mountain pine beetle outbreaks, wildfire severity, and postfire tree regeneration in the US Northern Rockies. *Proceedings of the National Academy of Sciences*, 111(42), 15120-15125.
- Hermosilla, T., Wulder, M. A., White, J. C., Coops, N. C., & Hobart, G. W. (2015a). Regional detection, characterization, and attribution of annual forest change from 1984 to 2012 using Landsat-derived time-series metrics. *Remote Sensing of Environment*, 170, 121-132.
- Hermosilla, T., Wulder, M. A., White, J. C., Coops, N. C., & Hobart, G. W. (2015b). An integrated Landsat time series protocol for change detection and generation of annual gap-free surface reflectance composites. *Remote Sensing of Environment*, 158, 220-234.
- Hermosilla, T., Wulder, M. A., White, J. C., Coops, N. C., Hobart, G. W., & Campbell, L. B. (2016). Mass data processing of time series Landsat imagery: pixels to data products for forest monitoring. *International Journal of Digital Earth*, 9(11), 1035-1054.
- Hill, R. A., Wilson, A. K., George, M., & Hinsley, S. A. (2010). Mapping tree species in temperate deciduous woodland using time - series multi - spectral data. *Applied Vegetation Science*, 13(1), 86-99.
- Huang, C., Goward, S. N., Masek, J. G., Thomas, N., Zhu, Z., & Vogelmann, J. E. (2010). An automated approach for reconstructing recent forest disturbance history using dense Landsat time series stacks. *Remote Sensing of Environment*, 114(1), 183-198.
- Hughes, M. J., Kaylor, S. D., & Hayes, D. J. (2017). Patch-based forest change detection from Landsat time series. *Forests*, 8(5), 166.

- Ilisson, T., & Chen, H. Y. (2009). Response of six boreal tree species to stand replacing fire and clearcutting. *Ecosystems*, 12(5), 820-829.
- Kennedy, R. E., Cohen, W. B., & Schroeder, T. A. (2007). Trajectory-based change detection for automated characterization of forest disturbance dynamics. *Remote Sensing of Environment*, 110, 370 – 386.
- Kennedy, R. E., Yang, Z., & Cohen, W. B. (2010). Detecting trends in forest disturbance and recovery using yearly Landsat time series: 1. LandTrendr—Temporal segmentation algorithms. *Remote Sensing of Environment*, 114(12), 2897-2910.
- Kennedy, R. E., Yang, Z., Braaten, J., Copass, C., Antonova, N., Jordan, C., & Nelson, P. (2015). Attribution of disturbance change agent from Landsat time-series in support of habitat monitoring in the Puget Sound region, USA. *Remote Sensing of Environment*, 166, 271-285.
- Kennedy, R. E., Yang, Z., Gorelick, N., Braaten, J., Cavalcante, L., Cohen, W. B., & Healey, S. (2018). Implementation of the LandTrendr algorithm on Google Earth Engine. *Remote Sensing*, 10(5), 691.
- Key, C. H., & Benson, N. C. (2006). Landscape assessment (LA). In: Lutes, Duncan C.; Keane, Robert E.; Caratti, John F.; Key, Carl H.; Benson, Nathan C.; Sutherland, Steve; Gangi, Larry J. 2006. FIREMON: Fire effects monitoring and inventory system. Gen. Tech. Rep. RMRS-GTR-164-CD. Fort Collins, CO: US Department of Agriculture, Forest Service, Rocky Mountain Research Station. p. LA-1-55, 164.
- Knudby, A., Newman, C., Shaghude, Y., & Muhando, C. (2010). Simple and effective monitoring of historic changes in nearshore environments using the free archive of Landsat imagery. *International Journal of Applied Earth Observation and Geoinformation*, 12, S116-S122.
- Kurz, W. A., Stinson, G., Rampley, G. J., Dymond, C. C., & Neilson, E. T. (2008). Risk of natural disturbances makes future contribution of Canada's forests to the global carbon cycle highly uncertain. *Proceedings of the National Academy of Sciences*, 105(5), 1551-1555.
- Lechowicz, M. J. (1984). Why do temperate deciduous trees leaf out at different times? Adaptation and ecology of forest communities. *The American Naturalist*, 124(6), 821-842.
- Leckie, D., Tinis, S., Henley, M., Eichel, F., Walsworth, N., Hardman, D., Burt, W., Dechka, J., Paradine, D., Landry, R., & Yuan, X. (2016). Deforestation and Forest Harvest Mapping with Integrated Automated and Manual Methods: Pilot Study Prince George, British Columbia, Canada (No. BC-X-438).
- Liang, L., Chen, Y., Hawbaker, T. J., Zhu, Z., & Gong, P. (2014). Mapping mountain pine beetle mortality through growth trend analysis of time-series Landsat data. *Remote Sensing*, 6(6), 5696-5716.
- Lu, D., Mausel, P., Brondizio, E., & Moran, E. (2004). Change detection techniques. *International Journal of Remote Sensing*, 25(12), 2365-2401.

- Mantovani, A. D. M., & Setzer, A. W. (1996). A Change Detection Methodology for the Amazon Forest Using Multitemporal NOAA/AVHRR Data and GIS—Preliminary Results. In *Remote Sensing and GIS for Site Characterization: Applications and Standards*. ASTM International.
- Mather, W. J., Simard, S. W., Heineman, J. L., & Sachs, D. L. (2010). Decline of planted lodgepole pine in the southern interior of British Columbia. *The Forestry Chronicle*, 86(4), 484-497.
- McRae, D. J., Duchesne, L. C., Freedman, B., Lynham, T. J., & Woodley, S. (2001). Comparisons between wildfire and forest harvesting and their implications in forest management. *Environmental Reviews*, 9(4), 223-260.
- NRCan (2020a). How much forest does Canada have? Natural Resources Canada. <https://www.nrcan.gc.ca/our-natural-resources/forests-forestry/state-canadas-forests-report/how-much-forest-does-canada-have/17601> [Accessed on 2020-10-30].
- NRCan (2020b). Deforestation in Canada—what are the facts? Canadian Forest Service Science-Policy Notes, May 2018. Natural Resources Canada. <https://cfs.nrcan.gc.ca/pubwarehouse/pdfs/28159.pdf> [accessed on 2020-10-30].
- NRCan (2020c). Top forest insects and diseases in Canada: Mountain pine beetle. Natural Resources Canada. <https://www.nrcan.gc.ca/forests/fire-insects-disturbances/top-insects/13381> [accessed on 2020-10-30].
- Pape, A. D., & Franklin, S. E. (2008). MODIS-based change detection for Grizzly Bear habitat mapping in Alberta. *Photogrammetric Engineering & Remote Sensing*, 74(8), 973-985.
- Peddle, D. R., Franklin, S. E., Johnson, R. L., Lavigne, M. B., & Wulder, M. A. (2003). Structural change detection in a disturbed conifer forest using a geometric optical reflectance model in multiple-forward mode. *IEEE Transactions on Geoscience and Remote Sensing*, 41(1), 163-166.
- Peddle, D. R., Huemmrich, K. F., Hall, F. G., Masek, J. G., Soenen, S. A., & Jackson, C. D. (2011). Applications of the BIOPHYS algorithm for physically-based retrieval of biophysical, structural and forest disturbance information. *IEEE Journal of Selected Topics in Applied Earth Observations and Remote Sensing*, 4(4), 971-982.
- Peddle, D. R., Johnson, R. L., Cihlar, J., & Latifovic, R. (2004). Large area forest classification and biophysical parameter estimation using the 5-Scale canopy reflectance model in Multiple-Forward-Mode. *Remote Sensing of Environment*, 89(2), 252-263.
- Piwowar, J. M., Peddle, D. R., & LeDrew, E. F. (1998). Temporal mixture analysis of Arctic sea ice imagery: a new approach for monitoring environmental change. *Remote Sensing of Environment*, 63(3), 195-207.
- Potapov, P. V., Turubanova, S. A., Hansen, M. C., Adusei, B., Broich, M., Altstatt, A., Mane, L., & Justice, C. O. (2012). Quantifying forest cover loss in Democratic Republic of the Congo, 2000–2010, with Landsat ETM+ data. *Remote Sensing of Environment*, 122, 106-116.

- Potapov, P. V., Turubanova, S. A., Tyukavina, A., Krylov, A. M., McCarty, J. L., Radeloff, V. C., & Hansen, M. C. (2015). Eastern Europe's forest cover dynamics from 1985 to 2012 quantified from the full Landsat archive. *Remote Sensing of Environment*, 159, 28-43.
- Potapov, P., Turubanova, S., & Hansen, M. C. (2011). Regional-scale boreal forest cover and change mapping using Landsat data composites for European Russia. *Remote Sensing of Environment*, 115(2), 548-561.
- Reyes, G. P., & Kneeshaw, D. (2008). Moderate-severity disturbance dynamics in *Abies balsamea*–*Betula* spp. forests: the relative importance of disturbance type and local stand and site characteristics on woody vegetation response. *Ecoscience*, 15(2), 241-249.
- Saskatchewan Research Council, 2014. Saskatchewan – Canada's sunniest province. The Saskatchewan Research Council, Canada. <https://www.src.sk.ca/blog/saskatchewan-canadas-sunniest-province>. [Accessed on 2020-10-30].
- Schroeder, T. A., Wulder, M. A., Healey, S. P., & Moisen, G. G. (2011). Mapping wildfire and clearcut harvest disturbances in boreal forests with Landsat time series data. *Remote Sensing of Environment*, 115(6), 1421-1433.
- Soenen, S. A., Peddle, D. R., & Coburn, C. A. (2005). SCS+ C: A modified sun-canopy-sensor topographic correction in forested terrain. *IEEE Transactions on Geoscience and Remote Sensing*, 43(9), 2148-2159.
- Soenen, S. A., Peddle, D. R., Coburn, C. A., Hall, R. J., & Hall, F. G. (2008). Improved topographic correction of forest image data using a 3-D canopy reflectance model in multiple forward mode. *International Journal of Remote Sensing*, 29(4), 1007-1027.
- Soenen, S. A., Peddle, D. R., Hall, R. J., Coburn, C. A., & Hall, F. G. (2010). Estimating aboveground forest biomass from canopy reflectance model inversion in mountainous terrain. *Remote Sensing of Environment*, 114(7), 1325-1337.
- Steinhaus, H. (1956). Sur la division des corp materiels en parties. *Bulletin de l'Acad'emie Polonaise des Sciences*, Classe III, 4(12), 801-804.
- Stueve, K. M., Housman, I. W., Zimmerman, P. L., Nelson, M. D., Webb, J. B., Perry, C. H., Chastain, R.A., Gormanson, D.D., Huang, C., Healey, S.P., & Cohen, W. B. (2011). Snow-covered Landsat time series stacks improve automated disturbance mapping accuracy in forested landscapes. *Remote Sensing of Environment*, 115(12), 3203-3219.
- Stumpf, A., Michéa, D., & Malet, J. P. (2018). Improved co-registration of Sentinel-2 and Landsat-8 imagery for earth surface motion measurements. *Remote Sensing*, 10(2), 160.
- Verbesselt, J., Hyndman, R., Newnham, G., & Culvenor, D. (2010). Detecting trend and seasonal changes in satellite image time series. *Remote sensing of Environment*, 114(1), 106-115.
- VRI (2020). VRI - Historical Vegetation Resource Inventory (2002 - 2018). The Ministry of Forests, Lands, Natural Resource Operations and Rural Development of British Columbia. <https://catalogue.data.gov.bc.ca/dataset/vri-historical-vegetation-resource-inventory-2002-2018-> [Accessed on 2020-10-30].

- White, J. C., Saarinen, N., Kankare, V., Wulder, M. A., Hermosilla, T., Coops, N. C., Pickell, P. D., Holopainen, M., Hyypä, J., & Vastaranta, M. (2018). Confirmation of post-harvest spectral recovery from Landsat time series using measures of forest cover and height derived from airborne laser scanning data. *Remote sensing of environment*, 216, 262-275.
- White, J. C., Wulder, M. A., Hermosilla, T., Coops, N. C., & Hobart, G. W. (2017). A nationwide annual characterization of 25 years of forest disturbance and recovery for Canada using Landsat time series. *Remote Sensing of Environment*, 194, 303-321.
- White, J. C., Wulder, M. A., Hobart, G. W., Luther, J. E., Hermosilla, T., Griffiths, P., Coops, N. C., Hall, R. J., Hostert, P., Dyk, A., & Guindon, L. (2014). Pixel-based image compositing for large-area dense time series applications and science. *Canadian Journal of Remote Sensing*, 40(3), 192-212.
- Wiken, E. B. (1986). *Terrestrial ecozones of Canada*. Environment Canada, Lands Directorate.
- Wulder, M. A., White, J. C., Luther, J. E., Strickland, G., Rimmel, T. K., & Mitchell, S. W. (2006). Use of vector polygons for the accuracy assessment of pixel-based land cover maps. *Canadian Journal of Remote Sensing*, 32(3), 268-279.
- Zhao, F., Huang, C., Goward, S. N., Schleeweis, K., Rishmawi, K., Lindsey, M. A., Denning, E., Keddell, L., Cohen, W. B., Yang, Z., & Dungan, J. L. (2018). Development of Landsat-based annual US forest disturbance history maps (1986–2010) in support of the North American Carbon Program (NACP). *Remote Sensing of Environment*, 209, 312-326.
- Zhu, Z. (2017). Change detection using landsat time series: A review of frequencies, preprocessing, algorithms, and applications. *ISPRS Journal of Photogrammetry and Remote Sensing*, 130, 370-384.
- Zhu, Z., & Woodcock, C.E. (2014). Continuous change detection and classification of land cover using all available Landsat data, *Remote Sensing of Environment*, (144):152-171.

CHAPTER 4

A COMPARISON OF THE UC-CHANGE AND C2C CHANGE DETECTION ALGORITHMS FOR MAPPING CUTBLOCKS AND ESTIMATING THE RATE OF FOREST HARVESTING IN BRITISH COLUMBIA, CANADA

Abstract

Two satellite-based forest change detection algorithms were evaluated for their ability to accurately map cutblocks and estimate the rate of forest harvesting. Generated maps were compared with forest inventories and official records for a large area (71 million ha) in the province of British Columbia, Canada, which has been subject to intense forest industry activity. The area covers multiple biogeoclimatic (BGC) zones and has a diverse terrain including several major mountain ranges. Our Unsupervised Classification to Change (UC-Change) technique and the Composite2Change (C2C) technique were used to map and date cutblocks that occurred between 1984 and 2015 using Landsat time-series data. The resulting maps were compared against the Vegetation Resources Inventory (VRI), the Consolidated Cutblocks (CC) dataset, and the National Forestry Database (NFD). VRI cutblock polygons were also used as validation data; they were produced by skilled interpreters based on stereo aerial photographs and reports from logging companies and, therefore, were expected to have a high spatial accuracy. The UC-Change algorithm detected 85.7% of reference cutblock pixels, whereas the C2C map had 69.5%. The former had a more consistent performance across BGC zones but was more sensitive to terrain slope and aspect conditions than the latter. It was estimated that the average rate of forest harvesting during the investigated time period and adjusted for commission and omission error was 251,000 ha/year (UC-Change) and 243,000 ha/year (C2C). This means that as much as 7.5 million ha of forest (33% of harvestable forest area in the province) were cleared between 1984

and 2015, well above the 6.7 million ha indicated by the VRI and CC datasets and 6.3 million ha derived from the NFD records. Based on this finding, the province may need to reduce the rate of timber extraction to meet its sustainability goals. The results show that highly automated techniques like UC-Change can detect cutblocks missing in forest inventory maps while providing temporally accurate information in a timely fashion and at no cost, although false detection is an issue that requires attention.

4.1. Introduction

Unlike deforestation, conversion of natural forests into managed forests has received far less attention, yet it has major effects on forest ecosystems. Clearcut harvesting, practiced in Canada (Bergeron and Fenton, 2012; Environmental Reporting BC, 2018a) and many other countries (Brassard and Chen, 2006; Lundmark *et al.*, 2013), results in even-aged stands that lack the diverse understory of old-growth forests and forests recovering from natural disturbances, such as fire¹⁰ and insect infestations (McRae *et al.*, 2001; Burton *et al.*, 2003; Bergeron and Fenton, 2012). Animal biodiversity is also much lower after clearcutting due to the lack of snags and coarse woody debris, which is a critical habitat component for small mammals (Carey and Johnson, 1995), birds (Carey *et al.*, 1991), and amphibians (Bury *et al.*, 1991; Corn and Bury, 1991). Accordingly, a better understanding of the scale and temporal dynamics of human-caused forest disturbances can facilitate the development of improved sustainable forest management practices. Given the vast areas and long time periods involved, this cannot be achieved without change detection techniques that use archive and current satellite image data to map and track changes in

¹⁰ High-intensity wildfires in forests dominated by lodgepole pine and other species with serotinous cones, which release seeds simultaneously when exposed to the heat of fire, may also produce even-aged stands, at least until subsequent disturbances (e.g., wind and insect infestations) transform them into more complex, multi-aged stands (Axelson *et al.*, 2009).

forest cover. Similarly, due to the large data volumes, areas, and time periods, it is not practical to do site-specific, manual satellite image analyses and, therefore, automated methods are required.

Mechanization and automation of the timber industry in the 1970s and 1980s caused a rapid growth in commercial harvesting of northern forests (Burton *et al.*, 2003; Environmental Reporting BC, 2018b). This dramatic expansion is well documented as it coincided with the launch of the first civilian Earth observation satellites. For example, the shape of individual cutblocks can be easily discerned in Landsat-1 Multispectral Scanner (MSS) imagery (nominal 57 m × 79 m spatial resolution; 18-day revisit; launched 1972). However, despite the long and continuous (i.e., with observations available for every year) record of satellite data acquisition, there are few detailed large-area maps of anthropogenic forest disturbances that are openly available today. Prior to the opening of the Landsat archive in 2008, satellite-based forest disturbance mapping was mostly limited to small-area medium-resolution (10 m – 100 m) or large-area but coarse-resolution (>100 m) studies (Banskota *et al.*, 2014; Zhu, 2017). Even today, the use of 1972 – 1983 Landsat data is hindered by the quality of data preprocessing (Wulder *et al.*, 2019). In contrast, the preprocessing of data acquired by Landsat 5 TM (launched in 1984) and newer sensors has been continuously improving (Zhu *et al.*, 2015; Qiu *et al.*, 2019a,b; Wulder *et al.*, 2019), resulting in analysis-ready imagery that can be used in multi-temporal studies without any additional or only minor preparation by the user.

Availability of free, geometrically-corrected and cloud-masked Landsat 5 TM and newer data (Landsat 7 and 8; Sentinel-2) created the opportunity and the need for the development of time-series change detection techniques that can automatically process vast amounts of remote sensing data to produce detailed forest disturbance maps. Two examples are the Composite2Change (C2C; White *et al.*, 2017) and the Global Forest Change (GFC; Hansen *et al.*,

2013) methods, which have both been used to produce 30m maps. The former shows stand-replacing forest disturbances (i.e., disturbances resulting in the removal of forest cover) that occurred between 1984 and 2015, while the latter is limited to the period 2000 – 2018.

Unsupervised Classification to Change (UC-Change) is a new approach that provides several important advancements and advantages and, thus, warrants a more extensive comparison with currently available products. In this Chapter, the UC-Change method was applied over the period 1984 – 2018 to assess stand-replacing disturbances at a spatial resolution of 30 m over a large area that contains almost all managed forests in British Columbia, Canada, and use the maps to estimate the rate of forest harvesting in the province (i.e., area harvested per year). The forest industry is vital to the economy of this province, producing an estimated \$18.4 billion (Canadian) of products and supporting more than 52 thousand jobs (Barnes, 2019; NRCan, 2020). Therefore, remote sensing data and techniques are required to monitor and promote sustainable use of forest resources.

A rigorous accuracy assessment of UC-Change map products was undertaken to estimate the rate of forest harvesting in the province (i.e., area harvested per year), with results compared to the Composite2Change (C2C) maps. The study area and dataset used provided a rare opportunity to conduct a thorough and challenging experiment, based on two main factors: 1) it presents a wide diversity of forest types, topography, and climate and, importantly, 2) it is one of the few regions for which highly detailed and extensive forest inventory data are available.

4.2. Study Area and Data

The study area encompasses 71 million ha of land and contains 99.98% of cutblocks that occurred in British Columbia between 1984 and 2015, based on the forest inventory data of

the province (VRI, 2020). The Pacific Ocean and several mountain chains create unusually diverse climatic conditions that support a wide variety of ecosystems, from dense temperate rainforests on Vancouver Island and along the mainland coast, to dry and sparse lodgepole pine forests in the interior of the province, as described in the Biogeoclimatic Ecosystem Classification system of British Columbia (BEC, 2020). The extent of the zones is shown in Figure 4-1, while Table 4-1 provides a description of each biogeoclimatic (BGC) zone in the study area (BEC, 2020).

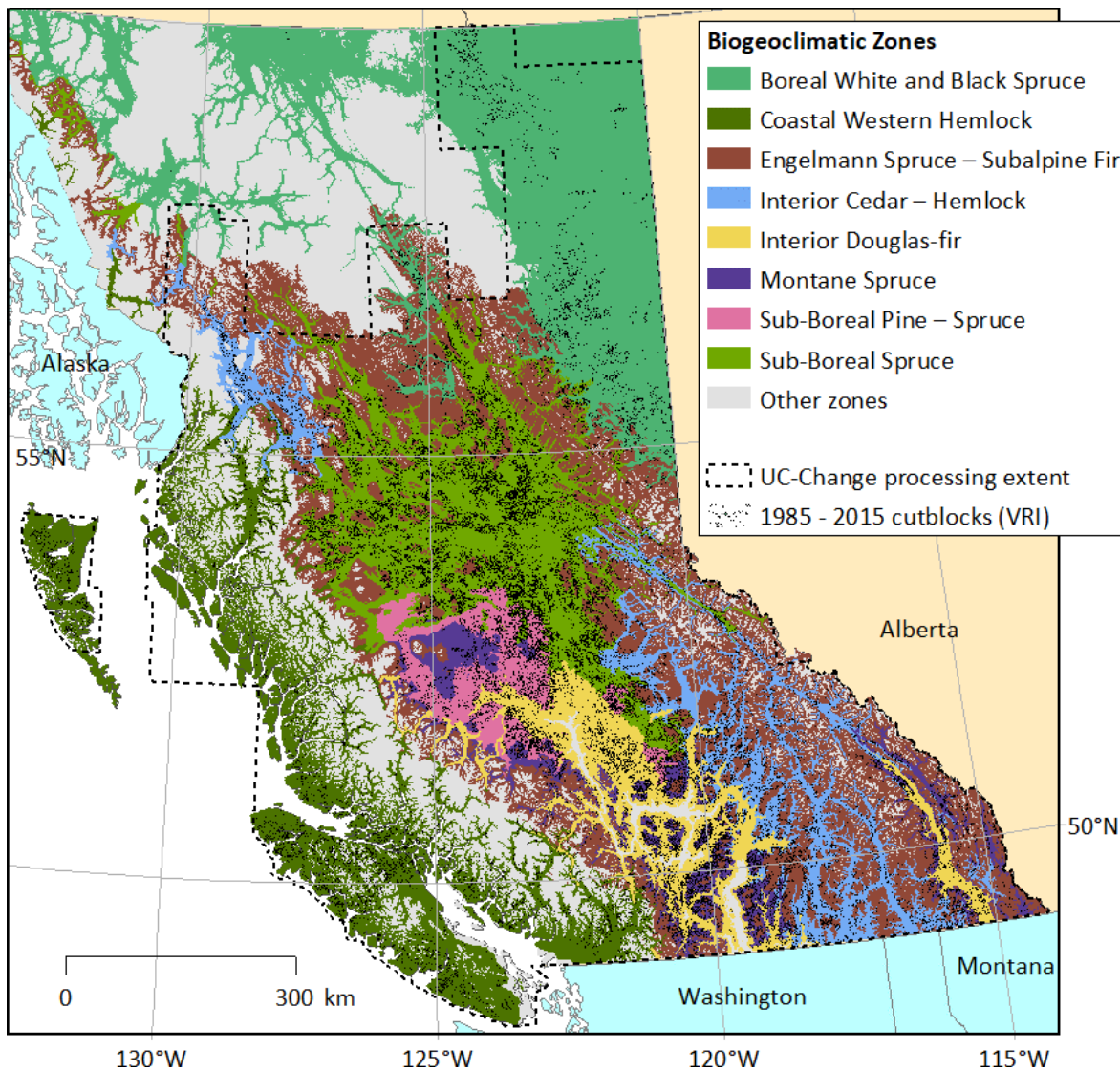


Figure 4-1. The extent of the study area (dashed line) and biogeoclimatic zones (based on BEC, 2020) in British Columbia. See also Table 4.1.

Table 4-1. The characteristics of forested BGC zones spanning the study area and information relevant to forest disturbance mapping (Meidinger and Pojar, 1991; BEC, 2020). Abbreviations: MAT – mean annual temperature (°C); MAP – mean annual precipitation (mm); MSP – mean summer precipitation (mm); Area – area occupied by the zone within the study area (km²); Slope – average terrain slope ± standard deviation (°); CS – average cutblock size (ha) calculated based on the Vegetation Resources Inventory data of British Columbia (VRI, 2020).

BGC zone	Climate	MAT	MAP	MSP	Area	Slope	CS	Dominant species and relevant information
Boreal	Cold	-1.8	455	220	103,109	3.9	33.7	White spruce, black spruce, lodgepole pine. Two main ecosystems: upland forests and muskeg.
White and Black Spruce (BWBS)	continental to hyper-continental with short summers	to 2.8	to 1297	to 403		± 5.8		Upland areas: mixed white spruce and aspen or black spruce and lodgepole pine. Mossy black spruce on wetter sites and open lodgepole pine – lichen on drier sites. White spruce and balsam poplar along rivers. Logging is difficult due to numerous wetlands and relies on hardwood species (e.g., trembling aspen and balsam poplar) more than in other zones. Primary anthropogenic disturbance: oil and gas industry.
Coastal Western Hemlock (CWH)	Sub-maritime to hyper-maritime with long, wet, and cool summers	3.4 to 9.3	1181 to 3416	262 to 859	100,007	20.3 ±14.1	13.2	Western hemlock, western red cedar. Highly diverse and productive forests with deep, multilayered canopy. Most of the forests are old. Wind is a common disturbance factor. Soil conservation is a concern due to intensive silvicultural practices, mountainous topography, and high precipitation.
Englemann Spruce – Subalpine Fir (ESSF)	Subalpine boreal with very short summers	-0.5 to 2.5	602 to 1659	246 to 561	158,419	19.8 ±11.9	21.2	Englemann spruce and subalpine fir forests occupying high elevations. 2 – 3-m deep snowpacks are common in winter.
Interior Cedar – Hemlock (ICH)	Continental with relatively long, cool to warm summers	1.9 to 6.7	569 to 1175	196 to 378	50,752	17.0 ±11.3	17.4	Western hemlock and western red cedar. High productivity and species diversity. Wildfires can occur frequently in drier parts of the zone, producing a mosaic of young and old forest patches.
Interior Douglas-fir (IDF)	Temperate with cool dry summers (3 – 5 months)	1.7 to 6.0	336 to 601	164 to 239	42,989	10.7 ±10.3	25.8	Douglas-fir. Historically frequent low-intensity forest fires kill young trees and understory, producing open, uneven-aged stands of Douglas-fir. Older trees of this species develop fire-resistant bark. Selective cutting with frequent thinning of low-vigour and high-risk trees leaves many older trees intact to provide shelter during regeneration and prevent fires. This practice is meant to replicate and replace the natural fire regime and was common in this zone in the 1980s and 1990s. Soil water deficits are common in summer.

Table 4-1. Continued...

BGC zone	Climate	MAT	MAP	MSP	Area	Slope	CS	Dominant species and relevant information
Interior Douglas-fir (IDF)	Temperate with cool dry summers (3 – 5 months)	1.7 to 6.0	336 to 601	164 to 239	42,989	10.7	25.8 ±10.3	Douglas-fir. Historically frequent low-intensity forest fires kill young trees and understory, producing open, uneven-aged stands of Douglas-fir. Older trees of this species develop fire-resistant bark. Selective cutting with frequent thinning of low-vigour and high-risk trees leaves many older trees intact to provide shelter during regeneration and prevent fires. This practice is meant to replicate and replace the natural fire regime and was common in this zone in the 1980s and 1990s. Soil water deficits are common in summer.
Montane Spruce (MS)	Continental with moderately short (2 – 4 months), warm summers	-0.2 to 3.2	527 to 960	200 to 271	28,231	10.5	30.7 ±9.6	Lodgepole pine and hybrid spruce (Engelmann + white spruce). Contains numerous wetlands. Extensive mountain pine beetle outbreaks result in a large amount of forest fuel. This and extended period of drought in summer often lead to large, stand-replacing fires, resulting in even-aged and even-sized canopies. Trembling aspen is a common seral species.
Sub-Boreal Pine – Spruce (SBPS)	Sub-continental with cool, dry summers	0.7 to 4.6	411 to 540	195 to 270	21,877	3.7	35.3 ±4.0	Lodgepole pine. Other species are rare. The climate favours plants that can tolerate frequent frosts and droughts. Trembling aspen is a common seral species in wetter areas. Historically, stand-replacing wildfires occurred approximately every 75–125 years, resulting in even-aged pine stands typically no older than 120 years. Although mountain pine beetle numbers are usually low, salvage harvesting yields a significant portion of extracted timber.
Sub-Boreal Spruce (SBS)	Mild continental with short but warm and moist summers	-2.0 to 0.4	500 to 949	196 to 373	91,821	6.5	30.3 ±6.4	Hybrid spruce (Engelmann + white spruce) and subalpine fir. Dense, productive coniferous forests with a developed understory. Wetlands are common.

4.2.1. Forest disturbance maps

The authors' UC-Change map was compared to the Composite2Change map (C2C; White *et al.*, 2017). The latter is the only other Landsat-based map available for the entire province that separates cutblocks from other forest disturbances and, therefore, it is the only available product for comparison that can be used for the purpose of this study (harvest rate estimation). The

two maps were produced using completely different time-series change detection algorithms, which are described briefly in the next sections.

4.2.1.1. Unsupervised Classification to Change (UC-Change) map

To detect changes, the UC-Change technique uses images classified with an unsupervised (K-means) classifier. This approach uses categorical data (spectral classes), similar to commonly used bi-temporal classification-based change detection techniques (e.g., Gregory *et al.*, 1981; Hall *et al.*, 1991; El-Hattab, 2016). However, instead of using image pairs, it employs a time-series approach, using hundreds of Landsat and Sentinel-2¹¹ images to locate clearcuts and forest fire scars in time and space. The approach is based on four steps. In Step 1, the algorithm identifies areas where spectral class boundaries do not shift spatially for some duration of time (e.g., four years). Such areas are labelled as stable. This is done for every image in the time series. Based on this rule, clearcuts are stable in 10-class K-means classification maps for up to 5 – 6 years. However, forest stands within that period that are subsequently harvested are considered as not stable. In Step 2, primary change pixels are identified for every image by subtracting stable pixels identified for preceding images from the current stable pixels. Only 40% to 50% of cutblocks and burned areas are detected this way with very few false positives. To improve the detection of disturbances, primary change pixels are used as training areas in a series of multitemporal Maximum Likelihood classifications in Step 3. Finally, Step 4 is object-based and filters spatial clusters of change pixels based on their pre- and post-disturbance spectral class

¹¹ Although Sentinel-2 imagery was used in addition to Landsat data to produce the original 1985 – 2019 map covering the Province of British Columbia, the map was then truncated to 1985 – 2015 to match the period covered by other maps in this study. Therefore, the addition of Sentinel-2 data had a negligible effect on the results.

composition. This step not only removes false positives, but also provides information on forest recovery and can help classify changes by disturbance type (e.g., forest fire and harvest).

The user must specify two parameters: the length of the time window and the number of classes for the K-means classifier. The length of time for the temporal processing window is selected based on the availability of cloud-free data to ensure that the algorithm can find overlapping images within the time window. The number of classes is selected to ensure that disturbances of interest remain homogenous for the duration equal to the length of the time window. For example, clearcuts remain homogenous for 4 – 6 years in 10-class K-means classification maps and 5 – 6 years in 8-class maps. Consequently, the algorithm used two settings depending on the availability of spatially overlapping images (in particular, the cloud-free portions of images): a 4-year time window and 10-class K-means classification or a 5-year window and 8-class classification. In most scenarios, both settings would produce nearly identical results. However, the second option produced better results in areas with frequent cloud cover at the cost of longer processing time. Other, less important parameters are discussed in Chapter 3.

The UC-Change technique currently can detect disturbance from both logging and wildfires but does not separate the two. Therefore, the National Burned Area Composite (NBAC) database was used to remove fire scar pixels in the UC-Change map (NBAC, 2020). To make the comparison of maps fair, this procedure was also applied to the C2C map.

4.2.1.2. Composite2Change (C2C) map

The C2C is a pixel-based technique that analyzes the temporal trajectories of individual pixels, breaking down those trajectories into straight-line segments representing pre-

disturbance, disturbance, and post-disturbance states (Hermosilla *et al.*, 2015b). The technique uses yearly image composites of the Normalized Burn Ratio, calculated as:

$$\text{NBR} = \frac{\text{NIR} - \text{SWIR2}}{\text{NIR} + \text{SWIR2}}, \quad (4-1)$$

where NIR and SWIR2 are surface reflectance values for the near-infrared and second short-wave infrared Landsat spectral bands, respectively. The composites were derived from cloud-free mid-summer (July and August) Landsat data. The difference between pre- and post-disturbance NBR values must exceed a user-defined change magnitude threshold. The C2C map currently available online shows forest fires and logging that occurred between July-August 1984 and July-August 2015 (C2C, 2019). Clouds, agriculture, and water bodies were masked out prior to data processing to reduce the false detection of clearcuts (Hermosilla *et al.*, 2016), similar to UC-Change.

4.2.2. Forest inventory map and protected areas as validation data

British Columbia's Vegetation Resources Inventory (VRI, 2020) data were used to assess the spatial and temporal accuracy of clearcut detection. VRI clearcut polygons were delineated and time-stamped using airphoto interpretation at a scale ranging between 1:10,000 and 1:15,000, together with ground sampling, and a reporting system, as described in Bourgeois *et al.* (2018). Because aerial photos for any particular area are acquired approximately once a decade, VRI data were expected to be very accurate and precise spatially but not always temporally. While VRI contains information about the majority of cutblocks in the study area, some information was lost during re-inventories or was not yet added due to delays in submission of information by logging companies (Bourgeois *et al.*, 2018). In addition, VRI data do not contain harvest date information for forest stands that were affected by wildfires after they were harvested. For these two reasons, two VRI datasets, released in 2015 and 2018, were combined to provide a more complete set of 1985-2015 reference clearcut polygons. The 2015 set had harvest date information

for cutblocks that were not yet affected by devastating wildfires in BC in 2017 and 2018, while the 2018 set contained many 2013 – 2015 cutblocks that were not included in the 2015 dataset. It is also noteworthy that while many clearcuts contain small patches of remaining trees, patches smaller than 0.5 ha were not captured in the VRI data (Bourgeois *et al.*, 2018). This could result in a slight overestimation of false negatives in this study.

The Canadian Protected and Conserved Areas Database (CPCAD) was used to evaluate general false detection of clearcuts in protected areas. Because commercial timber harvest is not allowed in provincial parks and other protected areas, all change pixels detected in such areas were labeled as false detections. Forest inventory data (VRI) confirmed almost no harvesting in protected area (logging occurred only on 0.01% of park area).

4.2.3. Other datasets

Forest harvest rates estimated based on the UC-Change and C2C maps were compared against those listed in the National Forestry Database (NFD) and calculated using the Consolidated Cutblocks (CC) dataset. The NFD is maintained by the Canadian Forest Service and contains data reported by logging companies (NRCan, 2014; NFD, 2020), while the CC dataset is updated by the Ministry of Forests, Lands and Natural Resources Operations of British Columbia (BC Ministry of Forests, 2020a). The CC dataset was designed to fill gaps in the VRI map, which is produced by the same agency. It mostly consists of VRI polygons, with the addition of polygons generated using Landsat data and the Reporting Silviculture Updates and Land status Tracking System (RESULTS). The Landsat part was carried out by a contractor and was based on bi-temporal change detection (SWIR-1 band ratios), followed by spatial segmentation and classification and, finally, manual editing (BC Ministry of Forests, 2020b). The Ministry checks at least 10% of Landsat-derived polygons, of which 95% must pass the inspection (personal

communication, C. Butson of the Ministry of Forests, Lands, Natural Resource Operations and Rural Development of British Columbia, Victoria, BC). A visual comparison of the VRI and CC datasets revealed that some cutblocks present in the VRI are absent in CC. For this reason, a combined dataset ($VRI \cup CC$) will also be used in this study. To produce $VRI \cup CC$, polygons unique to the CC map were added to the VRI map.

4.3. Experimental Design

Two factors needed to be considered when evaluating the temporal aspect of forest harvest detection. On the one hand, the detection lag can be as long as a year or more depending on the availability of usable data (e.g., cloud-free July and August data in case of C2C and June-September data in case of UC-Change). The detection lag is the offset between the acquisition date of the image in which a change is first detected and the actual date of the change. On the other hand, disturbance dates listed in the reference VRI dataset are sometimes inaccurate, as mentioned previously. Therefore, some disagreement between the maps and VRI data in terms of date of harvest can be expected.

To assess the spatio-temporal accuracy of the reference dataset (VRI), 500 randomly selected iVRI cutblock pixels were analyzed using the LandTrendr Pixel Time Series Plotter (Kennedy *et al.*, 2018; GEE, 2020). This algorithm was used to plot yearly NBR, red, NIR, SWIR-1 and SWIR-2 values derived from atmospherically corrected July and August Landsat composites. These plots were then visually analyzed to identify the actual time of disturbance (Figure 4-2). To compare the temporal accuracy of the VRI map and the change detection maps, another 200 pixels were randomly selected in iVRI cutblocks where there was a greater than 2-year disagreement with the UC-Change and C2C maps.

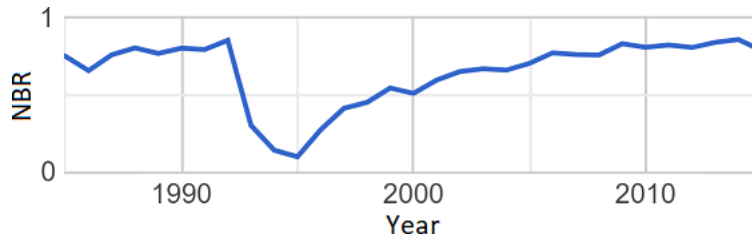


Figure 4-2. LandTrendr-generated NBR trajectory for a pixel in a clearcut dated 1993 in both the UC-Change and C2C maps and 1996 in the VRI. Based on the dramatic fall in NBR values, the forest was harvested some time between summer 1992 and summer 1993 (only July and August Landsat data were used to produce this plot). Therefore, the VRI timestamp was deemed incorrect.

VRI polygons accurately represent the full spatial extent of individual cutblocks and, therefore, make it possible to assess the detection of cutblock edges. Edge pixels present a problem when using 30-m Landsat data, as they contain a mixture of disturbed and undisturbed forest. As one way to handle this, a change detection algorithm could label such mixed pixels as either disturbed or undisturbed depending on which constituent contributes more than the other (i.e., more than 50% of a pixel). However, because disturbance events do not alter the spectral characteristics of mixed pixels as much as pure pixels, the detection of edge pixels depends more on user-defined thresholds and other parameters, such as the minimum number of image combinations in which a change pixel must be detected. In addition, remote sensing images contain positional or other geometric errors. Because change detection techniques use multiple images in large image stacks, geometric and registration errors across individual images may propagate and be compounded, further affecting the detection of clearcut edges while also potentially generating overlapping mixed pixels in terms of cutblock recognition in a time-series context. Depending on how a change detection algorithm handles boundary pixels, cutblocks may appear bigger or smaller in the map than they actually are. This affects total-harvest-area estimates.

To evaluate the detection of edge pixels, positive and negative 30-m buffers were applied to VRI polygons (Figure 4-3). The former produced polygons that will be referred to as

buffered VRI (bVRI), while the latter produced inner VRI (iVRI) polygons. Because the positional RMSE of Landsat 5 – 8 data is typically less than 12m (Wulder *et al.*, 2019), a buffer corresponding to the width of one Landsat pixel (30m) was chosen to eliminate the impact of geometric errors and account for inaccuracies caused by the mixed-pixel problem in this context. Importantly, the total area of all VRI polygons was 58,887 km² and the area of all iVRI polygons was 37,971 km², meaning that edge pixels account for 35.5% of rasterized VRI polygons on average. Therefore, accurate detection of edge pixels is extremely important if the goal is to produce accurate estimates of total harvested area.

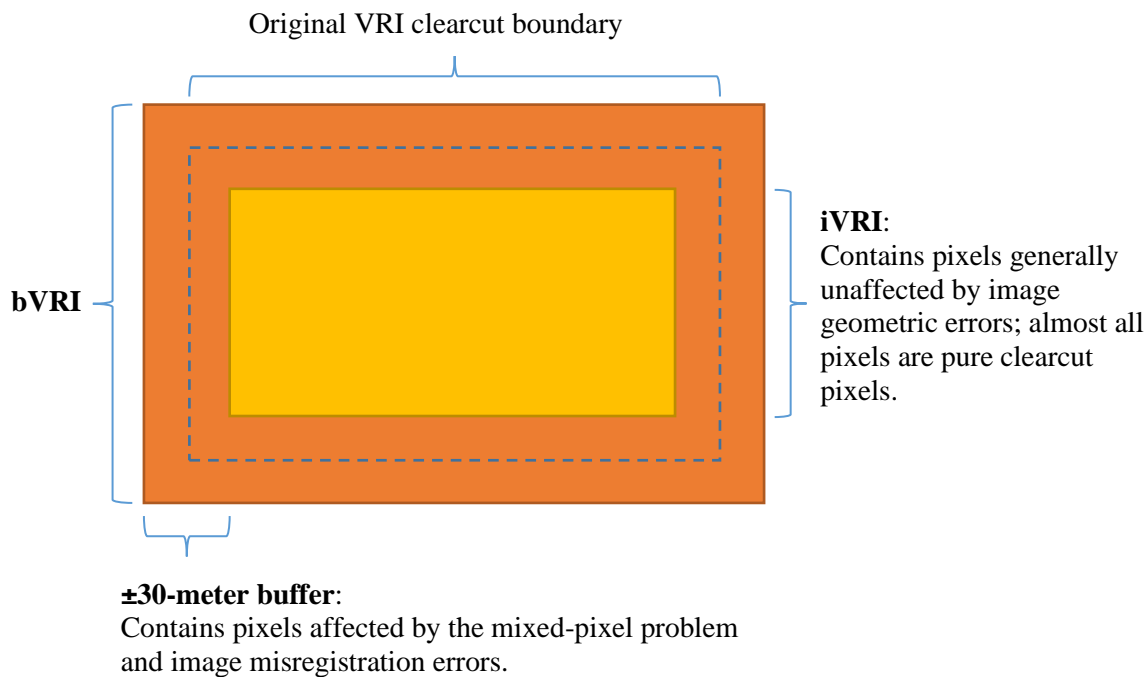


Figure 4-3. Positive and negative 30-m buffers were applied to each VRI clearcut polygon. The positive buffer allowed assessment of clearcut edge detections, which are subject to various geometric errors and the mixed-pixel problem. Inner VRI polygons (iVRI) were used to evaluate the ability of change detection techniques to detect pure clearcut pixels.

By comparing the detection of inner and edge pixels, it is possible to quantify whether cutblocks appear larger or smaller in the map compared to the corresponding VRI clearcut

polygons. The following formula compares the actual number of clearcut pixels detected in bVRI polygons with the number expected based on the detection of forest harvest pixels in iVRI polygons:

$$RSD_{\text{map/VRI}} = \frac{Ah_{\text{map}} \cap Ah_{\text{bVRI}}}{\text{Expected } Ah_{\text{map}} \cap Ah_{\text{bVRI}}} = \frac{Ah_{\text{map}} \cap Ah_{\text{bVRI}}}{(Ah_{\text{map}} \cap Ah_{\text{iVRI}}) \times \frac{Ah_{\text{bVRI}}}{Ah_{\text{iVRI}}}}, \quad (4-2)$$

where

$RSD_{\text{map/VRI}}$ is the relative size difference for cutblocks in the map and VRI data;

Ah_{map} is the total area mapped as harvested in the change detection map;

Ah_{VRI} , Ah_{iVRI} , and Ah_{bVRI} are the total areas of VRI, iVRI, and bVRI polygons;

$Ah_{\text{map}} \cap Ah_{\text{bVRI}}$ is the area inside bVRI polygons mapped as harvested; and

$Ah_{\text{map}} \cap Ah_{\text{iVRI}}$ is the area inside iVRI polygons mapped as harvested.

The more images used to derive a change map for a particular date, the more likely it was that geometric discrepancies among images resulted in inaccuracies in the detection of clearcut edges. For example, the UC-Change technique used nearly twice as much data for the period 1999 – 2015 compared to 1984 – 1998, whereas the C2C technique used one observation per year for all years. Therefore, the detection of clearcut edges was expected to be different depending on the period in the UC-Change maps, whereas in the C2C map, the level of error would be consistent across all years.

False detection caused by factors other than geometric errors and mixed pixels will be referred to as general commission errors. These errors typically occur in areas that have high inter-annual reflectance fluctuations, such as wetlands and mountainous areas near the snow line. General commission errors were evaluated using change pixels detected in protected areas, such as national and provincial parks. It was assumed that after a protected area was established, no forest harvesting occurred (Gawalko, 2004). A negative buffer of 30 m was applied to CPCAD

polygons to exclude errors already assessed using bVRI polygons. Commission errors were estimated for each year in the study period using parks established at least two years prior. For example, 37,683.7 km² of protected areas were used to assess false detections for the year 1985, and 90,426.0 km² (12.7% of the land area) for the year 2015.

Once the aforementioned factors are accounted for, it is possible to estimate the actual scale of forest harvesting in the study area. The harvested area estimates calculated from the C2C and UC-Change maps were adjusted based on the commission and omission error estimates using the following formula:

$$Ah = (Ah_{map} - \frac{Ah_{map} \cap A_{parks}}{A_{parks}} \times A_{study\ area}) \div \frac{Ah_{map} \cap Ah_{bVRI}}{Ah_{VRI}}, \quad (4-3)$$

where

Ah is the corrected estimate of the harvested area;

A_{parks} is the total area of protected areas;

$Ah_{map} \cap A_{parks}$ is the area inside protected areas mapped as harvested; and

$A_{study\ area}$ is the total land area in the study area. The part of the equation that is in brackets removes general commission errors, while the rest of the equation considers whether cutblocks in the map have smaller or larger area than the corresponding VRI polygons.

There are two main sources of error in estimates adjusted using Equation 4-3. First of all, this equation is based on the assumption that protected areas are representative of the whole study area in terms of general commission errors. However, this may not be the case, because most protected areas in BC were established in mountainous areas (the average terrain slope in protected areas was 20.5°, compared to 15.1° in the whole study area) and around water bodies. These areas contain dynamic land-cover types, such as wetlands and mountain glaciers. The spectral

characteristics of wetlands can change dramatically from year to year due to variation in water levels, and glaciers can retreat and advance. These spectral changes can be misidentified as forest disturbances. Therefore, relatively more false detections can be expected in protected areas than in the rest of the study area.

Another source of uncertainty in Equation 4-3 comes from the assumption that the VRI map is error free, which is also not true. For example, VRI polygons do not contain clearcut reserves smaller than 0.5 ha. There are also other errors in the VRI map, which will be evaluated in the next section.

Cutblock detection was evaluated for the entire study area and for each individual biogeoclimatic zone. This allowed to compare the performance of the UC-Change and C2C change detection techniques depending on forest type. The maps were expected to have lower accuracies in dry, open forests, where disturbance events produce less change in forest spectral characteristics.

Finally, to evaluate the effect of topography on the detection of clearcuts, VRI polygons were divided into four groups based on slope: 0° - 10° , 10° - 20° , 20° - 30° , and $>30^{\circ}$. Also, as an initial assessment of broad aspect influences on steeper slopes (clearcuts located on slopes $>30^{\circ}$), a second and preliminary assessment was conducted whereby results from two broad aspect classes were assessed and compared with those obtained without considering aspect at all. The aspect classes were designated simply as facing generally north ($<90^{\circ}$ and $>270^{\circ}$), or facing generally south (90° to 270°). These are very broad, general aspect classes and were selected to allow for an initial assessment of broad aspect influences, only. A digital elevation model with a base resolution of 0.75 arc-seconds (~ 25 m) was used to calculate slope and aspect (CDEM, 2013). These results are discussed in the next section.

4.4. Results

4.4.1. Evaluation of the VRI forest inventory map

Visual analysis of the temporal trajectories of 500 randomly selected 1988 – 2012 iVRI cutblock pixels revealed that 94.8% of them represented areas harvested between 1985 and 2015, whereas the remaining 5.2% were disturbed before 1985, after 2015, or showed no sign of disturbance. 95.1% of confirmed cutblock pixels had timestamps within ± 2 years of the harvest date identified using the LandTrendr Pixel Time Series Plotter (90.2% divided by 94.8%). This means that the VRI map and a change detection map produced using 1984 – 2015 data (e.g., the UC-Change or C2C map used in this study) cannot have a spatial agreement of more than 94.8% and a temporal agreement of more than 95.1%, unless there are commission errors common to both maps.

Table 4-2. Percent 1988–2012 iVRI pixels visually confirmed as cutblock pixels using the LandTrendr Pixel Time Series Plotter. The last column shows the total percentage of 1988 – 2012 iVRI cutblock pixels confirmed as 1985 – 2015 disturbances.

Forest Harvest Map	Difference between visually-determined dates and iVRI timestamps			
	± 1 year	± 2 years	± 3 years	1985 – 2015
iVRI	86.8%	90.2%	92.2%	94.8%

4.4.2. Evaluation of the UC-Change and C2C forest change maps

Overall, the UC-Change technique detected 85.7% of reference 1988 – 2012 iVRI cutblock pixels, whereas the C2C map contained only 69.5%. In both the UC-Change and C2C maps, 95.0% of the detected 1988 – 2012 iVRI cutblock pixels were dated within ± 2 years of the corresponding VRI timestamps (Table 4-3). Among the remaining 5.0%, it was the change detection maps that were more temporally accurate in 55% (UC-Change) and 57% (C2C) of cases,

whereas VRI timestamps were more accurate in 39% and 30% of cases, compared to UC-Change and C2C, respectively, based on 200 randomly selected sample pixels verified using the LandTrendr Pixel Time Series Plotter. This is consistent with the Landsat-based maps being more temporally accurate than the VRI map due to the fact that they were produced using data of much higher temporal resolution.

Table 4-3. Percent 1988 – 2012 iVRI clearcut pixels present in the UC-Change and C2C maps.

Forest Disturbance Map	Percent 1988–2012 iVRI pixels detected with a temporal agreement of			
	±1 year	±2 years	±3 years	±∞
UC-Change	76.6%	81.4%	83.0%	85.7%
C2C	61.5%	66.0%	67.4%	69.5%

UC-Change detected 84.2% of 1988–2012 VRI pixels with a spatial agreement of ±1 pixels and temporal agreement of ±2 years. In contrast, it detected 81.4% of iVRI pixels at ±2 years. In other words, UC-Change mapped more cutblock pixels inside bVRI polygons than what was expected based on the percentage iVRI pixels correctly mapped as harvested (Figure 4-4). Based on Equation 4-2, cutblocks were estimated 1.7% larger in the UC-Change map than in the VRI map in the period 1988 – 1998, for which only Landsat 5 TM imagery was used, and 4.6% larger in the period 1999 – 2012, where data from two sensors (Landsat 5 TM and Landsat 7 ETM+) were available (except 2012). This shows that the more images used per year, the more false positives were produced due to the mixed-pixel problem and image co-registration errors. Visual analysis confirmed this finding: clearcuts in the UC-Change map did appear bigger than the corresponding VRI polygons (Figure 4-5).

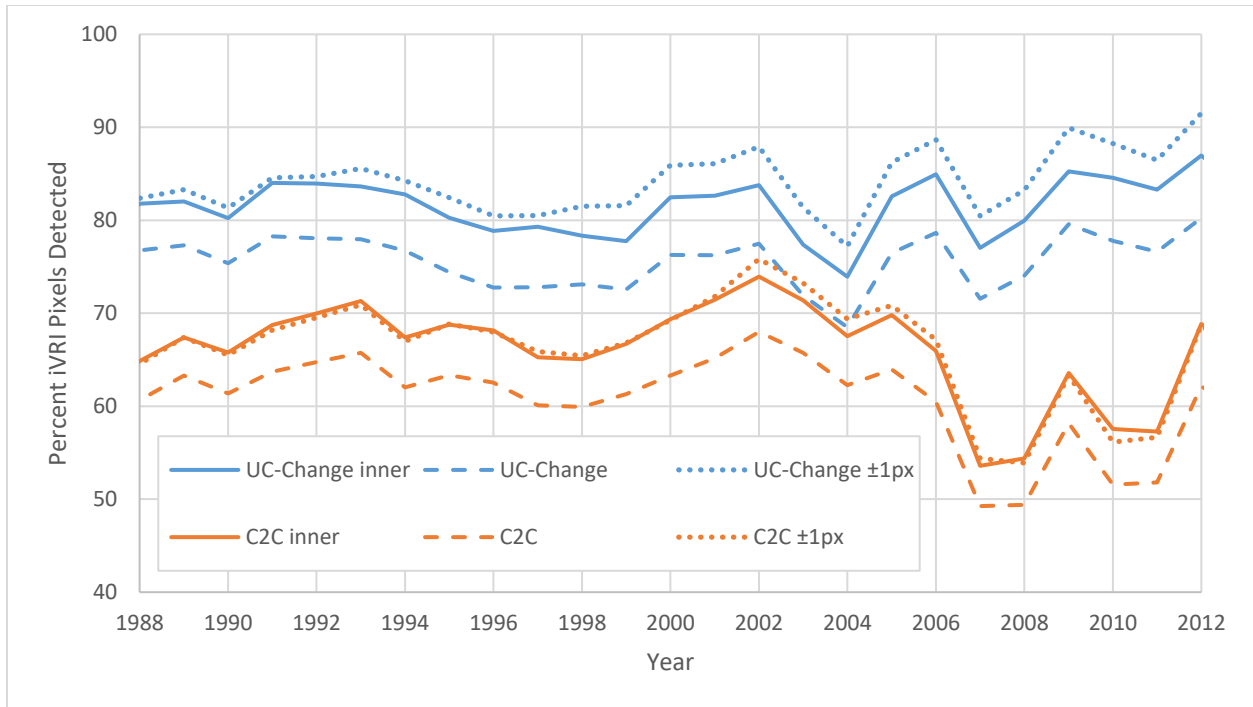


Figure 4-4. Percent reference clearcut pixels detected inside iVRI (e.g., UC-Change inner), VRI (UC-Change), and bVRI (UC-Change ± 1 pixel) polygons with a temporal agreement of ± 2 years, represented by solid, dashed, and dotted lines, respectively. If there were no geometric errors and mixed pixels were labelled accurately, the three lines per change detection technique would coincide. Using original VRI polygons for the assessment of clearcut detection produced the lowest numbers due to a misalignment between the map and reference dataset (VRI).

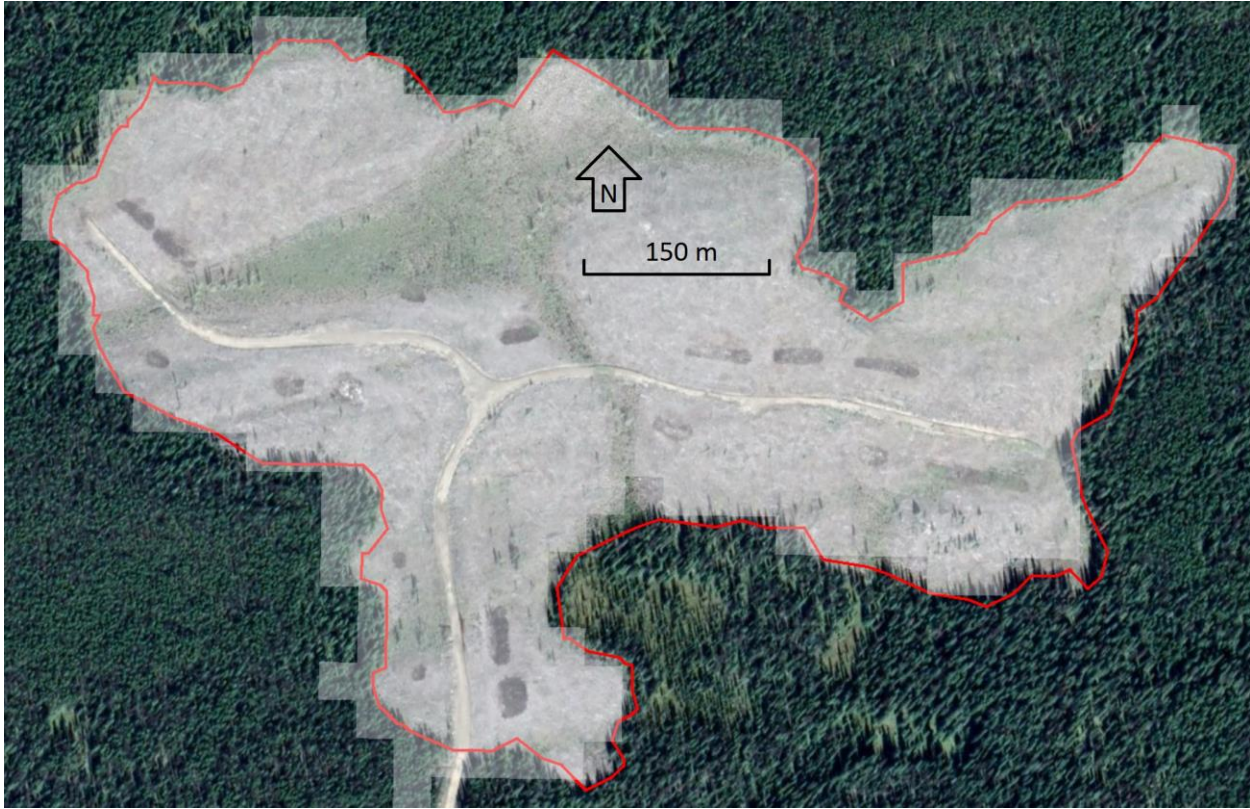


Figure 4-5. UC-Change map (translucent) and a VRI polygon (red) overlaid on top of a high-resolution Google Earth image (© Maxar Technologies). The size of the clearcut in the change map is clearly too large and the change pixels are shifted eastward relative to the actual location of the clearcut. This example illustrates false detection resulting from the mixed-pixel problem and image misregistration.

C2C mapped cutblock edges approximately as accurately as inner pixels (with respect to mixed pixels and co-registration errors). It mapped 66.2% of reference clearcut pixels at ± 30 m and a temporal agreement of ± 2 years. This number is very close to the percentage of iVRI pixels correctly mapped as harvested at ± 2 years (66.0%). Clearcuts appeared 0.2% smaller in the C2C map than the reference polygons for the years 1988-1998 and 0.7% larger for the years 1999 – 2012. However, the geographic location of clearcut pixels did not match that in the VRI map, because only 60.6% of clearcut pixels were detected in the original VRI polygons.

There were four times more false clearcut pixels in provincial parks and other protected territories in the UC-Change map than in the C2C map (0.82% of the total protected area vs. 0.19%; 0.01% in case of VRIUCC). Assuming the rate of false detection was consistent across the study area, given its larger size, these percentages would translate into as much as 5,809 km² and 1,347 km² of false “clearcuts” in the UC-Change and C2C maps, respectively, for the period 1984 - 2015. Most general commission errors in the UC-Change map were in fact unmasked fire scar pixels. This was not a problem for the C2C map because it contained accurate change type information. The current version of the UC-Change algorithm does not produce such information and the user has to rely on existing forest fire maps (e.g., NBAC) to separate cutblocks from fire scars. Some forest fires, such as the ones that occurred in Entiako Provincial Park and Tweedsmuir Provincial Park in 2001, were missing in the NBAC database and, therefore, were not masked out like most other fire scars, resulting in false positives. It is possible that this type of “error” attributed to UC-Change and C2C maps may in fact be a result of other similarly undocumented fires elsewhere in the NBAC database.

The accuracy of the UC-Change map was affected by slope (Figure 4-6). It detected 87.4%, 83.8%, 79.8%, and 74.7% of iVRI pixels on slopes ranging between: 0 – 10°, 10° – 20°, 20° – 30°, and > 30°, respectively. C2C was more consistent, detecting 67.9%, 72.7%, 71.8%, and 69.2%, respectively. Regarding aspect, from an initial assessment of broad aspect classes, both UC-Change and C2C found much fewer cutblock pixels on the generally more north-facing slopes (aspect: < 90° and >270°) than on the generally south-facing (aspect: 90° to 270°) slopes. UC-Change mapped 78.5% and 70.8% of forest harvest pixels on steep (>30°) south-facing and north-facing slopes, respectively, while C2C detected 72.9% on south-facing and 65.3% on north-facing slopes.

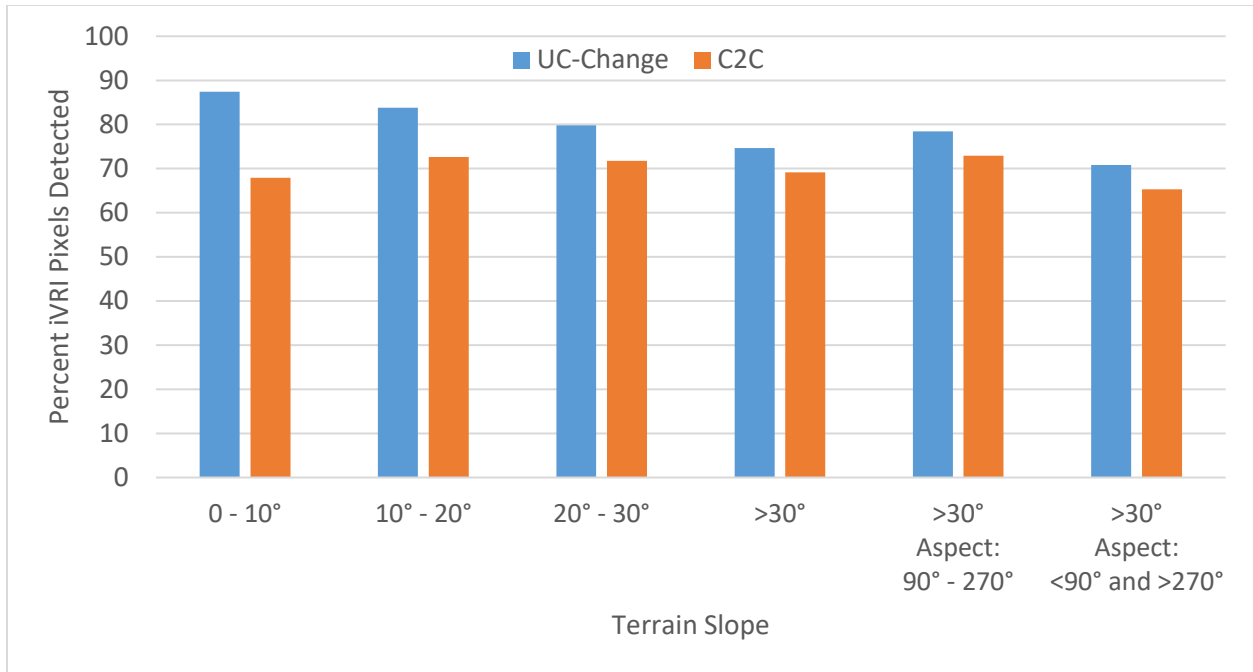


Figure 4-6. Percent iVRI clearcut pixels detected on different slope intervals for the years 1987 - 2013. An initial assessment of general terrain aspect was also done for steep slopes (>30°), as shown in the two right-most result sets.

The performance of the C2C technique varied greatly among BGC zones (Figure 4-7). It detected only 40.1% of iVRI pixels in the IDF zone, 51.1% in the SBPS zone, and 69.9% – 78.5% in other zones. The UC-Change map had higher accuracies in all cases compared with C2C, and was also more consistent, ranging between 82.9% and 90.7% in most zones except the IDF zone, where it detected only 68.3% of iVRI pixels (still a 28.1% improvement over C2C).

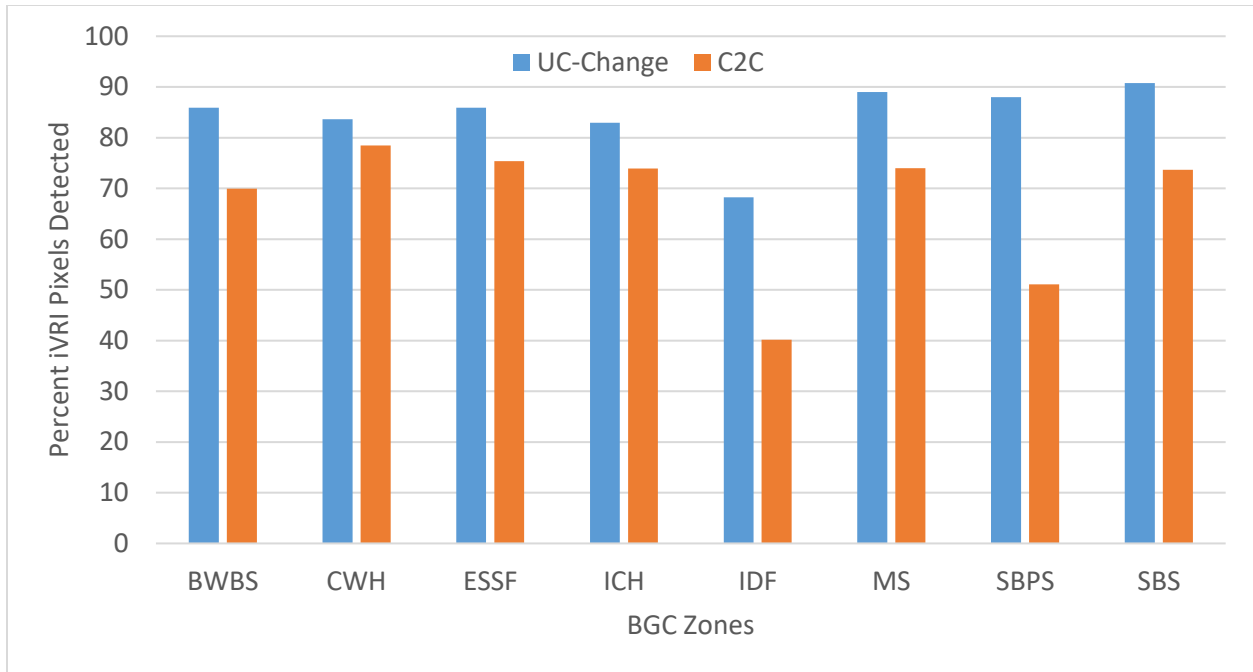


Figure 4-7. Percent iVRI clearcut pixels detected per BGC zone for the years 1987 - 2013.

4.4.3. Harvest rate estimation

All maps and datasets displayed very similar trends, with peak harvesting rates in the late 1980s, mid-2000s, and mid-2010s (Figure 4-8). Timber extraction rapidly increased in the second half of the 20th century due to mechanization and automation of the industry and peaked in the late 1980s, when it reached the Allowable Annual Cut (Burton *et al.*, 2003; Environmental Reporting BC, 2018b). The mid-2000s peak is also very distinct. During this period, the Allowable Annual Cut was increased to allow salvage and preemptive harvest in lodgepole pine forests affected by a major MPB outbreak (Kurz *et al.*, 2008). This was followed by a steep decline in harvest rates due to the global financial crisis of 2007 – 2008 (Masek *et al.*, 2011).

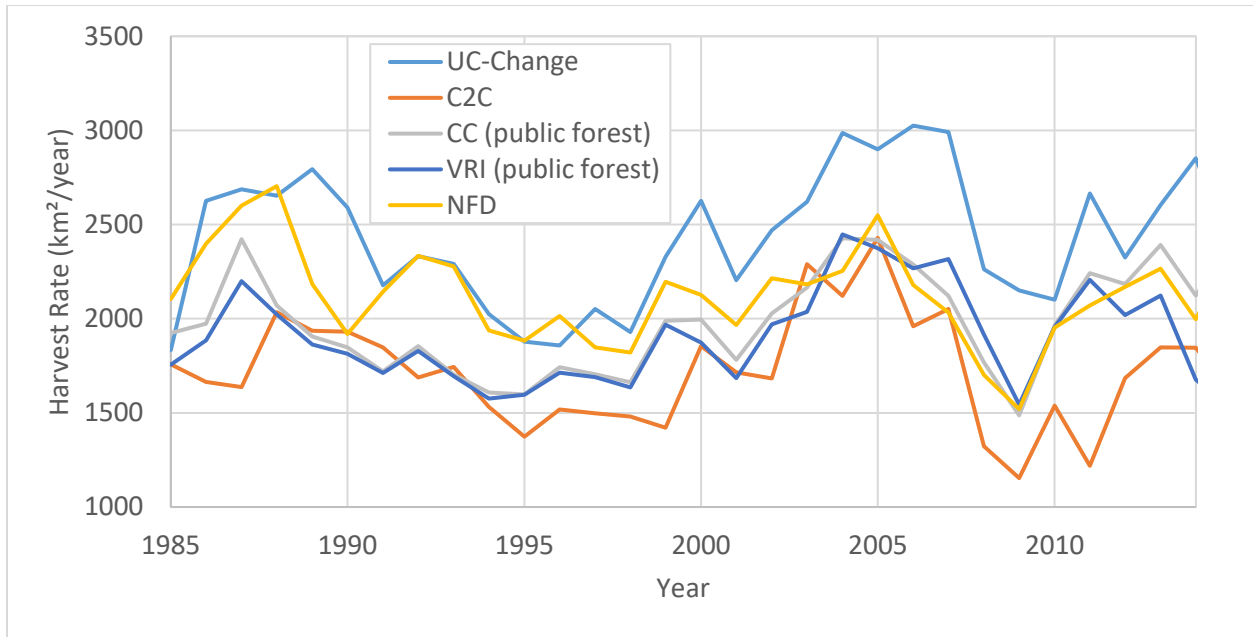


Figure 4-8. Forest harvest rates in British Columbia, estimated using five different sources.

The UC-Change map showed 40.6% higher average yearly forest harvest rates than the C2C map (2428 km²/year vs. 1726 km²/year). VRI, CC, VRI∪CC, and NFD showed intermediate numbers (1912 km²/year, 1970 km²/year, 2115 km²/year, and 2118 km²/year, respectively). The large discrepancy between the NFD dataset and the other two government datasets (VRI and CC) for the years 1985 – 2002 is noteworthy, even considering the fact that the VRI and CC maps do not contain information about privately owned forests and the NFD does.

Adjustment for commission and omission errors based on Equation 4-3 made the UC-Change and C2C results more similar: 2,513 km²/year and 2,425 km²/year, respectively (Figure 4-9). Assuming that logging in public forests accounted for approximately 95% of all logging by area in the province (BC Ministry of Forests, 2020c), a total average rate of 2,226 km²/year (2,115 km²/year divided by 0.95) can be calculated based on the VRI∪CC data. Resulting estimates of total harvested area derived from maps produced using automated change detection

algorithms (UC-Change and C2C) were 14.5% to 24.9% higher than the numbers taken from datasets developed by government agencies (VRI, CC, and NFD, individually) (Table 4-4).

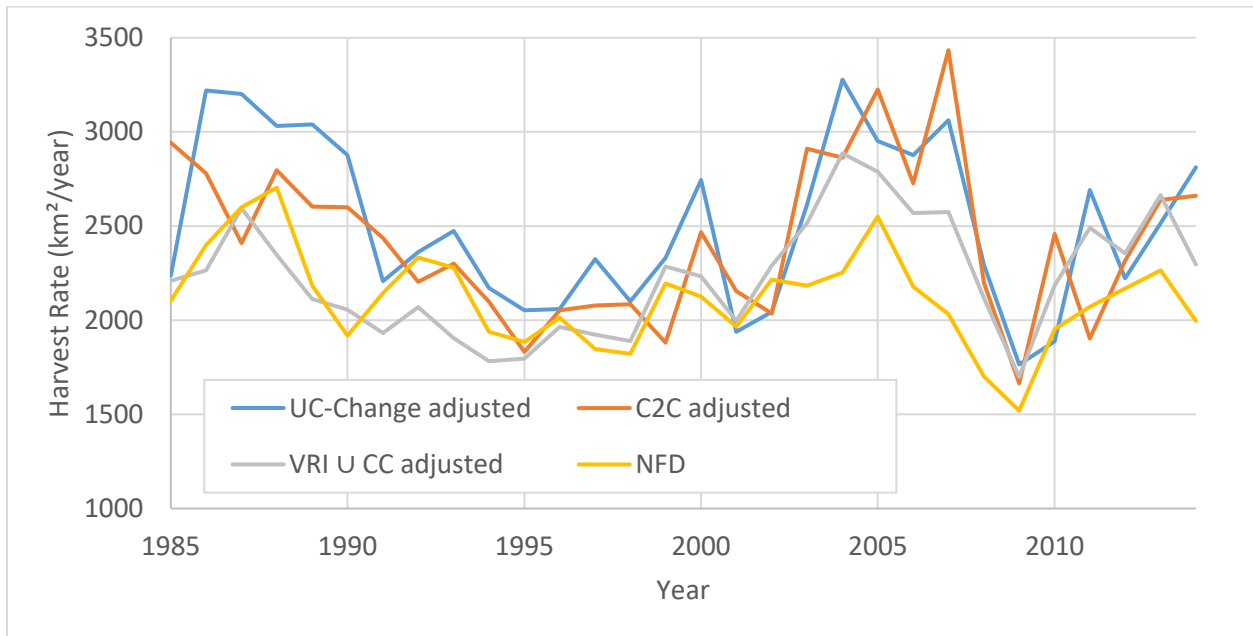


Figure 4-9. Forest harvest rate estimates with UC-Change and C2C results adjusted for commission and omission errors. The “VRI \cup CC adjusted” numbers were produced by merging VRI and CC maps and dividing the results by 0.95 to produced estimates for the entire province (the original VRI and C2C maps contain information about logging occurring on public lands only, which accounts for approximately 95% of all logging in the province).

Overall, 72,835 km² were harvested between June-September 1984 and June-September 2014, according to the UC-Change results (Table 4-4). The C2C map had 28.9% fewer cutblock pixels (51,780 km² for the period July-August 1984 – July-August 2014). However, adjustment for commission and omission errors produced similar estimates of 75,383 km² (UC-Change) and 72,758 km² (C2C). These estimates were much higher than the 63,543 km² derived from the NFD records (January 1985 – December 2014). The combined VRI \cup CC map showed 63,453 km² of cutblocks on public lands (January 1985 – December 2014). Assuming that 5% of logging in the province occurred on private lands (BC Ministry of Forests, 2020c), one can estimate a total of 67,000 km² based on this source.

Table 4-4. Total area (km²) and percent of BC forest (~55 million ha) harvested between 1985 and 2014 (inclusive). UCC = UC-Change.

	UCC	C2C	VRI	CC	NFD	UCC adjusted	C2C adjusted	$\frac{VRI \cup CC}{0.95}$
Area (km ²)	72,835	51,780	57,359	59,107	63,543	75,383	72,758	6.7×10⁴
% of BC forest	13	9	10	11	12	14	13	12

4.5. Discussion

4.5.1. VRI as validation data

British Columbia’s forest inventory data (VRI) proved to be a great source of reference data for the assessment and comparison of time series change detection products. The VRI dataset contains detailed spatial information about the vast majority of forest harvest activities in the province (i.e., hundreds of thousands of cutblocks). However, there are certain limitations given that this dataset was produced by visual interpretation of aerial photos. Because aerial photos are acquired approximately once a decade for any particular area in the province, they cannot be a source of accurate harvest date information. Instead, this information is provided by logging companies (BC Ministry of Forests, 2016). As a result, incorrect harvest dates were assigned to some VRI polygons. For example, the UC-Change technique detected 85.7% of cutblocks that were dated between 1988 and 2012 in the VRI map. However, when some VRI pixels were analyzed using the LandTrendr Pixel Time Series Plotter, it was found that 5.2% of the cutblocks they represented were actually cleared before 1984, after 2015, or showed no spectral changes and, therefore, could not be possibly detected in the 1984 – 2015 Landsat data that were used to produce the UC-Change map. Due to such temporal inaccuracies in the VRI dataset, using it as validation data can result in an underestimation of accuracy of change detection products.

Another reason why the UC-Change and C2C maps likely detected more cutblocks than what VRI data indicated is that VRI polygons do not show patches of forest smaller than 0.5 ha (5.5 Landsat pixels), which are present in many cutblocks. While clearcutting was by far the most common silvicultural practice in British Columbia in the 20th century, a method called “clearcutting with reserves” became widespread in the 2000s and accounted for 85% of logging on public lands in 2012 by area (Environmental Reporting BC, 2018a). This silvicultural system is similar to clearcutting but leaves patches of intact forest of various size called reserves. Based on the visual analysis of high-resolution Google Earth satellite imagery, many reserves are smaller than 0.5 ha and, thus, are not represented in the VRI map. Therefore, pixels in these reserves correctly labelled as undisturbed by a change detection algorithm may be flagged as false negatives if VRI polygons are used as reference data. This is yet another instance where the UC-Change product may in fact be more accurate than the VRI map.

Overall, the maps had a good temporal agreement with the forest inventory data. In total, 95% of cutblocks present in both UC-Change and VRI had similar harvest dates in the two maps (within two years). Among the remaining 5%, the UC-Change map had a higher temporal accuracy in the vast majority of cases. The same was true when comparing C2C and VRI data. This confirmed the finding that many VRI polygons had incorrect timestamps. This was not surprising as the change detection techniques used data of much higher temporal frequency than what was available to photo interpreters who delineated and dated VRI polygons.

4.5.2. False detection of cutblock pixels in the UC-Change and C2C maps

Cutblocks appeared larger in the UC-Change map than in the VRI and C2C maps. There were two main reasons for this. First of all, UC-Change classifies numerous combinations of multitemporal images to produce a change map for each date in the time series of satellite

images. For example, the algorithm used 5 - 15 different combinations of images for each date and tile in the period of 1984 – 1998, for which only Landsat 5 TM data were available, and 15 – 20 combinations for the years 1999 – 2015, where data from two sensors (Landsat 5 TM and Landsat 7 ETM+ or Landsat 7 ETM+ and Landsat 8 OLI) were available for all years except 2012. The UC-Change algorithm required that change pixels for a particular date were detected in at least two combinations of images. This allowed it to detect more change pixels and assign accurate harvest dates even to cutblocks that were obscured by clouds during the year of harvest. However, the more combinations of images were used to create a map for a particular date, the larger the clearcuts appeared in the UC-Change map due to misregistration errors among images (the spatial resolution was the same for all 1984 – 2015 Landsat 5 – 8 images). This is why 1999 – 2012 cutblocks were 4.6% bigger in the UC-Change map than the corresponding VRI polygons, whereas 1988 – 1998 cutblocks were “only” 1.7% larger. Setting a stricter threshold can solve this issue. For example, when change pixels for a particular date were required to appear in at least 20% of image combinations (instead of just 2 regardless the number of combinations), cutblocks were mapped almost true to their actual size. However, this also resulted in a proportionally reduced overall percentage of detected iVRI pixels. Using higher resolution data (e.g., 10-m Sentinel-2 data instead of Landsat’s 30 m) is one way to produce less excessive edge detection when using UC-Change without sacrificing producer’s accuracy.

Because the C2C algorithm used one observation per pixel per year, it was not surprising that cutblocks in the C2C map appeared close to their actual size in both periods (0.2% smaller than VRI polygons in the period 1988 – 1998 and 0.7% larger in 1999 – 2012). The difference for the two periods in this case can be explained by the change in silvicultural practices. Clearcutting was the dominant practice in the years 1988 – 1998. This practice was largely replaced

by the system called clearcutting with reserves. Because VRI polygons do not contain reserves smaller than 0.5 ha, using VRI polygons as reference data led to a slight overestimation of the relative size of cutblocks in both the C2C and UC-Change maps (see Equation 4-2).

The UC-Change map had more false cutblock pixels in national parks and other protected areas than the C2C map (0.82% vs. 0.19%). The UC-Change algorithm maps both forest harvesting activities and fire scars, but, unlike C2C, cannot yet separate the two types of disturbances effectively. An existing forest fire map (NBAC) was used to mask burned areas in the UC-Change map (NBAC, 2020). However, this resulted in false positives because some forest fires were missing in the NBAC map. Therefore, future efforts will focus on improving the ability of the UC-Change algorithm to classify change, as well as reducing false detections in dynamic land-cover types, such as wetlands and agricultural areas.

4.5.3. Effect of terrain slope and aspect on cutblock detection

The performance of UC-Change was more sensitive to terrain slope and aspect due to the algorithm's scene-based nature (as defined in §2.1.4). UC-Change processes data in tiles (i.e., original multispectral images are subset into 104 km × 104 km scenes¹²) and relies on a K-means algorithm to produce initial classification maps. In turn, K-means is sensitive to topography-related variation in reflectance and illumination because it assigns classes based on the absolute values of pixels (Section 3.3.1). One of the key requirements of the UC-Change technique is that undisturbed and recently disturbed forest are classified into different spectral classes. This is not always the case for tiles containing mountainous terrain because depending on the slope and aspect, cutblocks can be classified into the same spectral class as some forest types and vice versa. As a result,

¹² The tiling system used in this study is based on the one used for Sentinel-2 data (110 km × 110 km), but results in a smaller overlap among neighboring tiles (2 km on each side instead of 5 km). This system was used to avoid mosaicking of Sentinel-2 data.

UC-Change struggled to detect some clearcuts in mountainous areas. Using topographically corrected data (e.g., Soenen *et al.*, 2005, 2008) or including slope and aspect information in K-means classification should improve the spatial consistency of resulting classification maps and, therefore, improve the performance of the UC-Change technique in topographically diverse areas.

In contrast, C2C is a pixel-based technique, which means that the processing of one pixel is completely independent of the processing of other pixels. Therefore, it was expected to perform more consistently across different slope conditions. Analysis of results for the entire study area showed that C2C performed better on slopes ranging between 10° and 30° than $0 - 10^\circ$ and $>30^\circ$, indicating that other factors, such as forest type, likely had a greater role. However, from the general assessment of broad terrain aspect classes on steep ($>30^\circ$) slopes, the effect of terrain aspect was as strong in the C2C map (72.9% of cutblock pixels detected on south-facing slopes vs. 65.3% on north-facing) as it was in the UC-Change map (78.5% vs. 70.8%), however, as noted earlier, the fact these aspect classes are so broad means that only very general interpretations can be drawn from that preliminary analysis. North-facing slopes receive less sunlight than south-facing slopes in the Northern Hemisphere. SWIR bands are particularly affected, because there is less atmospheric scattering in the SWIR part of the electromagnetic spectrum than in the VNIR part. A stronger absorption of incident SWIR radiation by vegetation (due to oblique solar incidence angles) and soil moisture (due to relatively higher soil moisture on north-facing slopes; Macyk *et al.*, 1978; Gemmell, 1995) also contributed to relatively low pixel values. For this reasons, higher NBR values and smaller difference between pre- and post-disturbance NBR values on north-facing slopes than south-facing slopes would be expected (Verbyla *et al.*, 2008). Because C2C relies on NBR to detect change, it missed many cutblock pixels on north-facing slopes as pre- and post-disturbance values were not sufficiently different to meet the change threshold

requirement. Therefore, C2C should also benefit from topographic correction of data acquired over mountainous areas.

4.5.4. Effect of forest type and harvest practices on cutblock detection

UC-Change performed similarly across different BGC zones. Most of the variation can be explained by differences in topography rather than forest type. Out of the eight zones included in the analysis, the best UC-Change results were obtained in the four zones with the lowest average terrain slope values (BWBS, MS, SBPS, and SBS). However, the IDF zone stands out. UC-Change detected much fewer reference cutblock pixels in this zone compared to other zones (68.3% vs. 82.9% – 90.7% in other zones) despite the relatively even terrain. Selective (partial) harvesting was widely practiced in this zone in the 1980s and 1990s with the purpose of mimicking natural disturbances typical to the region (frequent low-intensity wildfires; Table 4-1). This type of harvesting is a non-stand-replacing forest disturbance (Figure 4-10) and, thus, is more difficult to detect in Landsat images than clearcuts and clearcuts with reserves. Frequent thinning in resulting partially harvested stands makes it even more difficult to accurately map the spatial extent of disturbances. The accuracy of forest harvest detection in this zone improved greatly in the 2000s and 2010s, when the province abandoned selective harvesting in favor of clearcutting with reserves (Environmental Reporting BC, 2018a). Similar to the use of improved terrain data (e.g. Soenen *et al.*, 2005, 2008), the incorporation of methods proven to be well suited for partial harvested forests (Peddle *et al.*, 2003) could be either integrated into UC-Change, or, owing to the flexibility of UC-Change to ingest multisource spatial products, the results from processing using those and related methods (e.g. Peddle *et al.*, 2004, 2011; Soenen *et al.*, 2010) could be utilized as an intermediate product for direct analysis by UC-Change. As C2C is less flexible for such inputs and multisource integration, those methods may not be compatible with C2C.



Figure 4-10. 1998 (bottom) and 1989 (middle) partial cuts (examples of selection management) next to a 2002 clearcut with reserves (top-left) as seen in a 2004 high-resolution Google Earth image. Location: 51°40'55"N, 121°51'12"W; Biogeoclimatic zone: IDF. Imagery © Maxar Technologies.

The performance of the C2C technique varied much more among BGC zones compared to the UC-Change technique. There are three main factors that affect the C2C algorithm: the magnitude of difference between pre- and post-disturbance NBR values; the length of time it takes NBR values to reach pre-disturbance levels; and availability of cloud-free data for July and August. For example, temperate rainforests in the CWH zone are characterized by very high pre-disturbance NBR values (0.7 – 0.8). C2C performed better in this zone than anywhere else in the province (78.5% of iVRI pixels detected vs. 40.1% – 75.4%) because the difference between pre- and post-disturbance NBR values was particularly large (Figure 4-11). In contrast, the SBPS zone had the lowest pre-disturbance NBR values (0.3 – 0.5) due to a combination of MPB, low canopy cover, and dry climate. Only 51.1% of reference cutblock pixels were detected in this zone by the C2C algorithm. Similar to UC-Change, C2C performed the worst in the IDF zone (40.1%) as post-disturbance NBR values were very high (i.e., similar to pre-disturbance levels) due to the selective harvesting method that was widely practiced in this zone in the 1980s and 1990s. Selective harvesting reduced the NBR of stands in the IDF zone from approximately 0.6 to only 0.4.

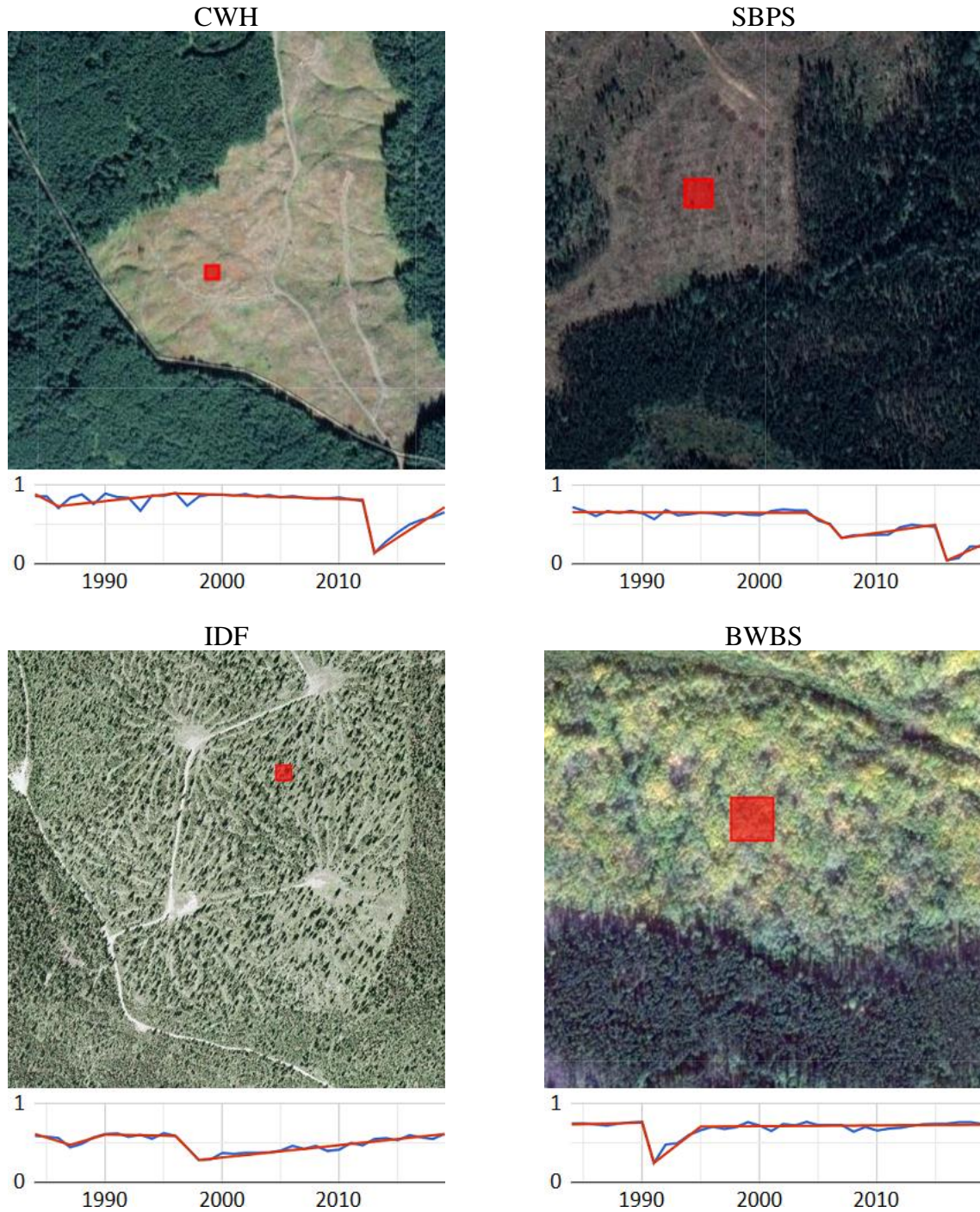


Figure 4-11. NBR trajectories (blue lines) of Landsat pixels (red squares in high-resolution Google Earth images; 30 m \times 30 m) in cutblocks representative of various BGC zones. Y-axis = NBR; X-axis = year. Red lines are LandTrendr-fitted segments. Imagery \copyright CNES / Airbus, Province of British Columbia, and Maxar Technologies.

While the difference between post- and pre-disturbance NBR values was relatively high in the BWBS zone (0.1 – 0.2 vs. 0.6 – 0.7), it typically only lasted 2 – 4 years. There are two factors that can explain such a fast spectral recovery: vegetative regeneration by remnant species and, secondly, the presence of mineral-rich soils (Bartels *et al.*, 2016). Many clearcuts in this zone occur in deciduous stands, where trees can quickly regenerate through root suckering, stem sprouting, and layering (Greene *et al.*, 1999; Bartels *et al.*, 2016). The C2C algorithm looks for long-lasting deviations in time series of NBR values and rejects short-term changes as noise. Because NBR values increased so quickly after disturbance in this zone, the C2C algorithm was unable to identify segments in the temporal profiles of pixels representing the disturbance event and post-disturbance recovery, which resulted in a poor cutblock detection (69.9%).

Availability of cloud-free data can also be an issue for the C2C technique as it can only utilize July and August data. The four BGC zones where C2C performed the worst (BWBS, IDF, SBPS, and SBS) have their wettest months in the summer, whereas other zones have the most precipitation in December or January. Data availability is much less of an issue for the UC-Change technique as it can use June to September imagery.

4.5.5. Accuracy of harvest rate estimation

UC-Change and C2C maps produced very different estimates of total harvested area in the province. The UC-Change map showed much higher rates of forest harvesting than official governmental reports and datasets (2,428 km²/year on average vs. 2,118 km²/year in the NFD), whereas the C2C map showed much lower rates (1,726 km²/year). White *et al.* (2017) found a similarly vast difference between a Canada-wide C2C map and NFD records but were not able to fully explain it, citing the lack of spatial information in the NFD dataset. The study presented in this Chapter used VRI data as reference data for the evaluation of cutblock detection. These data

contain detailed spatial information about the vast majority of cutblocks that occurred in the province during the investigated time period (1985 – 2014). Using VRI polygons, it was found that the C2C technique underestimated the rate of forest harvesting in the province because its performance was sensitive to forest type, biotic disturbance factors, and data availability.

There are two possible reasons why UC-Change estimates were higher relative to the other techniques. Firstly, the algorithm may have detected cutblocks unaccounted for in the NFD. Secondly, it is possible that commission errors may have been higher than what was estimated based on the VRI data and protected areas.

Overall, commission errors in the UC-Change map were largely offset by omission errors, resulting in more accurate forest harvest rate estimates compared to the C2C map. In addition, UC-Change demonstrated a consistent and predictable performance across the province independent on forest type. The main weaknesses of the algorithm, such as excessive mapping of cutblock edges, sensitivity to terrain slope and aspect, and misclassification of burned areas as clearcuts, can be addressed in the future to make UC-Change maps even more reliable.

4.6. Conclusions

This Chapter has compared forest harvest rate estimates for the Province of British Columbia based on four different sources: 1) maps generated by automated time-series change detection algorithms from Landsat data (C2C and UC-Change); 2) a map produced by visual interpretation of aerial photography (VRI); 3) a map derived from both Landsat images and aerial photography (CC); and 4) a database summarizing reports from logging companies (NBD). UC-Change and C2C produced the highest (2428 km²/year on average for the years 1985 - 2014) and lowest (1726 km²/year) estimates, respectively. The other information products indicated

harvest rates ranging between 2013 km²/year and 2118 km²/year. Such a large gap between the Landsat-based maps was assumed to be due to high omission errors in the C2C map and commission errors in the UC-Change map, which necessitated a thorough evaluation of the two maps.

This study used the forest inventory data of British Columbia (VRI) as a rich, open, and independent source of reference data. This approach has strengths and weaknesses that both stem from the fact that the VRI dataset was produced using visual interpretation of high-definition, large-scale stereo aerial photos. The dataset contains highly detailed spatial information about the majority of cutblocks in the province, making it possible to assess many aspects of forest change detection maps. It is freely available to the public, allowing a reproducible and transparent assessment of maps produced from different algorithms. Because VRI polygons are produced using a different set of data (i.e., not Landsat), they allow an unbiased evaluation of Landsat-based maps, such as the ones compared in this study (UC-Change and C2C). However, the user must be aware of two caveats: a relatively low temporal accuracy and, secondly, a lack of information about small (< 0.5 ha) patches of residual forest that can be found in many clearcuts. Nonetheless, where available, forest inventory data can be an invaluable resource for the development and comparison of change detection algorithms.

Provincial parks and other protected areas were used to assess general commission errors in the UC-Change and C2C maps. This approach makes it easy to assess false detection of logging in a transparent and reproducible way. However, it is based on the assumption that protected areas are representative of the region they are in, which is not always the case. For example, most protected areas in BC are located in areas where false cutblock detections are somewhat more likely, such as wetlands and mountains. In addition, this approach may not be

applicable for many developing countries, where illegal logging still occurs in protected areas (Tacconi, 2007; Geldmann *et al.*, 2017). Therefore, these results must be interpreted with caution.

The UC-Change technique performed consistently better than C2C in all biogeoclimatic zones and across all years and terrain slope and aspect conditions due to its ability to utilize spatial information, more spectral bands (in this study, five bands vs. two), and more images per year and over a longer intra-annual time window (multiple June – September images vs. one July – August image composite). Overall, UC-Change detected 85.7% of reference iVRI cutblock pixels, whereas the C2C map contained only 69.5%. The C2C technique perform poorly in the period 2007 – 2011 (inclusive), as well as in deciduous and dry and open coniferous forests. A much more consistent performance across different forest types makes UC-Change a more reliable tool for mapping cutblocks and estimating the rate of forest harvesting. However, it was found that the UC-Change map had more false positives than the C2C map, mainly due to mislabelling of mixed pixels and burned areas.

The main strength of the UC-Change algorithm is its ability to accurately map forest harvest activities, even in areas heavily affected by MPB. This compares favorably against other time-series change detection algorithms, such as C2C. UC-Change is a truly multivariate change detection method as it uses spatial information and multiple spectral bands together. This allows it to detect change even when the difference in pre- and post-disturbance values is subtle in any individual spectral band but is present in all or most bands, like in stands killed by MPB. The automatic multitemporal retraining routine in the UC-Change algorithm further improves the detection of subtle changes and separates these from phenological changes in reflectance. In contrast, C2C is a univariate technique that detects change based on a single spectral index (NBR);

this could be the reason why many cutblocks were missing in the C2C map, especially in MPB-affected areas.

Our analysis showed that more forest area was likely harvested between 1985 and 2014 than what existing maps (e.g., C2C and VRI) and databases (NFD) indicate. For example, approximately 7.5 million ha of forest were cleared in the 30-year period, according to the UC-Change map (compared to 6.5 million ha based on NFD). According to Environmental Reporting BC (2018b), about as much was harvested between ~1910 and 1985. Of approximately 55 million ha of forests, only 23 million ha are made available for logging in the province (BC Ministry of Forests, 2017; Gilani and Innes, 2020). This means that as few as 8 million ha remain harvestable. Therefore, the province may need to reduce the rate of timber extraction to meet its sustainability goals.

In conclusion, the results of this study support the use of satellite-based maps as important for proper decision-making and long-term planning. Such maps can be updated frequently for the entire province at almost no cost using highly automated algorithms. In comparison, British Columbia's Forest Inventory is primarily based on human interpretation of aerial photographs (Bourgeois *et al.*, 2018). An estimated \$15 million (Canadian) was required to map one tenth of the province per year using this method (Bourgeois *et al.*, 2018). However, the budget has decreased substantially since the 1990s and is now well below this number. Due to the 10-year gap between subsequent aerial photo acquisitions, the temporal information for disturbances is often inaccurate and many recent disturbances are missing. In contrast, the UC-Change algorithm can detect recent cutblocks and accurately identify the date of harvest by using temporally dense stacks of Landsat and Sentinel-2 images. These datasets are more readily available, more are available now at no cost, earlier images (e.g., Landsat MSS imagery dating

back to 1972) are increasingly being reprocessed with improved quality, and furthermore, there are increasingly more satellites being launched with improved sensors, area coverage, and revisit frequency. All of these factors point to the adoption of satellite image time-series data sets for forest management, including longer term and future disturbance monitoring and planning. This highlights the need for robust and high-quality time series analysis algorithms, such as UC-Change.

4.6.1. Future work

This study identified three opportunities to further improve on the current version of the UC-Change algorithm: excessive detection of cutblock edges, sensitivity to topographic effects, and inaccurate change attribution. Excessive mapping of edge pixels (i.e., labelling of pixels containing mostly undisturbed forest as cutblock pixels) can be addressed by parameter adjustment, but this can have a negative effect on the detection of inner cutblock pixels. Alternatively, Spectral Mixture Analysis or Temporal Mixture Analysis could be used to filter detected change pixels based on the proportion of undisturbed forest (Piwowar et al., 1999). Finally, using higher-resolution imagery (e.g., 10-m and 20-m Sentinel-2 data) should allow the UC-Change technique to map the extent of individual cutblocks more accurately, but only if it also comes with higher geometric accuracy. This can potentially make it possible to identify forest management methods (e.g., clearcutting, clearcutting with reserves, and selective harvesting) on a cutblock-by-cutblock basis and monitor the implementation of sustainable practices.

There are several possible ways to reduce sensitivity to topographic illumination effects. One way is to include terrain slope and aspect information in input data. This should prevent classification routines in the UC-Change algorithm from, for example, classifying cutblocks on north-facing slopes into the same spectral classes as intact forest stands on south-

facing slopes. Another solution is to subset data based on the slope and aspect. Finally, topographic correction of input data can potentially improve the spatial consistency of image classification and, therefore, change detection.

Currently, the UC-Change algorithm lacks a dedicated algorithm for change attribution. As a result, it cannot effectively separate cutblocks from burned forest. Because this study focused entirely on forest harvesting, detected forest change pixels representing fire scars had to be masked using an existing forest fire map (NBAC). However, some burned areas remained unmasked because they were missing in the NBAC map, resulting in false positives. Therefore, future work should focus on improving change classification accuracy. Existing change attribution approaches could be adopted for classifying disturbances detected by the UC-Change technique, as they have been shown to be highly effective (e.g., Hermosilla *et al.*, 2015a). A change attribution algorithm could use existing maps (e.g., maps of protected areas and forest fires) as training data to better identify fire scars and false positives.

In conclusion, the results of this study demonstrate a strong potential of the UC-Change technique as a tool for mapping and quantifying forest harvest activities. Future work is clearly warranted to further improve and expand its functionality. The study also showed that forest inventory maps can be used for the evaluation and comparison of change detection products, although the inconsistent temporal accuracy of such maps is an issue that must be considered in the process.

4.7. References

Banskota, A., Kayastha, N., Falkowski, M. J., Wulder, M. A., Froese, R. E., & White, J. C. (2014). Forest monitoring using Landsat time series data: a review. *Canadian Journal of Remote Sensing*, 40(5), 362-384.

- Barnes, A., 2019. 2018 Economic state of the B.C. forest sector. The Ministry of Forests, Lands, Natural Resource Operations and Rural Development of British Columbia, Canada. https://www2.gov.bc.ca/assets/gov/farming-natural-resources-and-industry/forestry/forest-industry-economics/economic-state/2018_economic_state_of_bc_forest_sector-with_appendix.pdf [Accessed on 2020-11-10]
- Bartels, S. F., Chen, H. Y., Wulder, M. A., & White, J. C. (2016). Trends in post-disturbance recovery rates of Canada's forests following wildfire and harvest. *Forest Ecology and Management*, 361, 194-207.
- BC Ministry of Forests (2016). RESULTS Information Submission Specifications: Form and Manner of Reporting (Licensee Submissions), 4th Edition. The Ministry of Forests, Lands, Natural Resource Operations and Rural Development of British Columbia, Canada. https://www2.gov.bc.ca/assets/gov/farming-natural-resources-and-industry/forestry/silviculture/silviculture-results/infosubmissionspecsmar_2016_final.pdf [Accessed on 2020-10-27].
- BC Ministry of Forests (2017). Provincial Timber Management Goals, Objectives & Targets. The Ministry of Forests, Lands, Natural Resource Operations and Rural Development of British Columbia, Canada. https://www2.gov.bc.ca/assets/gov/farming-natural-resources-and-industry/forestry/silviculture/timbergoalsobjectives2017apr05_revised.pdf [Accessed on 2020-08-20].
- BC Ministry of Forests (2020a). Harvested Areas of BC (Consolidated Cutblocks). The Ministry of Forests, Lands, Natural Resource Operations and Rural Development of British Columbia, Canada. <https://catalogue.data.gov.bc.ca/dataset/harvested-areas-of-bc-consolidated-cutblocks-> [Accessed on 2020-10-31].
- BC Ministry of Forests (2020b). Forest Disturbance Monitoring. The Ministry of Forests, Lands, Natural Resource Operations and Rural Development of British Columbia, Canada. <https://www2.gov.bc.ca/gov/content/industry/forestry/managing-our-forest-resources/forest-inventory/forest-cover-inventories/forest-disturbance-monitoring> [Accessed on 2020-08-20].
- BC Ministry of Forests (2020c). Harvest Levels. The Ministry of Forests, Lands, Natural Resource Operations and Rural Development of British Columbia. <https://www.for.gov.bc.ca/hfd/pubs/docs/mr/mr113/harvest.htm> [Accessed on 2020-10-31].
- BEC (2020). Biogeoclimatic Ecosystem Classification Program. The Ministry of Forests, Lands, Natural Resource Operations and Rural Development of British Columbia. <https://www.for.gov.bc.ca/hre/becweb/> [Accessed on 2020-10-30].
- Bergeron, Y., & Fenton, N. J. (2012). Boreal forests of eastern Canada revisited: old growth, nonfire disturbances, forest succession, and biodiversity. *Botany*, 90(6), 509-523.
- Bourgeois, W., Binkley, C., LeMay, V., Moss, I., & Reynolds, N. (2018). British Columbia forest inventory review panel technical background report. Prepared for the Office of the Chief

- Forester Division, British Columbia Ministry of Forests, Lands, *Natural Resource Operations and Rural Development*. https://www2.gov.bc.ca/assets/gov/farming-natural-resources-and-industry/forestry/stewardship/forest-analysis-inventory/brp_technical_document_final.pdf [Accessed 2020-10-31].
- Brassard, B. W., & Chen, H. Y. (2006). Stand structural dynamics of North American boreal forests. *Critical reviews in plant sciences*, 25(2), 115-137.
- Burton, P. J., Messier, C., Weetman, G. F., Prepas, E. E., Adamowicz, W. L., & Tittler, R. (2003). The current state of boreal forestry and the drive for change. *Towards sustainable management of the boreal forest*, 1-40.
- Bury, R. B., Corn, P. S., & Aubry, K. B. (1991). Regional patterns of terrestrial amphibian communities in Oregon and Washington. Pages 341-352 in L. E Ruggiero, K. B. Aubry, A. B. Carey, and M. H. Huff, technical coordinators. Wildlife and vegetation of unmanaged Douglas-fir forests. *United States Forest Service General Technical Report PNW-285*.
- C2C (2019). Satellite Forest Information for Canada. Canadian Council of Forest Ministers. https://opendata.nfis.org/mapserver/nfis-change_eng.html [Maps downloaded on 2019-02-10].
- Carey, A. B. (1991). The biology of arboreal rodents in Douglas-fir forests. *United States Forest Service General Technical Report PNW-276*.
- Carey, A. B., & Johnson, M. L. (1995). Small mammals in managed, naturally young, and old-growth forests. *Ecological applications*, 5(2), 336-352
- CDEM (2013). Canadian Digital Elevation Model: Product Specifications. Edition 1.1. Natural Resources Canada. https://ftp.maps.canada.ca/pub/nrcan_rncan/elevation/cdem_mnec/doc/CDEM_product_specs.pdf [Map downloaded on 2020-07-17].
- Corn, P. S., & Bury, R. B. (1991). Terrestrial amphibian communities in the Oregon Coast Range. Pages 305-318 in L. F Ruggiero, K. B. Aubry, A. B. Carey, and M. H. Huff, technical coordinators. Wildlife and vegetation of unmanaged Douglas-fir forests. *United States Forest Service General Technical Report PNW-285*.
- ECCC (2020). Canadian Protected and Conserved Areas Database (CPCAD). Environment and Climate Change Canada (ECCC), Government of Canada. <https://www.canada.ca/en/environment-climate-change/services/national-wildlife-areas/protected-conserved-areas-database.html> [Map downloaded on 2020-02-30]
- El-Hattab, M. M. (2016). Applying post classification change detection technique to monitor an Egyptian coastal zone (Abu Qir Bay). *The Egyptian Journal of Remote Sensing and Space Science*, 19(1), 23-36.
- Environmental Reporting BC (2018a). Trends in Silviculture in B.C. (1987-2016). The Ministry of Forests, Lands, Natural Resource Operations and Rural Development of British

- Columbia, Canada. <http://www.env.gov.bc.ca/soe/indicators/land/silviculture.html> [Accessed on 2020-10-31].
- Environmental Reporting BC (2018b). Trends in Timber Harvest in B.C. The Ministry of Forests, Lands, Natural Resource Operations and Rural Development of British Columbia, Canada. <http://www.env.gov.bc.ca/soe/indicators/land/timber-harvest.html> [Accessed on 2020-10-31].
- Gawalko, L. (2004). Mountain pine beetle management in British Columbia parks and protected areas. *Information Report-Pacific Forestry Centre, Canadian Forest Service, (BC-X-399)*, 79-86.
- GEE (2020). LandTrendr Pixel Time Series Plotter. Google Earth Engine. <https://emaprplab.users.earthengine.app/view/lt-gee-pixel-time-series> [Accessed on 2020-08-25].
- Geldmann, J., Manica, A., Burgess, N. D., Coad, L., & Balmford, A. (2019). A global-level assessment of the effectiveness of protected areas at resisting anthropogenic pressures. *Proceedings of the National Academy of Sciences*, 116(46), 23209-23215.
- Gilani, H. R., & Innes, J. L. (2020). The State of British Columbia's Forests: A Global Comparison. *Forests*, 11(3), 316.
- Greene, D. F., Zasada, J. C., Sirois, L., Kneeshaw, D., Morin, H., Charron, I., & Simard, M. J. (1999). A review of the regeneration dynamics of North American boreal forest tree species. *Canadian Journal of Forest Research*, 29(6), 824-839.
- Gregory, M. S., Walsh, S. J., & Vitek, J. (1981). Mechanics of monitoring forest clear cuts and their regeneration. *Proceedings of the 7th International Symposium on Machine Processing of Remotely Sensed Data with Special Emphasis on Range, Forest, and Wetlands Assessment, Purdue University, West Lafayette, IN, USA* (West Lafayette, IN: Purdue University), pp. 520–527.
- Hall, F. G., Botkin, D. B., Strebel, D. E., Woods, K. D., & Goetz, S. J. (1991). Large - scale patterns of forest succession as determined by remote sensing. *Ecology*, 72(2), 628-640.
- Hansen, M. C., Potapov, P. V., Moore, R., Hancher, M., Turubanova, S., Tyukavina, A., Thau, D., Stehman, S. V., Goetz, S. K., Loveland, T. R., Kommareddy, A., Egorov, A., Chini, L., Justice, C. O., & Townshend, J. R. G. (2013). High-resolution global maps of 21st-century forest cover change. *Science*, 342(6160), 850-853.
- Hermosilla, T., Wulder, M. A., White, J. C., Coops, N. C., & Hobart, G. W. (2015a). Regional detection, characterization, and attribution of annual forest change from 1984 to 2012 using Landsat-derived time-series metrics. *Remote Sensing of Environment*, 170, 121-132.
- Hermosilla, T., Wulder, M. A., White, J. C., Coops, N. C., & Hobart, G. W. (2015b). An integrated Landsat time series protocol for change detection and generation of annual gap-free surface reflectance composites. *Remote Sensing of Environment*, 158, 220-234.

- Hermosilla, T., Wulder, M. A., White, J. C., Coops, N. C., Hobart, G. W., & Campbell, L. B. (2016). Mass data processing of time series Landsat imagery: pixels to data products for forest monitoring. *International Journal of Digital Earth*, 9(11), 1035-1054.
- Jarvis, A., Reuter, H. I., Nelson, A., & Guevara, E. (2008). Hole-filled SRTM for the globe Version 4, available from the CGIAR-CSI SRTM 90m Database. The International Center for Tropical Agriculture. <http://srtm.csi.cgiar.org> [Accessed on 2020-07-02].
- Kennedy, R. E., Yang, Z., Gorelick, N., Braaten, J., Cavalcante, L., Cohen, W. B., & Healey, S. (2018). Implementation of the LandTrendr algorithm on Google Earth Engine. *Remote Sensing*, 10(5), 691.
- Kurz, W. A., Stinson, G., Rampley, G. J., Dymond, C. C., & Neilson, E. T. (2008). Risk of natural disturbances makes future contribution of Canada's forests to the global carbon cycle highly uncertain. *Proceedings of the National Academy of Sciences*, 105(5), 1551-1555.
- Lundmark, H., Josefsson, T., & Östlund, L. (2013). The history of clear-cutting in northern Sweden—driving forces and myths in boreal silviculture. *Forest Ecology and Management*, 307, 112-122.
- Masek, J. G., Cohen, W. B., Leckie, D., Wulder, M. A., Vargas, R., de Jong, B., Healey, S., Law, B., Birdsey, R., Houghton, R. A., & Mildrexler, D. (2011). Recent rates of forest harvest and conversion in North America. *Journal of Geophysical Research: Biogeosciences*, 116(G4).
- Macyk, T. M., Lindsay, J. D., & Pawluk, S. (1978). Relief and microclimate as related to soil properties. *Canadian Journal of Soil Science*, 58(3), 421-438.
- McRae, D. J., Duchesne, L. C., Freedman, B., Lynham, T. J., & Woodley, S. (2001). Comparisons between wildfire and forest harvesting and their implications in forest management. *Environmental Reviews*, 9(4), 223-260.
- Meidinger, D., & Pojar, J. (1991). Ecosystems of British Columbia. *Special Report Series-Ministry of Forests, British Columbia*, (6).
- NBAC (2020). Canadian Wildland Fire Information System: National Fire Database fire polygon data. Natural Resources Canada. <http://cwfis.cfs.nrcan.gc.ca/datamart> [Accessed on 2020-10-30].
- NFD (2020). Forest area harvested on private and Crown lands in Canada. Canadian Forest Service, Natural Resources Canada. <http://nfdp.ccfm.org/en/data/harvest.php> [Accessed on 2020-10-31].
- NRCan (2014). The State of Canada's Forests: Annual Report 2014. Canadian Forest Service, Natural Resources Canada. <https://cfs.nrcan.gc.ca/pubwarehouse/pdfs/35713.pdf> [Accessed on 2020-10-31].
- NRCan (2020). Forest industry employment (British Columbia). Natural Resources Canada. <https://cfs.nrcan.gc.ca/statsprofile/employment/bc> [Accessed on 2020-11-10]

- Peddle, D. R., Franklin, S. E., Johnson, R. L., Lavigne, M. B., & Wulder, M. A. (2003). Structural change detection in a disturbed conifer forest using a geometric optical reflectance model in multiple-forward mode. *IEEE Transactions on Geoscience and Remote Sensing*, 41(1), 163-166.
- Peddle, D. R., Huemmrich, K. F., Hall, F. G., Masek, J. G., Soenen, S. A., & Jackson, C. D. (2011). Applications of the BIOPHYS algorithm for physically-based retrieval of biophysical, structural and forest disturbance information. *IEEE Journal of Selected Topics in Applied Earth Observations and Remote Sensing*, 4(4), 971-982.
- Peddle, D. R., Johnson, R. L., Cihlar, J., & Latifovic, R. (2004). Large area forest classification and biophysical parameter estimation using the 5-Scale canopy reflectance model in Multiple-Forward-Mode. *Remote Sensing of Environment*, 89(2), 252-263.
- Piwowar, J. M., Peddle, D. R., & Davidson, D. P. (1999). Assessing annual forest ecological change in western Canada using temporal mixture analysis of regional scale AVHRR imagery over a 14 year period. In, *Proceedings of the 4th International Airborne Remote Sensing Conference and Exhibition, /21st Canadian Symposium on Remote Sensing, Ottawa, Canada.*
- Qiu, S., Lin, Y., Shang, R., Zhang, J., Ma, L., & Zhu, Z. (2019a). Making Landsat Time Series Consistent: Evaluating and Improving Landsat Analysis Ready Data. *Remote Sensing*, 11(1), 51.
- Qiu, S., Zhu, Z., & He, B. (2019b). Fmask 4.0: Improved cloud and cloud shadow detection in Landsats 4–8 and Sentinel-2 imagery. *Remote Sensing of Environment*, 231, 111205.
- Soenen, S. A., Peddle, D. R., & Coburn, C. A. (2005). SCS+ C: A modified sun-canopy-sensor topographic correction in forested terrain. *IEEE Transactions on Geoscience and Remote Sensing*, 43(9), 2148-2159.
- Soenen, S. A., Peddle, D. R., Coburn, C. A., Hall, R. J., & Hall, F. G. (2008). Improved topographic correction of forest image data using a 3-D canopy reflectance model in multiple forward mode. *International Journal of Remote Sensing*, 29(4), 1007-1027.
- Soenen, S. A., Peddle, D. R., Hall, R. J., Coburn, C. A., & Hall, F. G. (2010). Estimating aboveground forest biomass from canopy reflectance model inversion in mountainous terrain. *Remote Sensing of Environment*, 114(7), 1325-1337.
- Tacconi, L. (ed.) 2007. *Illegal logging: law enforcement, livelihoods and the timber trade.* Earthscan, London.
- Verbyla, D. L., Kasischke, E. S., & Hoy, E. E. (2008). Seasonal and topographic effects on estimating fire severity from Landsat TM/ETM+ data. *International Journal of Wildland Fire*, 17(4), 527-534.
- VRI (2020). *VRI - Historical Vegetation Resource Inventory (2002 - 2018).* The Ministry of Forests, Lands, Natural Resource Operations and Rural Development of British Columbia.

[https://catalogue.data.gov.bc.ca/dataset/vri-historical-vegetation-resource-inventory-2002-2018-](https://catalogue.data.gov.bc.ca/dataset/vri-historical-vegetation-resource-inventory-2002-2018) [Accessed on 2020-10-30].

- White, J. C., Wulder, M. A., Hermosilla, T., Coops, N. C., & Hobart, G. W. (2017). A nationwide annual characterization of 25 years of forest disturbance and recovery for Canada using Landsat time series. *Remote Sensing of Environment*, 194, 303-321.
- Wulder, M.A., Loveland, T.R., Roy, D.P., Crawford, C.J., Masek, J.G., Woodcock, C.E., Allen, R.G., Anderson, M.C., Belward, A.S., Cohen, W.B. & Dwyer, J. (2019). Current status of Landsat program, science, and applications. *Remote Sensing of Environment*, 225, 127-147.
- Zhu, Z. (2017). Change detection using Landsat time series: a review of frequencies, preprocessing, algorithms, and applications. *ISPRS Journal of Photogrammetry and Remote Sensing*, 130, 370-384.
- Zhu, Z., Wang, S., & Woodcock, C. E. (2015). Improvement and expansion of the Fmask algorithm: Cloud, cloud shadow, and snow detection for Landsats 4–7, 8, and Sentinel 2 images. *Remote Sensing of Environment*, 159, 269-277.

CHAPTER 5

CONCLUSIONS AND FUTURE WORK

5.1. Conclusions

The goal of this research was to develop new methods in time-series analysis suitable for modern forestry and other needs (e.g., environmental monitoring), specifically that could improve cutblock detection and offer new, ecologically-based forest recovery metrics. It has potential use for multiple stakeholders, ranging from reporting, inventory, environmental sustainability, and the forest industry who have significant needs for harvest and planning information to optimize operations, yields, and future resource extraction. Logging has various negative effects on ecosystems, even in areas affected by natural disturbances, such as fire and mountain pine beetle (MPB) (Lindenmayer *et al.*, 2012); therefore, there is a need for algorithms that can accurately map forest harvesting regardless of the type and health condition of forest. Using remote sensing data time-series analysis is the only way to map where and when forest was harvested in a consistent, transparent, cost-effective, and timely fashion and for large areas. In addition, the long and continuous record of Earth observation image data makes it possible to monitor forest recovery in disturbed areas almost anywhere in the world. This information can help researchers, policy makers, and the logging industry to develop site-optimized sustainable silvicultural practices.

To achieve these goals, four objectives were defined:

1. Develop a truly multisensor and multispectral approach for the detection of cutblocks and fire scars in various forest types over large areas despite the presence of other disturbance factors.
2. Develop object-based forest recovery metrics indicative of stand composition.

3. Develop a framework for the evaluation of forest disturbance maps using open-access data.
4. Compare generated maps with existing forest-disturbance maps and databases with an emphasis on their ability to provide accurate area and rate estimates for forest harvesting at a regional scale.

For the first objective, a new technique named Unsupervised Classification to Change (UC-Change) was developed. It detects changes in the spatial distribution of spectral classes in classification maps produced with an unsupervised clustering algorithm. Because the technique does not compare pixel values directly, it is designed to be insensitive to radiometric differences among images caused by factors such as the temporal variation in BRDF effects, different sensors and sensor parameters, differences in image properties such as spectral response functions of sensors, and variability in vegetation phenology. Therefore, it can use data acquired during any part of the growing season without atmospheric correction, BRDF adjustment (except for mountainous areas), inter-sensor and other types of radiometric normalization, which makes this newly developed UC-Change technique highly flexible. This also substantially improves the ability to use a much greater portion of available image data in time series, especially in areas more prone to cloud cover. This flexibility allowed the algorithm to use June 1 – September 20 data, as opposed to only July and August data used by other approaches that are sensitive to phenological changes in reflectance (Kennedy *et al.*, 2010; Hermosilla *et al.*, 2015a,b). UC-Change detected 9.5% more 1985 – 2015 reference cutblock pixels using June 1 – September 20 data than using July and August data (86.6% vs. 79.0%), mainly because the wider range of dates reduced the data gaps in the time series. The technique performed very well when tested on data of marginal quality (Landsat 1 – 5 MSS data acquired 1972 – 1990), where it detected over 85% of cutblocks. In addition, unlike any existing pixel-based time-series change detection technique, UC-Change can

fully utilize images with a different number of spectral bands (Landsat 5 - 8 and Sentinel-2) including those with different spectral ranges. This opens up important multi-sensor and multi-source analysis possibilities, which are becoming increasingly more relevant with new sensors available today (e.g., Sentinel-1 and Sentinel-2) and planned for the near future.

Because the UC-Change technique can use any number of images per year and can detect changes up to the third last image in the time series, it can map changes that occurred only weeks before the last image was acquired as long as that level of temporal resolution is available, which is increasingly the case. Besides UC-Change, only curve-fitting time-series change detection techniques, such as the Continuous Change Detection and Classification (CCDC) technique (Zhu and Woodcock, 2014), have such a capability. However, those techniques require a very large amount of cloud-free and snow-free data for both summer and winter. This can be an issue for areas with persistent winter snow cover, such as for most of British Columbia's territory (Zhu and Woodcock, 2014).

The new technique produced excellent results for a 100 km × 100 km test area in the interior British Columbia. It detected more reference cutblock (88.3% detected at a ±1 year agreement with the reference data) and forest-fire pixels (75.3%) than the LandTrendr (32.7% of cutblock pixels and 60.8% of fire-scar pixels detected at ±1 year), Composite2Change (C2C; 41.9% and 62.9%, respectively), and Global Forest Change (GFC; 72.2% and 58.2%, respectively) techniques for the period 2002 – 2014 (Kennedy *et al.*, 2018; C2C, 2019; GFC, 2020). Unlike these other techniques, it also performed well in areas characterized by low canopy cover and/or severe mountain pine beetle damage.

The second objective was to evaluate the utility of the two forest recovery metrics offered by the new technique. Unlike the metrics used in other approaches, which measure spectral

recovery of individual pixels, the UC-Change metrics monitor the spatial distribution of spectral classes in disturbed areas at the object level (see also Figure 3.8). These metrics (percentage of pre- and post-disturbance spectral classes) are mainly determined by the spatial distribution of different tree species and other vegetation, and therefore, can provide information about stand composition, a critical aspect of forest recovery from an ecological perspective. Compared to the index-based spectral recovery metrics of existing techniques (e.g., C2C and LandTrendr), the UC-Change metrics took longer to return to pre-disturbance values (27 years compared to 20 years in this study) and showed different recovery patterns as was expected based on the forest type. For many clearcuts, the UC-Change metrics plateaued before reaching pre-disturbance values. Analysis of the forest inventory data of British Columbia showed that many of these clearcuts had a stand composition very different from the surrounding intact forest (e.g., more lodgepole pine and/or deciduous species), which was consistent with the results obtained using UC-Change.

The third objective was to design an approach for a comprehensive assessment of forest change detection maps using open-access data for validation. This study used the Vegetation Resources Inventory (VRI) data of British Columbia to assess cutblock detection; the National Burned Area Composite (NBAC) dataset to assess the detection of burned areas; and polygons representing protected areas, such as national and provincial parks, to evaluate false detection (ECCC, 2020; NBAC, 2020; VRI, 2020). The VRI dataset contains detailed information about the vast majority of cutblocks that occurred in the province from the early 20th century to present time (~450,000 cutblock polygons). Likewise, the NBAC database includes information on over 5500 forest fires that occurred since 1986. Finally, there are over 1000 protected areas covering 14.4% of the province.

It is noteworthy that VRI and NBAC data are not error-free; therefore, accuracy assessment based on these datasets was expected to produce lower results than if a smaller set of verified polygons (e.g., 600 polygons) had been used instead. In all cases of comparison with other reference products, the assessment is based on agreement with a product of established quality and acceptable accuracy, but ultimately, at these scales, it is not possible to do anywhere close to sufficient field validation. This is more than compensated for by the use of multiple reference validation sources that increase the integrity of agreement-based assessments. Using unedited VRI and NBAC datasets allows for very detailed, granular, unbiased, transparent, and reproduceable analyses and comparison of maps. Due to the enormous amount of reference data used in the study, a very high level of confidence can be attributed to any differences that were found among and within change detection maps. In addition, VRI polygons accurately characterize the spatial extent of individual cutblocks, which makes it possible to evaluate the detection of cutblock edges. This is important, because edge pixels in change detection maps are affected by the mixed-pixel problem and geometric inaccuracies in input data.

The final objective was to compare UC-Change maps against existing forest disturbance maps and databases for their ability to estimate the area and rate of forest harvesting in the entire province of British Columbia. This region has a wide variety of forest types, terrain (from flat to mountainous) and climatic conditions (a large range of biogeoclimatic zones). In addition, it was heavily affected by an MPB outbreak in the 2000s. UC-Change was much more consistent throughout the study area compared with the C2C map, the only other change-detection maps available that distinguishes between stand-replacing and other disturbances. C2C performed poorly in areas with low stand density and areas affected by the MPB. In addition, it struggled to detect cutblocks characterized by fast spectral recovery (e.g., in many deciduous stands where

trees can regenerate vegetatively). The UC-Change map did not have these issues, but it was more sensitive to topography (e.g., fewer reference pixels were detected on steep north-facing slopes than on south-facing slopes) and had more false positives than the C2C map. Nonetheless, it performed consistently better than C2C in all biogeoclimatic zones and across all years and terrain slope and aspect conditions due to its ability to utilize spatial information, more spectral bands (in this study, five bands vs. two), and more images per year (multiple June – September images vs. one July – August image composite). Overall, it detected 85.7% of reference inner cutblock pixels, whereas the C2C map contained only 69.5%.

The analysis showed that more forest area has likely been harvested between 1985 and 2014 than what existing maps and databases indicate. According to the UC-Change map, 7.3 million ha of forest were cleared during this period. In contrast, the C2C, VRI, and Consolidated Cutblocks (CC) maps showed a total of 5.2, 5.7, and 5.9 million ha of forest harvested over the same period, respectively. However, once adjusted for commission and omission error estimates, both the UC-Change and C2C results indicated that there could be as much as 7.5 million ha of 1985 – 2014 cutblocks.

In conclusion, UC-Change proved to be a highly flexible technique that can map cutblocks and fire scars consistently well in forests of various species composition, stand density, and health. The UC-Change forest recovery metrics behaved as expected based on the pre-disturbance forest type and post-disturbance recovery dynamics. This makes these metrics more useful for monitoring forest recovery from the ecological perspective than existing pixel-based metrics. UC-Change represents a new approach to time-series change detection and monitoring, the full potential of which is yet to be realized.

5.2. Future work

There are multiple ways in which the functionality of the UC-Change technique could be even further improved and expanded. The first priority would be to improve the UC-Change algorithm in regards to handling topographic effects, as well as addressing the false detection of forest change in wetlands and mountainous areas, and detection of some repeat disturbances when those occur within a few years from each other. Future work could also focus on adding forest-disturbance and land-cover classification, as well as support for data of variable spatial resolution without resampling.

Digital elevation data can potentially be used to make the performance of the technique more consistent across different terrain slope and aspect conditions. Integration of slope and aspect data has been shown to improve image classification in mountainous areas (Frank, 1988; Peddle and Duguay, 1995; Eiumnoh and Shrestha, 2000; Chen *et al.*, 2017) as have improved terrain correction procedures (Soenen *et al.*, 2005, 2008). Because UC-Change relies on image classification to detect change, it should also benefit from the addition of topographic information. Open-access digital elevation models (DEMs) with a sufficiently high spatial resolution (~30 m) and near-global coverage could be used for this purpose (Farr *et al.*, 2007; CDEM, 2013; O'Loughlin *et al.*, 2016). The flexibility and versatility of UC-Change to ingest and use multisource and variable format data sets opens up extensive new opportunities for using terrain and other types of regional/global data sets.

Automatic parameter adjustment based on data availability can make the technique more automated and help address many issues identified in the thesis. This would be good to implement and test. To reduce commission errors, stricter parameters could be used for geographical areas and time periods for which more data are available. On the other hand, using a

very small temporal processing window (two images) for the last year in the time series would make it possible to map very recent forest disturbances, although possibly at the cost of user accuracy. Sensitivity analysis showed that UC-Change can perform similarly well under a wide range of input parameters and in different biogeoclimatic zones, which indicates that it is already highly robust. However, dynamic parameter adjustment is likely required to map very large areas (e.g., countries or even continents) in a fully automated fashion.

To improve the detection of clearcut edges, access roads, and forest reserves inside clearcuts, which all suffer from the mixed-pixel problem, a higher than 30-m spatial resolution would generally be required. The next version of the UC-Change algorithm will use 10-m and 20-m Sentinel-2 data without spatial resampling. This is possible because only one part of the UC-Change algorithm (Secondary Change Pixel Detection, see Section 3.3.4) requires that images in the processing window have the same resolution. This part of the algorithm processes four images at a time, and it can be limited to using only data of the same resolution for each set of images. The 10-m and 20-m spectral bands of a Sentinel-2 image can be treated as two separate images. While they contain different spectral information, the iterative retraining algorithm should improve the consistency of unsupervised classification of 10- and 20-m data as it did when processing 5-band Landsat images and 9-band Sentinel-2 images in this study. Using Sentinel-2 data with the original spatial resolution can potentially make it possible to identify forest management methods used by different logging companies on a cutblock-by-cutblock basis and monitor the implementation of sustainable practices. Using 10-m data will also reduce overestimation of logged area by the UC-Change algorithm, which tends to label more mixed pixels as forest change, even when the percentage of bare ground is low.

Currently, the UC-Change algorithm lacks a dedicated change attribution algorithm that could classify changes based on the disturbance factor. As a result, it cannot easily separate cutblocks from burned forest. Existing change attribution approaches could be adopted for classifying disturbances detected by the UC-Change technique, as they have proved to be highly effective (e.g., Hermosilla *et al.*, 2015a).

Finally, time-series land-cover classification is possible even with the current version of UC-Change. The iterative retraining routine in the UC-Change algorithm uses classification results for individual images to improve the unsupervised classification of other images in the time series by reducing deviation in the spatial distribution of spectral classes caused by phenological changes and clouds. The same routine could use an existing land-cover map for any particular year to label spectral classes in all images in the time series. Alternatively, an automated procedure could be used to label classes using a spectral library derived from hyperspectral imagery, such as Hyperion (Parshakov *et al.*, 2014). Such time-series land-cover classification could also make the UC-Change forest recovery metrics even more meaningful as it would allow them to track changes in the distribution of thematic classes (e.g., vegetation types) rather than unlabeled spectral classes.

Given the flexibility, level of automation, level of testing (both validation and challenging terrain and highly variable land cover), large-area datasets, and lengthy time series considered in this research, there are many other possible opportunities to further build and test even more extensive capabilities based on this new UC-Change approach.

5.3. References

C2C (2019). Satellite forest information for Canada: C2C map. Canadian Council of Forest Ministers. https://opendata.nfis.org/mapserver/nfis-change_eng.html [Maps downloaded on 2019-02-10].

- CDEM, 2013. Canadian Digital Elevation Model: Product Specifications. Edition 1.1. Natural Resources Canada.
https://ftp.maps.canada.ca/pub/nrcan_rncan/elevation/cdem_mnec/doc/CDEM_product_specs.pdf [Accessed on 2020-07-17].
- Chen, B., Huang, B., & Xu, B. (2017). Multi-source remotely sensed data fusion for improving land cover classification. *ISPRS Journal of Photogrammetry and Remote Sensing*, 124, 27-39.
- ECCC (2020). Canadian Protected and Conserved Areas Database (CPCAD). Environment and Climate Change Canada (ECCC), Government of Canada.
<https://www.canada.ca/en/environment-climate-change/services/national-wildlife-areas/protected-conserved-areas-database.html> [Accessed on 2020-10-30].
- Eiumnoh, A., & Shrestha, R. P. (2000). Application of DEM data to Landsat image classification: Evaluation in a tropical wet-dry landscape of Thailand. *Photogrammetric Engineering and Remote Sensing*, 66(3), 297-304.
- Farr, T.G., Rosen, P.A., Caro, E., Crippen, R., Duren, R., Hensley, S., Kobrick, M., Paller, M., Rodriguez, E., Roth, L. & Seal, D. (2007). The shuttle radar topography mission. *Reviews of Geophysics*, 45(2).
- Frank, T. D. (1988). Mapping dominant vegetation communities in the Colorado Rocky Mountain Front Range with Landsat Thematic Mapper and digital terrain data. *Photogrammetric Engineering and Remote Sensing*, 54(12): 1727-1734.
- GFC (2020). Hansen Global Forest Change v1.7 (2000-2019). Google Earth Engine.
https://developers.google.com/earth-engine/datasets/catalog/UMD_hansen_global_forest_change_2019_v1_7 [Accessed on 2020-10-31].
- Hermosilla, T., Wulder, M. A., White, J. C., Coops, N. C., & Hobart, G. W. (2015a). Regional detection, characterization, and attribution of annual forest change from 1984 to 2012 using Landsat-derived time-series metrics. *Remote Sensing of Environment*, 170, 121-132.
- Hermosilla, T., Wulder, M. A., White, J. C., Coops, N. C., & Hobart, G. W. (2015b). An integrated Landsat time series protocol for change detection and generation of annual gap-free surface reflectance composites. *Remote Sensing of Environment*, 158, 220-234.
- Kennedy, R. E., Yang, Z., & Cohen, W. B. (2010). Detecting trends in forest disturbance and recovery using yearly Landsat time series: 1. LandTrendr—Temporal segmentation algorithms. *Remote Sensing of Environment*, 114(12), 2897-2910.
- Lindenmayer, D. B., Burton, P. J., & Franklin, J. F. (2012). *Salvage logging and its ecological consequences*. Island Press.
- NBAC (2020). Canadian Wildland Fire Information System: National Fire Database fire polygon data. Natural Resources Canada. <http://cwfis.cfs.nrcan.gc.ca/datamart> [Accessed on 2020-10-30].

- O'Loughlin, F. E., Paiva, R. C. D., Durand, M., Alsdorf, D. E., & Bates, P. D. (2016). A multi-sensor approach towards a global vegetation corrected SRTM DEM product. *Remote Sensing of Environment*, 182, 49-59.
- Parshakov, I., Coburn, C., & Staenz, K. (2014). Automated class labeling of classified Landsat TM imagery using a Hyperion-generated hyperspectral library. *Photogrammetric Engineering & Remote Sensing*, 80(8), 797-805.
- Peddle, D. R., & Duguay, C. R. (1995). Incorporating topographic and climatic GIS data into satellite image analysis of an alpine tundra ecosystem, Front Range, Colorado Rocky Mountains. *Geocarto International*, 10(4), 43-60.
- Soenen, S. A., Peddle, D. R., Coburn, C. A., Hall, R. J., & Hall, F. G. (2008). Improved topographic correction of forest image data using a 3-D canopy reflectance model in multiple forward mode. *International Journal of Remote Sensing*, 29(4), 1007-1027.
- Soenen, S. A., Peddle, D. R., & Coburn, C. A. (2005). SCS+ C: A modified sun-canopy-sensor topographic correction in forested terrain. *IEEE Transactions on Geoscience and Remote Sensing*, 43(9), 2148-2159.
- Zhu, Z., & Woodcock, C.E. (2014). Continuous Change Detection and Classification of Land Cover Using All Available Landsat Data. *Remote Sensing of Environment*, (144):152-171.

APPENDIX 1

PSEUDOCODE

This appendix contains pseudocode detailing the main processing steps of the UC-Change algorithm: 1) unsupervised classification; 2) stable pixel detection and iterative retraining; 3) primary change pixel detection; 4) secondary pixel detection; and 5) object-based filtering and forest recovery information extraction (Figure 3-6). Parameters used in this study are listed first, followed by the list of variables, and, finally, the pseudocode.

1. Parameters

`max_processing_window_length = 4`

Stable pixels are detected for a period of four or fewer years.

`size_of_processing_window = 4`

The number of images used for stable pixel detection is four. This means that one primary image and three secondary images are used to detect stable pixels.

`min_overlap = 70%`

Minimum non-masked-area overlap between the primary image *p* and individual secondary image candidates is 70%.

`n_retrainings = 2`

Number of iterations of retraining. Can be set to 0 to skip iterative retraining.

`n_classes_with_change = 1`

Number of spectral classes in classified images from which to extract primary change pixels. This parameter can be set to >1 if multimodal distribution of pixel values in disturbed forest is expected; however, `n_classes_with_change = 1` still works for such disturbances because of temporal redundancies.

`change_likelihood_threshold = 0.2`

Minimum proportion of multitemporal maximum likelihood maps that contain a change class representing a particular disturbance date that are represented by that change class in a particular pixel.

`MMU = 40 pixels`

Minimum mapping unit: spatial clusters of change pixels smaller than 40 pixels are automatically rejected.

`cluster_clearsky_threshold = 65%`

Minimum percentage of non-masked pixels in a spatial cluster of change pixels is 65%.

`pre_in_post_threshold = 0.5`

Proportion of dominant pre-disturbance spectral classes in post-disturbance data must be less than 50%.

`post_in_pre_threshold = 0.5`

Proportion of dominant post-disturbance spectral classes in pre-disturbance data must be less than 50%.

2. Global Variables

`image`

Array of images containing original multispectral images.

`date`

Array containing the acquisition dates of all images in the time series.

`year`

Array containing the year of image acquisition of all images in the time series.

`blank_image`

Blank image with the same number of rows and columns as input images. A value of zero is assigned to all pixels.

`kmeans`

Array of images containing K-means classification outputs.

`classified`

Array of images containing either K-means classification maps (if `n_retrainings = 0`) or single-date maximum likelihood classification maps (if `n_retrainings > 0`) with unlabelled classes.

`classified_SWIR2_ranked`

Array of images containing single-date classification outputs (K-means or Maximum Likelihood) where spectral classes are ranked based on the average SWIR-2 values (e.g., in 10-class `classified_SWIR2_ranked`, Class 1 has the lowest average SWIR-2 value and Class 10 has the highest average SWIR-2 value).

`multitemporal_mlh`

Array of images containing multitemporal maximum likelihood classification outputs. Class labels are the image acquisition dates associated with the stable pixels and primary change pixels used as training data.

`stable`

Array of images where non-zero values represent stable pixels not only in primary images `p`, but also in secondary images `s`.

`primary_change`

Array of images where non-zero values represent primary change pixels. Derived from `stable`.

`secondary_change`

Array of images where non-zero values represent secondary change pixels. Derived from `multitemporal_mlh`.

`primary_and_secondary_indices`

Non-image 2d array containing the indices of secondary images for each primary image `p` (Table A1-1).

`change_detection_maps`

Array of images where each image is a forest disturbance map for a particular date.

`recovery_to_pre`

Array of images where pixel values represent the percentage of dominant pre-disturbance classes after disturbance.

`recovery_from_post`

Array of images where pixel values represent the percentage of dominant post-disturbance classes after disturbance.

`n_...` (e.g., `n_images`, `n_classes`)

Number of elements in an array (e.g., number of images or number of spectral classes).

3. Local Variables

The following variables are re-declared for every primary image:

`p`

The index of the primary image currently being processed. Any image in the time series except the last three (if `size_of_processing_window = 4`) can be primary.

`w_indices`

The indices of all images within the processing window for primary image `p`. For example, if `max_processing_window_length = 4`, then these are all images acquired within four years after the primary image that is currently being processed.

o_indices

The indices of images within the processing window which individually have a >70% overlap with image p (if `min_overlap = 70%`).

s_indices

The indices of three images within the processing window which together have the largest overlap (typically 95% - 99%) with image p. These are the indices of secondary images to primary image p.

p_number_of_mlh

Total number of multitemporal Maximum Likelihood classification maps where a pixel can be labelled `date[p]`.

secondary_change_p_number_of_mlh

Total number of multitemporal Maximum Likelihood classification maps where a pixel is labelled `date[p]`.

Table A1-1. The values of some of the variables for the nineteenth image (1990-06-23_L5.dat) in a hypothetical dataset.

Variable	Value	Acquisition Date
p	18	1990-06-23
w_indices	19, 20, 21, 22, 23, 24, 25, 26, 27, 28, 29, 30, 31, 32, 33, 34	1990-08-10, 1990-08-26, 1990-09-11, 1991-06-10, 1991-07-28, 1991-08-13, 1991-08-22, 1991-09-07, 1992-07-23, 1992-08-15, 1992-08-24, 1993-08-11, 1993-09-03, 1994-06-02, 1994-07-20, 1994-07-29
o_indices	19, 20, 21, 27, 28, 29, 30, 31, 32, 33	1990-08-10, 1990-08-26, 1990-09-11, 1992-07-23, 1992-08-15, 1992-08-24, 1993-08-11, 1993-09-03, 1994-06-02, 1994-07-20
s_indices	28, 31, 33	1992-08-15, 1993-09-03, 1994-07-20
primary_and_secondary_indices[p]	18, 28, 31, 33	1990-06-23, 1992-08-15, 1993-09-03, 1994-07-20

4. Functions

where

Returns indices of array elements that match a user-defined criterion / criteria (e.g., `where(image = 10)` returns the x and y of pixels with a value of 10).

`array(n, value = z)`

Returns an array of n elements with a value of z. The parameter `value` is optional.

`image_array(n, value = z)`

Returns an array of `n` images (2D arrays) where a value of `z` is assigned to all pixels. The parameter `value` is optional.

`overlap(image0; image1, image2, ...)`

Returns the percentage of non-masked pixels in `image0` that are also not masked in `image1`, `image2`, ...

`mode(array, n_modes)`

Returns the most commonly occurring value (`n_modes = 1`) or values (`n_modes > 1`) in an array.

`stack(image0, image1, image2, ...)`

Returns a stack of input images (e.g., four images that each have six spectral bands are stacked to produce one 24-band image stack).

`maximum_likelihood_classification(input_data, training_rois)`

Returns a Maximum Likelihood classification map.

`kmeans_classification(input_data, number_of_classes, number_of_kmeans_iterations)`

Returns a K-means classification map.

`segmentation`

This function identifies contiguous spatial clusters of change pixels and returns the `x` and `y` coordinates of pixels for each cluster.

`percent_clearsky`

Returns the proportion of non-masked pixels.

`sum`

Returns the sum of all elements in an array.

`rank_classes(map, spectral_band = SWIR2)`

Returns a classification map where spectral classes are ranked based on the average SWIR-2 values.

`merge(image0, image1)`

This function uses non-zero pixels in `image1` to replace pixels with a value of 0 in `image0`.

5. Processing

Step 1: Unsupervised Classification

```
for each image i
    kmeans[i] = kmeans_classification(input_data = image[i], number_of_classes
    = 10, number_of_kmeans_iterations = 5)
```

Step 2: Stable Pixel Detection and Iterative Retraining

```
for each primary image p
    w_indices = where(date > date[p] and year ≤ year[p] +
    max_processing_window_length)

    // Reduce the number of secondary image candidates by selecting only those that match the
    min_overlap requirement.
    for each index w in w_indices
        if (overlap(kmeans[p]; kmeans[w]) > min_overlap)
            add w to o_indices

    // Check every combination of the primary image p and three secondary image candidates for
    maximum overlap.
    max_overlap = 0
    s_indices = array(3)
    for (o1 = 0; n_o_indices - 3; o1++)
        for (o2 = o1 + 1; n_o_indices - 2; o2++)
            for (o3 = o2 + 1; n_o_indices - 1; o3++)
                percent_overlap = overlap(kmeans[p]; kmeans[o_indices[o1]],
                kmeans[o_indices[o2]], kmeans[o_indices[o3]])
                if (percent_overlap > max_overlap)
                    max_overlap = percent_overlap
                    s_indices = [o1,o2,o3]

    primary_and_secondary_indices[p,*] = [p, s_indices[0], s_indices[1],
    s_indices[2]]

    primary_and_secondary = kmeans[primary_and_secondary_indices[p,*]]
    last_secondary_date[p] = date[s_indices[2]]

    // Stable pixel detection and iterative retraining.
```

```

for (r = 0; r < n_retrainings; r++)

    // combine the primary classification map and all three secondary classification maps into
    one image. Each original map has pixel values ranging between 0 (masked) and 10
    (spectral class 10). The output image has pixel values ranging 101010100 (for pixels
    masked in all four images) to 111111110 (for pixels that are in spectral class 10 in all
    four images).

    primary_and_secondary_combined = (100 + primary_and_secondary[0]) +
    (100 + primary_and_secondary[1])*100 + (100 +
    primary_and_secondary[2])*10,000 + (100 +
    primary_and_secondary[3])*1,000,000

    // Detect stable pixels for the primary image and all three secondary images.
    for (s = 0; s < size_of_processing_window; s++)
        stable_s = blank_image
        for (c = 0, c < n_classes)

            // Subset kmeans_combined based on class c in image s.

            primary_and_secondary_combined_c =
            primary_and_secondary_combined[where(primary_and_secondary[s] =
            c)]

            // Find the most common multitemporal combination of spectral classes.

            primary_and_secondary_combined_c_mode =
            mode(primary_and_secondary_combined_c, n_modes = 1)

            // Find the x and y coordinates of stable pixels in class c in image s.

            stable_s[where(primary_and_secondary_combined =
            primary_and_secondary_combined_c_mode)] = c

        stable[p,s] = stable_s

    // Use detected stable pixels as training data in single-date maximum likelihood
    classification.

    if (r != n_retrainings - 1)
        primary_and_secondary[s] =
        maximum_likelihood_classification(input_data =
        image[primary_and_secondary_indices[p,s]], training_rois =
        stable[p,s])

// Replace original K-means maps with the output of retraining.
classified[p] = primary_and_secondary[0]

```

Step 3: Primary Change Pixel Detection

```
for each primary image p
    // Primary change pixels are derived from stable pixels.
    primary_change_p = stable[p,0]

    // Subtract stable pixels detected for previous images.
    pre_where = where(last_secondary_date >= date[p] and date < date[p])
    for each pre-disturbance image pre in pre_where
        for (s = 0; s < size_of_processing_window; s++)
            if (date[primary_and_secondary_indices[pre,s]] < date[p])
                primary_change_p[where(stable[pre,s] != 0)] = 0

    // Remove clusters of change pixels smaller than 40 pixels.
    primary_change_p = sieve(primary_change_p, cluster_size > MMU)

    // Find the class that has the most remaining pixels.
    change_class = mode(primary_change_p[where(primary_change_p > 0)], n_modes
    = n_classes_with_change)
    temp = blank_image
    temp[where(primary_change_p = change_class)] = 1
    primary_change[p] = temp
```

Step 4: Secondary Change Pixel Detection

// Perform multitemporal supervised classification on every set of primary and secondary images to produce secondary change pixels. Unlike classifications performed in previous steps, the resulting maps have labelled classes where labels are the dates of forest change.

```
for each primary image p
    // Produce a stack of four multispectral images. Example: 1990-06-23_L5.dat, 1992-08-
    15_L5.dat, 1993-09-03_L5.dat, 1994-07-20_L5.dat → 1990-06-23_L5-1994-07-
    20_L5_stack (24 bands).
    stack_p = stack(image[secondary_image_indices[p,*]])

    // Training data: stable pixels detected for all ten classes in the primary image and primary
    change pixels detected for the entire processing window. Example:
    1990-06-23_L5_c1_stable, 1990-06-23_L5_c2_stable, 1990-06-23_L5_c3_stable,
```

1990-06-23_L5_c4_stable, 1990-06-23_L5_c5_stable, 1990-06-23_L5_c6_stable,
 1990-06-23_L5_c7_stable, 1990-06-23_L5_c8_stable, 1990-06-23_L5_c9_stable,
 1990-06-23_L5_c10_stable,
 1990-08-10_L5_primary_change, 1990-08-26_L5_primary_change,
 1990-09-11_L5_primary_change, 1991-06-10_L5_primary_change,
 1991-07-28_L5_primary_change, 1991-08-13_L5_primary_change,
 1991-08-22_L5_primary_change, 1991-09-07_L5_primary_change,
 1992-07-23_L5_primary_change, 1992-08-15_L5_primary_change,
 1992-08-24_L5_primary_change, 1993-08-11_L5_primary_change,
 1993-09-03_L5_primary_change, 1994-06-02_L5_primary_change,
 1994-07-20_L5_primary_change (24 classes in total).

```
training_rois_p = [stable[p,0], primary_change[p+1 :  

secondary_image_indices[p,3]]
```

```
multitemporal_mlh_p = maximum_likelihood_classification(input_data =  

stack_p, training_rois = training_rois_p, class_labels =  

training_rois_p.date)
```

// Remove stable pixels from the resulting Maximum Likelihood classification.

```
multitemporal_mlh_p[where(class_labels = date[p])] = 0
```

```
multitemporal_mlh[p] = multitemporal_mlh_p
```

// extract secondary change pixels from multitemporal_mlh.

for each primary image p except the first one

```
secondary_change_p_number_of_mlh = blank_image
```

```
p_number_of_mlh = blank_image
```

```
secondary_change_p = blank_image
```

```
pre_where = where(last_secondary_date >= date[p] and date < date[p])
```

for each pre-disturbance image pre in pre_where

```
change_class_p_where = where(multitemporal_mlh[pre].class_labels =  

date[p])
```

```
secondary_change_p_number_of_mlh[where(multitemporal_mlh[pre] =  

change_class_p_where)]++
```

```
temp = blank_image
```

```
temp[where(image[s] != 0)] = 1
```

```
p_number_of_mlh[p] += temp
```

```
secondary_change_likelihood_p = secondary_change_p_number_of_mlh /  

p_number_of_mlh
```

```

secondary_change_p[where(secondary_change_likelihood_p >
change_likelihood_threshold)] = 1

secondary_change[p] = secondary_change_p

// combine primary and secondary change pixels for each date.

primary_and_secondary_change[p] = merge(primary_change[p],
secondary_change[p])

```

Step 5: Object-Based Filtering and Forest Recovery Information Extraction

// rank spectral classes in single-date classification maps based on the average SWIR-2 values. This is required for the next step to work.

```

for each image i

    classified_SWIR2_ranked[i] = rank_classes(classified[i], spectral_band =
    SWIR2)

```

// Filter false positives and extract forest recovery information.

```

recovery_to_pre = image_array(n_images, value = 0)
recovery_from_post = image_array(n_images, value = 0)
change_detection_maps = image_array(n_images, value = 0)

```

for each primary image p except the first one

```

primary_and_secondary_change_sieved =
sieve(primary_and_secondary_change[p], cluster_size > MMU)

spatial_clusters_p = segmentation(primary_and_secondary_change_sieved)

pre_where = where(year >= year[p] - 4)
post_where = where(year <= year[p] + 4)

```

// The remaining steps are object-based, meaning they are performed on subsets of images representing individual patches of potentially disturbed forest. In this thesis, object is defined as a spatially contiguous cluster of pixels.

```

for each spatial cluster d in spatial_clusters_p

    spatial_cluster_d = spatial_clusters_p[d]

    pre_class_percentages_sum = array[n_classes, value = 0]

    n_clearsky_pre = 0

```

```

    for each pre-disturbance image pre in pre_where

```

```

classified_pre = classified_SWIR2_ranked[pre]
classified_pre_cluster_d = classified_pre[spatial_cluster_d]

if (percent_clearsky(classified_pre_cluster_d) >
cluster_clearsky_threshold) // if (n_nonmasked_px_in_cluster >
n_nonmasked_px_in_cluster_min)
  n_clearsky_pre++
  for each spectral class c
    pre_class_percentages_sum[c] += percentage of the non-masked portion
of cluster d represented by class c in classified_SWIR2_ranked[pre]

// calculate multitemporal average percentage for each class in pre-disturbance data.
pre_class_percentages = pre_class_percentages_sum/n_clearsky_pre

dominant_pre_class_indices = class or classes with the highest
pre_c_multitemp_avg_percentage that cumulatively account for 90% or more pixels in
spatial_cluster_d

post_class_percentages = calculate the same way as
pre_c_multitemp_avg_percentage but using
classified_SWIR2_ranked[p:post_where[n_post_where - 1]]

dominant_post_class_indices = determine dominant post-disturbance classes the
same way as dominant_pre_class_indices

pre_in_pre = sum(pre_class_percentages[dominant_pre_class_indices])
pre_in_post = sum(post_class_percentages[dominant_pre_class_indices])
post_in_post = sum(post_class_percentages[dominant_post_class_indices])
post_in_pre = sum(pre_class_percentages[dominant_post_class_indices])

// Reject cluster if pre- and post-disturbance distributions of spectral classes are not
sufficiently different.

if (pre_in_post/pre_in_pre < pre_in_post_threshold or
post_in_pre/post_in_post < post_in_pre_threshold)
  add spatial_cluster_d to change_detection_maps[p]

// Extract forest recovery information.
for (i = p; i < n_images; i++)
  classified_i = classified_SWIR2_ranked[i]
  classified_i_cluster_d = classified_i[spatial_cluster_d]

```

```

if (percent_clearsky(classified_i_cluster_d) >
cluster_clearsky_threshold)

    // recovery_to_pre[i] contains recovery information for spatial clusters that
    // have already been processed and, therefore, it should not be overwritten
    temp = recovery_to_pre[i]

    temp[spatial_cluster_d] = percentage of the non-masked portion of
    cluster d represented by dominant pre-disturbance spectral classes
    recovery_to_pre[i] = temp

    temp = recovery_from_post[i]

    temp[spatial_cluster_d] = percentage of the non-masked portion of
    cluster d represented by dominant post-disturbance spectral classes
    recovery_from_post[i] = temp

```